MARTIN MARIETTA ENERGY SYSTEMS LIBRARIES
3 4456 0354935 5

NUREG/CR-5565
(ORNL/TM-11548)

The Response of BWR Mark II Containments to Station Blackout Severe Accident Sequences

Prepared by
S. R. Greene, S. A. Hodge, C. R. Hyman, M. L. Tobias

Oak Ridge National Laboratory

OAK RIDGE NATIONAL LABORATORY
CENTRAL RESEARCH LIBRARY
CIRCULATION SECTION
4500N ROOM 175
LIBRARY LOAN COPY
DO NOT TRANSFER TO ANOTHER PERSON
If you wish someone else to see this report, send in name with report and the library will arrange a loan.
UCN-7969 (3 9-77)

Prepared for
U.S. Nuclear Regulatory Commission

AVAILABILITY NOTICE

Availability of Reference Materials Cited in NRC Publications

Most documents cited in NRC publications will be available from one of the following sources:

1. The NRC Public Document Room, 2120 L Street, NW, Lower Level, Washington, DC 20555

2. The Superintendent of Documents, U.S. Government Printing Office, P.O. Box 37082, Washington, DC 20013-7082

3. The National Technical Information Service, Springfield, VA 22161

Although the listing that follows represents the majority of documents cited in NRC publications, it is not intended to be exhaustive.

Referenced documents available for inspection and copying for a fee from the NRC Public Document Room include NRC correspondence and internal NRC memoranda; NRC Office of Inspection and Enforcement bulletins, circulars, information notices, inspection and investigation notices; Licensee Event Reports; vendor reports and correspondence; Commission papers; and applicant and licensee documents and correspondence.

The following documents in the NUREG series are available for purchase from the GPO Sales Program: formal NRC staff and contractor reports, NRC-sponsored conference proceedings, and NRC booklets and brochures. Also available are Regulatory Guides, NRC regulations in the *Code of Federal Regulations*, and *Nuclear Regulatory Commission Issuances*.

Documents available from the National Technical Information Service include NUREG series reports and technical reports prepared by other federal agencies and reports prepared by the Atomic Energy Commission, forerunner agency to the Nuclear Regulatory Commission.

Documents available from public and special technical libraries include all open literature items, such as books, journal and periodical articles, and transactions. *Federal Register* notices, federal and state legislation, and congressional reports can usually be obtained from these libraries.

Documents such as theses, dissertations, foreign reports and translations, and non-NRC conference proceedings are available for purchase from the organization sponsoring the publication cited.

Single copies of NRC draft reports are available free, to the extent of supply, upon written request to the Office of Information Resources Management, Distribution Section, U.S. Nuclear Regulatory Commission, Washington, DC 20555.

Copies of industry codes and standards used in a substantive manner in the NRC regulatory process are maintained at the NRC Library, 7920 Norfolk Avenue, Bethesda, Maryland, and are available there for reference use by the public. Codes and standards are usually copyrighted and may be purchased from the originating organization or, if they are American National Standards, from the American National Standards Institute, 1430 Broadway, New York, NY 10018.

DISCLAIMER NOTICE

This report was prepared as an account of work sponsored by an agency of the United States Government. Neither the United States Government nor any agency thereof, or any of their employees, makes any warranty, expressed or implied, or assumes any legal liability of responsibility for any third party's use, or the results of such use, of any information, apparatus, product or process disclosed in this report, or represents that its use by such third party would not infringe privately owned rights.

NUREG/CR-5565
ORNL/TM-11548
RX, 1S, XA

The Response of BWR Mark II Containments to Station Blackout Severe Accident Sequences

Manuscript Completed: April 1991
Date Published: May 1991

Prepared by
S. R. Greene, S. A. Hodge, C. R. Hyman, M. L. Tobias

Oak Ridge National Laboratory
Operated by Martin Marietta Energy Systems, Inc.

Oak Ridge National Laboratory
Oak Ridge, TN 37831-8057

Prepared for
Division of Safety Issue Resolution
Office of Nuclear Regulatory Research
U.S. Nuclear Regulatory Commission
Washington, DC 20555
NRC FIN B0853
Under Contract No. DOE-AC05-84OR21400

THE RESPONSE OF BWR MARK II CONTAINMENTS TO STATION BLACKOUT SEVERE ACCIDENT SEQUENCES

S. R. Greene
S. A. Hodge
C. R. Hyman
M. L. Tobias

ABSTRACT

This report describes the results of a series of calculations conducted to investigate the response of BWR Mark II containments to short-term and long-term station blackout severe accident sequences. The BWR-LTAS, BWRSAR, and MELCOR codes were employed to conduct quantitative accident sequence progression and containment response analyses for several station blackout scenarios. The accident mitigation effectiveness of automatic depressurization system actuation, drywell flooding via containment spray operation, and debris quenching in Mark II suppression pools is assessed.

FIN No. B0853 - BWR Mark II and III Parametrics

*Research sponsored by the Office of Nuclear Regulatory Research, Division of Safety Issue Resolution, U.S. Nuclear Regulatory Commission under Interagency Agreement DOE 1886-8085-3B with the U.S. Department of Energy under contract DE-AC05-84OR21400 with Martin Marietta Energy Systems, Inc.

CONTENTS

	Page
ABSTRACT	iii
CONTENTS	v
LIST OF TABLES	ix
LIST OF FIGURES	xi
FOREWORD	xxi
NOMENCLATURE	xxiii
EXECUTIVE SUMMARY	1
1. INTRODUCTION	9
2. BWR-LTAS AND BWRSAR BWR-4 MODEL DESCRIPTION	13
3. BWR-4 SHORT-TERM STATION BLACKOUT CORE DEGRADATION ANALYSES	17
3.1 INTRODUCTION	17
3.2 SEQUENCE WITH ADS ACTUATION AND SIMPLIFIED EUTECTICS	18
3.3 SEQUENCE WITH ADS ACTUATION AND BEST-ESTIMATE EUTECTICS	22
3.4 SEQUENCE WITH SIMPLIFIED EUTECTICS AND NO ADS ACTUATION	24
4. BWR-4 LONG-TERM STATION BLACKOUT CORE DEGRADATION ANALYSES	59
4.1 INTRODUCTION	59
4.2 THE INITIAL PHASE (BEFORE THE CORE IS UNCOVERED)	59
4.3 THE FINAL PHASE (CORE DEGRADATION AND RELOCATION)	63
5. MARK II CONTAINMENT DESIGN DESCRIPTION	87
6. MARK II CONTAINMENT FAILURE MODES AND MECHANISMS	93
7. MARK II CONTAINMENT MODEL DESCRIPTION	97
8. MARK II CONTAINMENT RESPONSE TO UNMITIGATED SHORT-TERM STATION BLACKOUT	103
8.1 INTRODUCTION	103
8.2 SEQUENCE WITH ADS ACTUATION (ALL CORE DEBRIS RETAINED IN DRYWELL PEDESTAL)	103
8.3 SEQUENCE WITHOUT ADS ACTUATION (ALL CORE DEBRIS RETAINED IN DRYWELL PEDESTAL)	108
8.4 SEQUENCE WITH ADS ACTUATION AND DRYWELL SPRAY ACTUATION (ALL CORE DEBRIS RETAINED IN DRYWELL PEDESTAL)	114

CONTENTS (continued)

Page

9. MARK II CONTAINMENT RESPONSE FOR UNMITIGATED SHORT-TERM STATION BLACKOUT WITH ADS ACTIVATION AND WETWELL POOL-DEBRIS INTERACTION 145
   9.1 INTRODUCTION 145
   9.2 SEQUENCE WITH 95% DRYWELL/5% WETWELL DEBRIS SPLIT 146
   9.3 SEQUENCE WITH 80% DRYWELL/20% WETWELL DEBRIS SPLIT 150
   9.4 SEQUENCE WITH 60% DRYWELL/40% WETWELL DEBRIS SPLIT 157
   9.5 SEQUENCE WITH 0% DRYWELL/100% WETWELL DEBRIS SPLIT 163
   9.6 SUMMARY OF MARK II DUAL CAVITY CALCULATIONS 166
10. MARK II CONTAINMENT RESPONSE FOR UNMITIGATED LONG-TERM STATION BLACKOUT 207
   10.1 INTRODUCTION 207
   10.2 ANALYSIS RESULTS 207
11. UNCERTAINTIES 219
   11.1 INTRODUCTION 219
   11.2 IN-VESSEL PHENOMENOLOGY 219
   11.3 EX-VESSEL PHENOMENOLOGY 220
   11.4 PLANT-SPECIFIC DESIGN CHARACTERISTICS 222
   11.5 EMERGENCY OPERATING PROCEDURE IMPLEMENTATION .. 223
12. SUMMARY OF TECHNICAL FINDINGS 225
   12.1 INTRODUCTION 225
   12.2 CONTAINMENT DESIGN DIFFERENCES 225
   12.3 MARK II CONTAINMENT FAILURE MECHANISMS AND CRITERIA 226
   12.4 IMPACT OF ADS ACTUATION TIMING ON SHORT-TERM BLACKOUT ACCIDENT PROGRESSION 226
   12.5 IMPACT OF IN-VESSEL DEBRIS EUTECTIC FORMATION ASSUMPTIONS ON SHORT-TERM BLACKOUT ACCIDENT PROGRESSION 226
   12.6 TIME REQUIRED TO EXCEED CONTAINMENT DESIGN PRESSURE FOR STATION BLACKOUT SEQUENCES 227

CONTENTS (continued)

Page

12.7 IMPACT OF ADS ACTUATION ON CONTAINMENT FAILURE TIMING 227

12.8 IMPACT OF DRYWELL SPRAY ACTUATION ON CONTAINMENT FAILURE TIMING 228

12.9 IMPACT OF SUPPRESSION POOL-DEBRIS INTERACTIONS ON CONTAINMENT FAILURE TIMING 228

12.10 CONTAINMENT FAILURE TIMING FOR LONG-TERM STATION BLACKOUT 229

13. REFERENCES 235

APPENDIX A. BWRSAR/MELCOR INTERFACE 239

APPENDIX B. BWR-LTAS INPUT DECK FOR BWR-4 243

APPENDIX C. BWRSAR INPUT DECK FOR BWR-4 245

APPENDIX D. MELCOR INPUT DECK FOR BWR MARK II CONTAINMENT 251

LIST OF TABLES

Table	Title	Page
ES.1	Mark II short-term station blackout scenario summary	6
1.1	BWR Mark I, II, and III containment characteristics	12
1.2	Domestic BWR Mark II units	12
3.1	BWRSAT program calculational methodology employed to represent events between onset of core degradation and pour of molten materials from reactor vessel for BWRs	27
3.2	Best-estimate BWR bottom head debris compositions	28
3.3	Initial conditions calculated by BWR-LTAS and employed as initial conditions in the BWRSAR analyses	29
3.4	Calculated sequence of events for BWR Mark II short-term station blackout with ADS actuation (with simplified eutectics)	29
3.5	Composition of the debris released from the reactor vessel by the end of the BWR Mark II calculation with ADS (with simplified eutectics)	30
3.6	Bottom head debris composition sets utilized in the two BWRSAR calculations	31
3.7	Integrated masses (lb) of debris expelled from the reactor vessel for the two sets of debris compositions	32
3.8	Debris pour rates (lb/min) for the two sets of debris compositions	33
3.9	Calculated sequence of events for BWR Mark II short-term station blackout without ADS actuation	34
3.10	Composition of the debris released from the reactor vessel by the end of the calculation without ADS	35
4.1	Calculated vessel and containment parameters at the time of battery failure for two methods of pressure control during station blackout	66
4.2	Calculated sequence of events for BWR Mark II long-term station blackout	67
4.3	Composition of the debris released from the reactor vessel by the end of the long-term station blackout calculation	68
5.1	Domestic BWR Mark II design parameter	89

LIST OF TABLES (continued)

Table	Title	Page
5.2	Mark II downcomer design characteristics	89
6.1	Mark II drywell head closure design data	95
7.1	ORNL Mark II containment model parameters	100
12.1	Mark II short-term station blackout scenario summary	230

LIST OF FIGURES

Figure	Title	Page
ES.1	Effect of debris-wetwell pool interactions on Mark II primary containment (wetwell) pressure response	7
3.2.1	Reactor vessel pressure for BWR-4/Mark II short-term station blackout sequence with ADS (simple eutectics)	36
3.2.2	Swollen reactor vessel water level for BWR-4/Mark II short-term station blackout accident sequence with ADS (simple eutectics)	37
3.2.3	Total SRV gas flow for BWR-4/Mark II short-term station blackout accident sequence with ADS (simple eutectics)	38
3.2.4	Total hydrogen generated in-vessel for BWR-4/Mark II short-term station blackout sequence with ADS (simple eutectics)	39
3.2.5	Integrated debris mass expelled from reactor vessel for BWR-4/Mark II short-term station blackout sequence with ADS (simple eutectics)	40
3.2.6	Mass-averaged debris pour temperature for BWR-4/Mark II short-term station blackout sequence with ADS (simple eutectics)	41
3.2.7	Decay power in ex-vessel debris for BWR-4/Mark II short-termstation blackout sequence with ADS (simple eutectics)	42
3.2.8	Downward movement of separated portions of the bottom head beneath the skirt would be limited to about 34 inches by the CRD housing support structure	43
3.3.1	Zirconium metal pours from the reactor vessel for the short-termstation blackout sequence with ADS actuation	44
3.3.2	Uranium dioxide pours from the reactor vessel for the short-term station blackout sequence with ADS actuation	45
3.3.3	Total debris pours from the reactor vessel for the short-term station blackout sequence with ADS actuation	46
3.3.4	Mass-averaged temperature of the debris pours from the reactor vessel for the short-term station blackout sequence with ADS actuation	47
3.4.1	Reactor vessel pressure for BWR-4/Mark II short-term station blackout sequence without ADS (simple eutectics)	48
3.4.2	Swollen reactor vessel water level for BWR 4/Mark II short-term station blackout sequence without ADS (simple eutectics)	49

LIST OF FIGURES (continued)

Figure	Title	Page
3.4.3	Total SRV gas flow for BWR-4/Mark II short-term station blackout sequence without ADS (simple eutectics)	50
3.4.4	Total hydrogen generated in-vessel for BWR-4/Mark II short-term station blackout sequence without ADS (simple eutectics)	51
3.4.5	Zirconium metal pours from the reactor vessel for BWR-4/Mark II short-term station blackout sequence without DS (simple eutectics)	52
3.4.6.	Uranium dioxide pours from the reactor vessel for BWR-4/Mark II short-term station blackout sequence with ADS (simple eutectics)	53
3.4.7	Total debris pours from the reactor vessel for BWR-4/Mark II short-term station blackout sequence without ADS (simple eutectics)	54
3.4.8	Mass-averaged temperature of the debris pours from the reactor vessel for the short-term station blackout sequence without ADS actuation.	55
3.4.9	Integrated debris mass expelled from the reactor vessel for BWR-4/Mark II short-term station blackout sequence with ADS (simple eutectics)	56
3.4.10	Decay power in ex-vessel debris for BWR-4/Mark II short-term station blackout sequence without ADS (simple eutectics)	57
4.2.1	Reactor vessel pressure and number of open safety/relief valves for the BWR-4/Mark II long-term station blackout sequence	69
4.2.2	Combined steam flow from the reactor vessel to the RCIC turbine, HPCI turbine, and safety/relief valves for the BWR-4/Mark II long-term station blackout sequence	70
4.2.3	Flow injected into the reactor vessel by the RCIC system for the BWR-4/Mark II long-term station blackout sequence	71
4.2.4	Actual reactor vessel water level (inches above vessel zero) for the BWR-4/Mark II long-term station blackout sequence	72
4.2.5	Mixed-mean temperature of the drywell atmosphere for the BWR-4/Mark II long-term station blackout sequence	73
4.2.6	Drywell pressure for the BWR-4/Mark II long-term station blackout sequence	74

LIST OF FIGURES (continued)

Figure	Title	Page
4.2.7	Pressure suppression pool water level and average temperature for the BWR-4/Mark II long-term station blackout sequence	75
4.3.1	Reactor vessel pressure for BWR-4/Mark II long-term station blackout sequence	76
4.3.2	Swollen reactor vessel water level for BWR-4/Mark II long-term station blackout sequence	77
4.3.3	Total SRV gas flow for BWR-4/Mark II long-term station blackout sequence	78
4.3.4	Total hydrogen generated in-vessel before bottom head penetration failure in the BWR-4/Mark II long-term station blackout sequence	79
4.3.5	Zirconium metal pours from the reactor vessel for BWR-4/Mark II long-term station blackout sequence. The initial bottom head penetration failure is predicted to occur 986 minutes after the inception of the accident	80
4.3.6	Uranium dioxide pours from the reactor vessel for BWR-4/Mark II long-term station blackout sequence	81
4.3.7	The combined metal and oxide pours from the reactor vessel for the BWR-4/Mark II long-term station blackout sequence	82
4.3.8	Mass-averaged temperature of the debris pours from the reactor vessel for the long-term station blackout sequence	83
4.3.9	Integrated combined metal and oxide release from the reactor vessel for BWR-4/Mark II long-term station blackout sequence	84
4.3.10	Decay power in ex-vessel debris for BWR-4/Mark II long-term station blackout sequence	85
5.1	Limerick Mark II containment	90
5.2	La Salle Mark II containment	91
5.3	Mark II reactor pedestal designs	92
7.1	ORNL Mark II containment model	101
7.2	Mark II vacuum breaker model	102

LIST OF FIGURES (continued)

Figure	Title	Page
8.2.1	Effect of concrete structure degassing on ex-pedestal wetwell pressure as calculated by MELCOR for the single cavity Mark II short-term station blackout sequence with ADS actuation	123
8.2.2	Primary containment pressure distribution for the single cavity Mark II short-term station blackout sequence with ADS actuation	124
8.2.3	Primary containment temperature distribution for the single cavity Mark II short-term station blackout sequence with ADS actuation	125
8.2.4	Debris layer temperatures for the single cavity Mark II short-term station blackout sequence with ADS actuation	126
8.2.5	Debris gas releases for the single cavity Mark II short-term station blackout sequence with ADS actuation	127
8.2.6	Maximum cavity dimensions for the single cavity Mark II short-term station blackout sequence with ADS actuation	128
8.2.7	Debris layer thicknesses as predicted by MELCOR for the single cavity Mark II short-term station blackout sequence with ADS actuation	129
8.3.1	Primary containment pressure distribution for the single cavity Mark II short-term station blackout sequence without ADS actuation	130
8.3.2	Primary containment temperature distribution as predicted by MELCOR for the single cavity Mark II short-term station blackout sequence without ADS actuation	131
8.3.3	Debris layer temperatures for the single cavity Mark II short-term station blackout sequence without ADS actuation	132
8.3.4	Debris gas releases for the single cavity Mark II short-term station blackout sequence without ADS actuation	133
8.3.5	Maximum cavity dimensions for the single cavity Mark II short-term station blackout sequence without ADS actuation	134
8.3.6	Debris layer thicknesses for the single cavity Mark II short-term sta tion blackout sequence without ADS actuation	135
8.4.1	Primary containment pressure distribution for the sequence with ADS and drywell spray actuation, and all debris retained in the dry-well pedestal	136

LIST OF FIGURES (continued)

Figure	Title	Page
8.4.2	Primary containment atmospheric temperature distribution for the sequence with ADS and drywell spray activation, and all debris retained in the drywell pedestal	137
8.4.3	Drywell spray flow rate for the sequence with ADS and drywell spray activation, and all debris retained in the drywell pedestal	138
8.4.4	Drywell floor (in-pedestal and ex-pedestal) pool elevations (swollen and collapsed) for the sequence with ADS and drywell spray activation, and all debris retained in the drywell pedestal	139
8.4.5	Drywell floor (in-pedestal and ex-pedestal) pool temperatures for the sequence with ADS and drywell spray activation, and all debris retained in the drywell pedestal	140
8.4.6	Drywell floor debris temperatures for the sequence with ADS and drywell spray activation, and all debris retained in the drywell pedestal	141
8.4.7	Drywell floor debris gas releases for the sequence with ADS and drywell spray activation, and all debris retained in the drywell pedestal	142
8.4.8	Maximum cavity boundaries for the sequence with ADS and drywell spray activation, and all debris retained in the drywell pedestal	143
8.4.9	Debris layer thicknesses for the sequence with ADS and drywell spray activation, and all debris retained in the drywell pedestal	144
9.2.1	Primary containment pressure distribution for the dual cavity (95% drywell/5% wetwell) Mark II short-term station blackout with ADS actuation	168
9.2.2	Primary containment temperature distribution for the dual cavity (95% drywell/5% wetwell) Mark II short-term station blackout with ADS actuation	169
9.2.3	In-pedestal drywell debris layer temperatures for the dual cavity (95% drywell/5% wetwell) Mark II short-term station blackout with ADS actuation	170
9.2.4	In-pedestal drywell debris gas releases for the dual cavity (95% drywell/5% wetwell) Mark II short-term station blackout with ADS actuation	171
9.2.5	In-pedestal drywell maximum cavity dimensions for the dual cavity (95% drywell/5% wetwell) Mark II short-term station blackout with ADS actuation	172

LIST OF FIGURES (continued)

Figure	Title	Page
9.2.6	In-pedestal drywell debris layer thicknesses for the dual cavity (95% drywell/5% wetwell) Mark II short-term station blackout with ADS actuation	173
9.2.7	Integrated steam generation from debris/wetwell pool interaction for the dual cavity (95% drywell/5% wetwell) Mark II short-term station blackout with ADS actuation	174
9.2.8	In-pedestal wetwell debris layer temperatures for the dual cavity (95% drywell/5% wetwell) Mark II short-term station blackout with ADS actuation	175
9.3.1	Primary containment pressure distribution for the dual cavity (80% drywell/20% wetwell) Mark II short-term station blackout with ADS actuation	176
9.3.2	Primary containment temperature distribution for the dual cavity (80% drywell/20% wetwell) Mark II short-term station blackout with ADS actuation	177
9.3.3	In-pedestal drywell debris layer temperatures for the dual cavity (80% drywell/20% wetwell) Mark II short-term station blackout with ADS actuation	178
9.3.4	In-pedestal drywell debris gas releases for the dual cavity (80% drywell/20% wetwell) Mark II short-term station blackout with ADS actuation	179
9.3.5	In-pedestal drywell maximum cavity dimensions for the dual cavity (80% drywell/20% wetwell) Mark II short-term station blackout with ADS actuation	180
9.3.6	In-pedestal drywell debris layer thicknesses for the dual cavity (80% drywell/20% wetwell) Mark II short-term station blackout with ADS actuation	181
9.3.7	In-pedestal wetwell debris layer temperatures for the dual cavity (80% drywell/20% wetwell) Mark II short-term station blackout with ADS actuation	182
9.3.8	In-pedestal wetwell debris gas releases for the dual cavity (80% drywell/20% wetwell) Mark II short-term station blackout with ADS actuation	183
9.3.9	In-pedestal wetwell maximum cavity dimensions for the dual cavity (80% drywell/20% wetwell) Mark II short-term station blackout with ADS actuation	184

LIST OF FIGURES (continued)

Figure	Title	Page
9.3.10	In-pedestal wetwell debris layer thicknesses for the dual cavity (80% drywell/20% wetwell) Mark II short-term station blackout with ADS actuation	185
9.3.11	Integrated steam generation from debris/wetwell pool interaction for the dual cavity (80% drywell/20% wetwell) Mark II short-term station blackout with ADS actuation	186
9.4.1	Primary containment pressure distribution for the dual cavity (60% drywell/40% wetwell) Mark II analysis of short-term station blackout with ADS actuation	187
9.4.2	Primary containment temperature distribution for the dual cavity (60% drywell/40% wetwell) Mark II short-term station blackout with ADS actuation	188
9.4.3	In-pedestal drywell debris layer temperatures for the dual cavity (60% drywell/40% wetwell) Mark II short-term station blackout with ADS actuation	189
9.4.4	In-pedestal drywell debris gas releases for the dual cavity (60% drywell/40% wetwell) Mark II short-term station blackout with ADS actuation	190
9.4.5	In-pedestal drywell maximum cavity dimensions for the dual cavity (60% drywell/40% wetwell) Mark II short-term station blackout with ADS actuation	191
9.4.6	In-pedestal drywell debris layer thicknesses for the dual cavity (60% drywell/40% wetwell) Mark II short-term station blackout with ADS actuation	192
9.4.7	In-pedestal wetwell debris layer temperatures for the dual cavity (60% drywell/40% wetwell) Mark II short-term station blackout with ADS actuation	193
9.4.8	In-pedestal wetwell debris gas releases for the dual cavity (60% drywell/40% wetwell) Mark II short-term station blackout with ADS actuation	194
9.4.9	In-pedestal wetwell maximum cavity dimensions for the dual cavity (60% drywell/40% wetwell) Mark II short-term station blackout with ADS actuation	195

LIST OF FIGURES (continued)

Figure	Title	Page
9.4.10	In-pedestal wetwell debris layer thicknesses for the dual cavity (60% drywell/40% wetwell) Mark II short-term station blackout with ADS actuation	196
9.4.11	Integrated steam generation from debris/wetwell pool interaction for the dual cavity (60% drywell/40% wetwell) Mark II short-term station blackout with ADS actuation	197
9.5.1	Primary containment pressure distribution for the dual cavity (0% drywell/100% wetwell) Mark II analysis of short-term station blackout with ADS actuation	198
9.5.2	Primary containment temperature distribution for the dual cavity (0% drywell/100% wetwell) Mark II short-term station blackout with ADS actuation	199
9.5.3	Cumulative wetwell leakage for the dual-cavity (0% drywell/100% wetwell) Mark II short-term station blackout with ADS actuation	200
9.5.4	In-pedestal wetwell debris layer temperatures for the dual cavity (0% drywell/100% wetwell) Mark II short-term station blackout with ADS actuation	201
9.5.5	In-pedestal wetwell debris gas releases for the dual cavity (0% drywell/100% wetwell) Mark II short-term station blackout with ADS actuation	202
9.5.6	In-pedestal wetwell maximum cavity dimensions for the dual cavity (0% drywell/100% wetwell) Mark II short-term station blackout with ADS actuation	203
9.5.7	In-pedestal wetwell debris layer thicknesses for the dual cavity (0% drywell/100% wetwell) Mark II short-term station blackout with ADS actuation	204
9.5.8	Integrated steam generation from debris/wetwell pool interaction for the dual cavity (0% drywell/100% wetwell) Mark II short-term station blackout with ADS actuation	205
9.6.1	Effect of debris/wetwell pool interactions on Mark II primary containment (wetwell) pressure response	206
10.2.1	Primary containment pressure distribution for the single cavity Mark II long-term station blackout sequence with ADS actuation	212

LIST OF FIGURES (continued)

Figure	Title	Page
10.2.2	Primary containment temperature distribution as predicted by MELCOR for the single cavity Mark II long-term station blackout sequence	213
10.2.3	Debris layer temperatures for the single cavity Mark II long-term station blackout sequence	214
10.2.4	Debris layer thicknesses for the single cavity Mark II long-term station blackout sequence	215
10.2.5	Debris gas releases for the single cavity Mark II long-term station blackout sequence	216
10.2.6	Maximum cavity dimensions for the single cavity Mark II long-term station blackout sequence	217
12.6.1	Predicted containment pressurization histories for Mark II station blackout sequences	231
12.7.1	Impact of ADS actuation on containment pressurization history for short-term station blackout sequence	232
12.8.1	Impact of drywell spray activation on short-term station blackout sequence with ADS actuation	233
12.9.1	Containment pressurization histories for dual cavity short-term station blackout sequences with ADS actuation	234

FOREWORD

The ability of containments to successfully survive some severe accident challenges, as indicated in draft NUREG-1150, is uncertain. In SECY-88-147, "Integration Plan for Closure of Severe Accident Issues" (dated May 25, 1988) the NRC staff presented to the Commission a program plan to evaluate generic severe accident containment vulnerabilities via the Containment Performance Improvement (CPI) program. This effort was based on the presumption that there are generic severe accident challenges for each light water reactor containment type and was intended to focus on the evaluation of hardware and procedural issues related to generic containment challenges.

The purpose of this report is to provide BWR Mark II owners with information they may find useful in assessing their plants as part of their Individual Plant Examination (IPE) program. Generic Letter 88-20, Supplement 3, dated July 6, 1990, gives specific guidance to industry on the use of this, and similar, reports. No requirements are contained in this report and it is being provided for information only.

The BWR Mark II and III Parametrics Program was established at Oak Ridge National Laboratory in 1988. The program's focus has been to provide best-estimate analyses of generic Mark II and III severe accident behavior and to assess the potential value of procedural and hardware improvements which could impact severe accident containment performance.

This report summarizes the results of the Mark II containment response analyses. Special issues relating to Mark II severe accident containment performance are dealt with in a companion report, NUREG/CR-5623, "BWR Mark II Ex-vessel Corium Interaction Analyses." Mark III containment response analysis results are described in NUREG/CR-5571, "The Response of BWR Mark III Containments to Short-term Station Blackout Severe Accident Sequences."

Detailed plant models which accurately reflect the most important design features of Mark II containments were developed for this study. The cooperation of Pennsylvania Power and Light Company (PP&L) and the staff of the Susquehanna Steam Electric Station is greatly appreciated. PP&L provided site access, and detailed plant design and procedural data which have contributed significantly to the quality and applicability of these analyses. Sandia National Laboratories (A. C. Payne) provided a copy of their MELCOR deck for the La Salle County Station which was reviewed prior to formulating the Mark II containment model employed in these analyses. The insights gained from this review accelerated the development of ORNL's model. Finally, appreciation is expressed to PP&L, Philadelphia Electric Company, and Dr. Michael Corradini of the University of Wisconsin for their review of and comments on the draft report.

Sherrell R. Greene, Manager
Mark II and III Parametrics
Program

NOMENCLATURE

AC	Alternating Current
ADS	Automatic Depressurization System
ASEP	Accident Sequence Evaluation Program
ATWS	Anticipated Transient Without Scram
BWR	Boiling Water Reactor
CPI	Containment Performance Improvement
DC	Direct Current
EPRI	Electric Power Research Institute
ECCS	Emergency Core Cooling System
EDF	External Data File
EPG	Emergency Procedure Guidelines
FDI	Fuel Dispersal Interactions
FSAR	Final Safety Analysis Report
est	Estimated
ft	Feet
h	Hour(s)
HCOG	Hydrogen Control Owner's Group
HPCI	High Pressure Coolant Injection
HPCS	High Pressure Core Spray
HVAC	Heating, Ventilation, and Air Conditioning
in.	Inches
INEL	Idaho National Engineering Laboratory
IPE	Individual Plant Examination
lb	Pound(s)
LOCA	Loss of Coolant Accident
LPCS	Low Pressure Core Spray
MCCI	Molten Core-Concrete Interactions
min	Minutes
MSIV	Main Steam Isolation Valve
MW	Megawatts
N/A	Not Applicable
NRC	Nuclear Regulatory Commission
ORNL	Oak Ridge National Laboratory
PRA	Probabilistic Risk Assessment
psia	pounds force per square inch absolute
psid	pounds force per square inch differential
psig	pounds force per square inch gauge
RCIC	Reactor Core Isolation Cooling
RHR	Residual Heat Removal
RPV	Reactor Pressure Vessel
RWCU	Reactor Water Cleanup
SERI	System Energy Resources Incorporated
SGTS	Standby Gas Treatment System
SNL	Sandia National Laboratories
SPMS	Suppression Pool Makeup System
SRV	Safety/Relief Valve

EXECUTIVE SUMMARY

Introduction

The purpose of this report is to provide BWR Mark II owners with information they may find useful in their Individual Plant Examination (IPE). No requirements are contained in this report (that is, the report is provided for information only).

Detailed analyses of BWR Mark II short-term station blackout sequences were conducted. A short-term station blackout is an accident sequence involving loss of all AC power with concurrent failure of the high pressure reactor vessel injection systems. Since AC power is needed for operation of the existing containment purge valves, it would not be possible to vent the containment via existing hardware under station blackout conditions.

Seven short-term station blackout analyses were conducted. The description of these seven scenarios is given in Table ES.1. The BWR-LTAS, BWRSAR, and MELCOR codes were employed to provide an analysis of the accident sequence from its inception until several hours after reactor vessel failure. The first three calculations were intended to investigate the role of automatic depressurization system (ADS) and drywell spray activation (a dedicated alternate power supply system is assumed) on Mark II severe accident containment performance. These calculations were halted at the time of drywell floor burn-through (due to the core-concrete interaction), because MELCOR does not have the capability to model the prompt debris-pool interactions (and containment pressure increase) that would occur following this event. The last four calculations were intended to investigate the potential implications of early entry of core-concrete debris into the wetwell via failed inpedestal drywell drainlines or downcomers.

One unmitigated long-term station blackout sequence was analyzed. A long-term station blackout is an accident sequence involving loss of all AC power, but high pressure reactor vessel injection is maintained until the unit batteries are exhausted.

Mark II Reactor Pedestal/Cavity Designs

The evaluations of Mark II containment designs completed during this study revealed that there is no "generic" configuration which acceptably represents all Mark II facilities. Each of the six domestic Mark II designs differ in a manner which could

significantly affect ex-vessel core-concrete interaction phenomena and containment performance. The designs differ in terms of depth of an in-pedestal cavity, the thickness of the in-pedestal drywell floor, and the presence of penetrations (downcomers or floor drains) in the in-pedestal floor.

Since it was not feasible to perform plant-specific evaluations for each of the six pedestal/cavity designs during the course of this project, a single deep-cavity design (representative of La Salle and WNP-2) was selected. The choice of this design was dictated by current CORCON and MELCOR code modeling limitations which preclude credible analyses of designs in which debris would be allowed to spread or flow outward from the in-pedestal to the ex-pedestal region of the drywell floor.

Mark II Containment Failure Mechanisms

Few detailed analyses have been conducted to evaluate failure modes and criteria for Mark II containments. The major threats to Mark II containment integrity during severe accidents appear to be either (a) static over-pressure failure of the outer containment boundary, air locks, and penetrations, (b) failure of the outer containment boundary in an over-pressure or missile-impingement mode resulting from ex-vessel steam explosions in the drywell or wetwell, or (c) combined over-pressure/over-temperature failure of the drywell head flange seals.

Mark II static over-pressure failure limits have been predicted to range between 120-160 psig. A failure pressure criterion of 135 psig (150 psia) was employed in these calculations. The best available information regarding drywell head flange seal failure indicates that these seals would fail after reaching 700°F if the pressure differential across the seals reaches 82 psid. There is great uncertainty regarding the generic applicability of this information, however, since the head flange closure design is *extremely* plant-specific.

Impact of ADS Actuation Timing on In-Vessel Short-term Blackout Accident Progression

BWRSAR calculations indicate that the timing of ADS actuation significantly impacts the rate of core degradation. Relocation of core debris begins 25 - 30 minutes later when the Revision 3 Emergency Procedure Guidelines (EPGs) are utilized than when the Revision 4 procedures are employed. This delay results from the superior

steam cooling provided by the Revision 3 approach. This delay could increase the probability of halting the accident prior to reactor vessel failure because additional time is provided for connection of alternate water and/or pumping power sources for use by in-vessel injection systems.

Impact of In-vessel Debris Eutectic Formation Assumptions on Short-Term Blackout Accident Progression

The potential impact of the most recent experimental findings regarding BWR debris eutectic formation in the lower head of the reactor vessel has been examined. These calculations indicate that more unoxidized zirconium would be expected to enter the containment early in the accident than is predicted by traditional modeling methods. This unoxidized zirconium would oxidize on the containment floor, heating the debris and providing a direct source of hydrogen to the drywell atmosphere. However, the calculations also indicate that any significant differences in the predicted containment response would be limited to the first 2 h after initial reactor vessel penetration failure.

Timing of Primary Containment Failure for Unmitigated Short-Term Station Blackout Sequence

Table ES.1 summarizes the results of all of the calculations performed for this study in terms of the estimated time to containment failure. Containment failure via the traditional over-pressure failure mode (at 135 psig) was predicted to occur in the depressurized reactor vessel scenario only when 100% of the debris is assumed to directly enter the wetwell pool. The predicted time to containment failure for this sequence is 8.5 h. This failure mode was also predicted for the scenario in which the reactor vessel is <u>not</u> depressurized and 100% of the debris remains in the drywell reactor pedestal. The predicted time to containment failure for this sequence is 10 h.

The maximum predicted primary containment pressure prior to drywell floor burn-through in the other unmitigated sequences ranged from 102 to 125 psig. While these pressures are lower than the assumed containment failure criterion of 135 psig, it is quite possible that containment failure would occur in these cases at the time of drywell floor failure This failure might result from the prompt burst of steam which is generated when the debris falls into the in-pedestal region of the pressure suppression pool (in all Mark IIs except LaSalle.) The associated times of drywell floor failure for these

scenarios ranged from 12.2 h to >26.7 h. These drywell floor failure timing estimates are believed to be conservatively low due to the use of a reactor pedestal and cavity model which confines all core debris to the in-pedestal region of the drywell.

Impact of ADS Failure on Short-term Blackout Containment Performance

Containment failure would probably occur (as a result of drywell floor failure) within 13 to 13.5 h for the short-term blackout sequence in which the ADS system is actuated, and (via over-pressure) within 10 h for the case in which the ADS system is not actuated. Thus, failure to actuate the ADS could shorten the time to gross containment failure by as much as 3 h - a 26% decrease in containment failure timing for this sequence.

Effectiveness of Drywell Flooding Via Containment Spray Operation

Flooding of the drywell floor via operation of the existing containment spray system reduces the ablation rate of the concrete drywell floor. The spray system employed in these calculations produces a 3 h delay (i.e., 16.6 h vs. 13.5 h) in the time of drywell floor burn-through for the short-term blackout case in which the reactor is depressurized. However, this retardation in floor ablation is gained at the expense of higher containment pressures associated with the vaporization of the spray water as it interacts with the hot core-concrete debris. The containment was predicted to be very near its failure pressure at the time of drywell floor burn-through. The overall effectiveness of existing systems can be limited because they often utilize low-head pumps (an 82.5 psid shut-off head was employed for this analysis). The drywell pressure exceeded the cutoff head of these pumps at 12 h into the accident. The existing pool of water generated by the pumps was depleted via boiling within 4.1 h after pump cutoff, and drywell floor burn-through was calculated to occur 0.6 h after the drywell pool water is exhausted. These results are subject to great uncertainty, however, since the actual heat transfer regime which would exist is unknown, and the effect of variable debris-to-pool heat transfer coefficients was not explored.

Potential Impact of Suppression Pool-Debris Interactions on Containment Performance

The last four short-term blackout calculations investigated the potential implications of early drywell drainline or downcomer melt-through and the interaction of core-concrete debris with the water contained in the in-pedestal wetwell region. The results of these preliminary calculations (Fig. ES.1) indicate that the early entry of very large fractions (80-100%) of the core-concrete debris could result in over-pressure failure of the containment within 9 h of accident inception, *even for cases in which steam explosions do not occur*. This finding (which is most relevant to the Nine Mile Point-2 and Shoreham designs that employ in-pedestal downcomers below the reactor vessel) is subject to great uncertainty due to the simplistic and limited models employed in MELCOR to represent debris-pool interactions.

Timing of Primary Containment Failure for Long-term Station Blackout Sequence

The long-term station blackout scenario is very similar to the short-term station blackout scenario in which the ADS is not actuated, except that the sequence is delayed due to the early availability of reactor vessel injection. Containment failure via over-pressurization is predicted to occur at 20.8 h in this sequence compared to 10 h for the short-term blackout case in which the ADS system is not actuated.

Table ES.1 Mark II short-term station blackout scenario summary

Case	ADS actuated?	Drywell sprays activated?	Debris split fraction % drywell	Debris split fraction % wetwell	Time to containment failure (h)	Time to drywell floor failure (h)	Wetwell pressure at time of floor failure (psia)
ST-1	yes	no	100	0	N/A	13.5	117
ST-2	no	no	100	0	10.0	12.2	173
ST-3	yes	yes	100	0	N/A	16.6	145
ST-4	yes	no	95	5	N/A	14.1	120
ST-5	yes	no	80	20	>20.4	>20.4	134[a]
ST-6	yes	no	60	40	>26.7	>26.7	140[b]
ST-7	yes	no	0	100	8.5	>12.9	145
LT-1	no	no	100	0	20.8	>22.1	165[c,d]

[a]Wetwell pressure at 20.4 h.

[b]Wetwell pressure at 26.7 h.

[c]Wetwell pressure at 22.1 h.

[d]Note: All containment failure mechanisms were disabled for the long-term station blackout calculation.

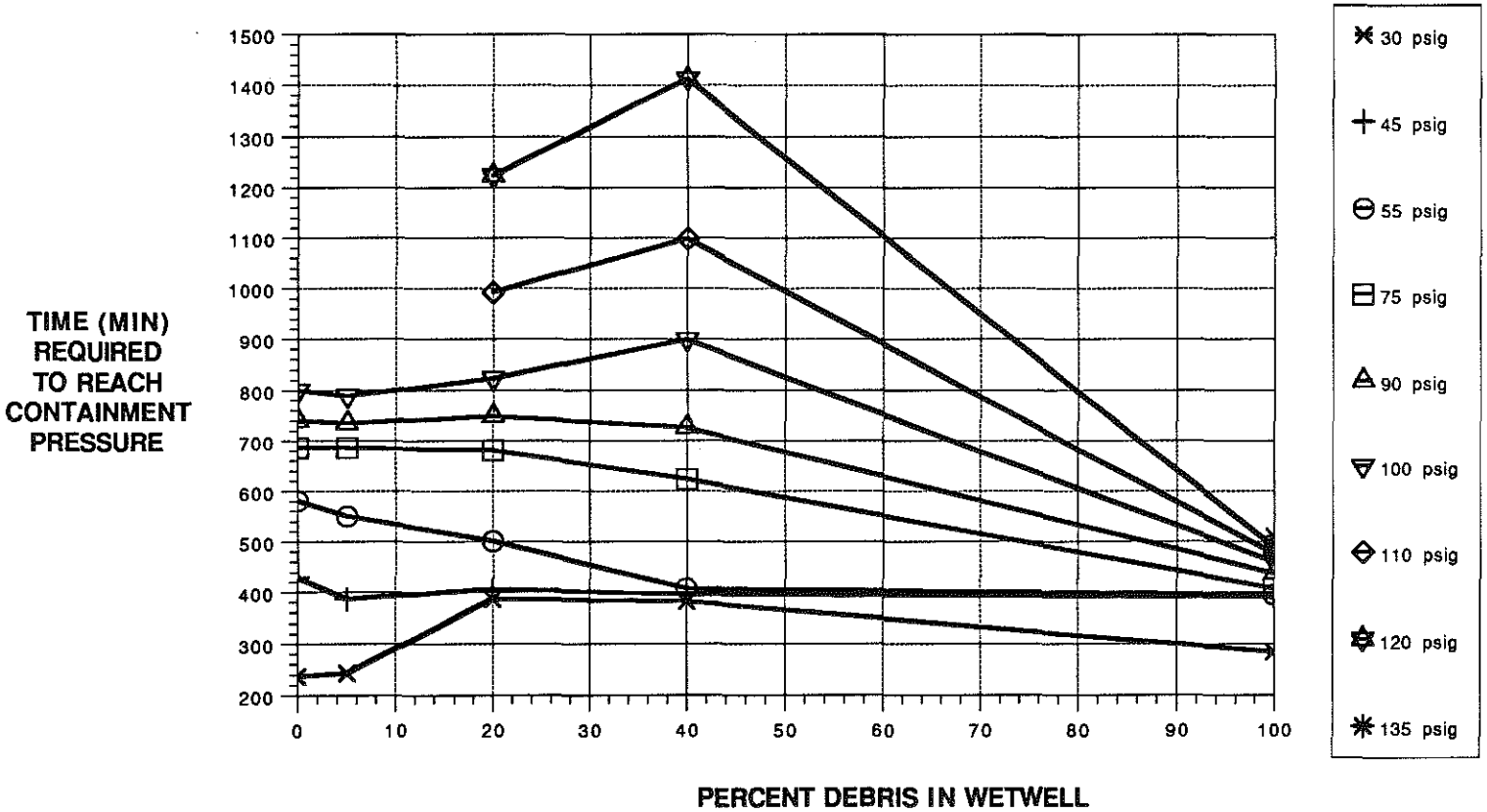

Fig. ES.1 Effect of debris-wetwell pool interactions on Mark II primary containment (wetwell) pressure response.

THE RESPONSE OF BWR MARK II CONTAINMENTS TO STATION BLACKOUT SEVERE ACCIDENT SEQUENCES

1. INTRODUCTION

Historically, the station blackout accident has been considered to be the sequence initiated by loss of offsite power combined with reactor scram and failure of the station diesels to start and load. Today, this accident sequence is classified as long-term station blackout, in which water is injected into the reactor vessel by the steam turbine-driven High Pressure Coolant Injection (HPCI) or Reactor Core Isolation Cooling (RCIC) systems to keep the core covered for as long as DC power for turbine governor control remains available from the unit batteries (a period of approximately 6 h). The reason for today's "long-term" designation is that the definition of station blackout implemented by the NRC-sponsored Accident Sequence Evaluation Program (ASEP) has been expanded to include two cases that, heretofore, were classified as Loss of Injection, or TQUV sequences in WASH-1400 (Ref. 1) parlance. In these short-term station blackout sequences, the capability for water injection to the reactor vessel is lost at the inception of the accident. (The short-term designation derives from the fact that the core is uncovered relatively quickly in these sequences.)

The early total loss of injection aspect of BWR/Mark II short-term station blackout might be initiated in either of two ways. First, there might be an independent failure of the RCIC system (and HPCI system if present) when it is called upon to keep the core covered during the period in which DC power remains available. Second, there might be a common-mode failure of the DC battery systems that, upon loss of offsite power, precludes starting of the diesel generators. Without DC power for valve operation and turbine governor control, the steam turbine-driven RCIC (and HPCI) system would not be operable.

The difference between long-term and short-term station blackout is that DC power remains available during the period of core degradation for short-term station blackout. The decay heat level is relatively high and the reactor vessel is depressurized during the period of core degradation and material relocation within and from the vessel. The core remains covered for more than 6 h in the long-term station blackout, so the decay heat level is approximately 30% lower during the period of core degradation. Since the safety relief valves (SRVs) cannot be manually operated without DC power, the

reactor vessel is pressurized at the time of bottom head penetration failure and initial release of debris from the vessel.

Much of the impetus for basing these BWR containment response studies upon the short-term station blackout severe accident sequence derives from the recent findings of the ASEP in support of the NUREG-1150 effort (Ref. 2). These findings provide the estimate that 97% of the core damage risk at Grand Gulf can be attributed to the overall threat of station blackout. Most recent BWR probabilistic risk assessments (PRAs) also indicate that station blackout is the dominant contributor to the total core melt probability.

The fundamental design characteristics of Mark I, II, and III containments are significantly different (Table 1.1). With respect to size, the major design difference is that the total containment free volume of the Mark II is 30-40% larger than that of the Mark I, while the total containment free volume of the Mark III is 500-600% greater than that of the Mark I. This difference alone would suggest that the basic severe accident performance of Mark II plants might be significantly different than the Mark I plants. However, the three containment designs also differ in shape and the location of the pressure suppression pool relative to the drywell floor.

There are nine domestic BWR Mark II units (six plants): Limerick-1 and -2, Susquehanna-1 and -2, La Salle-1 and -2, WNP-2, Nine Mile Point-2, and Shoreham. Limerick, Susquehanna, and Shoreham (five units) employ the BWR-4 reactor design; while La Salle, WNP-2, and Nine Mile Point-2 (four units) employ the BWR-5 reactor design. The basic design characteristics of these plants are summarized in Table 1.2. Although these plants share many generic containment features, the drywell reactor pedestal/cavity design is very plant-specific (see Chapter 5).

For the purpose of these analyses, a synthetic "Mark II CPI Plant" design is utilized. This CPI Plant integrates Susquehanna's BWR-4 reactor with a primary containment which incorporates elements of the Susquehanna, La Salle, and WNP-2 designs. This combination of features was chosen, in part, to minimize the impact of current core-concrete interaction analysis code (CORCON) limitations by utilizing a drywell pedestal/cavity design (La Salle/WNP-2) that prevents spreading of the core debris to the ex-pedestal region of the drywell.

This report describes the results of calculations for BWR-4/Mark II short- and long-term station blackout sequences. The BWR-LTAS (Ref. 3), BWRSAR (Ref. 4), and MELCOR (Ref. 5) codes were employed for analysis of the reactor and primary

containment response for a variety of short-term station blackout scenarios and for one long-term station blackout scenario.

Chapter 2 describes the BWR-LTAS and BWRSAR reactor models used in these calculations. Chapter 3 describes the results of the BWR-4 in-vessel core degradation analyses for short-term station blackout sequences. Chapter 4 describes the results of the BWR-4 in-vessel core degradation analyses for a long-term station blackout sequence. Chapter 5 describes the Mark II containment design. Mark II containment failure mechanisms are briefly discussed in Chapter 6. Chapter 7 describes the BWR Mark II MELCOR model developed for and utilized in this study. Chapters 8 and 9 describe the results of the Mark II short-term station blackout containment analyses. (The results of calculations conducted to investigate the impact of non-explosive debris/suppression pool interactions are described in Chapter 9.) The results of the Mark II long-term station blackout containment analyses are described in Chapter 10. Chapter 11 provides a summary of the uncertainties associated with the calculations. Finally, the technical findings of the study are summarized in Chapter 12.

Appendix A presents a brief description of the BWRSAR/MELCOR interface written at ORNL to provide an automated method for driving the MELCOR containment models with the BWRSAR SRV flows, vessel leakage flows, debris pours, and ex-vessel decay heat levels. Appendices B, C, and D present listings of prototypical BWR-LTAS, BWRSAR, and MELCOR input decks utilized for this study.

Table 1.1. BWR Mark I, II, and III containment characteristics

Parameter	Mark I Browns Ferry	Mark II Limerick	Mark III Grand Gulf
Drywell design pressure (psig)	56	55	30
Drywell design temperature (°F)	281	340	330
Drywell free volume (ft^3)	159,000	243,600	270,000
Wetwell design pressure (psig)	56	55	15
Wetwell design temperature (°F)	281	220	185
Min. wetwell free volume (ft^3)	126,200	147,700	1,400,000
Max. wetwell pool volume (ft^3)	127,800	127,800	136,000
Total containment free volume (ft^3)	285,200	391,200	1,670,000

Table 1.2. Domestic BWR Mark II units

Name	MWe	Location	Reactor type[a]	Commercial Operation
La Salle 1	1036	Seneca, IL	5	1/84
La Salle 2	1036	Seneca, IL	5	10/84
Limerick 1	1055	Pottstown, PA	4	2/86
Limerick 2	1055	Pottstown, PA	4	1/90
Nine Mile Pt. 2	1080	Scriba, NY	5	4/88
Shoreham	809	Brookhaven, NY	4	N/A
Susquehanna 1	1032	Berwick, PA	4	6/83
Susquehanna 2	1032	Berwick, PA	4	2/85
WNP-2	1095	Richland, WA	5	12/84

[a]The BWR-4 plants employ a High Pressure Coolant Injection (HPCI) steam-turbine pumping system to provide high pressure makeup to the reactor vessel via feedwater or core spray lines. This system is replaced in the BWR-5 plants by an electric motor-driven High Pressure Core Spray (HPCS) system.

2. BWR-LTAS AND BWRSAR BWR-4 MODEL DESCRIPTION

BWR-LTAS (Ref. 3) is a digital computer code written to calculate the effects of operator actions on the general thermalhydraulic behavior of the Browns Ferry Unit 1 BWR following a hypothetical station blackout event. The code consists of the differential and algebraic equations of mass and energy conservation and equations of state for the reactor vessel and containment. Some of the important variables calculated by the BWR-LTAS code include:

1. Reactor vessel water levels (above the fuel as well as in the downcomer annulus),
2. Reactor vessel pressure,
3. Average fuel temperature,
4. Reactor vessel injection flow,
5. Safety-relief valve flow,
6. Containment pressures and temperatures, and
7. Suppression pool water level and temperature.

The pumping systems that have been included in BWR-LTAS are the RCIC and HPCI systems, the control rod drive hydraulic system (CRDHS), the condensate/condensate booster pumps, and the low pressure emergency core cooling systems [the low pressure coolant injection (LPCI) mode of the RHR system and the core spray system]. The CRDHS and the RCIC and HPCI systems are capable of injecting adequate makeup flows against full reactor pressure. The steam-driven RCIC and HPCI systems are capable of running during station blackout. All the other pumps are driven by non-battery-backed electric motors that require a high voltage source of AC power.

The primary system variables calculated by BWR-LTAS are: core coverage, reactor vessel injection requirements, reactor vessel pressure, steam flow to the primary containment, and the transfer of heat from the surfaces of the reactor vessel and associated piping to the drywell atmosphere. The mathematical model is programmed to function at any reactor vessel pressure between atmospheric pressure and 1300 psia (well above the normal pressure of 1025 psia). The reactor vessel water inventory can range from nearly empty (water in the vessel lower plenum only) to nearly full. [For proper convergence, the pressure calculation assumes that there is always a steam space of at least 500 ft^3 volume (approximately 2% of vessel free volume)].

The BWR-LTAS code is intended to be used to investigate that portion of accident sequences up to, but not including, permanent core uncovery and subsequent

fuel damage. For this reason, no provision is made to calculate heatup of the fuel during periods of core uncovery. For modeling purposes, the thermalhydraulic processes within the reactor vessel are treated in two regions: the steam-only region, which normally comprises approximately the top third of the reactor vessel; and the steam-water region, which normally covers the reactor fuel. Given the injection flows and reactor vessel pressure, the steam/water region model calculates the reactor vessel water levels and the core steam production rate. The steam-only region calculation operates on the core steam production rate (and also on relief valve position information) to calculate reactor vessel pressure. Run-specific input includes:

1. Injection flow vs time or an algorithm to represent operator control of reactor vessel water level,
2. SRV opening(s) vs time or an algorithm to represent operator control of reactor vessel pressure with the SRVs, and
3. Initialization parameters: initial time elapsed since reactor trip, initial reactor vessel pressure and level, and initial containment pressures, temperatures, and suppression pool level.

The BWR-LTAS and BWRSAR code input decks for these calculations are based upon the Susquehanna Plant. Construction of the input decks was greatly facilitated by information provided by the Pennsylvania Power and Light (PP&L) Company with regard to plant-specific design features. One of the information items provided by PP&L in support of this study has general application to all types of BWRs. This item involves Susquehanna Plant data recorded during a plant test in which the main steam isolation valves were tripped with the reactor at power (Ref. 6). The data recorded included reactor vessel pressure and water level, feedwater flow, HPCI and RCIC system injected flow, and core inlet flow. Previous studies have neglected the effect of reactor vessel injection during feedwater turbine coastdown because the information necessary to estimate this effect was not available. The PP&L test, however, shows that the injection associated with feedwater pump coastdown is sufficient to increase the reactor vessel water level by approximately 57 inches. The higher initial reactor vessel water level causes a delay of approximately 16 min in the time of initial core uncovery and corresponding delays in the subsequent events of the accident sequence.

The BWRSAR code input deck utilized for these studies is considered to be an improvement over previous models in the following areas:

1. Nine-by nine fuel assemblies are represented,
2. Axial conduction is calculated for the fuel and cladding,
3. Reactor vessel leakage is reduced to conform to measured leak rates for Susquehanna,
4. SRV leakage is modeled in a manner consistent with Susquehanna's experience with Crosby valves,
5. The assumed control blade melting temperature (2450°F) is reduced in accordance with recent experimental (DF-4, CORA) observations,
6. Core plate and control rod guide tube creep-rupture failure temperatures (2100°F) are increased as recommended in recent group discussions with representatives from Sandia National Laboratories, Idaho National Engineering Laboratory and the Electric Power Research Institute (EPRI),
7. The ablation temperature (2660°F) for the debris material in the vessel bottom head is decreased,
8. The end-of-cycle axial power profile provided by PP&L for Susquehanna Unit 1 Cycle 4 (equilibrium core) is used,
9. Decay energy is release from the fuel in accordance with current recommendations of R. A. Lorenz of ORNL*. (Based on recent experiments, the energy release is slower than previously anticipated), and
10. Operator actions to control reactor vessel pressure are modeled in a manner consistent with Susquehanna procedures.

---

*R. A. Lorenz, "CORSOR - History and Status," ORNL Internal Memo, March 3, 1989.

3. BWR-4 SHORT-TERM STATION BLACKOUT CORE DEGRADATION ANALYSES

3.1 INTRODUCTION

The core degradation analyses performed in support of the studies discussed in this chapter were conducted with the Boiling Water Reactor Severe Accident Response (BWRSAR) code and are based upon the unmitigated short-term station blackout accident sequence at a BWR with a Mark II containment . The accident is assumed to occur at the end of core life. (Initial conditions for the calculation were provided by the BWR-LTAS code, as discussed in Sect. 3.2.) The purpose of these BWRSAR calculations is to provide the reactor vessel gas blowdown rates and the core and structural debris pour rates from the vessel for use as input to subsequent MELCOR calculations of the detailed containment response. Information concerning the BWRSAR code and its applications to short-term station blackout is provided in the following discussion. Additional and more detailed information concerning the operation of the BWRSAR code and its capabilities and limitations can be found in Refs. 4 and 7.

The BWRSAR code implements the BWR severe accident modeling strategy outlined in Table 3.1. It should be recognized that this methodology, developed at ORNL by L. J. Ott, results in significantly longer times to reactor vessel bottom head penetration failure than previous analytical approaches. This delay is a result of the contention that after the onset of core degradation and the initial local failures of the core plate, the very large amount of water in the BWR reactor vessel bottom head must first be boiled away and the quenched debris must then reheat (to approximately 2100°F) before the reactor vessel bottom head penetrations can fail.

The reactor vessel debris pours calculated by the BWRSAR code depend upon a user-input definition of the pure species and eutectic mixtures that will form in the vessel bottom head and their melting points. The current "best-estimate" debris composition (Table 3.2) is based upon the results of the small-scale BWR Core Debris Eutectic Formation and Melting Experiment (Ref. 8) performed at ORNL by G. W. Parker in December 1987. In the experiment, metal pours occurred in three mixtures over the range of 2640-2920°F. An oxide pour occurred at 4172°F, leaving the majority of the UO_2 pellets within the simulated lower plenum regions. This remaining UO_2 would be expected to melt at approximately 4800°F.

The CORCON module within MELCOR can not accommodate the "best-estimate" multi-eutectic treatment. Currently, CORCON can accept only UO_2, Zr, steel, ZrO_2, steel oxide, and B_4C. Therefore, debris pours intended for use with CORCON must be comprised of these materials. Two mixture compositions are used:

- All metals in one mixture melting at 2750°F (mole fractions Zr 0.210, Fe 0.579, Cr 0.151, Ni 0.060), and
- All ZrO_2 and UO_2 in a mixture melting at 4800°F material (mole fractions ZrO_2 0.170, UO_2 0.830).

The remaining oxides are also specified to melt at 4800°F.

While these melting temperatures are significantly higher than those of some of the pours observed in the small-scale experiment, temperatures of this magnitude are necessary with the version of CORCON implemented within MELCOR 1.80. Otherwise, the containment calculation would initially treat these introduced pours as frozen material, and the latent heat of fusion would be lost from the calculation. At any rate, use of these higher melting temperatures is conservative in that a more severe challenge to the containment is introduced at the time of the initial pour.

It should be noted that very little of the debris in the bottom head is molten at the time of penetration failure and, therefore, the subsequent debris pours from the reactor vessel are controlled by the rate of debris melting and begin sometime after penetration failure. However, if the reactor vessel is pressurized at the time of penetration failure, the metal-water reactions associated with the vessel blowdown through the bottom head debris would produce a large amount of hydrogen and associated energy release within the debris bed. Significant debris pours would begin almost immediately after bottom head penetration failure.

3.2 SEQUENCE WITH ADS ACTUATION AND SIMPLIFIED EUTECTICS

The initial conditions for the BWRSAR analyses (Table 3.3) were taken from the results of a BWR-LTAS calculation that covers the period of the accident sequence from 0.6 min -35 min. The initial conditions for the BWR-LTAS calculation were taken from the results of the Susquehanna main steam isolation valve closure test discussed in

Chapter 2. The BWRSAR calculation was initiated at time 35 min into the short-term station blackout accident sequence.

The sequence of events and event timing for the BWR Mark II short-term station blackout with ADS actuation accident sequence as calculated by the BWRSAR code are provided in Table 3.4. It is assumed that the reactor had been operating at 100% power at the time of scram and that no reactor vessel injection source is ever recovered.

Operator control of reactor vessel pressure during the period of the BWR-LTAS calculation and the period of the BWRSAR calculation before ADS actuation is modeled as follows:

Event	Time (min)
Begin manual control of reactor vessel pressure and begin depressurization to 765 psia.	2.00
Complete controlled depressurization; maintain vessel pressure in range 715-865 psia.	2.00-33.33
With water level near the top of the core, allow vessel pressure to increase. Then maintain vessel pressure in the range 935-1075 psia.	33.33-78.0
With water level at 257.5 in. above vessel zero, open one SRV; when vessel pressure falls to 715 psia, manually actuate the ADS.	78.0

The Susquehanna operating procedures are based upon Revision 3 of the BWR Owners Group Emergency Operating Procedures (EPGs) (Ref. 9). Revision 3 calls for manual ADS actuation at a water level equivalent to 28% of core height. This level is reached at approximately 84 min after scram in this sequence. However BWRSAR calculations indicate that a substantial amount of hydrogen (approximately 80 lb) would be generated by clad metal-steam reactions by this time. It is believed that general adherence to Revision 3 of the EPGs is better represented by earlier actuation of the ADS, before significant hydrogen has been generated. Accordingly, the BWRSAR calculations described here are based on manual ADS actuation at 78 min into the transient. At this time, the reactor water level is approximately 33% of core height, and less than 10 lb of

hydrogen has been generated. ADS actuation at this time provides steam cooling of the uncovered portion of the core and delays any further hydrogen generation for a period of approximately 20 min. The ADS maneuver is carried out in two steps in accordance with the provisions of Revision 3 of the EPGs. First, a single SRV is manually opened when the reactor vessel water level has fallen to one-third core height. As the vessel pressure decreases through 715 psia, the ADS is actuated, opening the remainder of the ADS family of valves. This results in a total of six open SRVs.

Plots of key parameters representing events within the reactor vessel as predicted by the BWRSAR code are provided in Figs. 3.2.1-3.2.7. These plots represent events from time 35 min, when the BWRSAR calculation is initiated, until time 300 min, which is approximately 37 min after reactor vessel bottom head penetration failure. As indicated in Fig. 3.2.1, the ADS maneuver is initiated at time 78 min, when the reactor vessel water level (Fig. 3.2.2) is at approximately one-third core height; this causes six SRVs to open. Since the SRVs are modeled as Crosby valves, the ADS valves remain open once actuated. (This would not be true of the Target Rock-type SRVs installed at earlier BWR plants such as Peach Bottom and Browns Ferry for which the open or closed status depends upon the differential pressure between reactor vessel and drywell.) The associated SRV flows from the reactor vessel to the pressure suppression pool are shown in Fig. 3.2.3.

The swollen reactor vessel water level, which includes consideration of the effects of voids, is shown in Fig. 3.2.2. The calculated water level rapidly falls below the core plate as a result of the water loss by flashing when the ADS valves are opened. Small temporary increases in level subsequently occur because of displacement of water in the bottom head whenever large masses of core debris are introduced after core plate failure. The decay heat associated with the fuel pellets relocated into the bottom head at time 220 min causes a boiloff of the remaining water in the reactor vessel. Bottom head dryout is predicted at time 263 min.

Figure 3.2.4 shows the hydrogen generation by metal-steam reaction in the core region. Approximately 23% of the clad, 10% of the channel box walls, and 1% of the control blade stainless steel are predicted to be oxidized during the in-vessel phase of the accident, producing approximately 1060 lb of hydrogen. This hydrogen does not accumulate within the reactor vessel, but is transferred into the wetwell via the open SRVs. Some additional hydrogen (approximately 25 lb) is generated by metal-water reactions instigated by the passage of steam through the bottom head debris bed during

the first 60 min after penetration failure. Hydrogen generation by this mechanism continues as long as water remains in the downcomer region of the reactor vessel. This water is boiled by radiative and conductive (through the vessel wall) heat transfer from the bottom head debris; since passage through the SRVs would require dislocation of the water occupying the lower 16 ft of the SRV tailpipes, the steam follows the path of least resistance and passes through the debris bed on its way out of the vessel.

A determination of the optimal timing for manual ADS actuation for the case in which the core is partially uncovered and no reactor vessel water injection systems are available should include a consideration of two issues. First, it is important to consider the temporary core cooling to be achieved by the ADS actuation. Secondly, the effect of the operation upon subsequent metal-water reactions after the core has reheated to runaway oxidation temperatures should also be considered.

Actuation of the ADS with the reactor vessel water level at either 71% (Ref. 10, EPG Revision 4) or 28% (EPG Revision 3) of core height will result in rapid core dryout and a drop in the reactor water level to below the core plate. There is, however, a significant difference in the amount of energy removed from the core in the two procedures. If Revision 4 procedures are followed, ADS actuation occurs when the core is relatively cool (i.e., when the highest clad temperatures are approximately 700°F). Thus, the quenching of the core structures removes only a relatively small amount of energy from the core.

Implementation of the Revision 3 procedures results in a delay in ADS actuation such that the maximum clad temperatures at the time of ADS initiation are much higher (approximately 1650°F), but still significantly below the temperature at which metal-steam oxidation reactions are a concern. Thus, the quenching of the core during this process removes significantly more energy than is removed via the Revision 4 approach. ORNL's analyses indicate that approximately 15 min are required for the clad temperatures to recover to the 1650°F range following the Revision 3 depressurization. Perhaps more importantly, the Revision 3 approach delays the onset of core degradation, debris relocation, and reactor vessel failure by 25-30 min relative to the timing of these events under Revision 4 procedures.

For the purposes of this calculation, the BWRSAR code input was modified as necessary to specify the formation of two eutectic mixtures discussed in Sect. 3.1. The integrated mass of material that has left the reactor vessel is shown as a function of time in Fig. 3.2.5. Although the initial bottom head penetration failure occurs at time 263 min,

the initial debris pour does not begin until time 270 min because of the time interval required for the metallic debris to heat to its assumed melting temperature of 2750°F. (The mass-averaged temperature of the release is shown in Fig. 3.2.6.) About 850,000 lb of debris is predicted to have left the vessel by the end of the calculation at time 900 min. This is equivalent to approximately 98% of the total original mass of bottom head debris. The composition of the released debris is provided in Table 3.5. The decay heat (proportional to the mass of UO_2) included in the released debris is shown in Fig. 3.2.7.

It should be noted that the BWRSAR code predicts that the portion of the reactor vessel bottom head beneath the point of attachment of the support skirt has been completely removed by time 483 min. (The removal is by the process of ablation of surrounding wall structure by the molten debris pouring through the failed bottom head penetration sites.) There are no specific models within BWRSAR to address this phenomenon since it is believed that the 340,000 lb of debris remaining within the vessel at this time would merely relocate downward approximately 3 ft onto the control rod drive housing support structure (see Fig. 3.2.8). The debris would continue to melt after relocation, with the molten portion flowing down onto the drywell floor in the same manner as if the portion of the bottom head surrounding the penetrations had remained intact. (This statement is true even if the debris were not held up by the housing support structure. The rate of release of molten material over the drywell floor is determined by the rate at which the debris melts, regardless of where the debris is located.) Within the BWRSAR code, heat transfer from the debris to the reactor vessel wall by convection and conduction is discontinued at the time that the debris is predicted to relocate onto the CRD housing support structure.

3.3 SEQUENCE WITH ADS ACTUATION AND BEST-ESTIMATE EUTECTICS

It is obviously desirable to consider the differences in the debris pours predicted by BWRSAR when the best-estimate (Parker) bottom head debris compositions are used, as opposed to the two-eutectic mixture compositions that drive the MELCOR calculations of containment response described in Chapter 8, and to attempt to determine if these differences are important. The two debris composition sets are compared in Table 3.6. The characteristics of the two resulting debris pours are compared in Tables 3.7 and 3.8 and in Figs. 3.3.1-3.3.4. The calculated results are identical through the time of initial

reactor vessel bottom head penetration failure, which is predicted to occur at 263 min after scram.

As indicated in Table 3.7, the best-estimate debris pours precede the two-eutectic debris pours during both the early metallic melting period (263-275 min) and the early oxidic melting period (345-385 min). There is, however, no significant difference in the debris masses accumulated on the drywell floor during the other periods of the pour calculation.

The differences in the rates of debris pour from the reactor vessel are shown in Table 3.8. The pour rates for the unoxidized zirconium metal are of special significance, since this metal will be oxidized on the drywell floor. (The zirconium metal pours are listed separately, but are also included in the adjacent "Metals" column.) The oxidation of zirconium releases large amounts of energy and increases the temperature of the debris.

As expected, the best-estimate eutectic representation of the lower-head debris results in a broader (and more finely structured) spectrum of pours from the reactor vessel. The zirconium metal, UO_2, and total debris pours are shown in Figs. 3.3.1-3.3.3 for both sets of debris compositions. The mass-averaged temperatures of the pours are compared in Fig. 3.3.4.

A satisfactory assessment of the impact of the different debris pours could only be obtained by performing the associated MELCOR containment response calculations for both sets of pours. For the reasons discussed previously, the MELCOR calculation for the best-estimate case cannot be run until improvements are implemented into the CORCON module. Nevertheless, it does seem probable that any significant difference in the predicted containment response would be limited to the 2 h period after initial penetration failure when the major metallic pours occur and the oxidic pours are being initiated. During this period, the best-estimate debris pours are more rapid and, thereby, provide a more severe containment loading. However, the total released masses are not sufficient to threaten the Mark II containment integrity. (These differences in initial debris pour characteristics would be of much more significance in the smaller Mark I containments.) As indicated in Figs. 3.3.3 and 3.3.4, differences in the overall characteristics of the two debris pour spectrums are small after 390 min into the accident sequence.

3.4 SEQUENCE WITH SIMPLIFIED EUTECTICS AND NO ADS ACTUATION

If the reactor vessel is not depressurized, liquid water will remain in the lower core region during the early portion of the core degradation phase of the short-term station blackout accident sequence. The result of a failure to actuate ADS is a much more extensive metal-water reaction within the core region and an accelerated core degradation rate.

The calculated sequence of events for short-term station blackout without ADS is provided in Table 3.9. For consistency with the assumption that the ADS is either not available or not actuated by the operators, the code input deck for this calculation had no provision for manual SRV actuation of any kind, including operator control of vessel pressure during the early part of the accident sequence. As indicated by a comparison of Tables 3.9 and 3.4, the absence of operator pressure control causes a one-minute delay in the calculated time of uncovering of the top of the core. This is not significant.

Plots of key parameters, as predicted by BWRSAR for this scenario, are shown in Figs. 3.4.1-3.4.10. These plots represent events from 35 min after the inception of the accident sequence, when the BWRSAR calculation is initiated, to time 250 min, which is approximately 4 min after the predicted initial failure of reactor vessel bottom head penetrations and onset of debris pours onto the drywell floor. As indicated in Fig. 3.4.1, the calculated vessel pressure decreases significantly after core plate dryout. This occurs because steam generation ceases within the core region while steam leakage and heat transfer from the vessel to the drywell atmosphere continue. Subsequently, the vessel pressure is restored to the range of the safety/relief valve setpoints after local core plate failures introduce core debris into the water in the lower plenum and restore in-vessel steam generation. The associated SRV flows are shown in Fig. 3.4.3.

The predicted swollen reactor vessel water level for the case without ADS is shown in Fig. 3.4.2. The decreasing water level initially traces a smooth curve through the core region, punctuated by spikes at each SRV actuation. After the onset of downward material relocation and quenching, the rate of level decrease is accelerated and proceeds in a more steplike fashion. Core plate dryout occurs with the water level just below the core plate (rather than several feet below, as in the case with ADS actuation). Water again enters the core region after core plate failure as a result of displacement of water in the lower plenum by the falling debris from the central region of the core. The

decay heat associated with the fuel pellet stack collapse at time 164 min causes a rapid boiloff of the remaining water and bottom head dryout occurs at time 194 min.

Figure 3.4.4 shows the total hydrogen generated in the core region as a function of time. Approximately 53% of the clad, 12% of the channel box walls, and 1% of the control blade stainless steel are predicted to be oxidized in the core region during the accident sequence, producing approximately 2210 lb of hydrogen. Comparison with Fig. 3.2.4 reveals that this is slightly more than twice the hydrogen produced in the core region during the accident sequence with ADS actuation. As indicated previously, the primary reason for this great increase in calculated hydrogen generation during core degradation is the presence of liquid water in the lower portion of the core region when large portions of the core have exceeded the runaway zirconium oxidation temperature. Steam generation by the submerged portion of the core and by quenching of the relocating debris then provides a steam-rich atmosphere (rather than the steam-starved atmosphere in the case with ADS actuation) to fuel the metal-water reactions in the core region. The additional hydrogen (approximately 2200 lb) is predicted to be generated by the passage of steam through the debris bed during the period of reactor vessel blowdown. (It is emphasized that this hydrogen generated within the bottom head debris bed is in addition to the approximately 2210 lb of hydrogen predicted to be generated in the core region.) The uncertainties associated with this BWRSAR calculation are large, but it is obvious that much more metal-water reaction would occur within the bottom head debris bed if the vessel were pressurized at the time of penetration failure than if it were not.

Based upon the two-eutectic-mixture approach described in Sect. 3.1, characteristics of the reactor vessel debris flows as calculated by the BWRSAR code for the case without ADS actuation are shown in Figs. 3.4.5-3.4.10. The large energy release associated with the blowdown of steam through the bottom head debris bed and the associated metal-water reactions is manifested by the very large initial pours of molten metals. Subsequent to the effects of the vessel blowdown, the releases of additional molten materials onto the drywell floor are controlled simply by decay heat and the melting temperatures of the component mixtures.

The composition of the debris that has been released from the reactor vessel by the end of the BWRSAR calculation at time 900 min is provided in Table 3.10. Comparison with the similar information for the case with ADS actuation provided in Table 3.5 shows that significantly less debris is predicted to have left the vessel at time

900 min for the case without ADS actuation. The reason for this can be discerned by noting the large difference in predicted zirconium metal release. The pressurized blowdown of steam through the bottom head debris bed for the case without ADS actuation converts much of the zirconium metal to ZrO_2 within the bed. Since the ZrO_2 is modeled to melt with the other oxides at 4800°F, whereas the zirconium metal melts with the metals at 2750°F, it will take longer (for the same decay heat rate) for the ZrO_2 to melt and pour from the vessel. The BWRSAR calculation predicts that 102,000 lb of ZrO_2 remains in the vessel at 900 min into the accident for the case without ADS.

Table 3.1. BWRSAR calculational methodology employed to represent events between onset of core degradation and pour of molten materials from reactor vessel for BWRs

1. As canister and control blade material becomes molten, it is relocated onto the core plate. This causes:

   a. a temporarily increased steaming rate,
   b. core plate dryout and cessation of steaming, and
   c. buildup of mass on the core plate and core plate heatup.

2. Each radial region of the core plate fails due to loss of strength when its calculated temperature reaches a user-specified value. Each core plate region and its accumulated debris falls into the lower plenum, producing a burst of steam and lowering the water level there as the fallen material is quenched.

3. Molten Zr metal flows downward over the lower core fuel rod nodes, leaving the UO_2 fuel pellets encased in thin ZrO_2 sheaths. Steam rising from the lower plenum cools the core nodes from which all unoxidized Zr has been removed. On the other hand, the rising steam causes energy release in the core peripheral nodes where Zr metal at elevated temperature still remains.

4. The standing portions of the core fall into the lower plenum by radial column. Each core column collapses when its average clad temperature reaches a user-input value, at which time very little of the UO_2 mass in the region has become molten. (The actual failure mechanism is weakening, by overtemperature, of the ZrO_2 sheaths surrounding the UO_2 fuel pellets.) The falling mass is quenched by the water in the lower plenum until the time of bottom head dryout. After bottom head dryout, the debris begins to reheat.

5. The structure of the control rod guide tubes in the lower plenum is heated by the surrounding core debris and is weakened to the point of failure when its temperature reaches a user-specified value. Failure of the control rod guide tubes causes all remaining standing portions of the core to immediately collapse. The control rod guide tube mass is added to the bottom head debris.

6. Bottom head penetrations fail by a simulated creep-rupture mechanism as the debris mass in their vicinity reaches about 2100°F. The reactor vessel depressurizes and equalizes with drywell pressure. When standing molten metal pools develop within debris nodes remote from the vessel wall, leakage pathways are opened through the wall via the instrument guide tubes.

7. The individual components of the debris mass leave the vessel in the order that they reach their melting points and become liquid. Solid metallic material surrounding the lower portion of the original instrument guide tube locations is ablated into the molten material flowing from the reactor vessel via these pathways.

Table 3.2. Best-estimate BWR bottom head debris compositions

Component	Composition	Melting Temperature (°F)
Eutectic 1	Zr - Fe - Cr	2642
Eutectic 2	Fe - Cr - Ni	2660
Eutectic 3	Zr - Fe - Ni	2912
Remaining Metals	Zr/Fe/Cr/Ni	2920
Eutectic 4	ZrO_2 - UO_2	4172
Remaining Non-fuel Oxides	FeO/Fe_3O_4 NiO/B_4C	4172
Fuel Pellets	UO_2	4800

Table 3.3 Initial conditions calculated by BWR-LTAS and employed as initial conditions in the BWRSAR analyses

Parameter	Value
Time (min)	35
Reactor Vessel Water Level (in.)	378.7
Reactor Vessel Pressure (psia)	997.9
Reactor Downcomer Water Temperature (°F)	521.4
Reactor Vessel Lower Plenum Water Temperature (°F)	527.0
Core Region Water Temperature (°F)	544.2

Table 3.4. Calculated sequence of events for BWR Mark II short-term station blackout with ADS actuation (with simplified eutectics)

Event	Time (min)
Station blackout-initiated scram from 100% power. Independent loss of the steam turbine-driven HPCI and RCIC injection systems.	0.0
Swollen water level falls below top of core	37.2
Open one SRV	78.0
ADS system actuation	79.5
Core plate dryout	81.2
Relocation of core debris begins	124.1
First local core plate failure	129.2
Collapse of fuel pellet stacks in central core	220.0
Reactor vessel bottom head dryout; structural support by control rod guide tubes fails; remainder of core falls into reactor vessel bottom head	263.2
Initial failure of bottom head penetrations	263.3

Table 3.5. Composition of the debris released from the reactor vessel by the end of the BWR Mark II calculation with ADS (with simplified eutectics)

Constituents	Integrated mass (lb)
Metals	
Zr	113,869
Fe	283,737
Cr	47,702
Ni	21,218
B_4C	768
Subtotal (metals)	467,294
Oxides	
ZrO_2	33,565
FeO	96
Fe_3O_4	184
Cr_2O_3	74
NiO	11
B_2O_3	39
UO_2	347,379
Subtotal (oxides)	381,348
Grand Total	848,642

Table 3.6. Bottom head debris composition sets utilized in the two BWRSAR calculations

The Two-Eutectic Mixture		The Best-Estimate (Parker) Eutectics	
Component	Melting Temperature (°F)	Component	Melting Temperature (°F)
All metals	2750	Zr-Fe-Cr	2642
		Fe-Cr-Ni	2660
		Zr-Fe-Ni	2912
		Remaining metals	2920
All oxides	4800	ZrO_2-UO_2	4172
		Remaining non-fuel oxides	4172
		Fuel pellets	4800

Table 3.7. Integrated masses (lb) of debris expelled from the reactor vessel for the two sets of debris compositions

Time[a] (min)	The Two-Eutectic Mixture			The Best-Estimate (Parker) Eutectics		
	Zr	Metals	Oxides	Zr	Metals	Oxides
265	0	0	0	926	3279	0
275	3499	11482	0	7871	27736	0
285	12610	41383	0	13055	45993	0
345	40108	80928	0	41036	82319	3606
365	40108	80928	0	50741	107475	31538
385	45792	95236	14782	53778	115726	35899
405	84273	192090	82745	85266	195405	79657
885	113869	466323	380184	113518	469493	384959

[a]The initial bottom head penetration failure occurs at 263 min after scram.

Table 3.8. Debris pour rates (lb/min) for the two sets of debris compositions

Period (min)[a]	The Two-Eutectic Mixture			The Best-Estimate (Parker) Eutectics		
	Zr	Metals	Oxides	Zr	Metals	Oxides
263-265	0	0	0	463	1640	0
265-275	350	1148	0	695	2446	0
275-285	911	2990	0	518	1826	0
285-305	1375	1977	0	1399	1816	180
305-325	0	0	0	0	0	0
325-345	0	0	0	0	0	0
345-365	0	0	485	1258	1397	
365-385	284	715	739	152	413	218
385-405	1924	4843	3398	1574	3984	2188
405-425	1221	3371	1767	1157	3479	2243

[a]The initial bottom head penetration failure occurs at 263 min after scram.

Table 3.9. Calculated sequence of events for BWR Mark II short-term station blackout without ADS actuation

Event	Time (min)
Station blackout-initiated scram from 100% power. Independent loss of the steam turbine-driven HPCI and RCIC injection systems.	0.0
Swollen water level falls below top of core	38.2
Relocation of core debris begins	90.6
Core plate dryout	135.3
First local core plate failure	155.8
Collapse of fuel pellet stacks in central core	163.8
Reactor vessel bottom head dryout; structural support by control rod guide tubes fails; remainder of core falls into reactor vessel bottom head bottom head	193.8
Initial failure of bottom head penetrations	246.1
Pour of molten debris from reactor vessel begins	246.5

Note: The bottom head debris is modeled to separate into a mixture of metals melting at 2750°F and a mixture of oxides melting at 4800°F (simplified eutectics).

Table 3.10. Composition of the debris released from the reactor vessel by the end of the calculation without ADS

Constituents	Integrated Mass (lb)
Metals	
Zr	38,045
Fe	263,391
Cr	49,062
Ni	21,825
B_4C	189
Subtotal (metals)	372,512
Oxides	
ZrO_2	37,217
FeO	25
Fe_3O_4	44
Cr_2O_3	18
NiO	2
B_2O_3	8
UO_2	326,073
Subtotal (oxides)	363,387
Total	735,899

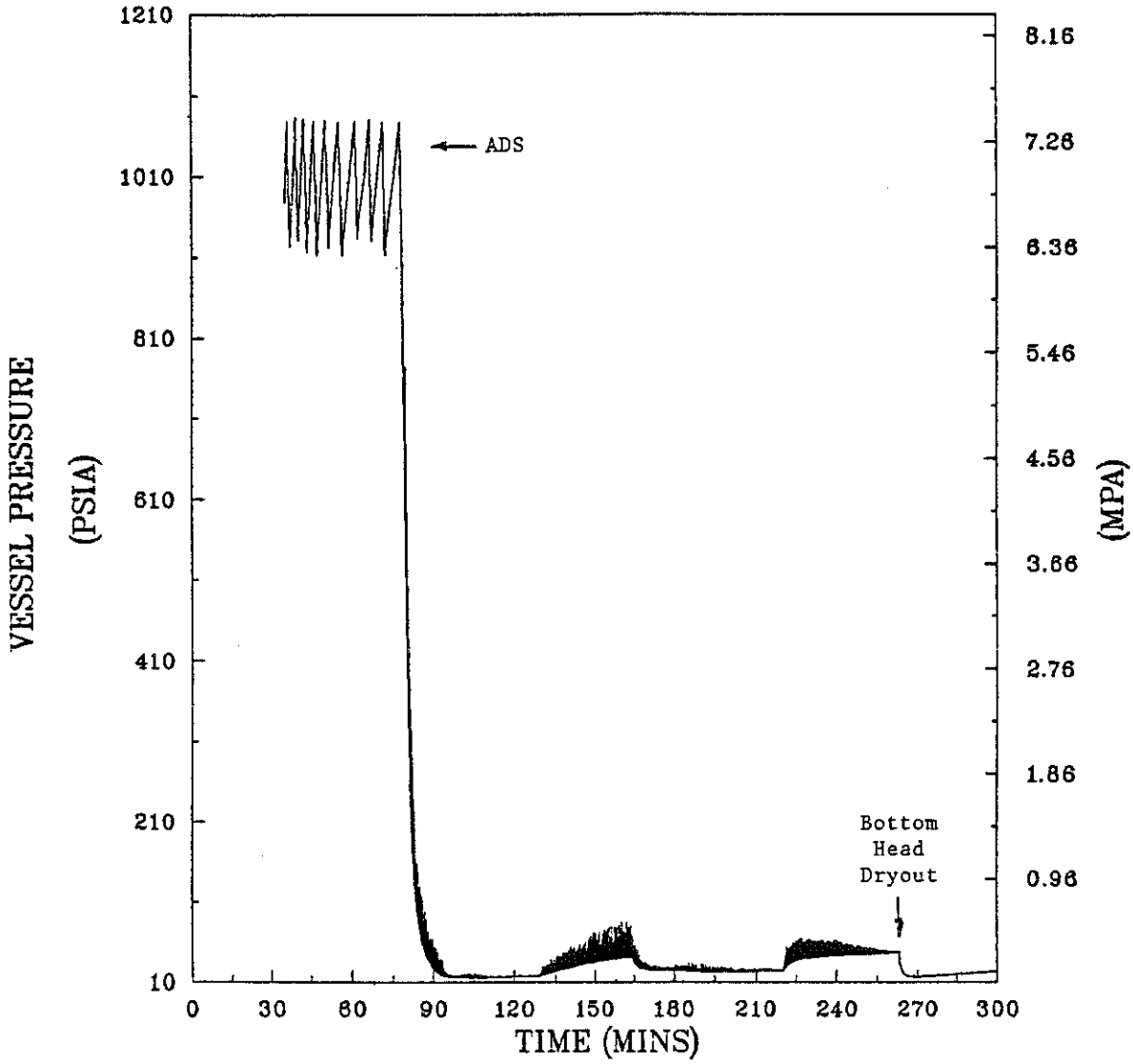

Fig. 3.2.1. Reactor vessel pressure for BWR-4/Mark II short-term station blackout sequence with ADS (simple eutectics).

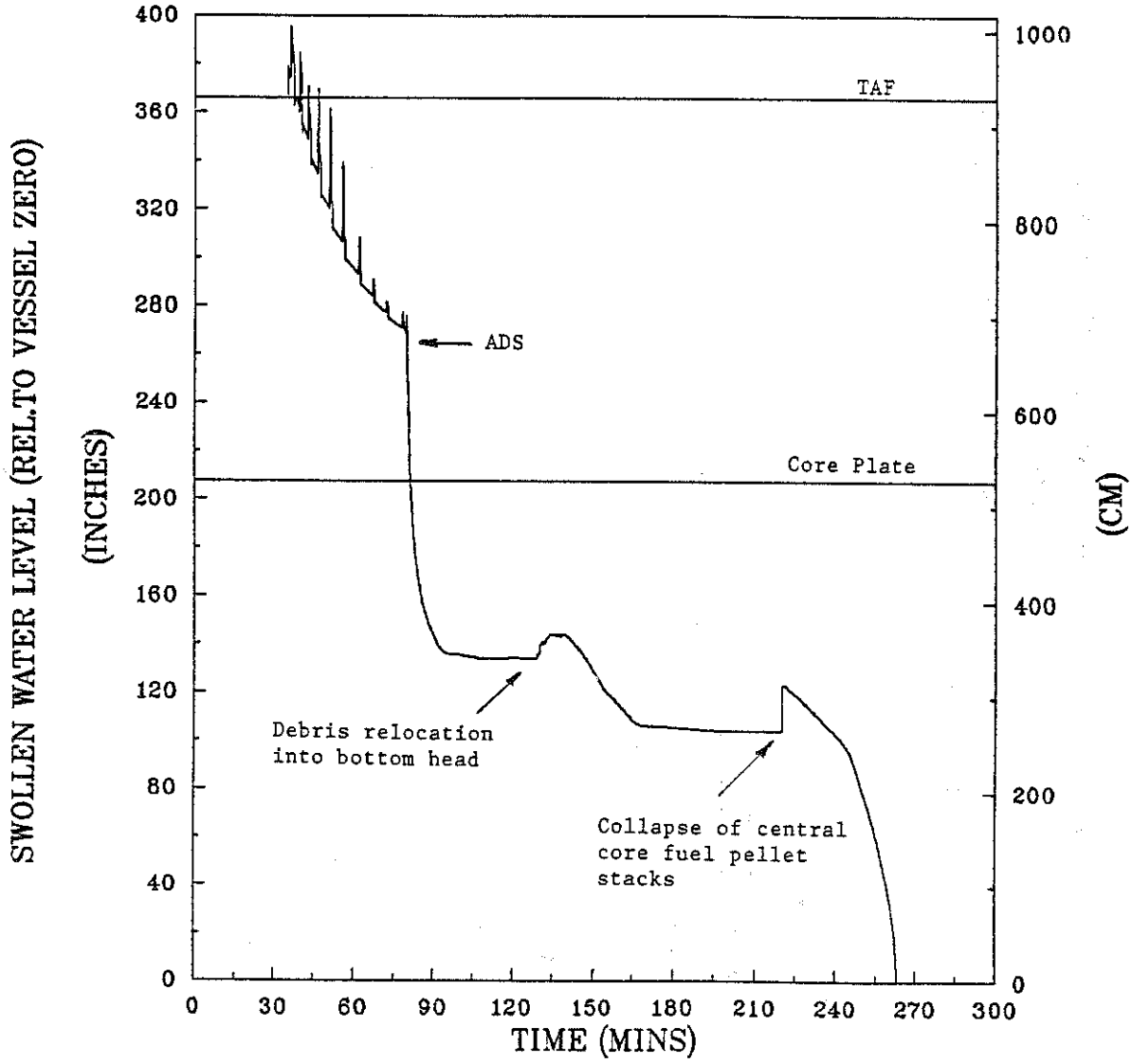

Fig. 3.2.2. Swollen reactor vessel water level for BWR-4/Mark II short-term station blackout accident sequence with ADS (simple eutectics).

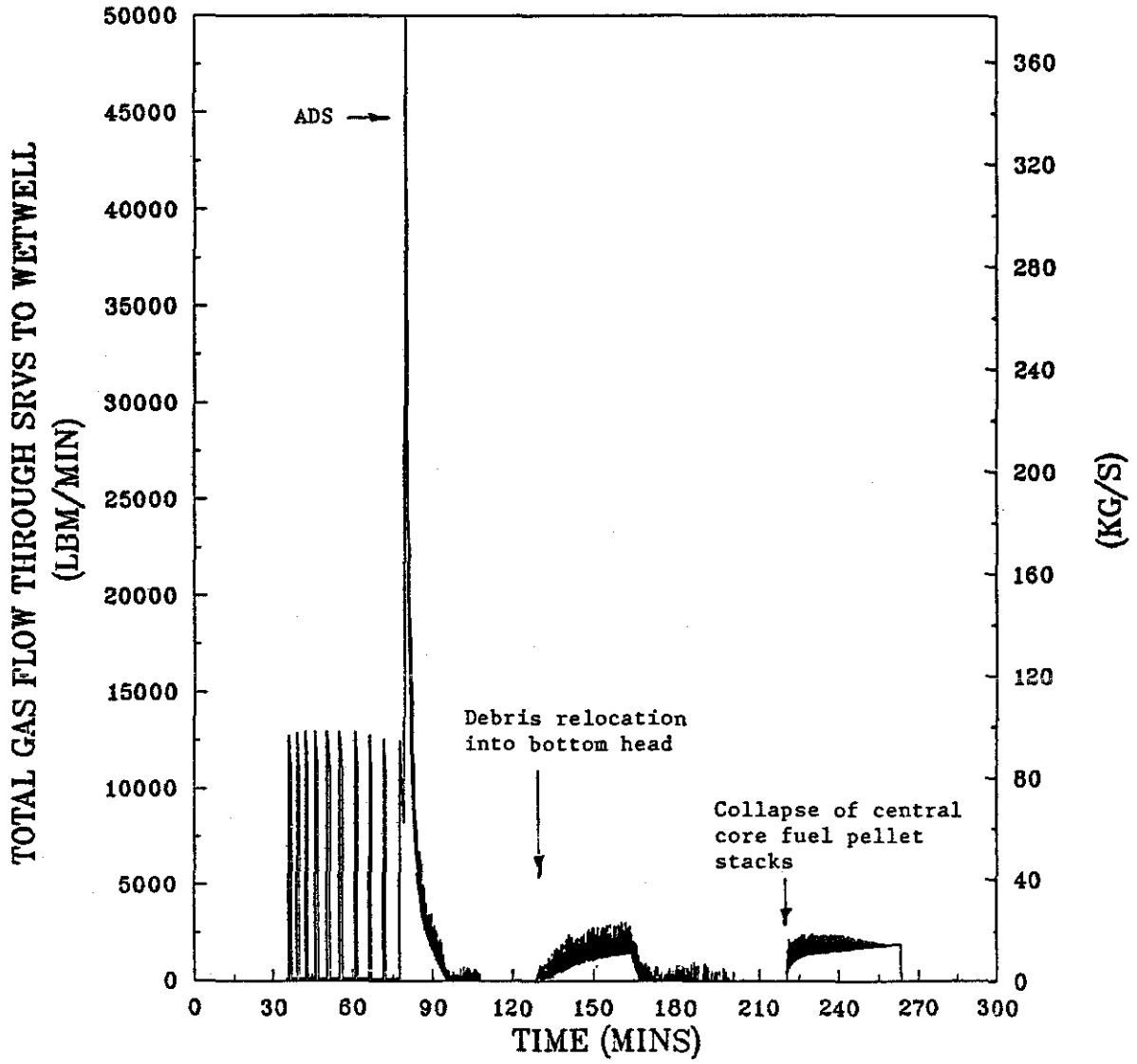

Fig. 3.2.3 Total SRV gas flow for BWR-4/Mark II short-term station blackout accident sequence with ADS (simple eutectics).

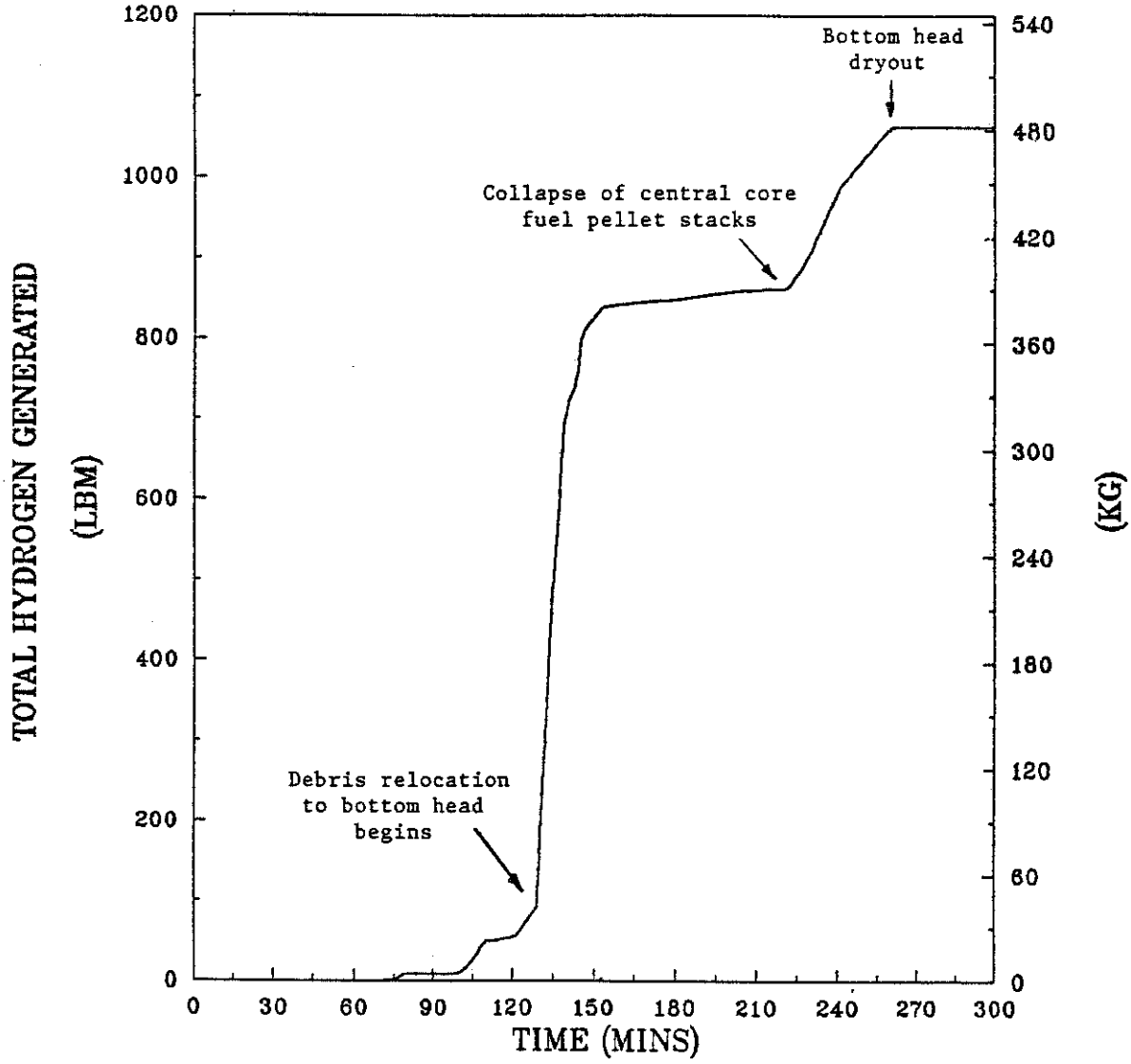

Fig. 3.2.4. Total hydrogen generated in-vessel for BWR-4/Mark II short-term station blackout sequence with ADS (simple eutectics).

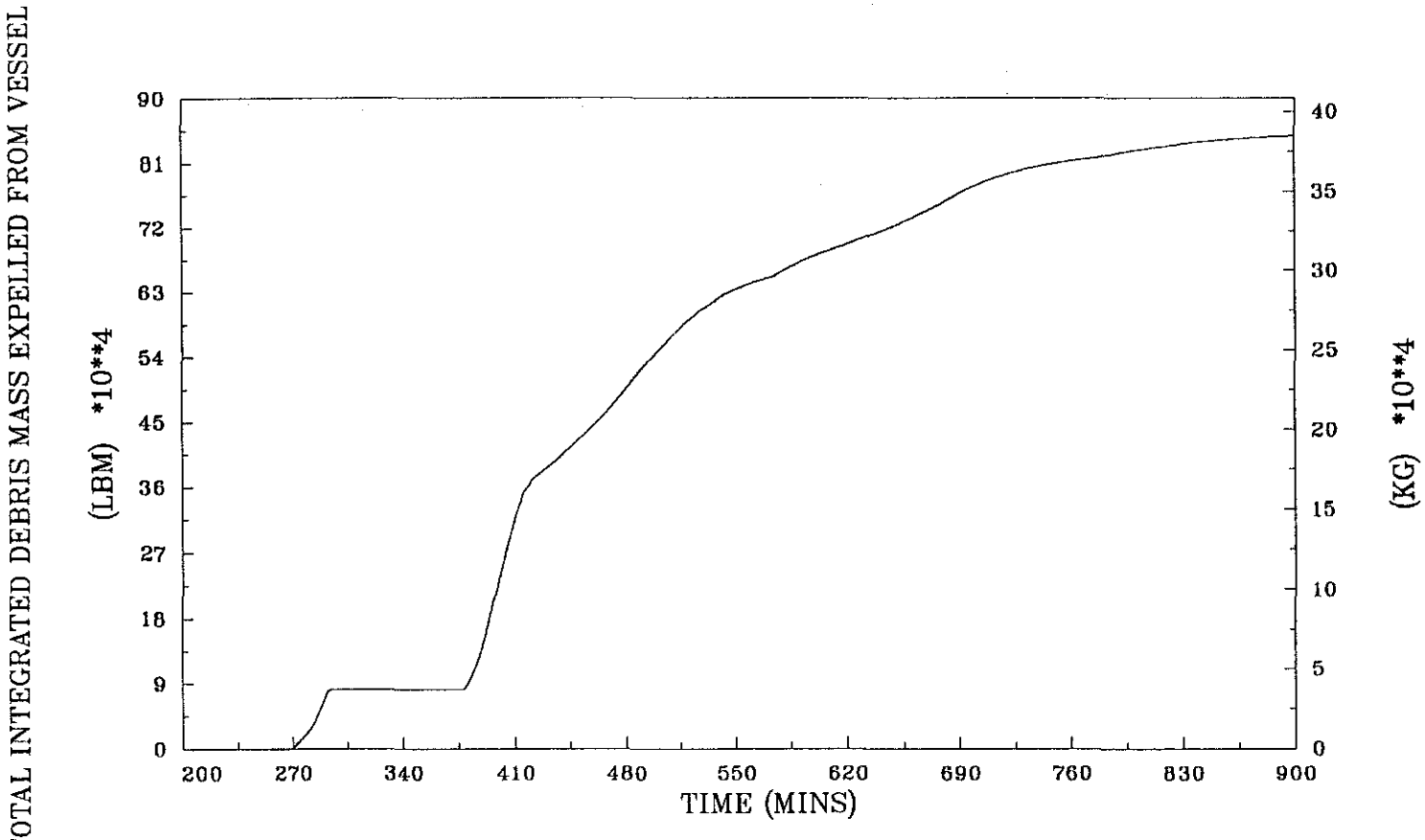

Fig. 3.2.5. Integrated debris mass expelled from reactor vessel for BWR-4/ Mark II short-term station blackout sequence with ADS (simple eutectics).

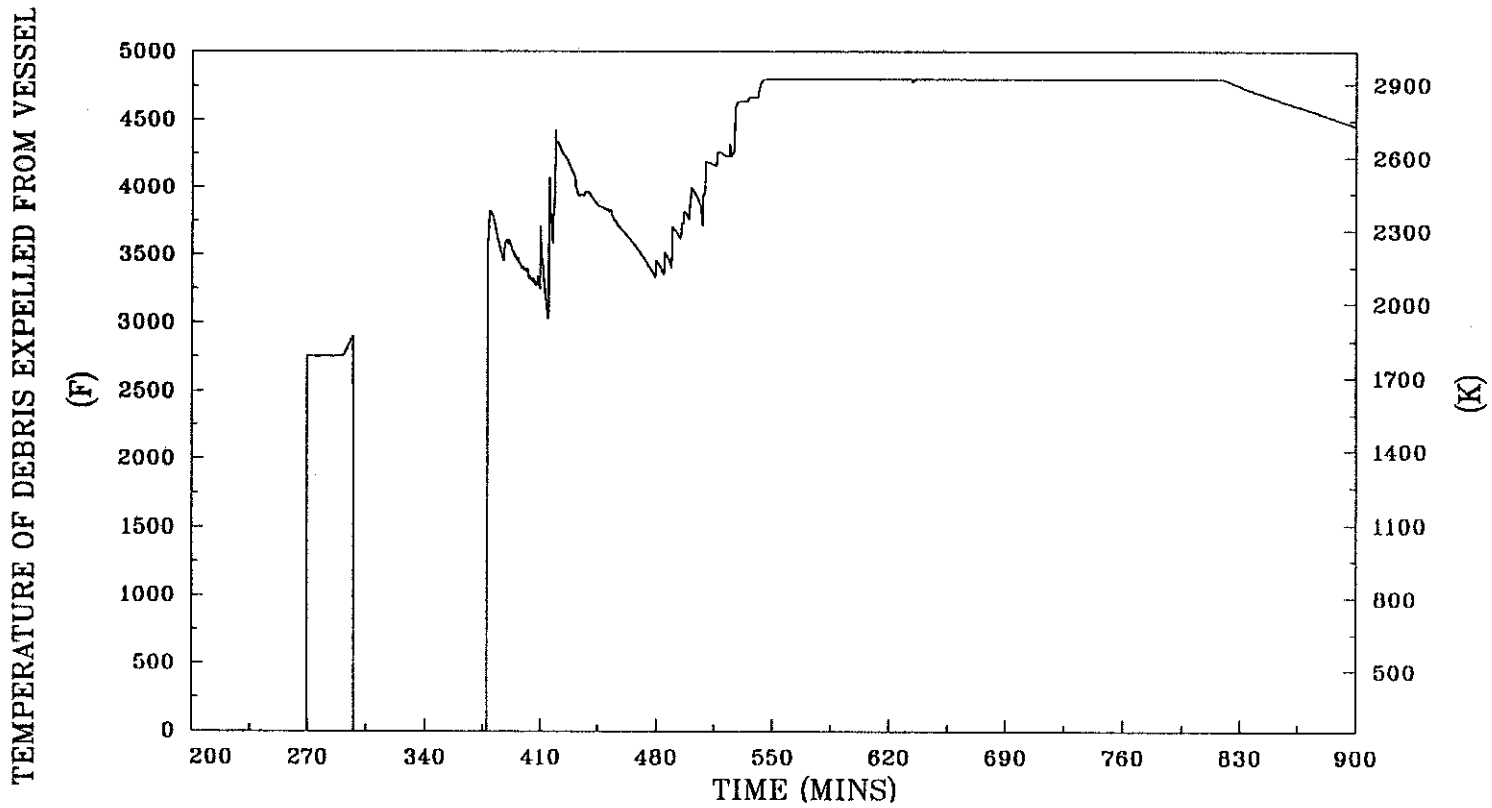

Fig. 3.2.6. Mass-averaged debris pour temperature for BWR-4/Mark II short-term station blackout sequence with ADS (simple eutectics).

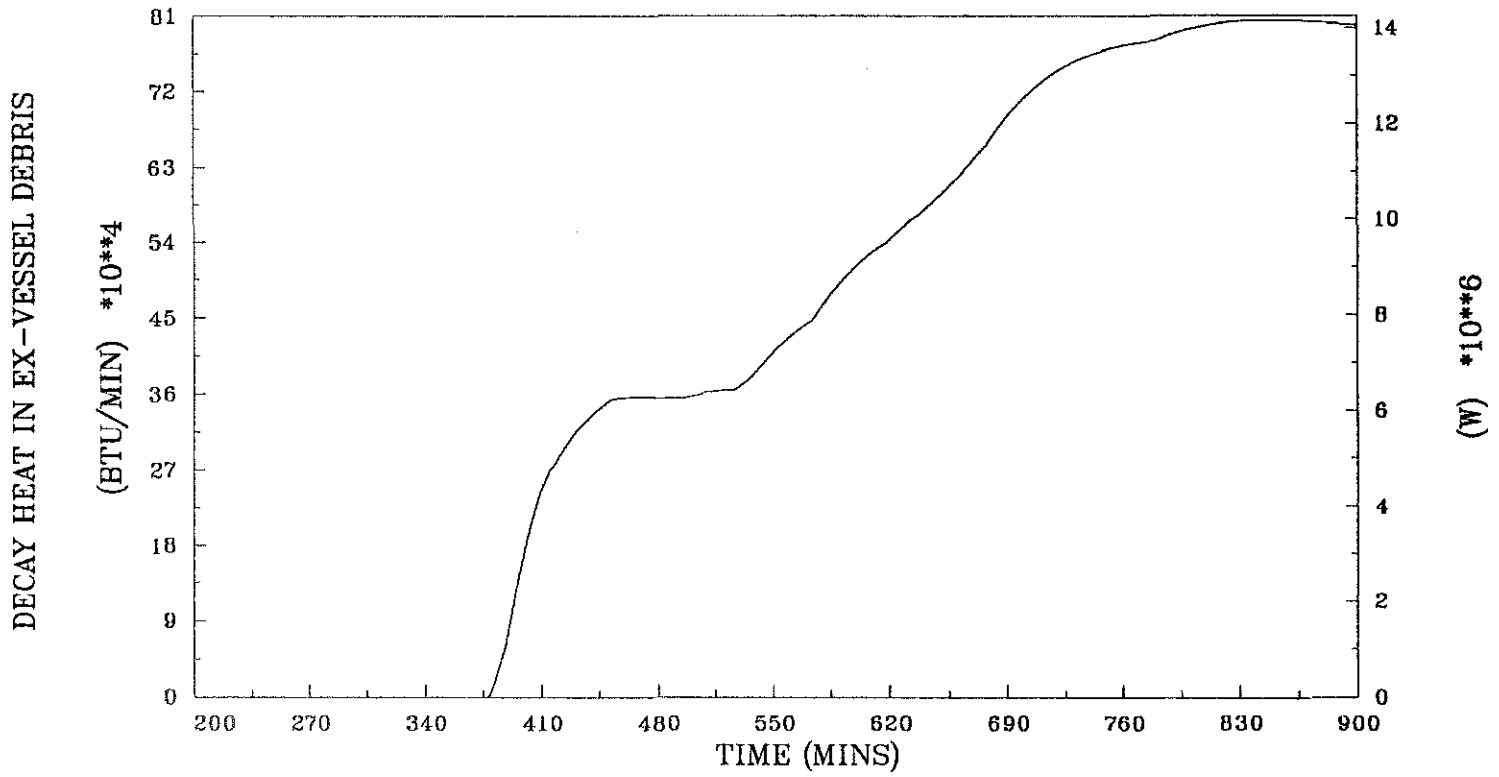

Fig. 3.2.7. Decay power in ex-vessel debris for BWR-4/Mark II short-term station blackout sequence with ADS (simple eutectics).

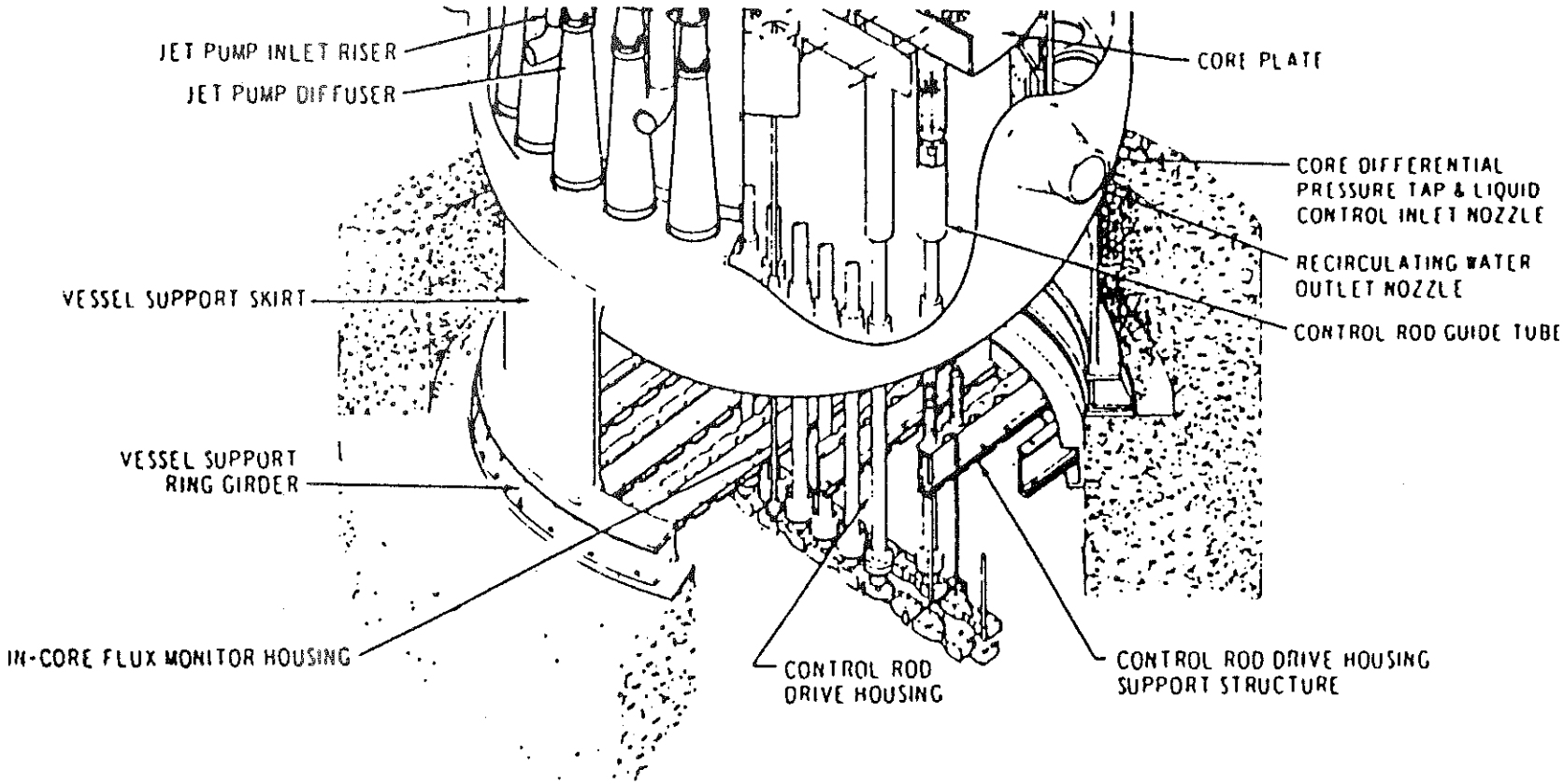

Fig. 3.2.8. Downward movement of separated portions of the bottom head beneath the skirt would be limited to about 34 inches by the CRD housing support structure.

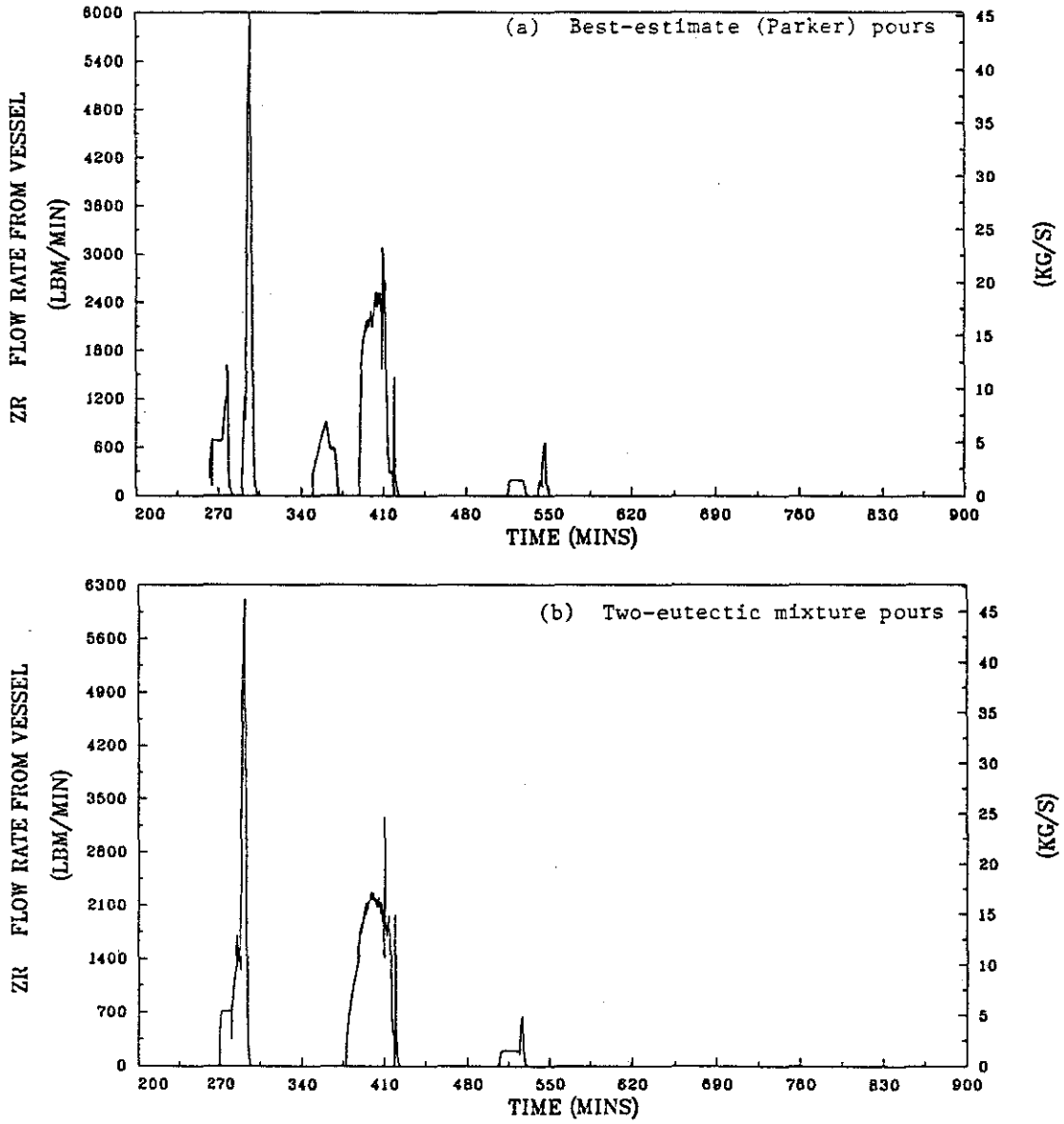

Fig. 3.3.1. Zirconium metal pours from the reactor vessel for the short-term station blackout sequence with ADS actuation.

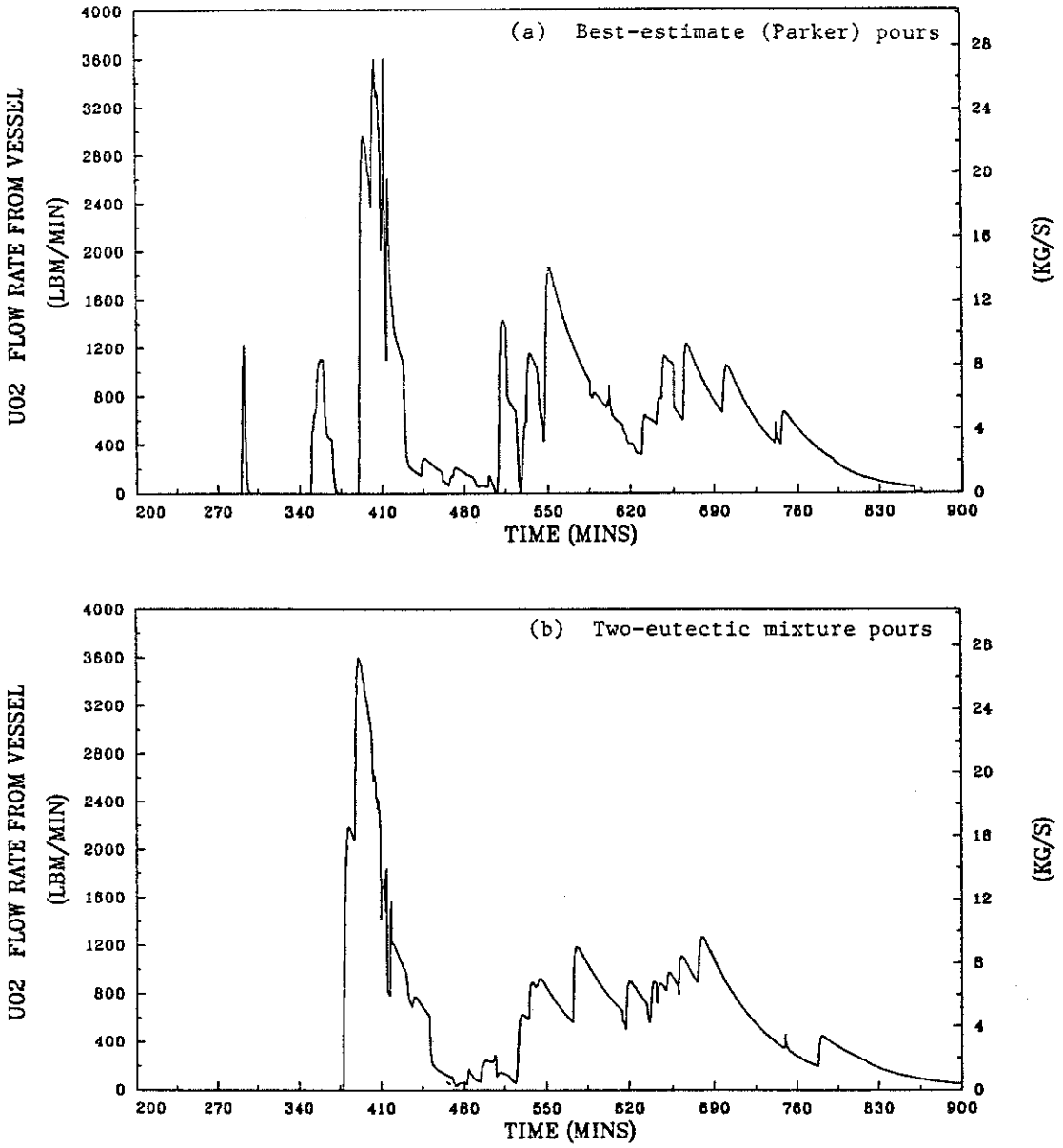

Fig. 3.3.2. Uranium dioxide pours from the reactor vessel for the short-term station blackout sequence with ADS actuation.

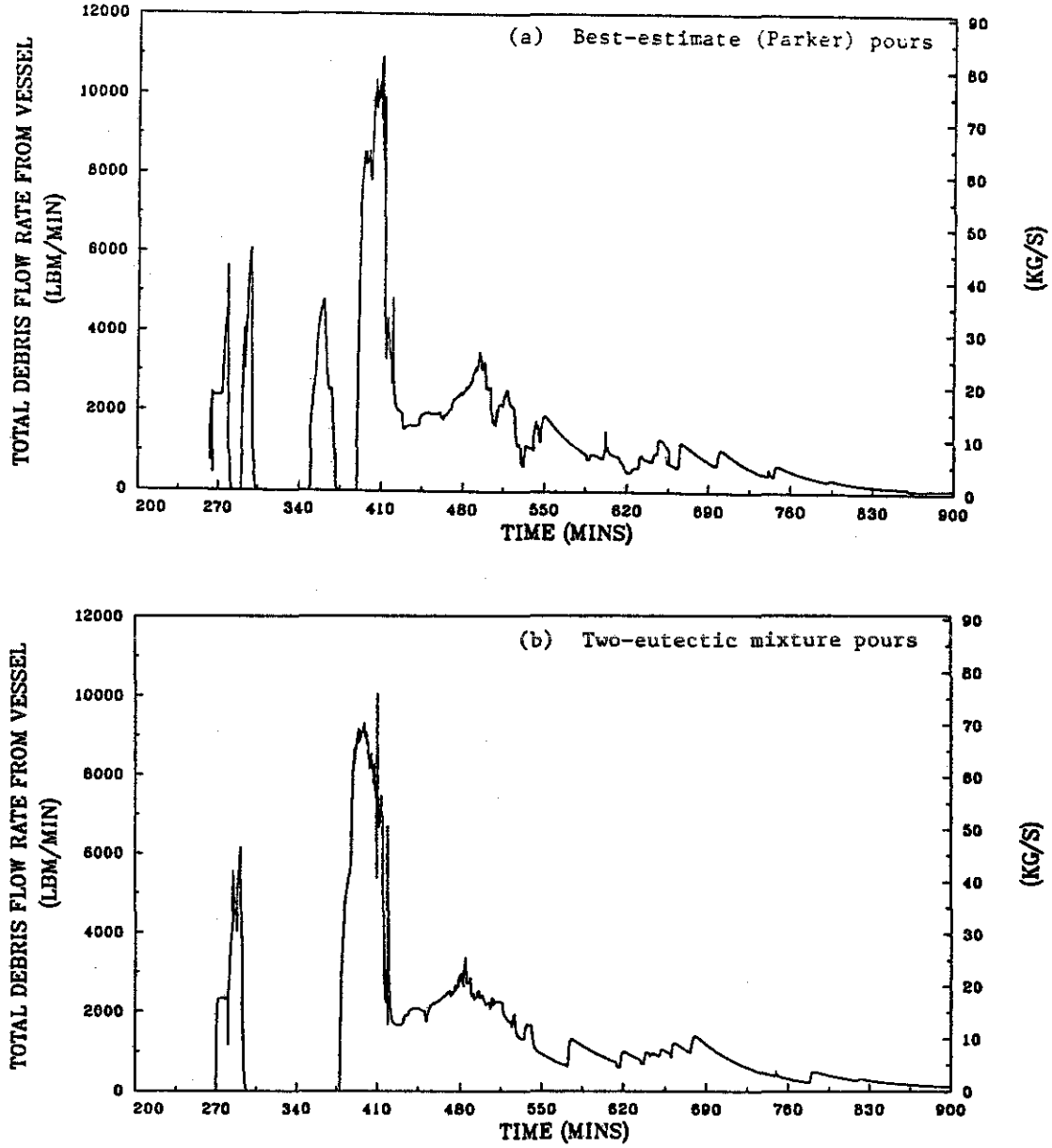

Fig. 3.3.3. Total debris pours from the reactor vessel for the short-term station blackout sequence with ADS actuation.

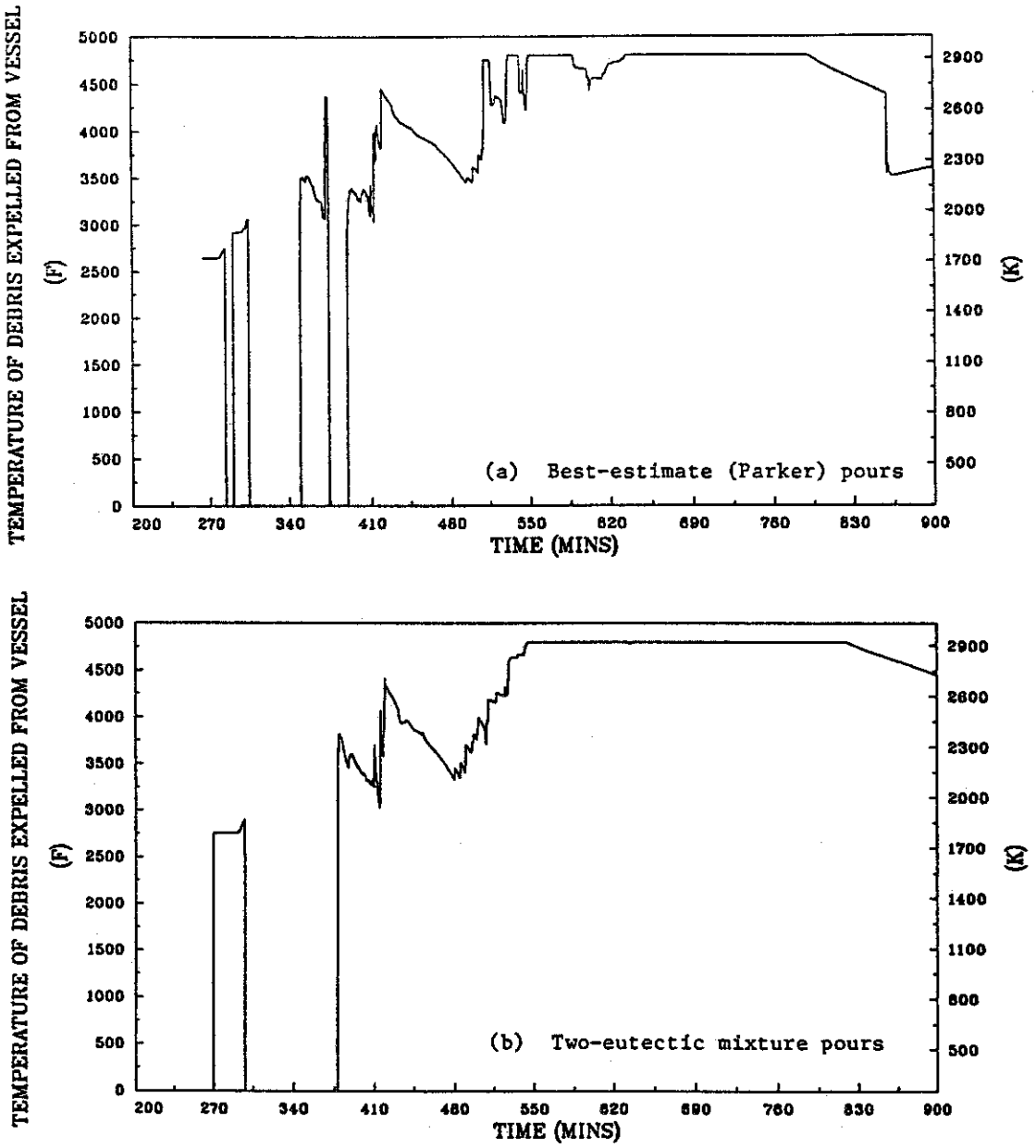

Fig. 3.3.4. Mass-averaged temperature of the debris pours from the reactor vessel for the short-term station blackout sequence with ADS actuation.

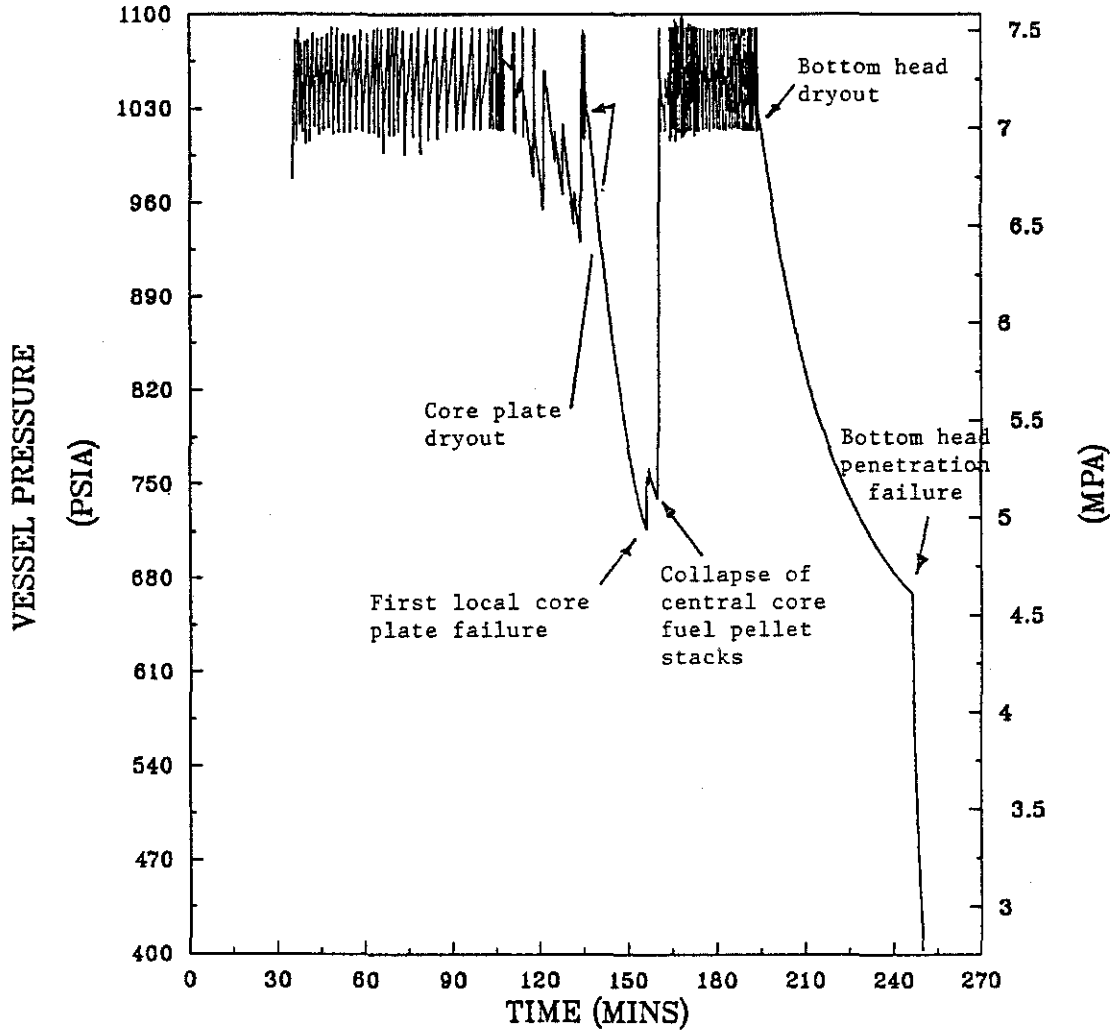

Fig. 3.4.1. Reactor vessel pressure for BWR-4/Mark II short-term station blackout sequence without ADS (simple eutectics).

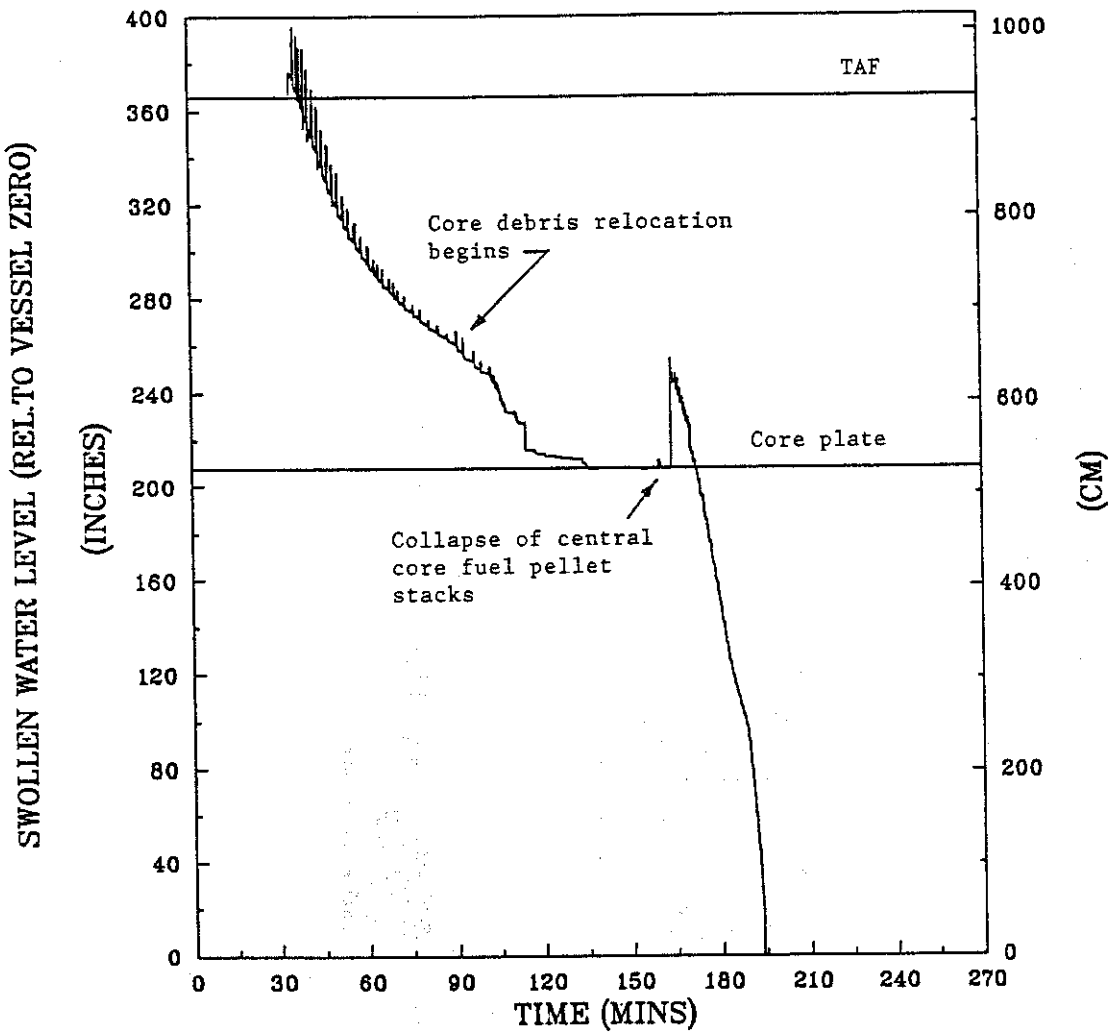

Fig. 3.4.2. Swollen reactor vessel water level for BWR-4/Mark II short-term station blackout sequence without ADS (simple eutectics).

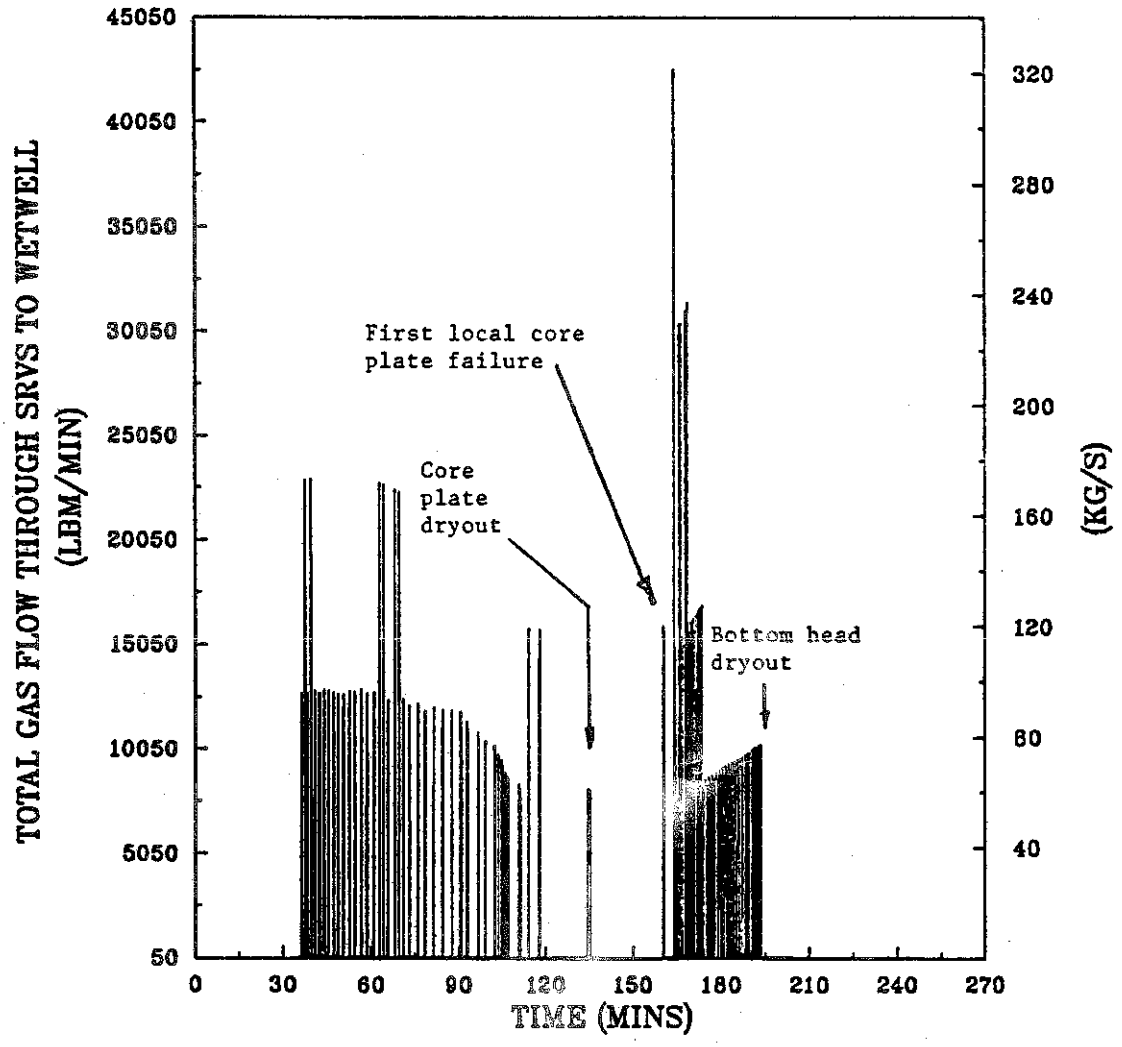

Fig. 3.4.3. Total SRV gas flow for BWR-4/Mark II short-term station blackout sequence without ADS (simple eutectics).

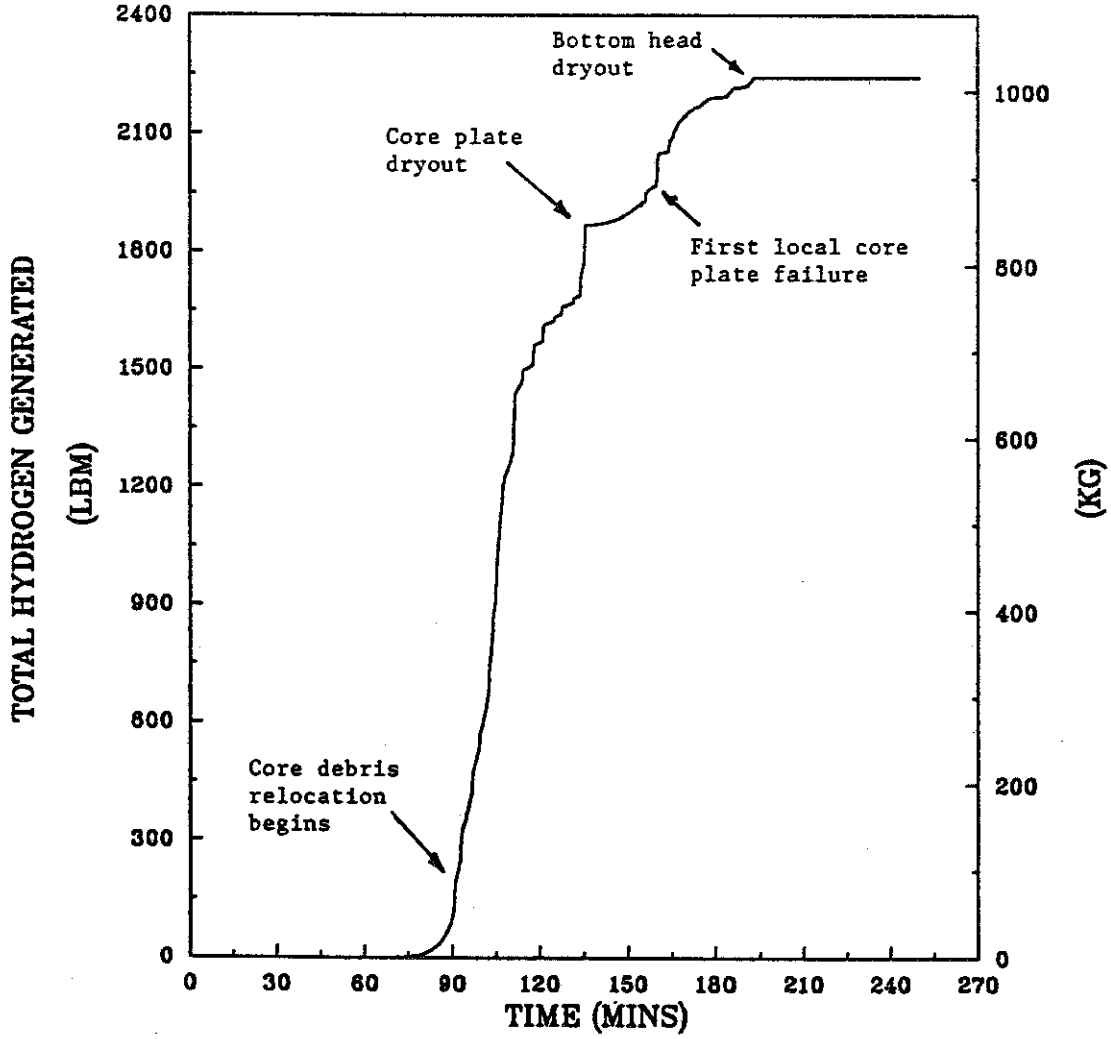

Fig. 3.4.4. Total hydrogen generated in-vessel for BWR-4/Mark II short-term station blackout sequence without ADS (simple eutectics).

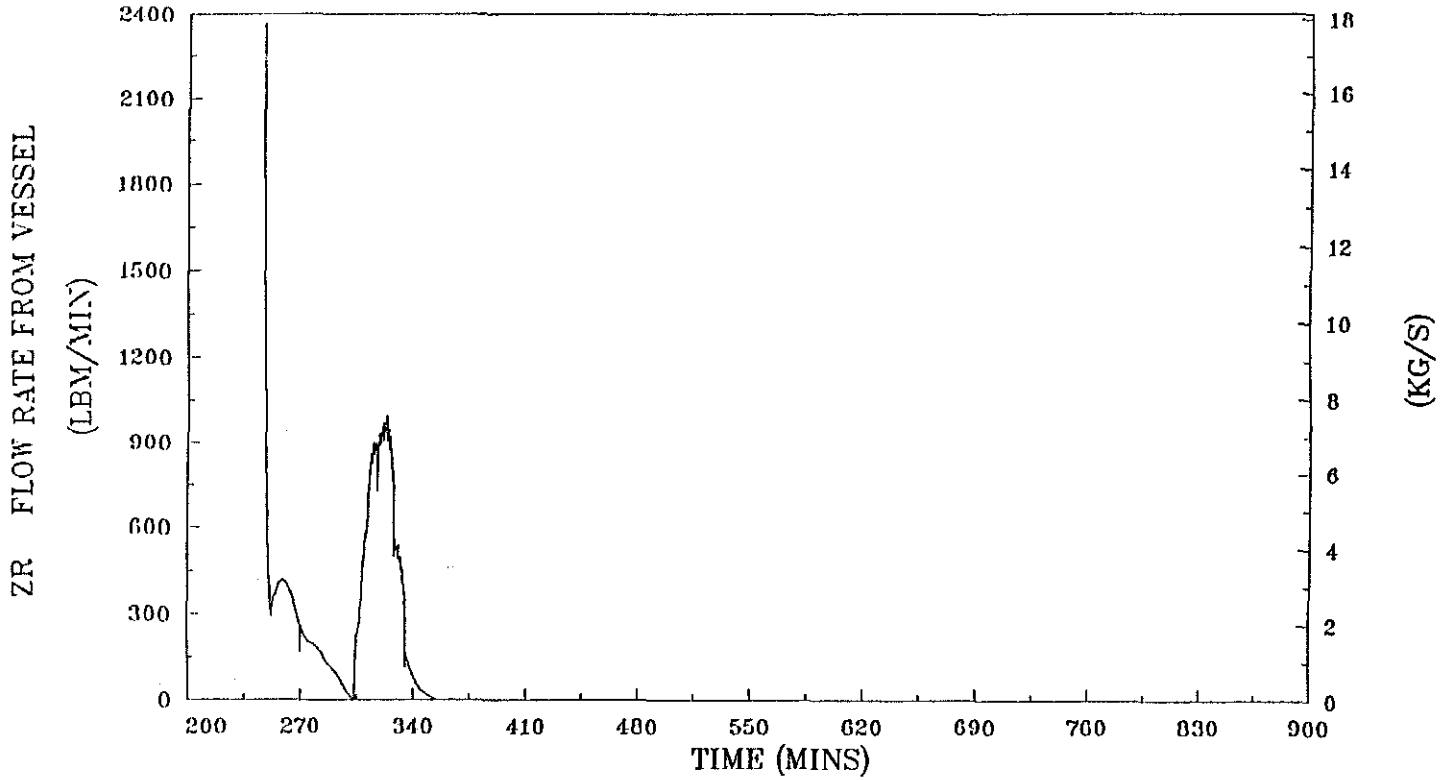

Fig. 3.4.5. Zirconium metal pours from the reactor vessel for BWR-4/Mark II short-term station blackout sequence without ADS (simple eutectics).

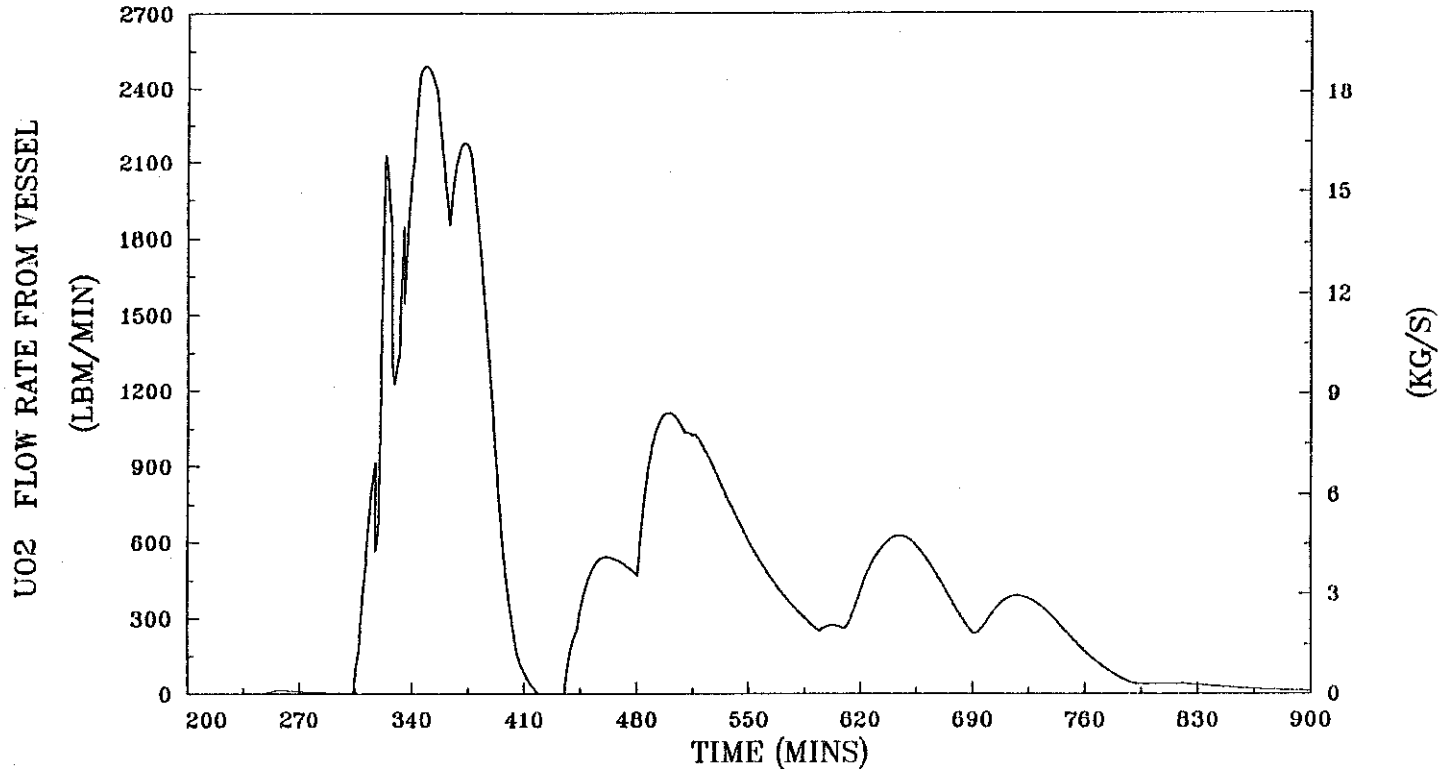

Fig. 3.4.6. Uranium dioxide pours from the reactor vessel for BWR-4/Mark II short-term station blackout sequence with ADS (simple eutectics).

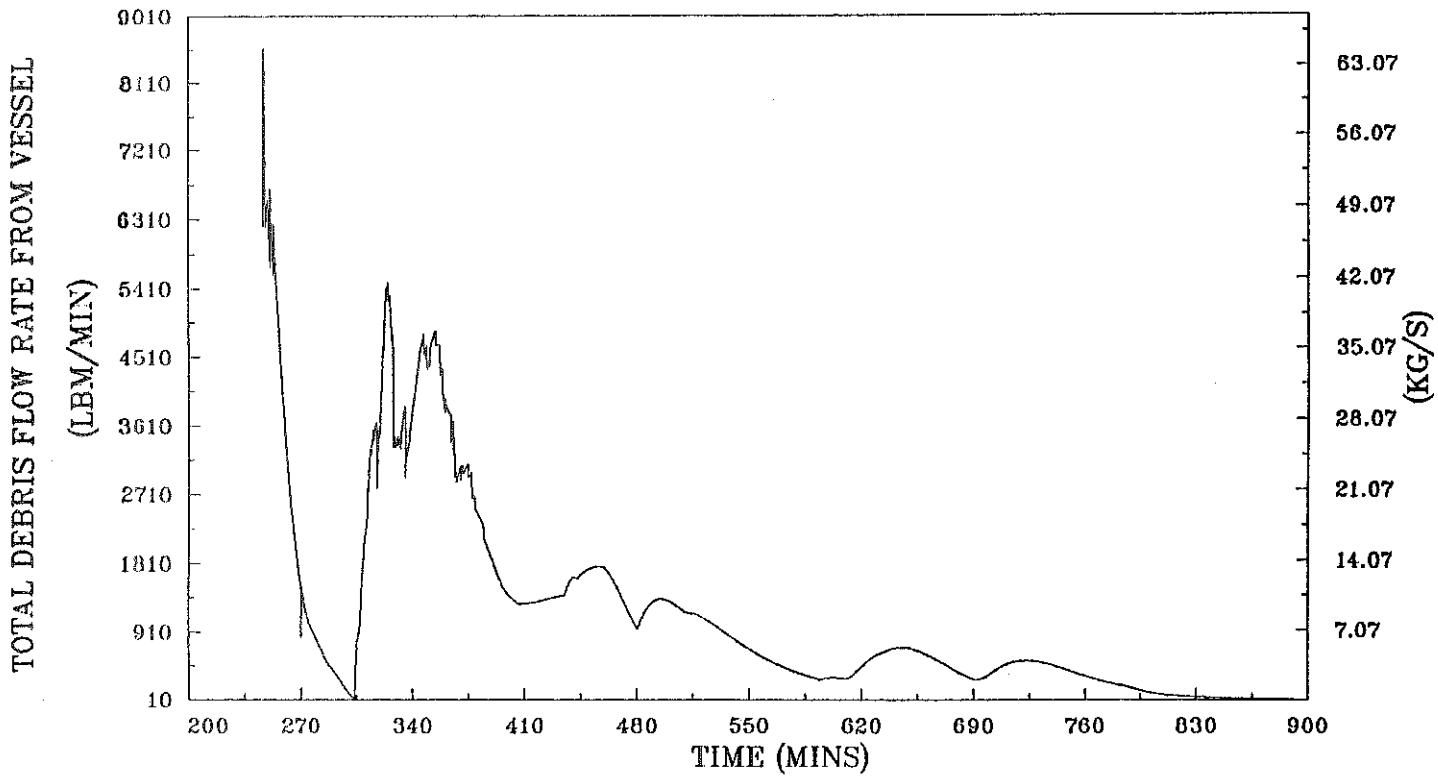

Fig. 3.4.7. Total debris pours from the reactor vessel for BWR-4/Mark II short-term station blackout sequence without ADS (simple eutectics).

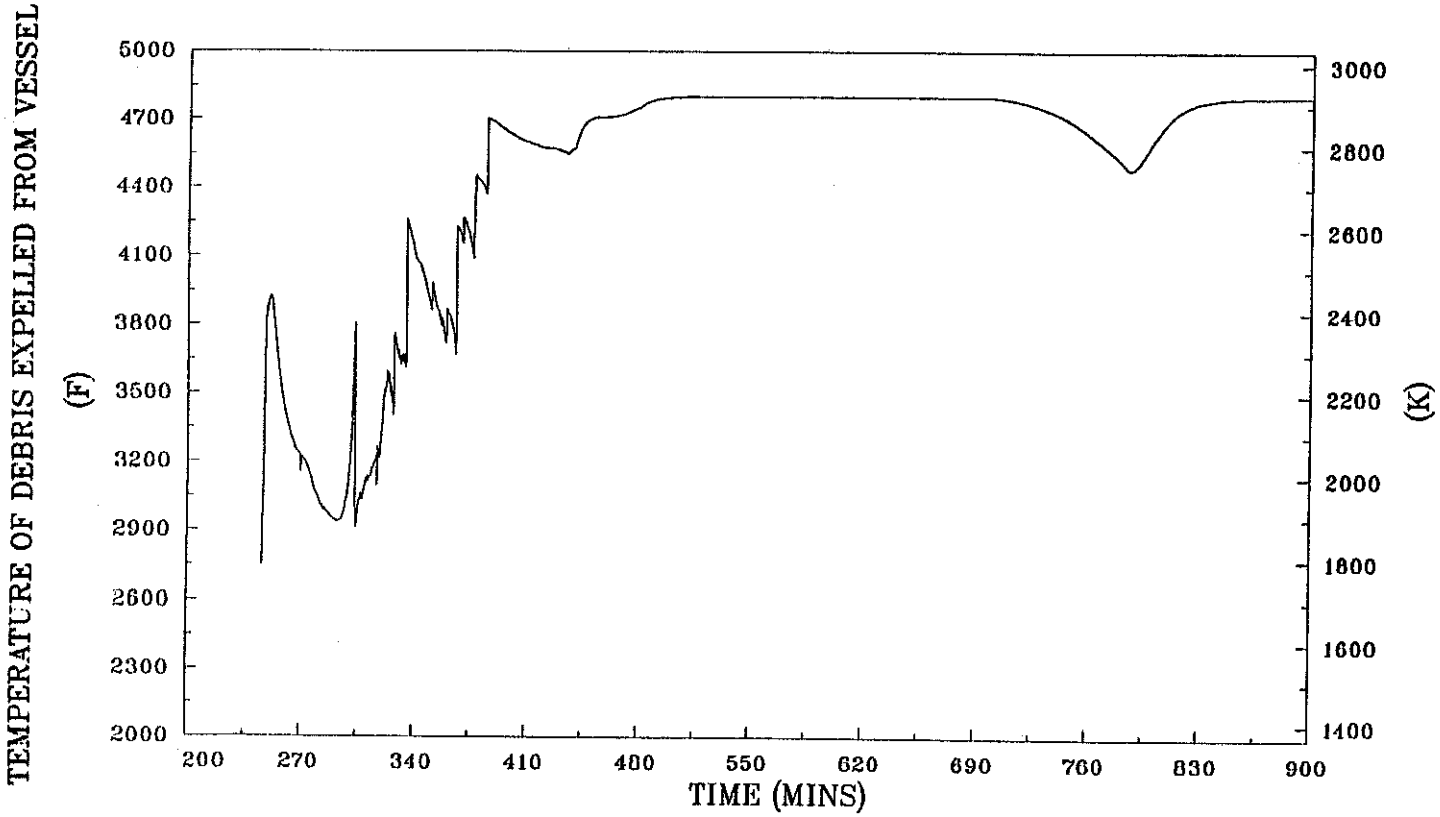

Fig. 3.4.8. Mass-averaged temperature of the debris pours from the reactor vessel for the short-term station blackout sequence without ADS actuation.

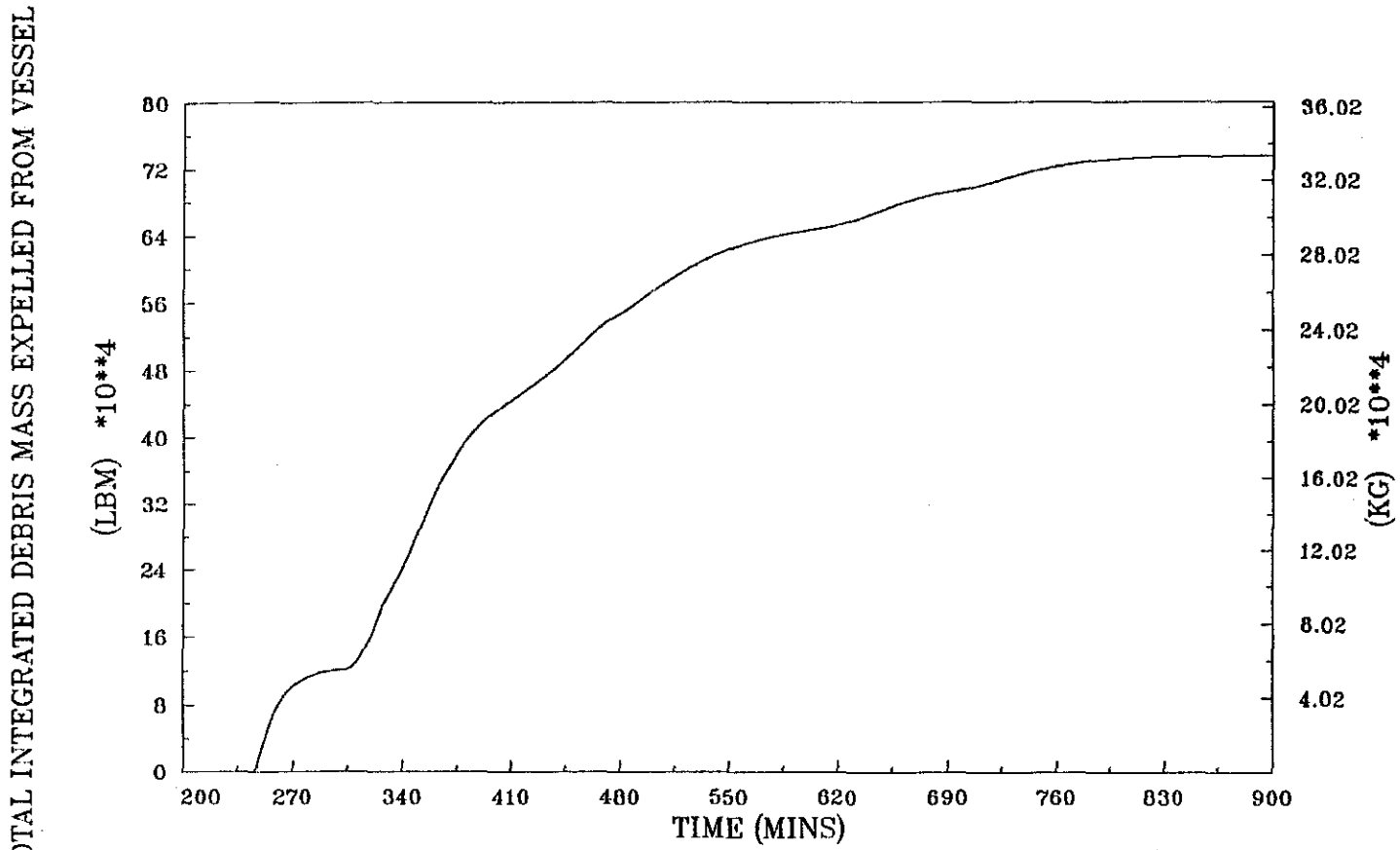

Fig. 3.4.9. Integrated debris mass expelled from the reactor vessel for BWR-4/Mark II short-term station blackout sequence without ADS (simple eutectics).

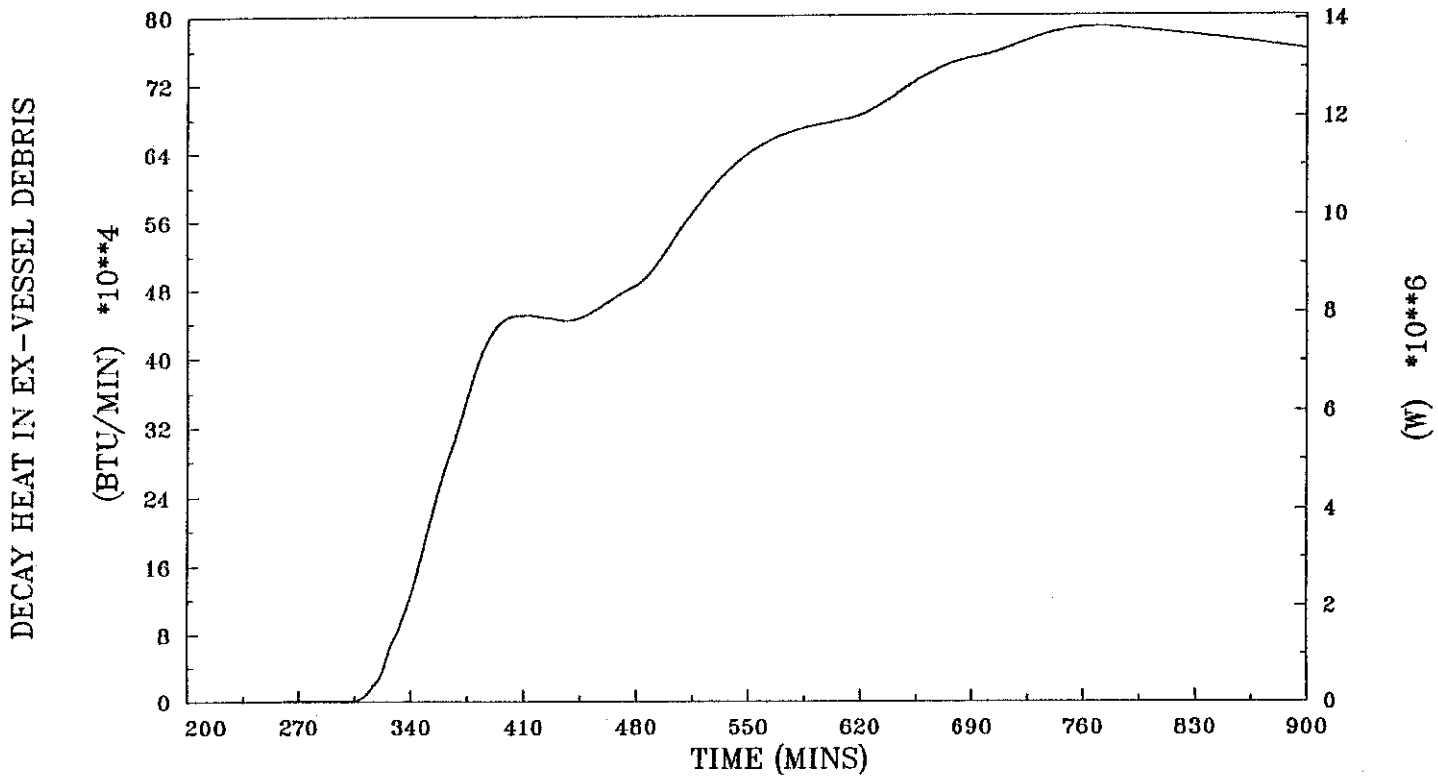

Fig. 3.4.10. Decay power in ex-vessel debris for BWR-4/Mark II short-term station blackout sequence without ADS (simple eutectics).

4. BWR-4 LONG-TERM STATION BLACKOUT CORE DEGRADATION ANALYSES

4.1 INTRODUCTION

Reactor vessel injection capability remains available in the long-term station blackout accident sequence (via the steam turbine-driven RCIC or HPCI systems) until the time that the unit battery is exhausted. Battery power is necessary for steam turbine valve and governor control. The time of battery exhaustion depends upon operator actions taken to reduce non-vital loads (such as feedwater turbine lube oil pumps) and could be between 4-8 h. A battery failure time of 6 h was assumed for this study.

For this accident sequence, Revision 4 of the BWR Owners Group Emergency Procedure Guidelines (Ref. 10) direct the operators to maintain the reactor vessel water level near the normal operating range (approximately 15 ft above the top of the core) and to depressurize the vessel in a controlled manner to approximately 200 psia. At the time of battery exhaustion, however, both injection capability and the ability to manually actuate the reactor vessel safety/relief valves would be lost. The reactor vessel pressure would subsequently increase to the setpoint for automatic relief valve actuation and boil-off of the vessel water inventory would begin. Uncovery of the upper core would then occur approximately 10 h after accident initiation.

The BWR-LTAS code was applied for the initial 10 1/2-h period of the accident while the core remains covered. The BWRSAR code was used for analyses of core degradation and relocation phase. The BWRSAR code results for gas releases and debris pours from the reactor vessel were used to drive a detailed MELCOR code simulation of the BWR Mark II containment response.

4.2 THE INITIAL PHASE (Before The Core Is Uncovered)

The BWR-LTAS calculation covers the period of the accident sequence from 0.6-630 min. The initial conditions for this calculation were taken from the results of the Susquehanna main steam isolation valve closure test discussed in Chapter 2. At 630 min, the reactor vessel water level has decreased to approximately 16 in. above the top of the core so the BWR-LTAS calculation is terminated and the BWRSAR calculation is

initiated. The BWR-LTAS results are discussed below and the BWRSAR results are discussed in Sect. 4.3.

The operator actions represented in the BWR-LTAS calculation are those specified by the BWR Owners Group EPGs. With the RCIC (or HPCI) steam turbine-driven reactor vessel injection available, the operators would delay core uncovery until after battery failure. The EPGs specify (Step RC/L-2) that the vessel water level should be maintained between the low- and high-level scram setpoints and that the RCIC (and HPCI) pump suction should be maintained on the condensate storage tank. The reactor vessel would be depressurized at a rate allowed by the plant Technical Specifications (corresponding to a coolant temperature decrease of approximately 100°F/h). Depressurization at this rate would require approximately 90 min to reduce the vessel pressure to 200 psia.

The operators would control reactor vessel pressure by running the HPCI turbine in the test mode. In this mode, the HPCI system pumps water (maximum capacity 5000 GPM) from the condensate storage tank through a test line back to the condensate storage tank. The operators adjust the steam demand from the reactor vessel by varying the amount of water being pumped. The HPCI and RCIC turbine exhaust is discharged to the pressure suppression pool. The reactor vessel pressure is lowered to approximately 200 psia simply by operating the HPCI turbine at maximum capacity, drawing approximately 48 lb/s of steam from the reactor vessel.

The calculated reactor vessel pressure throughout the initial phase of this accident sequence is shown in Fig. 4.2.1. As indicated, the vessel pressure has decreased to 200 psia by 107 min although the safety/relief valves (SRVs) cycle only a few times during this period. The HPCI system is subsequently shifted between operation at 25% capacity and full capacity as necessary to maintain the vessel pressure between 200-250 psia. After battery exhaustion at 360 min, the HPCI turbine can no longer be operated and the reactor vessel pressure steadily increases to the setpoint for automatic SRV operation. The lowest-set relief valve then continuously cycles.

Use of the HPCI system test mode for reactor vessel pressure control is preferred because the heatup rate of the pressure suppression pool is significantly reduced. This approach also virtually eliminates the threat of a stuck-open SRV during the period while battery power remains available by eliminating or reducing automatic cycling of the SRVs. (See Sect. 8.2 of Ref. 11 for the effect of a stuck-open SRV on station blackout accident progression.) It should be recognized, however, that a stuck-open SRV would

actually be beneficial during the period after battery failure since it would prevent vessel repressurization.

The steam flow from the reactor vessel during the initial phase of this accident sequence is shown in Fig. 4.2.2. With the reactor vessel at normal operating pressure, one open SRV takes approximately 250 lb/s, the HPCI system at full capacity in the test mode takes approximately 48 lb/s (Ref. 12), and the RCIC system injecting at full capacity into the reactor vessel would take approximately 9 lb/s (Ref. 13). The BWR-LTAS code adjusts these flows (and the turbine exhaust flows) as necessary to compensate for changing reactor vessel and containment pressures.

It should be noted that five of the Mark II plants in the United States employ the BWR-4, while the other four employ the BWR-5 design (see Table 1.2). This distinction is important because the BWR-5 plants do not have an HPCI system, but use an electric motor-driven high pressure core spray system (HPCS) that would not be available in station blackout. Reactor vessel depressurization could only be carried out by remote-manual operator actuation of the SRVs in BWR-5 plants. The increased heatup of the pressure suppression pool as a result of passing the steam released from the reactor vessel directly through an SRV, rather than through a turbine, will be briefly addressed at the conclusion of this Section.

The operator controls reactor vessel water level by continuous injection with the RCIC system, which has a maximum capacity of 600 GPM. With suction from the condensate storage tank at 80°F, this is equivalent to 83.3 lb/s. It was assumed for this calculation that the operator would monitor reactor vessel level on the reactor safeguards wide range instrument. The operator is assumed to increase or decrease the RCIC injection rate as necessary to approach a target level of + 12.5 in. (equivalent to 540 in. above vessel zero). The predicted injection history is shown in Fig. 4.2.3. The average injection is highest during the period while the reactor vessel is being depressurized.

The calculated (collapsed) reactor vessel water level above vessel zero is shown in Fig. 4.2.4. The operator is assumed to monitor vessel level on the reactor safeguards wide range instrument, which is calibrated for a reactor pressure of 1020 psia and a drywell temperature of 135°F. Since the drywell temperature is much higher than this during the accident sequence and the vessel pressure falls as low as 200 psia, the wide range instrument indicates a level that is higher than the actual level by as much as 30 in. (depending on the conditions). Thus, the actual water level falls entirely on the low side

of the target level, as indicated on Fig. 4.2.4, although the operator sees an indicated level that straddles the target level.

There are important advantages associated with reactor vessel depressurization while battery power remains available in this accident. First, this maneuver buys time. If the reactor vessel remained pressurized during the initial phase, the boiloff of vessel water inventory would begin with a water level near the target level indicated on Fig. 4.2.4, rather than the much higher level associated with a reactor vessel which repressurizes subsequent to operator-controlled depressurization. Simply stated, it requires more water mass to maintain a given water level at lower pressures than at higher pressures. As the vessel repressurizes, this larger mass is retained within the vessel.

A second major benefit of reactor vessel depressurization is that it reduces the drywell heat load. During normal operation, heat is transferred through the reactor vessel wall and surrounding mirror insulation to the drywell atmosphere, where it is removed by the drywell coolers. Under station blackout conditions, however, the drywell coolers do not operate, but the heat transfer to the drywell atmosphere remains unchanged as long as the temperature of the water/steam within the vessel remains the same. As indicated in Fig. 4.2.5, the temperature of the drywell atmosphere increases rapidly immediately after the drywell coolers are lost. The drywell atmospheric temperature then remains approximately constant because the rate of heat transfer to the drywell heat sinks matches the heat transfer from the reactor vessel. After battery exhaustion at 360 min, however, the vessel pressure and saturation temperature increase, and the temperature of the drywell atmosphere increases in turn. The corresponding drywell pressure is indicated in Fig. 4.2.6.

The calculated increases in pressure suppression pool water level and temperature are shown in Fig. 4.2.7. After battery exhaustion, these quantities remain approximately constant for approximately 2 h while the reactor vessel pressure slowly increases to the setpoint for automatic operation of the SRVs. Subsequently, the pool level and temperature again increase as mass and energy are transferred from the reactor vessel with each SRV cycle. At the time (630 min) the calculation is transferred to the BWRSAR code, the pool-average temperature is 202°F and the pool level has increased slightly more than 4 ft above its initial (23 ft) level.

The effect of reactor vessel pressure control by remote-manual SRV actuation rather than by operation of the HPCI turbine in the test mode is of interest because BWR-5 units do not have the HPCI option. With SRV pressure control, there is no need to maintain sufficient pressure (above 165 psia) to permit operation of the HPCI turbine. Accordingly, the vessel pressure could be maintained in the vicinity of 100 (rather than 200) psia. Table 4.1 indicates the calculated differences at the time of battery failure (6 h) for the two methods of pressure control for long-term station blackout. The most important difference is that the pressure suppression pool temperature is approximately 17 degrees higher for the case with SRV control. However, this disadvantage is partially offset by a lower reactor vessel pressure when injection capability is lost. While pressure control by the HPCI turbine is clearly desirable, either method is viable.

4.3 THE FINAL PHASE (Core Degradation And Relocation)

The BWRSAR calculation was initiated at time 630 min (10 1/2 h) into the long-term station blackout accident sequence. The calculated sequence of events and event timing are provided in Table 4.2. It should be noted that this sequence is similar to the case of short-term station blackout without ADS discussed in Sect. 3.4. Comparison of the event sequence listed in Table 4.2 with the short-term sequence listed in Table 3.9 illustrates the much slower progression of events for the long-term case, because of the lower decay heat. For example, approximately 99 min elapse between uncovering of the top of the core and the beginning of material relocation for the long-term sequence (Table 4.2) whereas only 52 min elapse between these two events in the short-term sequence (Table 3.9).

Plots of key parameters as calculated by BWRSAR for events within the reactor vessel during the long-term station blackout accident sequence are shown in Figs. 4.3.1-4.3.4. These plots represent events from 630 min after the inception of the accident sequence to time 1000 min, which is approximately 14 min after the predicted initial failure of reactor vessel bottom head penetrations and the beginning of debris pours onto the drywell floor. As indicated in Fig. 4.3.1, the calculated vessel pressure decreases significantly after core plate dryout. This occurs because steam generation ceases within the core region while steam leakage and heat transfer from the vessel to the drywell atmosphere continue. Subsequently, the vessel pressure is restored to the range of the safety/relief valve setpoints after local core plate failures introduce core debris into the

water in the lower plenum and restore in-vessel steam generation. The associated SRV flows are shown in Fig. 4.3.3.

After bottom head dryout, steam generation within the reactor vessel is limited to flashing of the water surrounding the jet pumps in the downcomer region as the vessel depressurizes due to continued leakage. As indicated in Fig. 4.3.1, the depressurization rate is reduced as the vessel pressure is reduced and the leakage rate is correspondingly decreased.

The predicted swollen reactor vessel water level is shown in Fig. 4.3.2. The decreasing water level initially traces a smooth curve through the core region, punctuated by spikes at each SRV actuation. Subsequently, after the onset of downward material relocation and quenching, the rate of level decrease is accelerated and proceeds in a more steplike fashion. Core plate dryout occurs with the water level just below the core plate. Water again enters the core region after core plate failure as a result of displacement of water in the lower plenum by the falling debris from the central region of the core. The decay heat associated with the fuel pellet stack collapse at 866 min causes a rapid boiloff of the remaining water and bottom head dryout occurs at time 892 min.

Figure 4.3.4 shows the total hydrogen generated in the core region as a function of time. Liquid water remains in the lower portion of the core at the time that large portions of the upper core have exceeded the runaway zirconium oxidation temperature. Steam generation by heat transfer to this water from the submerged portion of the core and by the mechanism of quenching of the relocating debris then provides a steam-rich atmosphere to fuel the metal-water reactions. Approximately 59% of the clad, 16% of the channel box walls, and 1% of the control blade stainless steel is predicted to be oxidized in the core region during the accident sequence, producing approximately 2560 lb of hydrogen. Since the reactor vessel is pressurized at the time of bottom head penetration failure in this accident sequence, the metal-water reactions associated with the vessel blowdown through the bottom head debris produce a large amount of hydrogen and energy release within the debris bed. Significant debris pours begin almost immediately after penetration failure.

The characteristics of the reactor vessel debris pours as calculated by the BWRSAR code for the long-term station blackout accident sequence are shown in Figs. 4.3.5-4.3.10. These results were obtained with the two-eutectic-mixture approach described in Sect. 3.1, for which all metals melt at 2750°F and all oxides melt at 4800°F.

As indicated on Figs. 4.3.7 and 4.3.8, there is a large initial flow of metals for approximately 12 min immediately after bottom head penetration failure. This initial pour consists of approximately 55,000 lb of metals from the central portion of the bottom head debris bed. This material is melted (and superheated) by the energy release associated with the blowdown of the reactor vessel through the bed. (About 28,000 lb of zirconium metal is predicted to be oxidized in the process.) Subsequently, the pour is terminated until the energy release associated with decay heating has increased the temperature of the upper regions of the bed to the melting temperature of the metals. The pour resumes at approximately time 1075 min, and is continuous thereafter.

As in the case for the calculations discussed in Chapter 3, the BWRSAR code predicts that the portion of the reactor vessel bottom head beneath the point of attachment of the support skirt is removed (ablated) long before the major portion of the in-vessel debris bed has melted. For the long-term station blackout calculation, this is predicted to occur approximately 2 h after the resumption of the pour, at time 1190 min. (The removal is by the process of ablation of surrounding wall structure by the molten debris pouring through the failed bottom head penetration sites.) There are no specific models within BWRSAR to relocate the solid debris. It is believed that the 420,000 lb of debris remaining within the vessel at this time would merely relocate downward approximately 3 ft onto the control rod drive housing support structure (see Fig. 3.2.8). After relocation, the debris would continue to melt, with the molten portion flowing down onto the drywell floor in the same manner as if the portion of the bottom head surrounding the penetrations had remained intact. (This statement is true even if the debris were not held up by the housing support structure; the rate of release of molten material over the drywell floor is determined by the rate at which the debris melts, regardless of where the debris is located.)

The temperature of the molten debris leaving the reactor vessel increases (Fig. 4.3.8) as the composition of the pour shifts from primarily metals to primarily oxides. A listing of the various constituents of the debris that are predicted to have become molten by the end of the calculation (1800 min) is provided in Table 4.3. About 85,000 lb of oxides are predicted to remain in the solid state at the end of the calculation. This is less than 10% of the total debris and, as indicated in Fig. 4.3.7, the release rate has become insignificant by this time.

Table 4.1. Calculated vessel and containment parameters at the time of battery failure for two methods of pressure control during station blackout

Parameter	HPCI turbine in test mode	SRV control
Vessel pressure (psia)	206.0	102.0
Vessel water level (in.)	529.5	518.4
Pressure suppresion pool temperature (°F)	173.7	190.8
Pressure suppression pool level (ft)	26.1	26.4
Drywell atmosphere temperature (°F)	201.0	193.5
Containment pressure (psia)	19.5	20.4

Table 4.2. Calculated sequence of events for BWR Mark II long-term station blackout

Event	Time (min)
Station blackout-initiated scram from 100% power. Independent loss of the steam turbine-driven HPCI and RCIC injection systems	0.0
BWRSAR calculation initiated	630.0
Swollen water level falls below top of core	637.8
Relocation of core debris begins	736.7
Core plate dryout	794.8
First local core plate failure	820.8
Collapse of fuel pellet stacks in central core	866.3
Reactor vessel bottom head dryout	892.1
Structural support by control rod guide tubes fails; Remainder of core falls into reactor vessel bottom head	926.4
Initial failure of bottom head penetrations	985.6
Pour of molten debris from reactor vessel begins	985.8

Note: The bottom head debris is modeled to separate into a mixture of metals melting at 2750°F and a mixture of oxides melting at 4800°F (simplified eutectics).

Table 4.3. Composition of the debris released from the reactor vessel by the end of the long-term station blackout calculation

Constituents	Integrated Mass (lb)
Metals	
Zr	52,230
Fe	287,481
Cr	49,056
Ni	21,825
B_4C	1,527
Subtotal (metals)	412,119
Oxides	
ZrO_2	57,218
FeO	99
Fe_3O_4	261
Cr_2O_3	95
NiO	17
B_2O_3	53
UO_2	317,684
Subtotal (oxides)	375,427
Total	787,546

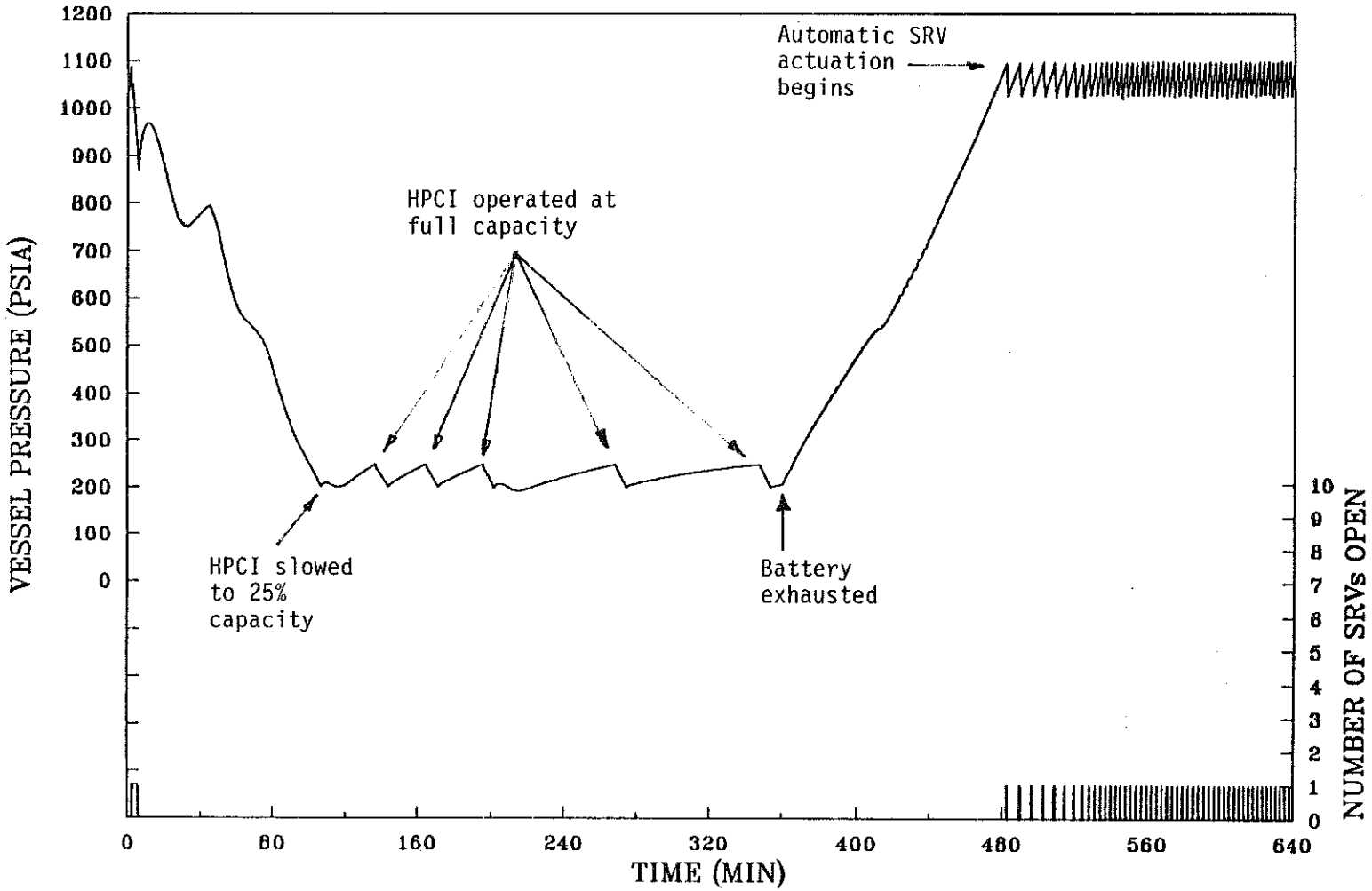

Fig. 4.2.1. Reactor vessel pressure and number of open safety/relief valves for the BWR-4/Mark II long-term station blackout sequence.

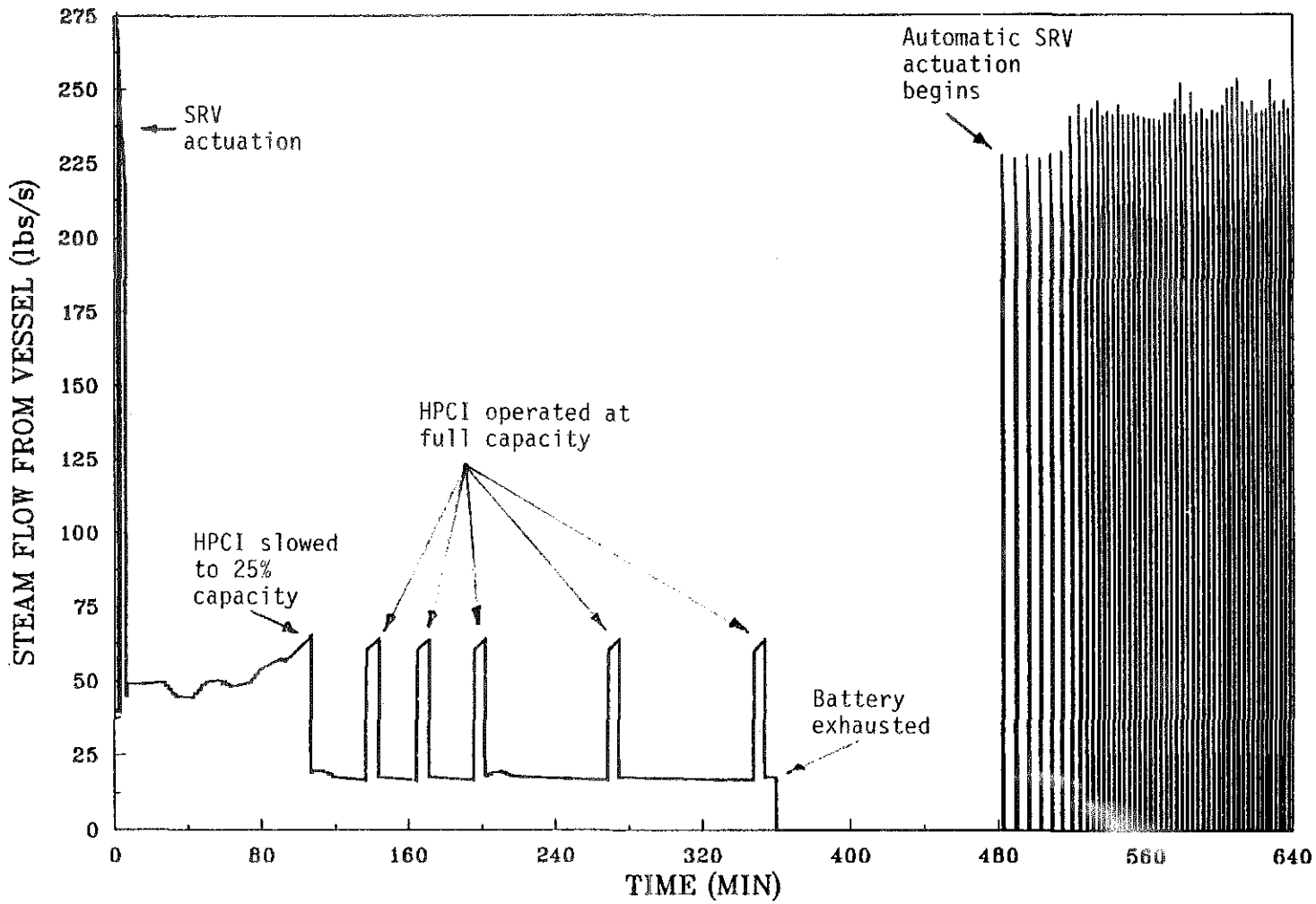

Fig. 4.2.2. Combined steam flow from the reactor vessel to the RCIC turbine, HPCI turbine, and safety/relief valves for the BWR-4/Mark II long-term station blackout sequence.

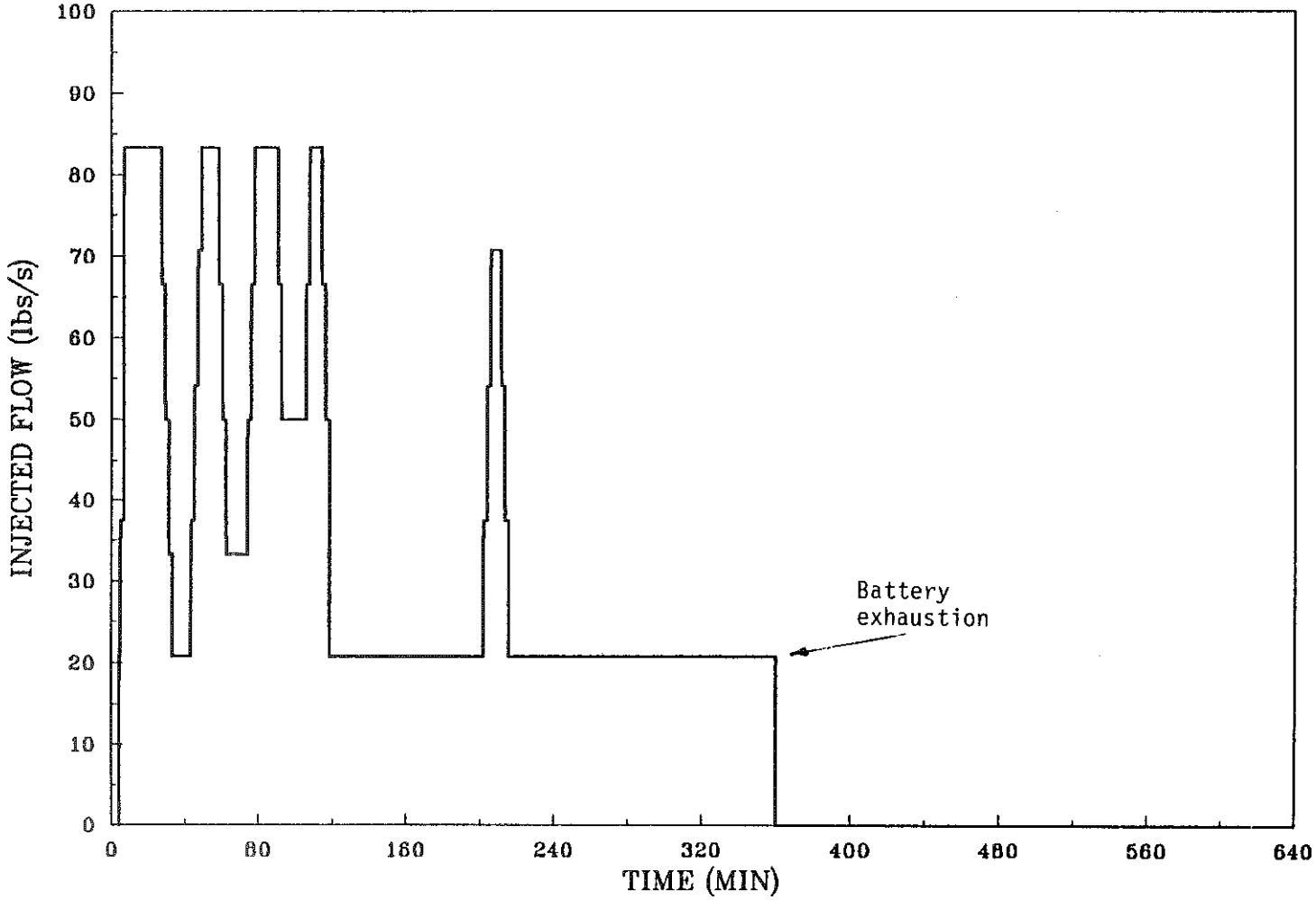

Fig. 4.2.3. Flow injected into the reactor vessel by the RCIC system for the BWR-4/Mark II long-term station blackout sequence.

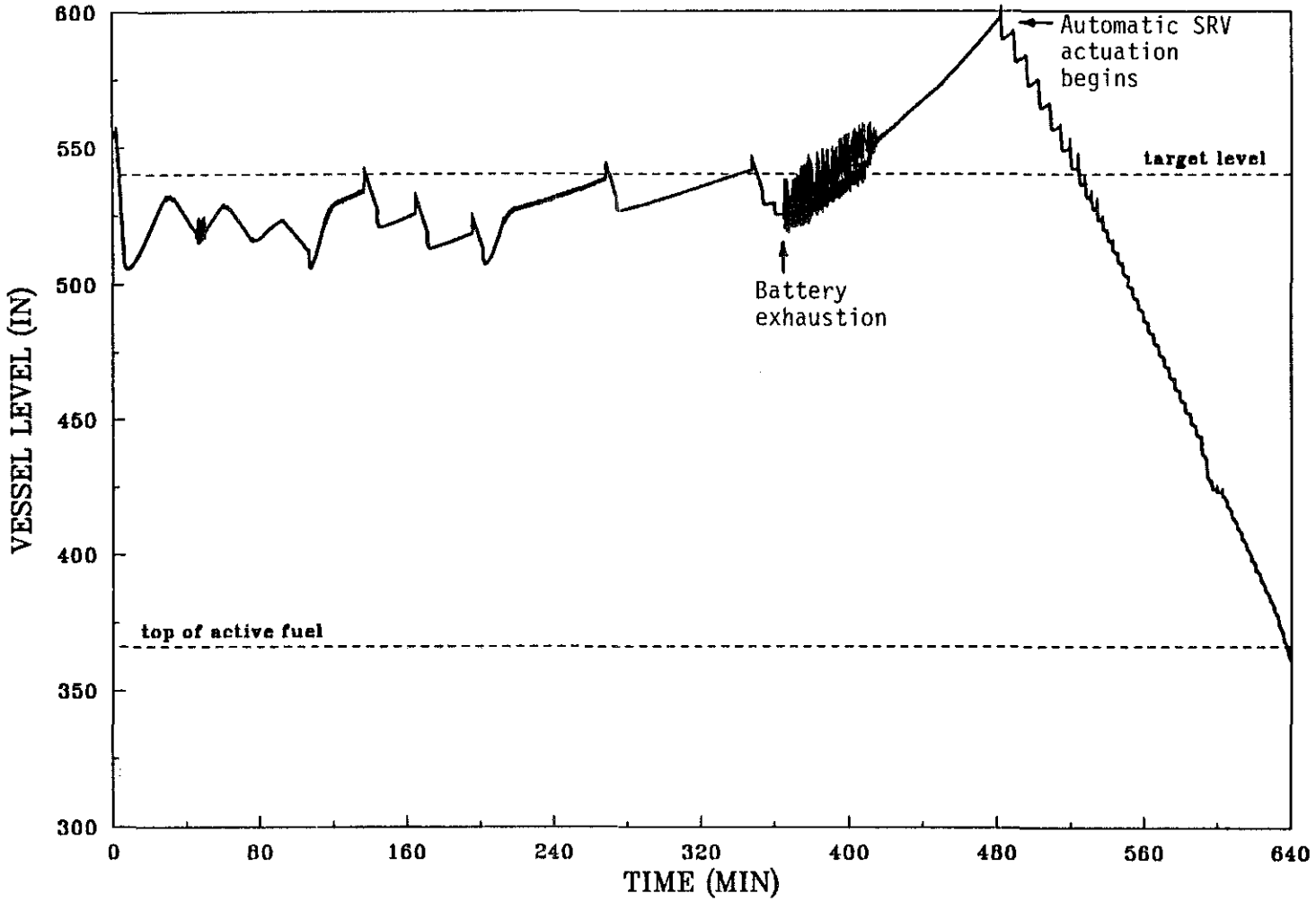

Fig. 4.2.4. Actual reactor vessel water level (inches above vessel zero) for the BWR-4/Mark II long-term station blackout sequence.

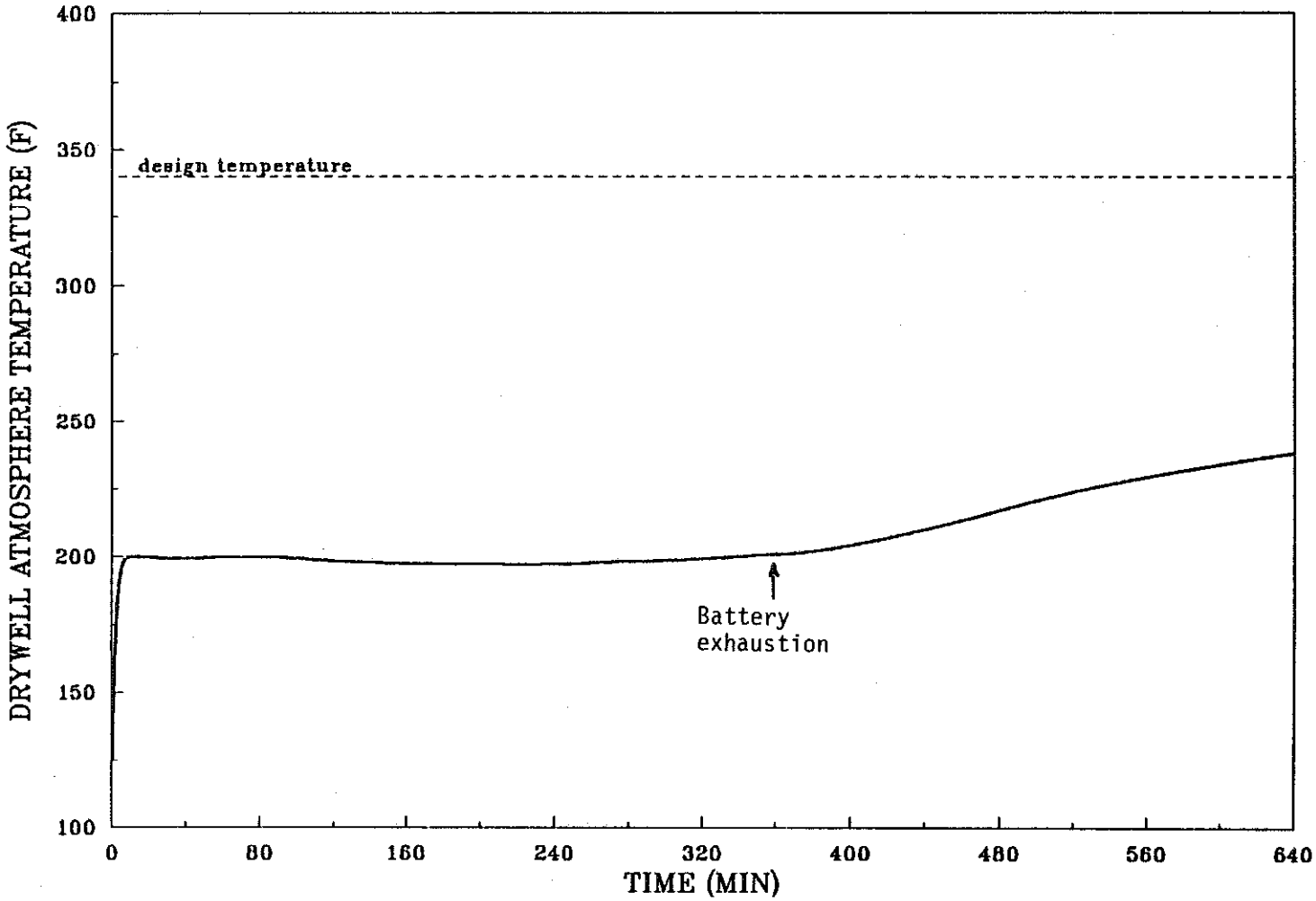

Fig. 4.2.5. Mixed-mean temperature of the drywell atmosphere for the BWR-4/Mark II long-term station blackout sequence.

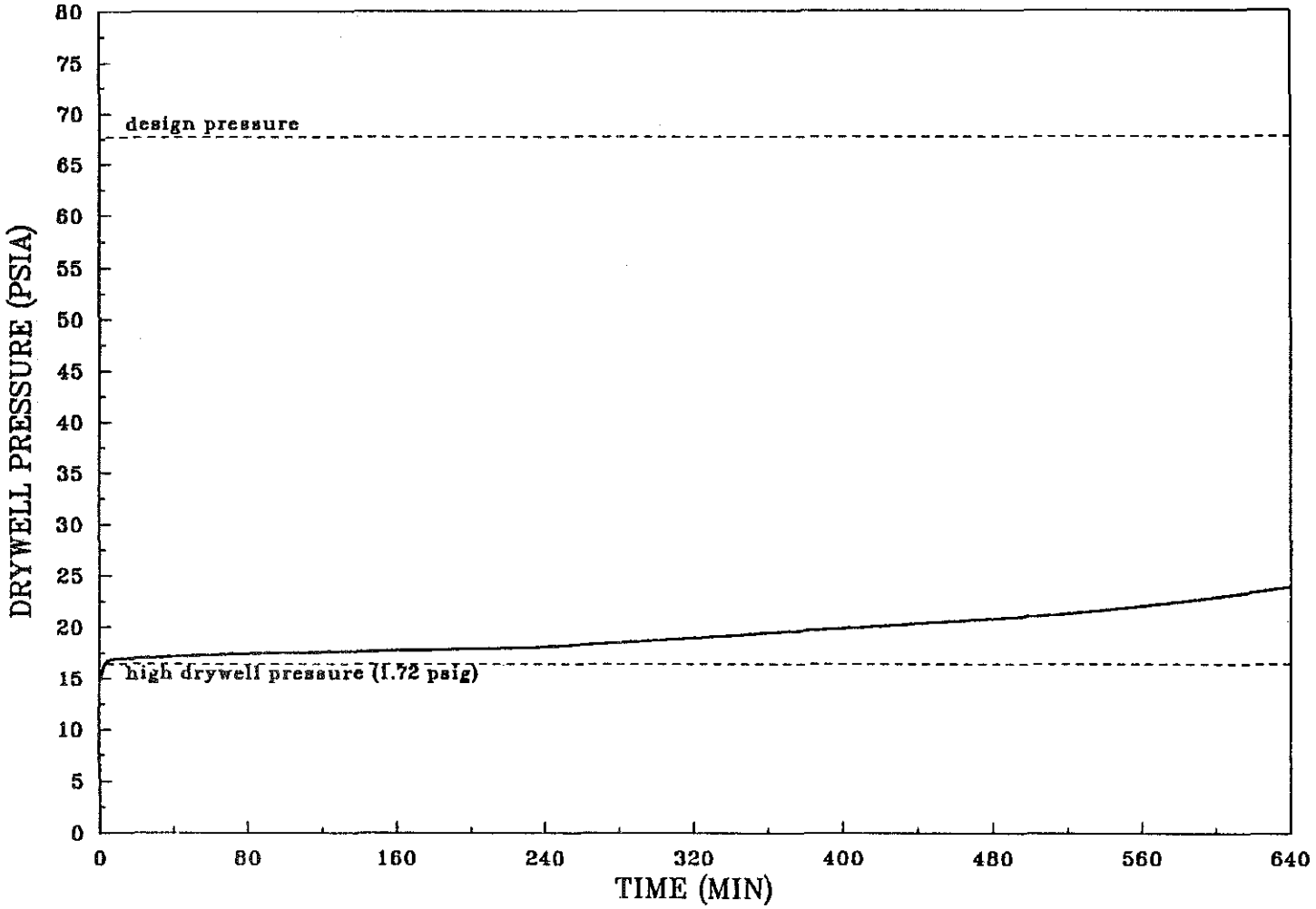

Fig. 4.2.6. Drywell pressure for the BWR-4/Mark II long-term station blackout sequence.

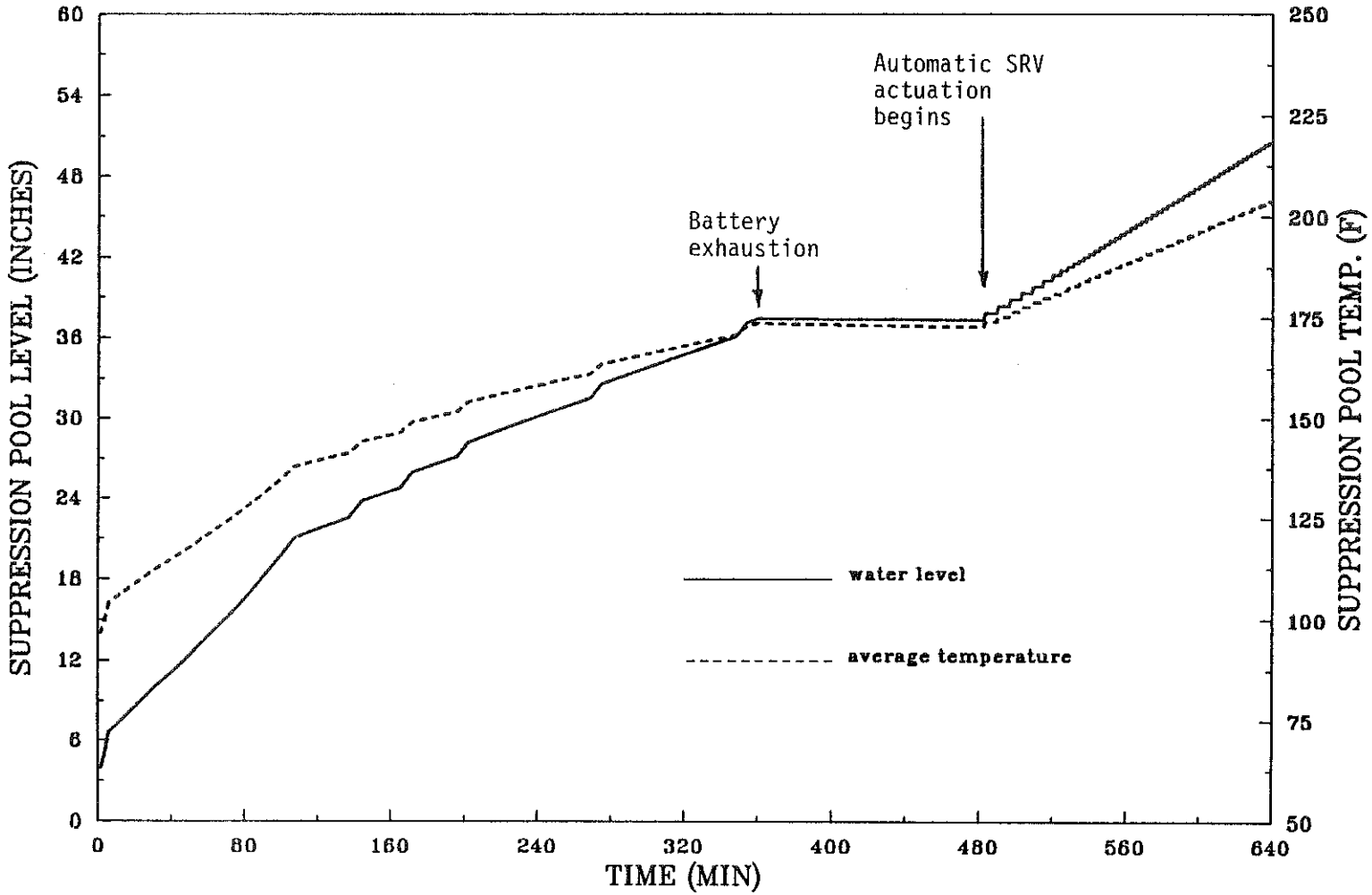

Fig. 4.2.7. Pressure suppression pool water level and average temperature for the BWR-4/Mark II long-term station blackout sequence.

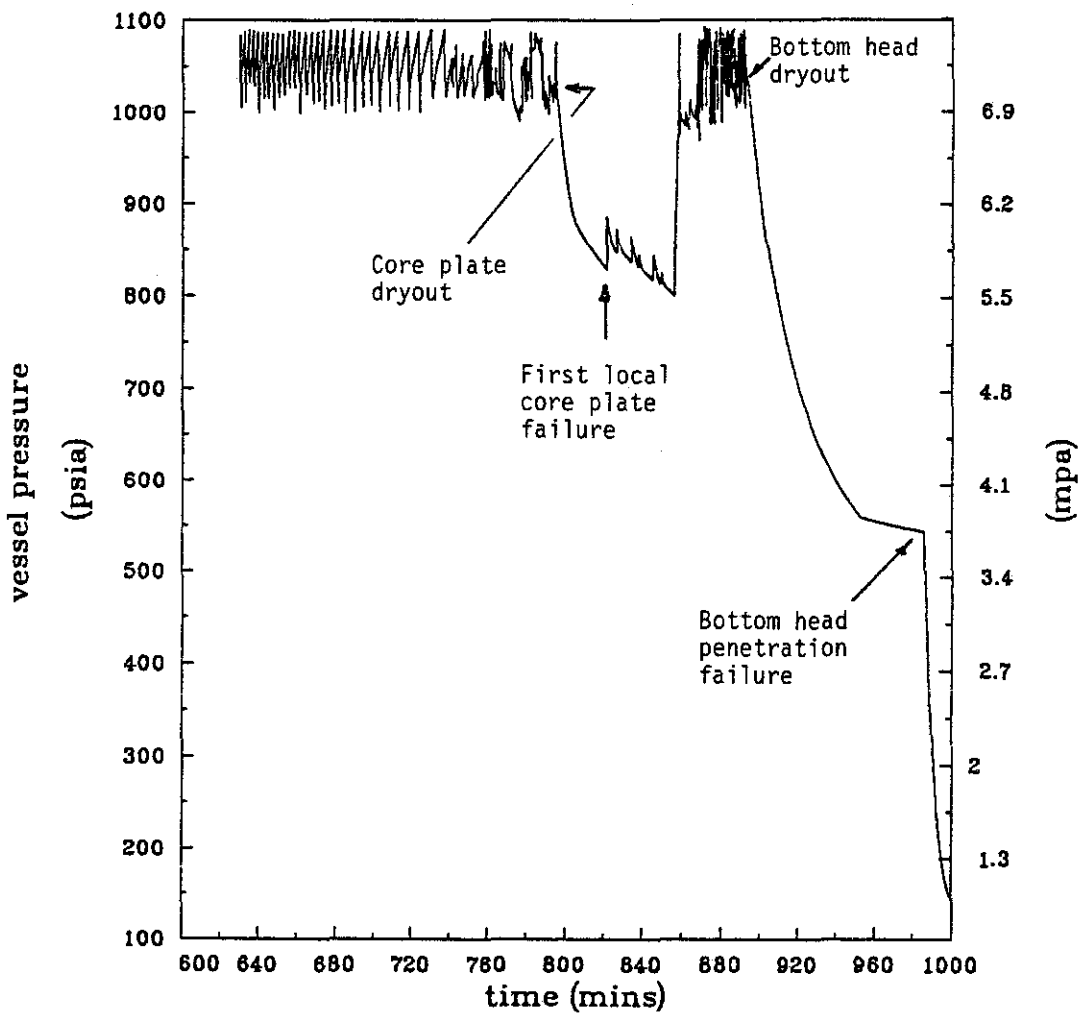

Fig. 4.3.1. Reactor vessel pressure for BWR-4/Mark II long-term station blackout sequence.

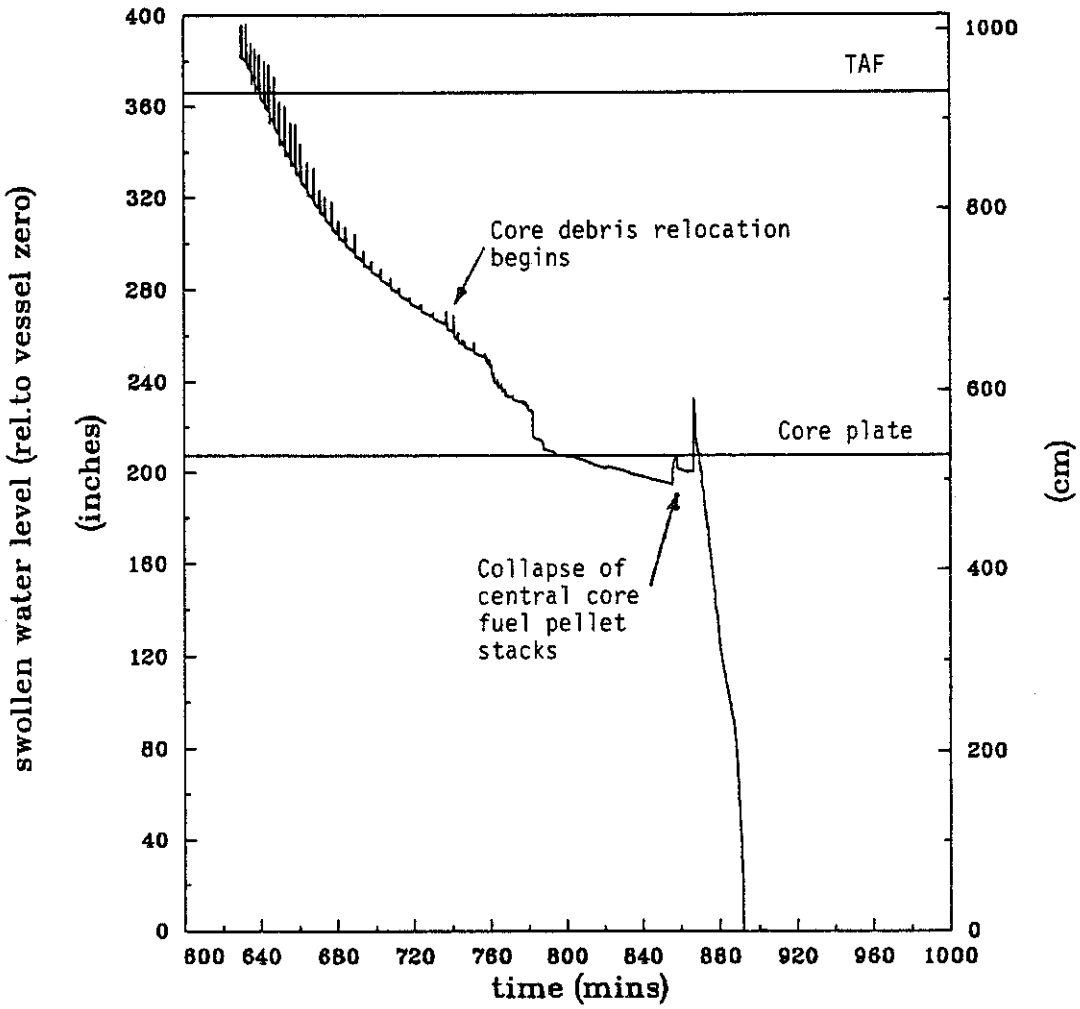

Fig. 4.3.2. Swollen reactor vessel water level for BWR-4/Mark II long-term station blackout sequence.

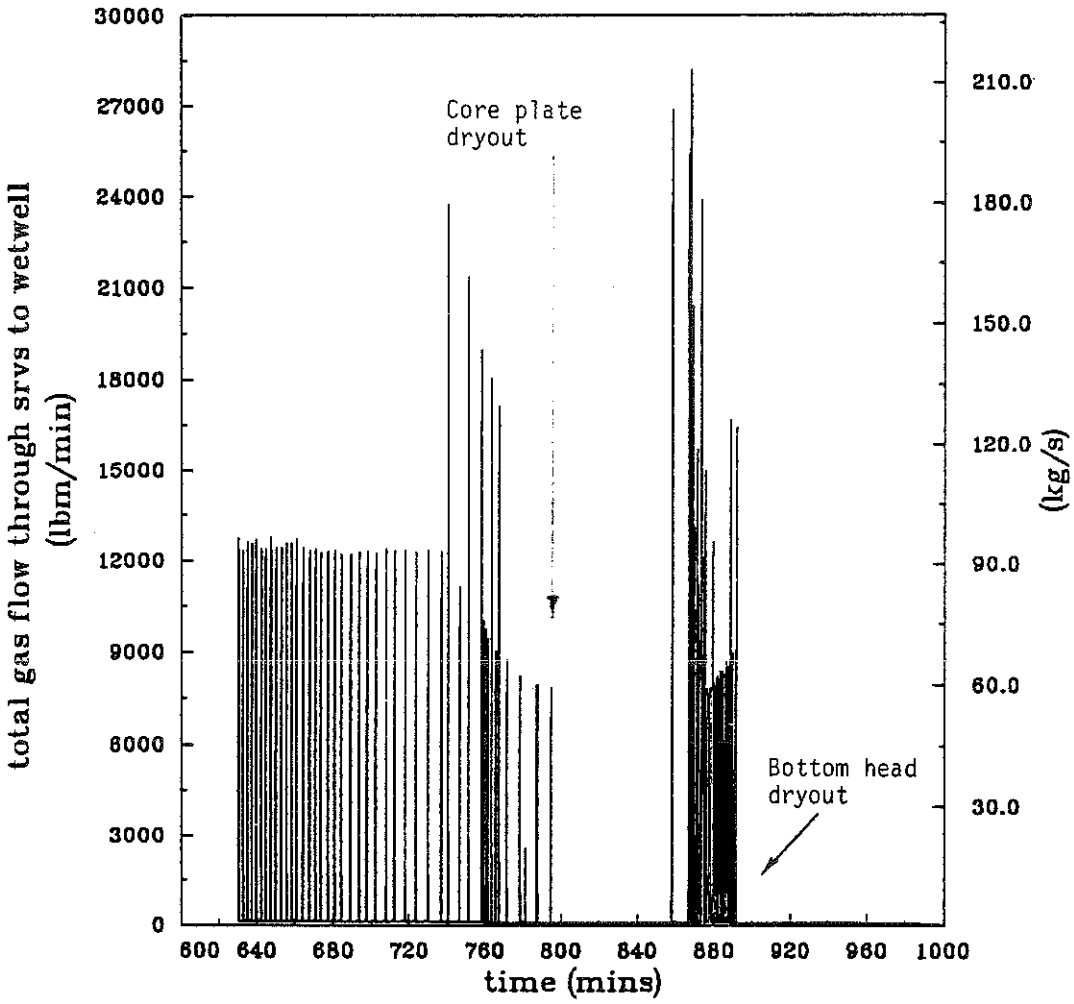

Fig. 4.3.3. Total SRV gas flow for BWR-4/Mark II long-term station blackout sequence.

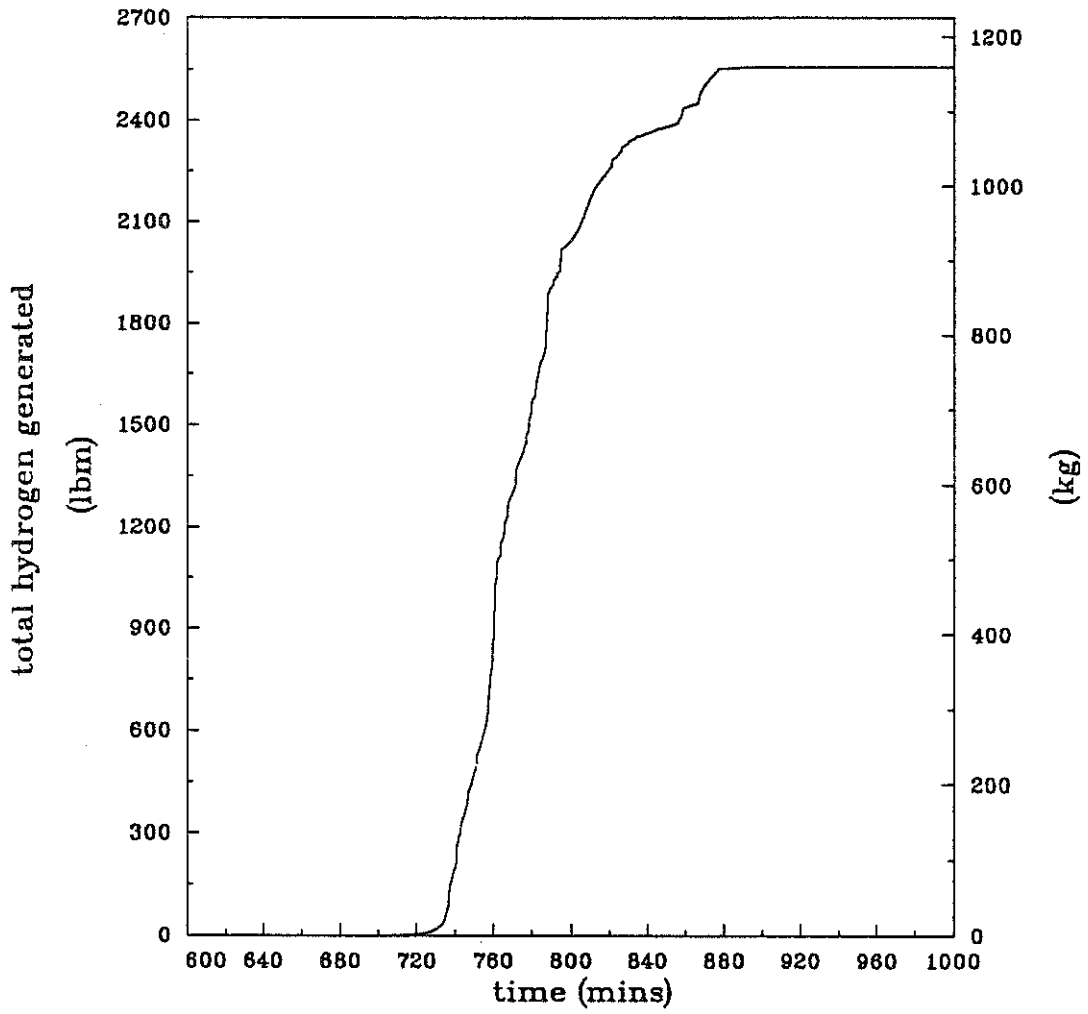

Fig. 4.3.4. Total hydrogen generated in-vessel before bottom head penetration failure in the BWR-4/Mark II long-term station blackout sequence.

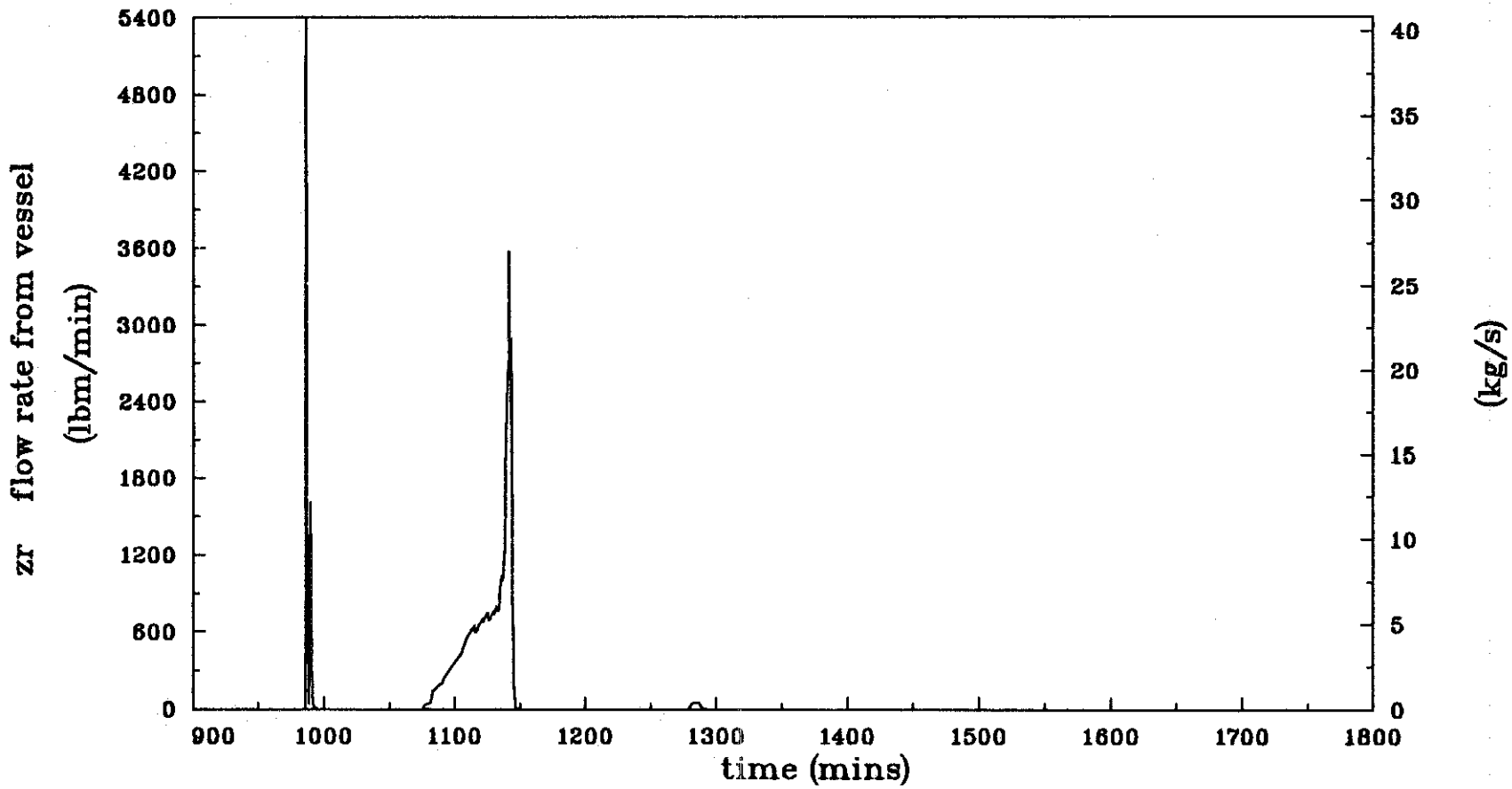

Fig. 4.3.5. Zirconium metal pours from the reactor vessel for BWR-4/Mark II long-term station blackout sequence. The initial bottom head penetration failure is predicted to occur 986 minutes after the inception of the accident.

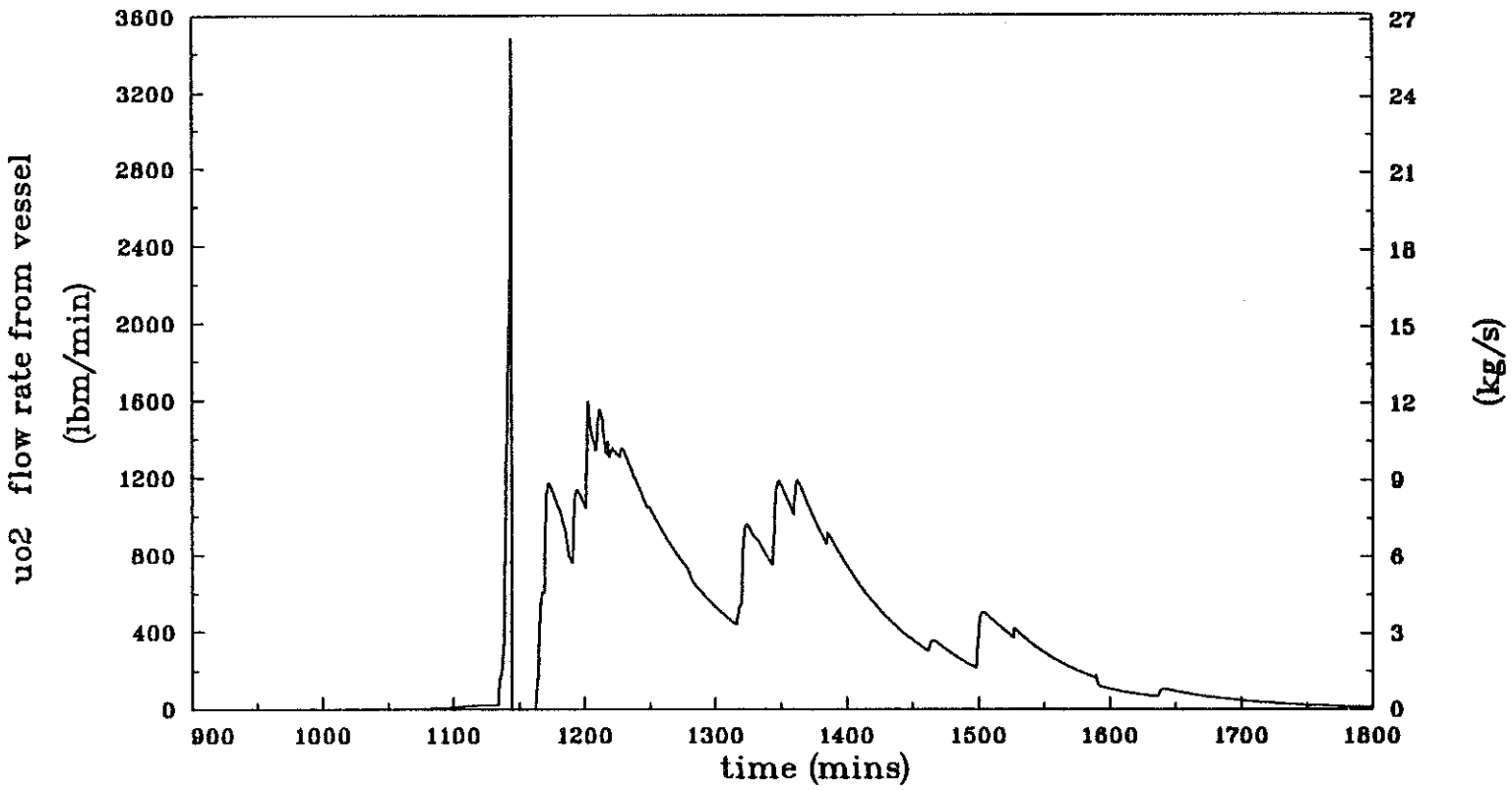

Fig. 4.3.6. Uranium dioxide pours from the reactor vessel for BWR-4/Mark II long-term station blackout sequence.

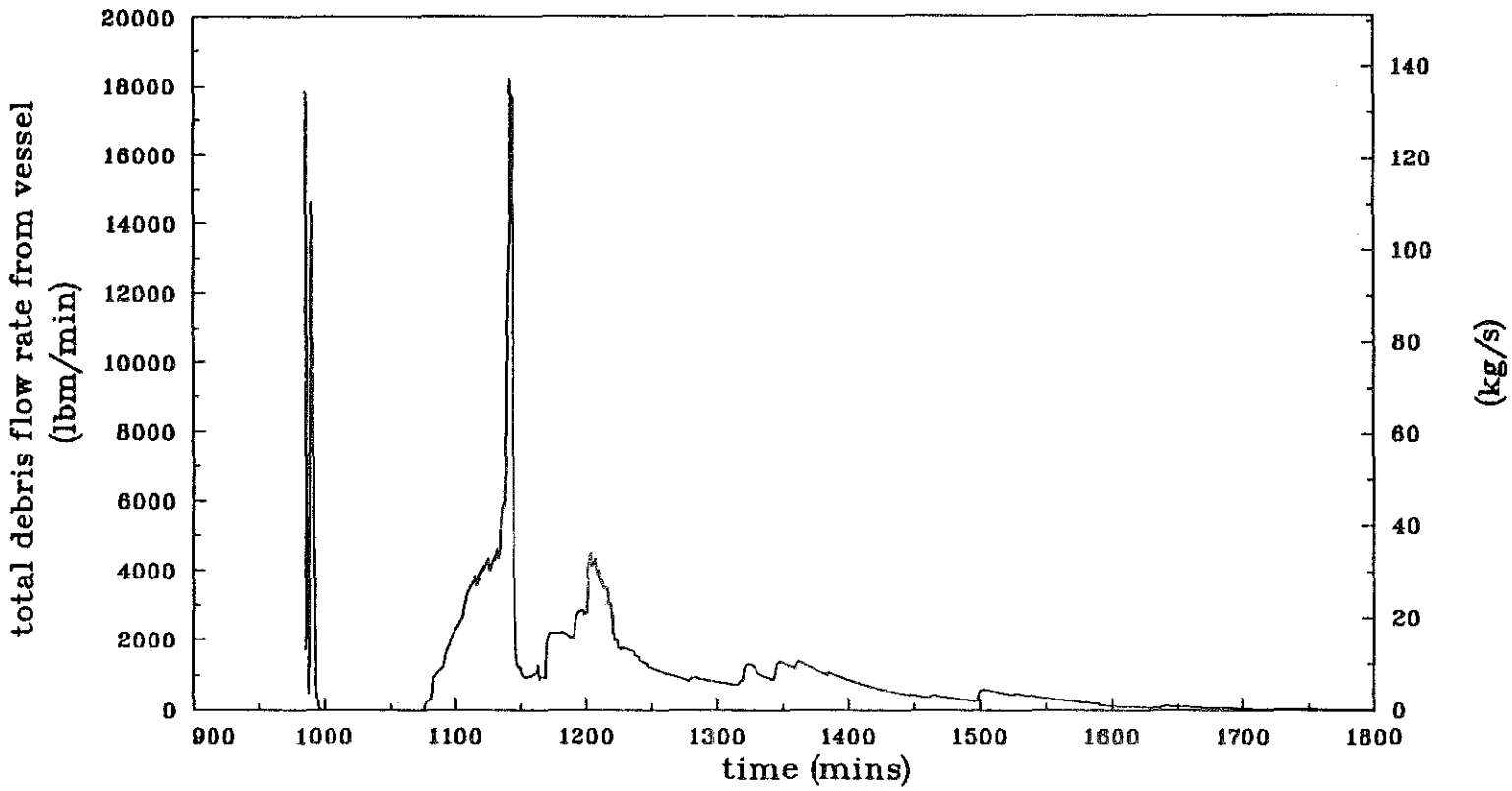

Fig. 4.3.7. The combined metal and oxide pours from the reactor vessel for the BWR-4/Mark II long-term station blackout sequence.

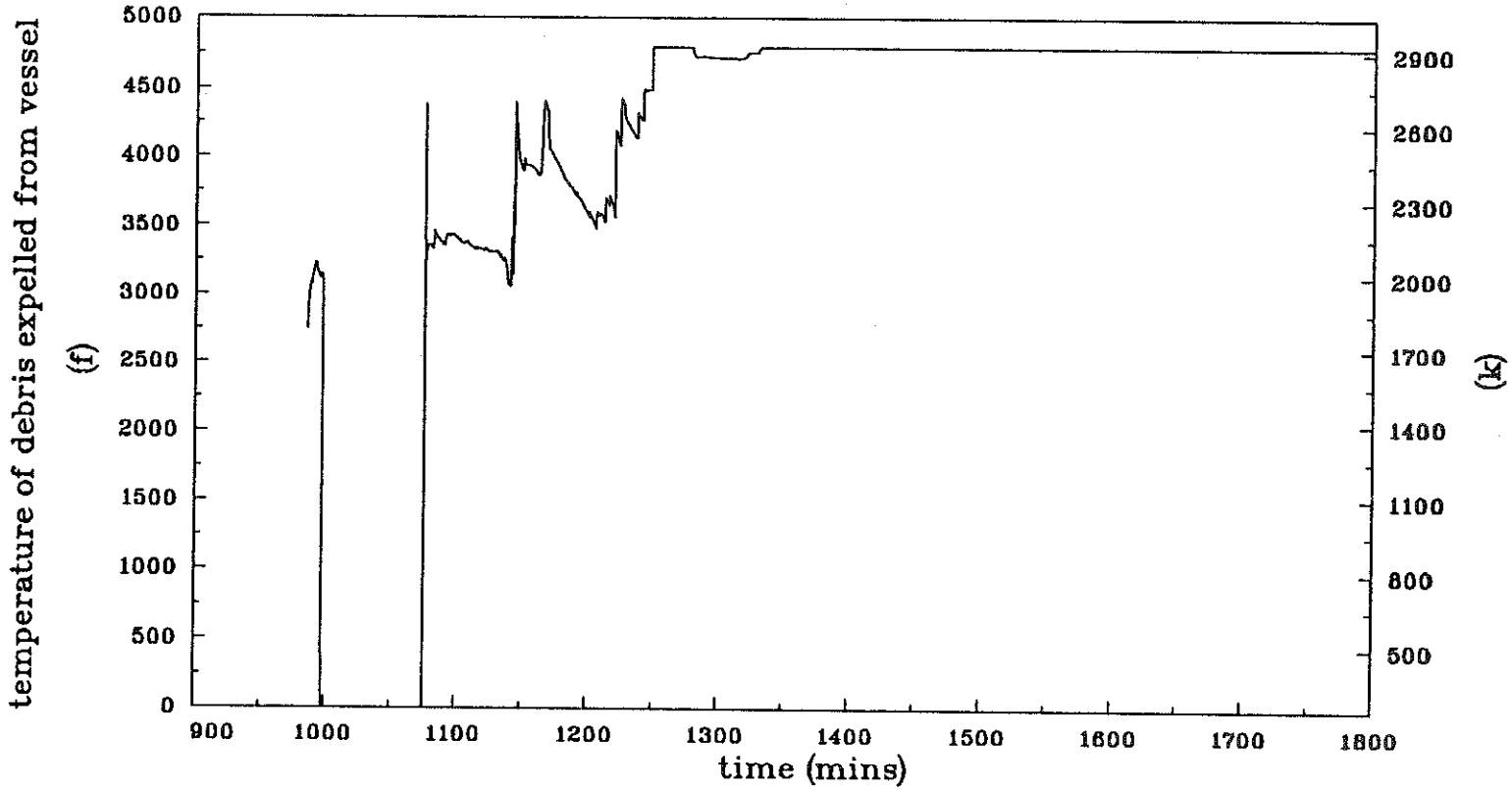

Fig. 4.3.8. Mass-averaged temperature of the debris pours from the reactor vessel for the BWR-4/Mark II long-term station blackout sequence.

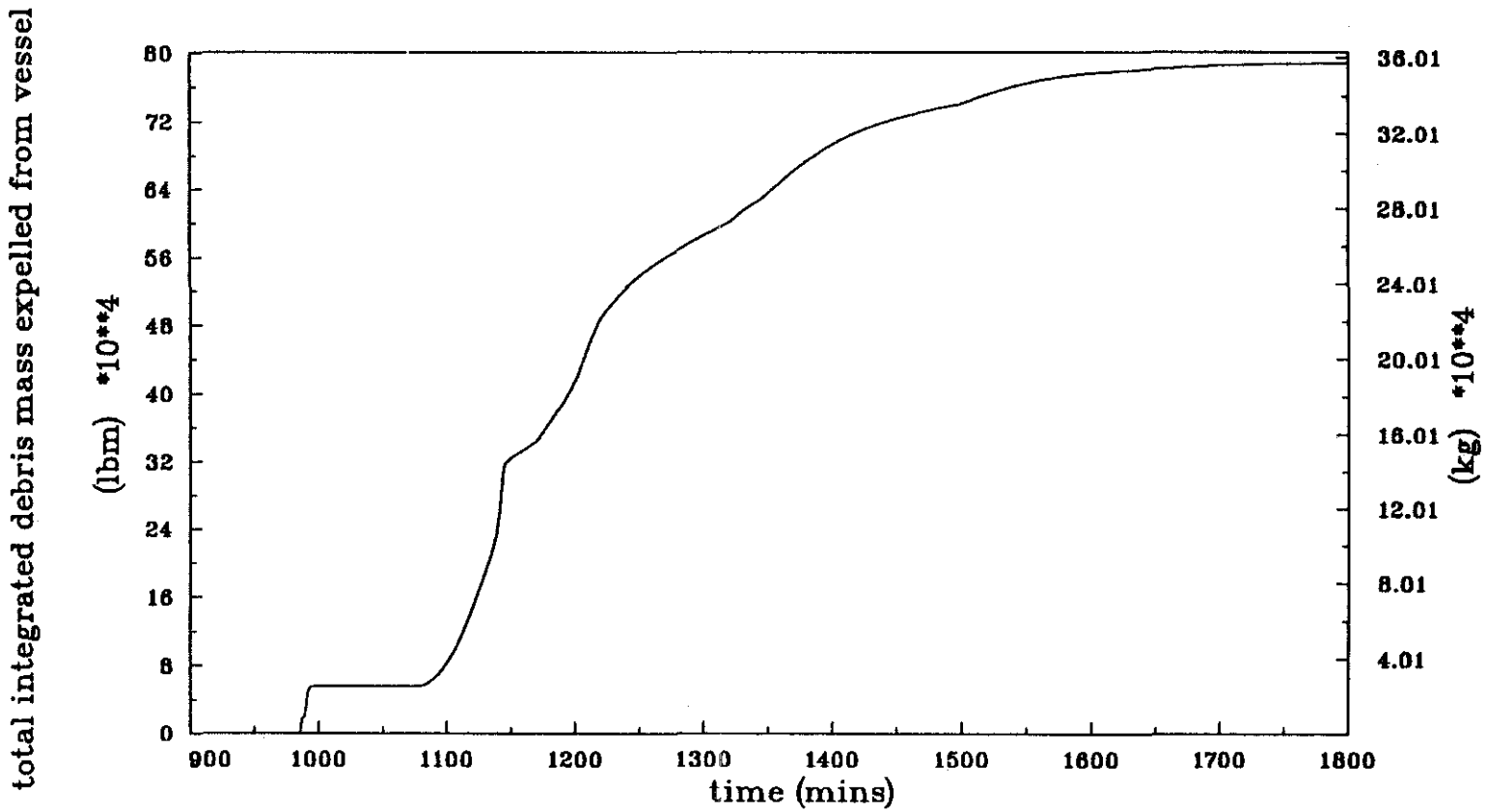

Fig. 4.3.9. Integrated combined metal and oxide release from the reactor vessel for the BWR-4/Mark II long-term station blackout sequence.

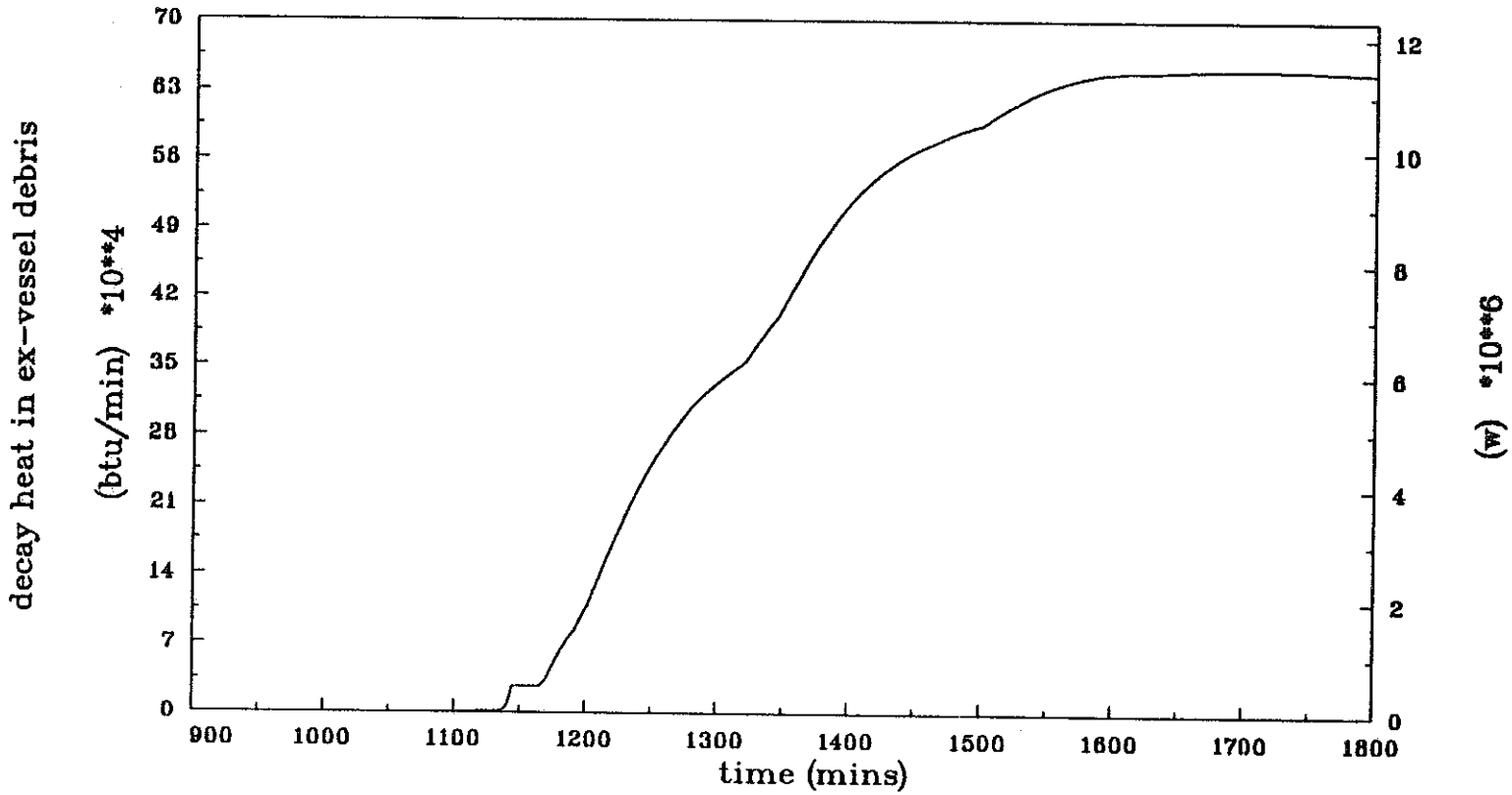

Fig. 4.3.10. Decay power in ex-vessel debris for the BWR-4/Mark II long-term station blackout sequence.

5. MARK II CONTAINMENT DESIGN DESCRIPTION*

The Mark II Containment utilizes the "over-under" design in its suppression pool arrangement. This type of containment is used on only five late-model BWR/4 and all BWR/5 reactors (Table 1.2). Typical Mark II containments are illustrated in Figs. 5.1 and 5.2. Mark II containment design specifications are listed in Tables 5.1 and 5.2.

The Mark II design provides a more compact arrangement of the pressure suppression system and reactor building than does the Mark I design. The containment is constructed with the suppression chamber located directly below the drywell in the same structure. The base foundation slab is a reinforced concrete mat approximately 7 ft thick.

The drywell and suppression pool are steel-lined structures constructed of either prestressed or reinforced concrete in the shape of a truncated cone and cylinder, respectively. The drywell head is bolted to a steel ring girder which is attached to the top of the concrete containment wall. The floor of the drywell serves as a pressure barrier between the drywell and suppression chamber and provides lateral positioning for the reactor pedestal and support for the downcomers. The drywell cone and suppression pool cylinder are 80 and 60 ft high, respectively. The drywell floor is approximately 3 ft thick.

The reactor pedestal wall thickness in the drywell region varies between 4-6 ft thick. The reactor pedestal stands 84 ft tall from its base in the pressure suppression pool to the vessel support lip. The pedestal may be either hollow (Fig. 5.1) or solid (Fig. 5.2) in the suppression pool region (plant-dependent). Figure 5.3 depicts the reactor pedestal designs employed in each of the six Mark II plants. All Mark II plants except La Salle have hollow pedestals in which the wetwell in-pedestal volume is open to the suppression pool via openings in the pedestal wall, and the region inside the pedestal is partially filled with water. The hollow pedestal region directly beneath the vessel in the drywell is accessible through open manways. In some plants, the drywell floor elevation inside the reactor pedestal is several feet lower than that outside the pedestal, forming a concrete cavity directly beneath the reactor vessel (Fig. 5.3). Shoreham and Nine Mile Point-2 have downcomers located within their reactor pedestal directly beneath the reactor vessel (four at Shoreham, eight at Nine Mile Point-2). At Shoreham, a curb was fitted around the inner circumference of the pedestal to contain the core debris within the in-pedestal region above the drywell floor. La Salle, Limerick, and WNP-2 have in-pedestal drain

*The discussion in this chapter is excerpted from Ref. 14.

lines which penetrate the in-pedestal drywell floor. Susquehanna-1 and-2 have no in-pedestal drywell floor penetrations.

Vacuum breakers are provided to equalize the static pressures between the suppression chamber and the drywell. They provide a controlled return flow path from the suppression chamber to the drywell to assure design operation of the suppression chamber in the event of a steam leak. In contrast to the Mark I system, only one of the Mark II plants (WNP-2) provides vacuum relief between the inside of the primary containment and the reactor building atmosphere. The concrete containment structure has the ability to accommodate subatmospheric (negative) pressures of approximately 5 psia (-9.7 psig).

The reactor building completely encloses the reactor and its primary containment. The structure provides secondary containment when the primary containment is closed and in service, and primary containment when the primary containment is open, as it is during the refueling period. The reactor building houses the refueling and reactor servicing equipment, the new and spent fuel storage facilities, and other reactor auxiliary or service equipment, including the reactor core isolation cooling system, reactor water cleanup system, standby liquid control system, control rod drive system, the emergency core cooling systems, and electrical equipment components.

The reactor building exterior walls and superstructure up to the refueling floor are constructed of reinforced concrete. Above the level of the refueling floor, the building structure in all Mark IIs except Limerick is fabricated of structural steel members, insulated siding, and a metal roof. Joints in the super-structure paneling are designed to assure leak tightness. Limerick's entire reactor building is constructed with a reinforced concrete superstructure. Penetrations of the reactor building are designed with leakage characteristics consistent with leakage requirements of the entire building. The reactor building is designed to limit the inleakage to 100% of the reactor building free volume per day at negative 0.25 in. H_2O gauge, while operating the standby gas treatment system. (Limerick's reactor enclosure is designed to limit inleakage to 100% free volume per day, and the refueling floor is designed to limit inleakage to 50% free volume per day.) The building structure above the refueling floor is also designed to contain a negative interior pressure of 0.25 in. H_2O gauge.

Table 5.1. Domestic BWR Mark II design parameter

Parameter	Lim	LaS	Sus	NMP	Sho	WNP
Power (Mwt)	3293	3293	3293	3300	2436	3293
Design (psig)	55	45	53	45	48	45
	-5	-5	-5	-5	-5	-2
Drywell Design Temp (°F)	340	340	340	340	340	340
Wetwell Design Temp (°F)	220	275	220	212	225	225
Drywell Free Volume (ft^3)	243600	230000	240000	303000	193000	201000
Wetwell Free Volume (ft^3)	282000	297000	282000	347000	215000	256000
Total P.C. (ft^3/Mwt)	160	160	158	197	167	139

Lim = Limerick
LaS = La Salle
Sus = Susquehanna
NMP = Nine Mile Point-2
Sho = Shoreham
WNP = WNP-2
P.C. = Primary Containment

Table 5.2 Mark II Downcomer Design Characteristics[a]

Plant	No. of Downcomers	Nominal Diam. (in.)	Lip Height[b] (in.)
Limerick	87 ex-pedestal	24	18
La Salle	98 ex-pedestal	23.5	18
Susquehanna	82 ex-pedestal	24	18
WNP-2	84 ex-pedestal	24	< 2 (est)
	18 ex-pedestal	18	< 2 (est)
Nine Mile Pt. 2	115 ex-pedestal	23.25	3-6
	8 in-pedestal	23.25	3-6
Shoreham	78 ex-pedestal	23.25	6
	4 in-pedestal	23.25	<0.5

[a]From Updated Final Safety Analysis Reports.

[b]Distance from surface of drywell floor to top of downcomer.

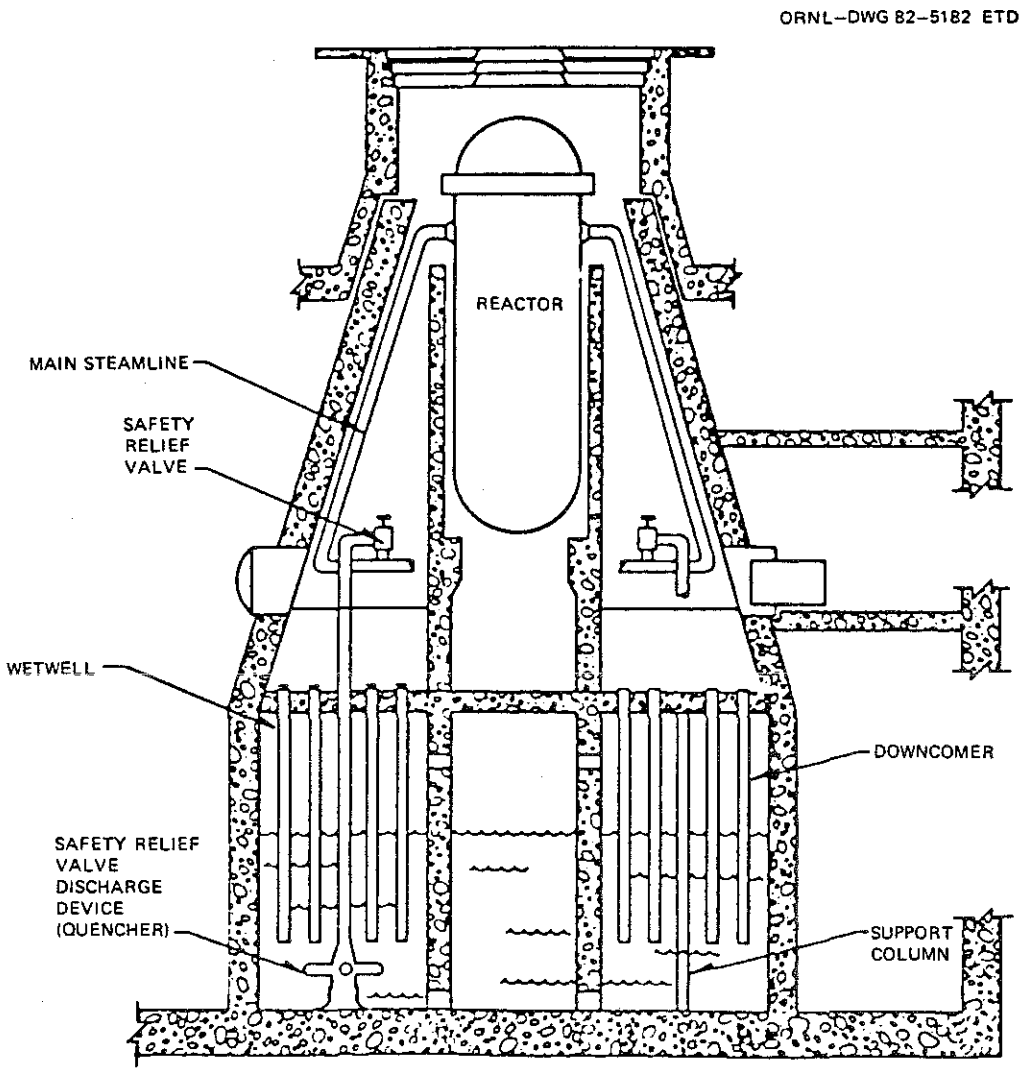

Fig. 5.1. Limerick Mark II containment.

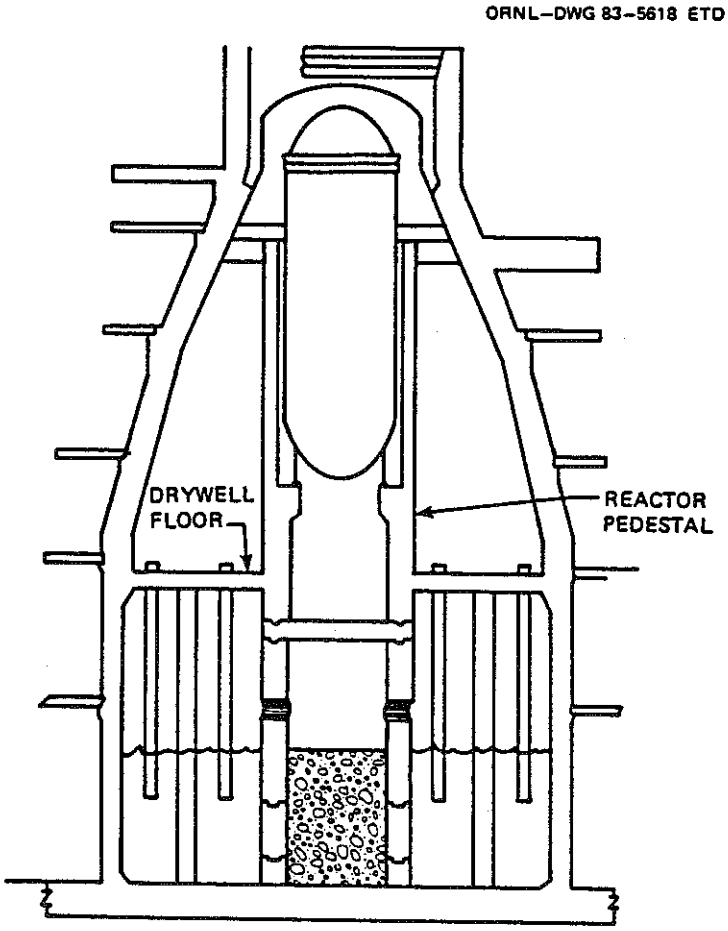

Fig. 5.2. La Salle Mark II containment.

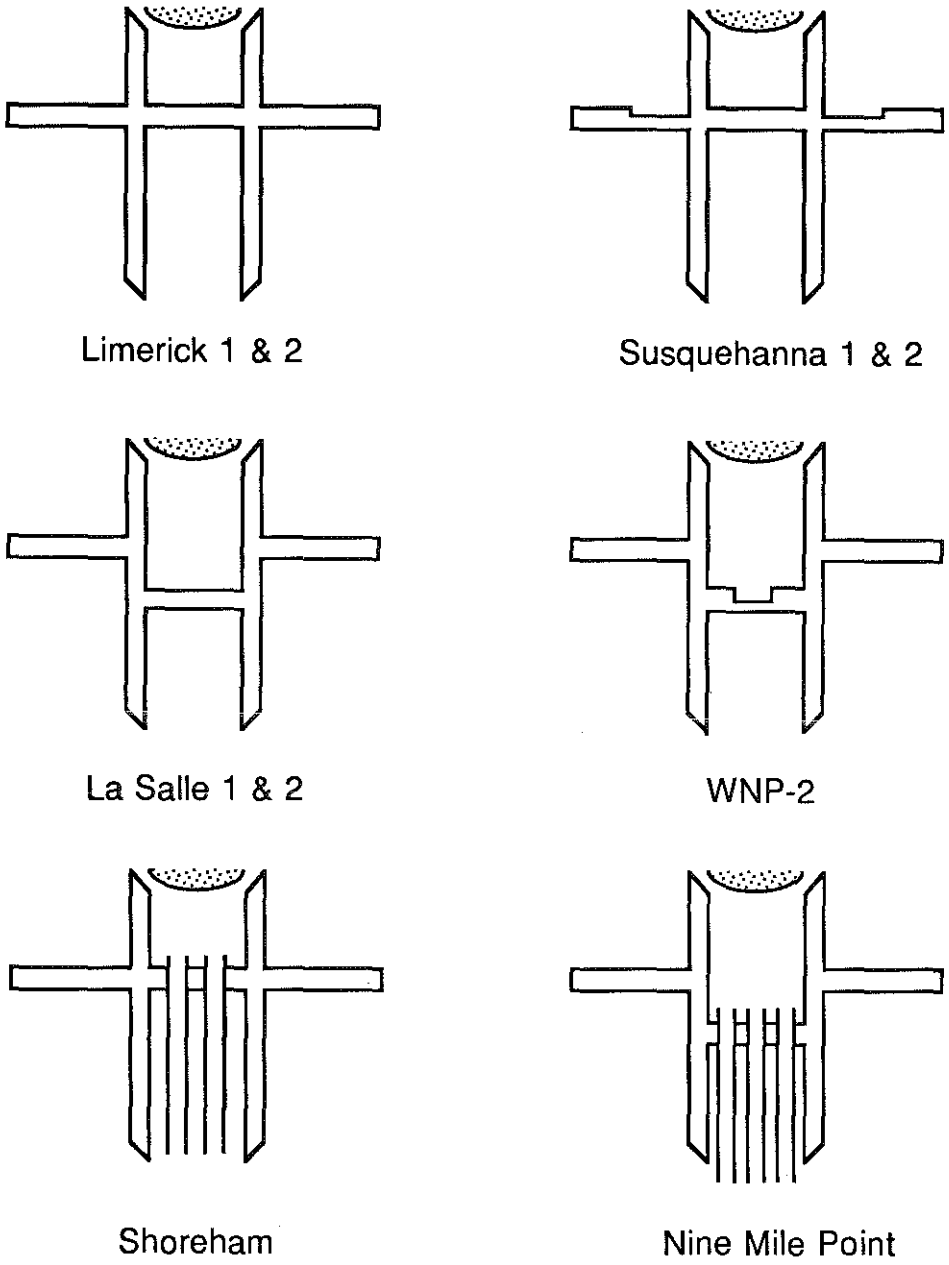

Fig. 5.3. Mark II reactor pedestal designs.

6. MARK II CONTAINMENT FAILURE MODES AND MECHANISMS

Historically, the dominant primary containment failure mechanism considered in BWR severe accident analyses was over-pressure failure of the steel primary containment shell (Refs. 15 and 16). The pressure and location at which failure would occur are plant-dependent. Failure pressures for Mark II containments have been predicted to range between 120-160 psig (Refs. 16-18). The most probable over-pressure failure location for Mark II plants appears to be the primary containment liner in the wetwell airspace above the surface of the pressure suppression pool (Ref. 16). A potentially important feature of this failure location is that primary containment blowdown would enter the lowest portions of the reactor building, thus affording the maximum opportunity for scrubbing of fission products and aerosols prior to their release to the environment. However, the associated release of steam into the building would inhibit any subsequent equipment recovery efforts in that locale.

A second potential mechanism for BWR primary containment failure is primary containment shell or penetration failure due to collapse of the reactor vessel caused by ablation of the reactor's concrete support pedestal or the drywell floor. Recent ORNL studies have revealed that more than 75% of the reactor pedestal wall thickness may be eroded due to concrete ablation for some pedestal designs (Ref. 19). The probability of the failure mode is a strong function of the amount of zirconium metal available for oxidation on the drywell floor. It should be noted that the weight of the reactor vessel and internals would be decreased prior to pedestal failure due to expulsion of the core and core support materials following reactor vessel failure. The resulting load on the reactor pedestal would, therefore, be significantly reduced. Unfortunately, the most probable location for primary containment failure following pedestal or drywell floor collapse is not known with certainty (and is probably plant-specific).

A third type of primary containment failure in Mark I and II plants is failure of the drywell head flange seals (Ref. 20). The Idaho National Engineering Laboratory and Sandia National Laboratories have recently conducted thermal performance tests of seals similar to those employed in BWRs (Refs. 21 and 22). These experiments indicate that the seals lose their elasticity and structural integrity when subjected to temperatures of 700°-750°F. Recent ORNL calculations indicate that drywell head flange temperatures of 900°-1068°F may be reached in some Mark I accident sequences. Failure of these head flange seals is a particular concern, since drywell blowdown via this pathway would

enter the region between the drywell head and the drywell shield plugs located in the floor of the refueling bay - and then directly into the refueling bay itself. The reactor building and the various reactor building fission product retention mechanisms could be bypassed in this scenario. The actual flow area available for leakage through this path is a function of both the seal elasticity (springback) and the drywell head flange clamping force (Ref. 20). The clamping force is a function of the reactor system pressure, head closure design (type of closure arrangement, number of closure bolts or pins, bolt length, bolt diameter, etc.), the thermal gradient across the closure fixtures, and the head flange bolt preload (Refs. 20, 23, and 24). Reference 20 indicates that head seal leakage at the Peach Bottom Plant would begin at 82 psig for zero gasket springback. These results are widely applied to other plants, *but are probably applicable only to Peach Bottom since the head closure designs (Table 6.1) and head flange bolt preload are highly variable, plant-specific characteristics.* It is, therefore, probable that the actual conditions under which the drywell head would leak are very plant-dependent.

Table 6.1. Mark II drywell head closure design data

Plant	Closure Type	Head Diam. (ft)	No. Bolts/ Pins	Bolt Diam. (in.)	Bolt Length (in.)
Peach Bottom[a]	Bolted Flange	32.25	68	2-1/2	44
Limerick	Bolted Flange	37.63	80	2-3/4	32
La Salle	Bolted Flange	31.45	60	3	30
Shoreham	Bolted Flange	30.17	128	2	19
Susquehanna	Bolted Flange	37.63	80	2-3/4	32
Nine Mile Pt. 2	Horizontal Finger Pin Joint	34.00	48	3	N/A

[a]Peach Bottom (Mark I) shown for reference only. Other Mark I plants have different drywell head closure designs.

7. MELCOR MARK II CONTAINMENT MODEL DESCRIPTION

The Mark II primary containment model employed for these calculations incorporates elements of the Susquehanna, La Salle, and WNP-2 designs. The containment volume and heat sink surface areas are based on the Susquehanna design, while the in-pedestal region of the drywell is based on the WNP-2 design. The WNP-2 and La Salle designs incorporate a deep in-pedestal drywell cavity with a volumetric capacity substantially larger than the volume of core debris resulting from a 100% core-melt accident. This cavity design was selected to minimize the impact of core-concrete interaction modeling limitations associated with the application of CORCON (stand-alone or as module in MELCOR) to pedestal designs that do not incorporate a cavity (such as the Limerick and Susquehanna designs). CORCON, which was originally developed to model the results of core-concrete interaction experiments in well defined crucible geometries, does not have the capability to model the flow and spreading of core/concrete debris that would occur in flat-floored designs.

Figure 7.1 is a schematic representation of the ORNL MELCOR Mark II containment model. Table 7.1 summarizes some of the more important model parameters. The model consists of nine control volumes representing the interior pedestal region of the wetwell, the remainder of the wetwell, the 87 downcomers (single cell), the interior pedestal region of the drywell, the remainder of the drywell (4 cells), and the annular gap between the reactor vessel and the inside of the reactor shield wall. Fifteen flow paths are employed to represent the architectural features (such as ports in the reactor pedestal and shield wall) which facilitate circulation between the drywell and wetwell, and between the in-pedestal and ex-pedestal regions of the drywell and wetwell.

Mark II drywell vacuum breakers do not require AC or DC power for operation. Susquehanna employs five 2.05 ft^2 vacuum breakers which fully open within one second under a 0.78 psi pressure differential (Ref. 25). The five drywell vacuum breakers are modeled as six independent, parallel flow paths between the wetwell airspace and the downcomers. Small variations in the as-built vacuum breakers will normally result in one breaker which begins to cycle at slightly lower pressure differentials than the others. This vacuum breaker would, therefore, tend to cycle more frequently than the other breakers. The complexity of the vacuum breaker model was dictated by a desire to provide a detailed analysis of the expected number of opening and closing cycles during an accident sequence. The vacuum breaker models are based on actual test data supplied

to ORNL by Pennsylvania Power and Light (PP&L), and may not be representative of those employed in other Mark II plants. The first four flow paths each represent 25% of the flow area of a *single* vacuum breaker, and are staged to open over the first 20% of the actual measured pressure differential required for full opening of a vacuum breaker valve (Fig. 7.2). The fifth flow path represents a second vacuum breaker (100% of the flow path area of a single vacuum breaker), and is programmed to open over the second 20% of the actual measured vacuum breaker opening pressure interval. The sixth flow path represents the remaining three vacuum breakers (300% of the flow area of a single vacuum breaker), and is programmed to open over the last 60% of the total opening pressure differential. Thus, the number of times the first "pseudo-vacuum-breaker" cycles represents the number of times 25 % of a vacuum breaker would be required. The number of times the second "pseudo-vacuum-breaker" cycles represents the number of times 50 % of a vacuum breaker would be required, etc.

Thirty-one heat slabs are incorporated in the model to represent the various floors, walls, and structures that provide heat sinks within the primary containment (Table 7.1). The cylindrical portion of the reactor pressure vessel (RPV) is represented as a heat sink which communicates with the reactor volume on one side and the shield wall annulus atmosphere on the other. A time-dependent boundary condition (temperature) is applied to the inner surface of the structure to maintain the surface at the temperature of the SRV discharge (which is employed as a mass/energy source to the pressure suppression pool).

Water vapor and CO_2 are released from concrete structures as the structures are heated. As implemented, the outgassing model assumes free water is released from concrete structures over an interval of 190°-221°F. The chemically-bound water is released from concrete structures over the interval of 221°-968°F. The CO_2 is assumed to be released from concrete structures over the interval of 1021°-1472°F. These input assumptions are based on experimental data from Sandia National Laboratories (Ref. 26).

The model incorporates two primary containment failure modes. The first failure mode is a simple over-pressure failure which opens a 0.1 ft^2 hole in the wetwell airspace region when the pressure in that region exceeds 135 psig. The second failure mode simulates the combined over-pressure/over-temperature failure of the drywell head flange seals (see Chapter 6). The model is constructed in accordance with the Chicago Bridge and Iron Company results for Peach Bottom (Ref. 20) so that the drywell head flange seals begin leaking when the drywell pressure is greater than 82 psig if the head flange temperature has exceeded 700°F at any previous time in the transient. The seal leakage

area ramps from 0.0 in.^{2} at 82 psid, to 662 in.^{2} at 200 psid. This leak enters the reactor well in the region between the reactor shield plugs (in the refueling bay floor) and the drywell head. This region is modeled as a separate control volume (Fig. 7.1).

Both a "single-cavity" and a "dual-cavity" version of the Mark II model were developed. The single-cavity version of the model employs a single active CORCON cavity (for core-concrete interaction simulation) in the in-pedestal region of the drywell. This model is useful for examination of scenarios in which all of the debris escaping the reactor vessel is held within the in-pedestal drywell region. The dual-cavity version of the model employs both the in-pedestal drywell cavity as well as a cavity representing the in-pedestal region of the wetwell. This model is useful for examination of scenarios in which debris enters the in-pedestal region of the wetwell via in-pedestal downcomers, or due to melt-through of the drywell floor drains.

The interface between the BWRSAR and MELCOR codes is provided via the External Data File (EDF) option in MELCOR. Utilization of the EDF option necessitated modification of an existing BWRSAR post processor routine, and the addition of an "interface" control volume to the ORNL containment model. Because MELCOR will not permit externally-sourced hydrogen to be injected into water pools, a special interface cell was added to the model to receive the hydrogen source and route it to the pressure suppression pool. The MELCOR code input is constructed to source the BWRSAR-generated SRV flows into the interface cell. The vessel leakage flows into the in-pedestal region of the drywell. The debris pours into the appropriate CORCON cavity (in-pedestal drywell or in-pedestal wetwell), as required for the specific case under investigation. The details of the method employed to interface BWRSAR and MELCOR are provided in Appendix A.

Table 7.1. ORNL Mark II containment model parameters

Control Volume Name	Free Volume (ft^3)	Heat Slab Name	Material Liner/Middle/Outer
Drywell:			
In-pedestal	11,018	pedestal wall 1	concrete
		pedestal wall 2	concrete
		RPV bottom head	steel
		floor	steel/concrete/steel
Ex-pedestal 705'-723'	65,685	exterior wall	steel/concrete
		floor	steel/concrete/steel
		misc. steel	steel
Ex-pedestal 723'-758'	91,677	exterior wall	steel/concrete
		shield wall	steel/concrete/steel
		misc. steel	steel
Ex-pedestal 758'-779'	25,497	exterior wall	steel/concrete
		misc. steel	steel
Ex-pedestal 779'-809'	37,151	drywell head	steel
		drywell head flange	steel
		RPV head	steel
		exterior wall	steel/concrete
		misc. steel	steel
Reactor-Shield Wall Annulus	636	shield wall	steel/concrete/steel
		RPV wall	steel
Downcomers	11,689	downcomer wall (airspace)	steel
		downcomer wall (submerged)	steel
Wetwell:			
In-pedestal	15,821	pedestal wall (airspace)	steel/concrete/steel
		pedestal wall (submerged)	steel/concrete/steel
		floor	steel/concrete
Ex-pedestal	264,330	exterior wall (airspace)	steel/concrete
		exterior wall (submerged)	steel/concrete
		support columns (airspace)	steel
		support columns (submerged)	steel
		floor	steel/concrete
Reactor Well	11,159	exterior wall	steel/concrete
		shield plugs	concrete

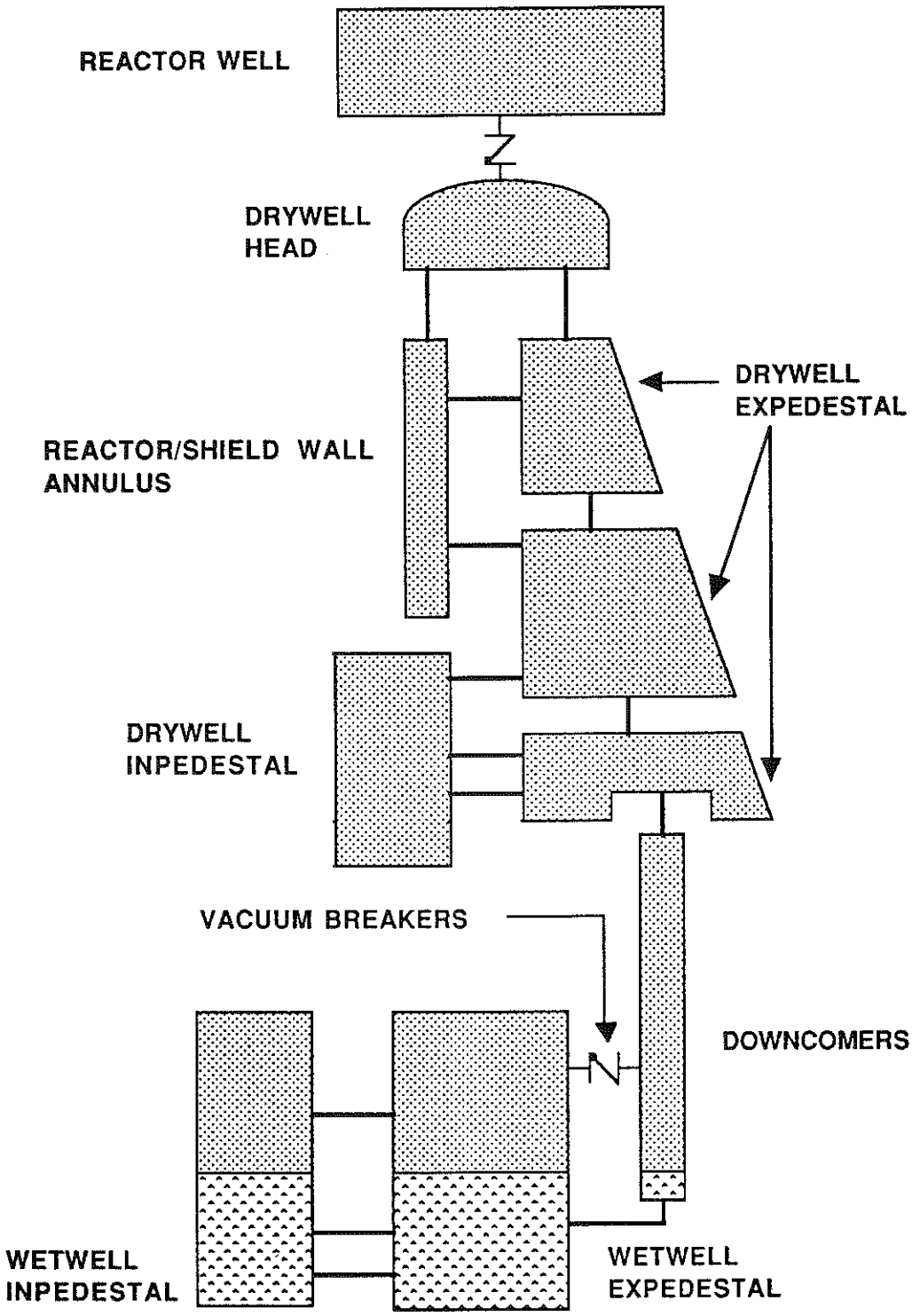

Fig. 7.1. ORNL Mark II containment model.

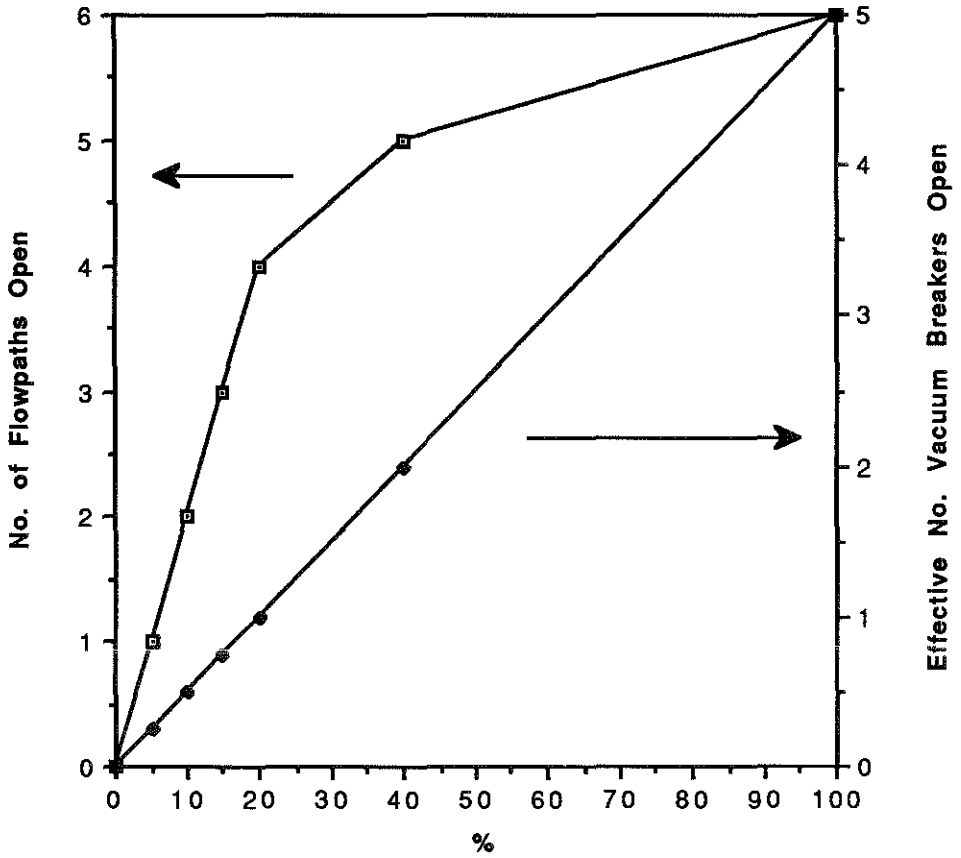

Fig. 7.2. Mark II vacuum breaker model characteristics.

8. MARK II CONTAINMENT RESPONSE TO UNMITIGATED SHORT-TERM STATION BLACKOUT

8.1 INTRODUCTION

This chapter presents the containment response results obtained by MELCOR analysis of three short-term station blackout scenarios The basic short-term station blackout scenario is described in Chapter 1. The first scenario analyzed is the "base case" short-term station blackout scenario in which the ADS is actuated in accordance with Revision 3 of the EPGs. The second scenario is the case in which the operator either fails to initiate the ADS, or a system failure results in an inability to depressurize the reactor. The third scenario is similar to the base case except it is assumed the diesel-driven fire protection system pump is used to spray water into the drywell via the existing drywell spray system header. The in-vessel BWRSAR analyses are reported in Chapter 3 and the primary containment model is described in Chapter 7. The containment failure models described in Chapter 7 were disabled for these calculations.

The MELCOR analysis of the containment response was performed subsequent to completion of the BWRSAR calculations and represents the same period of the accident sequence. The initial containment atmospheric conditions for MELCOR were specified to be the same as those used by BWRSAR and the time-dependent conditions were calculated in response to the mass and energy sources generated by BWRSAR. These sources consist of SRV discharges (steam and hydrogen) into the wetwell pool, leakage of water from the reactor coolant system, discharge of steam and hydrogen flows from the bottom head of the reactor vessel after the head penetrations fail, and debris pours from the failed reactor vessel bottom head. The containment calculations progressed from the time of core uncovery (35 min) and continued throughout the core degradation and relocation period.

8.2 SEQUENCE WITH ADS ACTUATION (All Core Debris Retained in Drywell)

The base case Mark II short-term station blackout analysis involves the following conditions:

1. ADS is initiated when core water level reaches one-third of core height in accordance with Revision 3 of the BWR Owners Group EPGs.
2. No AC power is available. Hence
   - HPCI & RCIC are unavailable, and
   - containment sprays are not available.
3. All containment failure mechanisms are disabled.

The calculation was terminated when the drywell floor within the in-pedestal region cavity was calculated to have been completely ablated in the axial direction (3.6 ft) at 810 min into the accident.

Because BWRSAR models the Mark II drywell as a single cell, it is not possible to specify the initial atmospheric temperature and composition spatial distributions. Likewise, it is not possible to specify the corresponding spatial temperature distributions of the drywell structures. For the current MELCOR analyses, uniform initial atmosphere temperatures and compositions were specified consistent with the BWRSAR results. (This is reasonable since significant intercell differences would not develop by time 35 min.) The thermal conditions for the structures were conservatively initialized to the steady state values consistent with the input atmospheric temperatures. This leads to a somewhat higher energy state within the structures than that corresponding to BWRSAR at the beginning of the calculation. This is conservative with respect to calculated containment pressures as the following paragraphs indicate.

The phenomenon of concrete degassing at elevated temperatures provides a source of containment water vapor in addition to the BWRSAR sources described above. Because containment atmosphere temperatures are elevated in the latter phases of severe accidents, the structures may reach temperatures high enough to cause significant gas loss and containment pressurization. Figure 8.2.1 presents the calculated ex-pedestal wetwell pressure for similar calculations differing only in whether or not degassing is modeled. The degassing case exhibits an initial pressure rise not calculated by the case in which structural degassing is not considered. This initial degassing pulse is due to the initial drywell concrete structural temperatures which are slightly above the threshold for steam evolution. The pressure rise is approximately 10 psi and is maintained/increased throughout the remainder of the calculation. This approach is conservative because the degassing calculation provides a continuous source of gas which pressurizes the containment.

Figure 8.2.2 presents the time-dependent pressure distribution calculated for the Mark II primary containment. As can be seen, the pressure for the in-pedestal drywell region experiences a large pressure spike (35 psi) due to the initial gas release from the concrete reactor pedestal. However, the containment does not reach the 135 psig level required for wetwell failure at any time during the calculation. The pressure is continuing to rise at the time of floor rupture. Thus, it would not be reasonable to conclude that the maximum pressure had been reached or that the containment would not fail due the the steam spike which is expected to occur when the drywell debris falls into the suppression pool.

There are distinct discontinuities exhibited by the pressure traces of Fig. 8.2.2. These are caused by significant events in the progression of the transient. At times 130 and 220 min, the pressure increases markedly due to the discharge of steam and hydrogen gases through the SRVs into the wetwell pool. At 270 min, another rise occurs as the reactor vessel bottom head is calculated to fail and debris begins to pour onto the drywell floor. Another break occurs as the second debris pour commences at 380 min. A final pressure increase is noted at 675 min. This corresponds to the rapid release of carbon monoxide from the debris as the carbon from the coking reaction begins to react with the carbon dioxide and water vapor released from the concrete (see discussion below).

Figure 8.2.3 depicts the primary containment atmospheric temperature distribution as a function of time. Once again, there are noticeable discontinuities in the temperature traces. At times 130 and 220 min, the temperatures rapidly increase in response to the SRV discharges mentioned earlier. It is also interesting to note that the maximum temperature occurs in the annulus between the biological shield and the outer surface of the reactor vessel. This is because the time-dependent temperature boundary condition employed at the inner surface of the reactor vessel wall. For these calculations, it was assumed that the inner surface was at the SRV gas discharge temperature.

Notice also that there is no obvious increase in the in-pedestal air temperature at the time of reactor vessel bottom head failure (270 min). This is because the debris falls into a shallow pool of water created by normal primary coolant system water leakage prior to failure of the bottom head. By 290 min, however, this water has been vaporized and the debris immediately begins to heat the in-pedestal atmosphere and the temperature increases rapidly. At 380 min, the second major debris pour commences and the in-pedestal air temperature rapidly increases. At approximately 550 min, the upper oxide layer top crust melts, and rapid heat transfer to the in-pedestal atmosphere ensues.

A final note on the atmosphere temperature distribution: as shown in Fig. 8.2.3, the drywell head atmosphere temperature reaches approximately 720°F by the end of the calculation at 810 min. In contrast, the calculated results also indicate that the drywell head flange reaches only 573°F. This is because the head flange is bounded on the inner surface by the drywell head atmosphere and on the outside by the cooler atmosphere within the reactor well. Although the calculated temperature of the atmosphere within the reactor well increased from 109°-427°F, the head failure criteria described in Chapter 6 were not met.

It should be noted that there is a substantial temperature difference (350°F at 810 min) between the hottest and coldest regions of the primary containment. The ability to consider regional temperature differentials within the containment is a result of the detailed nodalization scheme employed for the Mark II model. This phenomenon could not be calculated if simpler nodalizations were used. Determination of regional temperatures within the drywell is necessary if judgements concerning local effects such as failure of the drywell head flange seals are to be made.

Figure 8.2.4 depicts the calculated debris temperatures for the drywell floor in-pedestal cavity. Both the heavy oxide and metal layer temperatures rapidly increase as the debris begins pouring from the failed reactor vessel at 270 min. The layer temperatures reach a local peak of approximately 1900°F at 300 min due to the termination of the pour from the reactor vessel. The debris accumulated on the drywell floor up to this point consists mostly of metals and contains very little decay heat. Because there is no additional pour from 300-380 min, the debris cools and the temperatures decrease. The debris temperatures once again begin to increase as the second massive debris pour commences at 380 min.

At approximately 400 min, the debris reaches the ablation temperature of the limestone common sand concrete (2245°F) and concrete ablation begins. Because the pouring debris contains a mixture of low melting temperature metals (2750°F) and higher melting temperature oxides (4800°F), the debris pour temperature is between the two melting temperatures and the cavity debris temperatures continue to rise. The heavy oxide layer is at the bottom of the debris pool and it has a much higher melting temperature than the overlying metal layer. Thick crusts initially form that insulate the bulk of the oxide layer and the oxide layer temperature increases more rapidly than the overlying metals. This is the reason for the diverging layer temperatures between 400-490 min.

A light oxide layer is predicted to form on top of the metal layer at approximately 460 min. This is due to the small content of UO_2 in the debris pour after 460 min. Because UO_2 is extremely dense, and because it constituted a large fraction of the earlier portion (380-460 min) of the second pour, all of the oxide pouring from the reactor vessel from 300-460 min settled to the bottom of the debris pool and no upper oxide layer could form. After 460 min, the UO_2 content of the debris pour is small. When the debris pour oxide combines with the concrete oxide rising through the metal layer, a buoyantly stable upper oxide layer is formed.

After 490 min, the heavy oxide layer temperature begins to decrease due to the increased heat losses. The increased heat losses stem from the melting of the heavy oxide and metal layer crusts resulting in the calculation of large intralayer convective heat transfer coefficients. This results in effective homogenization of the debris temperature distribution -- decreasing the heavy oxide layer temperature while increasing the metal and light oxide layer temperatures. The melting of the heavy oxide layer is due to the increasing concentration of the concrete oxides in the heavy oxide layer. Since the concrete oxides (SiO_2 and CaO) melt at lower temperatures than the core debris oxides (UO_2 and ZrO_2), mixing the two oxides results in a lowering of the heavy oxide solidus temperature. Thus the heavy oxide layer experiences thinning of its crusts which lowered the thermal resistance to conduction heat transfer at the boundaries of the layer and the heavy oxide layer temperature began to decrease.

Concrete oxide dilution of the heavy oxide layer continued until approximately 585 min. At this time, the heavy oxide layer density was calculated to be less than the overlying metal layer density and the code performed a "layer flip" of the metal and heavy oxide layers. In addition, the material of the formerly heavy oxide layer was combined with that of the light oxide layer so that the resulting mixture of light oxides was placed on top of the metal layer.

At 675 min, the debris temperatures drop due to depletion of the unoxidized zirconium and the reduction of the chemical power supplied to the debris. The carbon inventory which had been accumulating in the metal layer begins to react with the CO_2 released by the ablation of concrete. The process produces large quantities of CO according to the following reaction:

$$C + CO_2 \rightarrow 2CO .$$

As can be seen, there are two moles of gas produced by this reaction for every mole of gas consumed. Figure 8.2.5 shows the cumulative debris gas releases for CO, CO_2, H_2, and H_2O. The CO release is very rapid and occurs only after the oxidation of all of the zirconium. This is the reason for the increased rate of pressure rise at 675 min as shown in Fig. 8.2.2.

Figure 8.2.6 depicts the axial and radial concrete ablation distances calculated for this transient. The concrete floor of the drywell is 3.74 ft thick and the cavity is 9.55 ft deep. Thus, the bottom (lower surface) of the drywell floor is located at the depth of 13.3 ft. The floor is penetrated at 810 min and the calculation is terminated.

These results should not be generalized to conclude that all Mark II drywell floors would be completely ablated for a depressurized short-term station blackout scenario. The main reason for this limitation is that the current calculation assumes a deep cavity exists and that the core debris will be maintained in a crucible geometry. Figure 8.2.7 shows that the total debris thickness is approximately 8.2 ft at 810 min, and is well below the 13.3 ft thickness required before overflow onto the remaining drywell floor can occur. In this configuration, the debris has limited surface area through which it can lose heat to the atmosphere. Thus, more heat is transferred downward into the underlying concrete and more concrete is ablated. Axial (downward) ablation would be less severe in Mark II designs (such as Limerick and Susquehanna) that do not incorporate a deep in-pedestal cavity. The results of this calculation may be summarized as follows:

- The drywell floor is predicted to fail due to ablation at 810 min into the transient.
- The containment does not reach the 135 psig level required for wetwell failure prior to drywell floor failure.
- The drywell head flange seals are not expected to fail prior to drywell floor failure.

8.3 SEQUENCE WITHOUT ADS ACTUATION (All Core Debris Retained In Drywell Pedestal)

This Mark II short-term station blackout analysis involves the following conditions.

1. The ADS is not initiated and the reactor fails to depressurize.
2. There is no AC power available, hence
   - HPCI & RCIC are unavailable, and
   - containment sprays are unavailable.
3. Containment failure mechanisms are disabled.

This section presents containment results obtained by MELCOR analysis of the short-term station blackout scenario assuming that ADS has not been actuated and that all debris leaving the failed reactor vessel is maintained within the in-pedestal portion of the drywell.

As stated in Sect. 8.2, degassing of concrete structures within the primary containment was conservatively modeled by allowing MELCOR to initialize the concrete structure temperature profiles to those that would exist at steady state conditions consistent with the user-input atmospheric temperatures. Under these conditions, MELCOR calculated that the initial structural temperatures were higher than the degassing temperature thresholds specified by user input. As a result, a portion of the concrete structure water vapor content was conservatively released at the beginning of the calculation and containment pressure was higher than that which would have been calculated had transient (but lower) initial structure temperature profiles been specified. Realistic initial structural temperature profiles were explicitly specified. These profiles were based on the results of BWR-LTAS and BWRSAR calculations.

The MELCOR calculation was terminated at 731 min when the drywell floor within the in-pedestal region cavity was calculated to have been completely ablated in the axial direction (3.7 ft). The debris temperatures at 731 min are approximately 450°F (505 K) above the concrete ablation temperature of 2246°F (1503 K), and the concrete ablation rate is 2 in. per h. The zirconium inventory of the debris is much smaller than that predicted to be present in short-term station blackout sequence with ADS actuation. (All of the zirconium in the debris is predicted to have been burned up by 375 min into the transient.)

As mentioned earlier, all of the debris is assumed to be maintained in a cavity directly beneath the reactor vessel. This has a direct bearing on the timing of drywell floor failure as the debris is several feet thick and debris heat losses are consistent with a distinctive cavity geometry. This is not the geometry that the debris would assume in many of the Mark II containments where no such cavity exists and debris would spread more extensively around the floor of the drywell. Debris in this geometry would experience greater heat losses than the debris considered in the current calculation. For these reactors, the event of drywell floor failure is more uncertain and the timing of the event would be later than the 731 min estimated in this calculation. From this standpoint, the current calculation provides a conservatively low estimate of the timing of drywell floor failure.

The time-dependent containment pressure distribution is presented in Fig. 8.3.1. Annotations on the figure identify the important events which influence the pressure response. The calculation begins at 35 min, with the first significant event being a pressure rise due to a SRV discharge of steam and hydrogen into the wetwell pool occurring at 100 min with a second SRV discharge at 170 min. Reactor vessel debris pouring first occurs at 247 min into the transient and is accompanied by a sharp 50 psi pressure rise in the containment. This pressure rise is due to the gas (steam and hydrogen) flow from the bottom head into the drywell as explained earlier and the heat transfer to the drywell atmosphere from the accumulating debris on the drywell floor. As mentioned earlier, the wetwell leakage pressure of 135 psig is reached at 600 min and the containment pressures at 731 min are 163 and 158 psig for the drywell and wetwell, respectively.

After 247 min, the containment pressure continuously increases as the debris directly heats the drywell atmosphere and the debris/concrete interaction releases hot gas from the debris to the atmosphere. This is most evident in Fig. 8.3.2 which presents the calculated containment atmospheric temperature distribution. There is a small temperature rise at 170 min due to the SRV discharge. The striking rise at 247 min occurs as hot debris and gas exit the failed reactor vessel.

At 731 min, the drywell pressure is 163 psig and the wetwell pressure is 158 psig. These pressures are well beyond the 135 psig required for leakage through the pressure boundary in the airspace of the wetwell. Although all containment failure modes were disabled for this calculation, containment failure (assuming a 135 psig wetwell failure pressure) would have occurred at approximately 600 min, some 2 h before drywell floor burn-through.

The drywell head atmosphere temperature is observed to be approximately 875°F at 731 min. Although the gas temperature exceeds the drywell head flange failure threshold of 700°F, the flange temperature itself is not calculated to exceed the failure threshold. The flange temperature is calculated to be 665°F (35°F below the leakage threshold) at the end of the calculation. This is because the drywell head is modeled to lie adjacent to the cool refueling bay atmosphere. Thus the exterior of the drywell flange is cooled while the interior is heated by hot drywell gases.

Containment pressures are significantly higher than those calculated for the short-term station blackout with ADS actuation sequence discussed in Sect. 8.2. This is because the reactor vessel water inventory is significantly reduced during ADS operation.

Steam generated by flashing during ADS actuation leaves the vessel via the SRVs and is condensed in the wetwell water pool. Significantly more water is in the vessel at the time of penetration failure for the case without ADS actuation than for the case with ADS actuation. This water is rapidly converted to steam and hydrogen as it flows under pressure through the bottom head debris bed and reacts with the zirconium in the lower head. This mechanism also explains the reduced inventory of zirconium pouring onto the drywell floor for the no ADS case compared to the case with ADS actuation. The resulting gas flow from the bottom head directly pressurizes the containment and containment pressures are higher than the case with ADS actuation.

Drywell floor debris temperatures are presented in Fig. 8.3.3. It is observed that the debris temperature almost instantly increases beyond the concrete ablation temperature of 2246°F and remains elevated above this temperature throughout the calculation. This is a result of debris heating by the zirconium/steam reaction within the reactor vessel bottom head prior to the debris leaving the reactor vessel. The typical debris pour temperature is 3500°F. This continuous elevation in the debris temperature is also a result of the continuous debris pour from the reactor vessel after the bottom head penetrations fail at 247 min.

In the case with ADS actuation, the initial debris pour is primarily metallic with little superheat. The pour lasts for only one-half hour and the drywell floor debris temperature does not exceed the concrete ablation temperature. In fact, the drywell floor debris temperature is calculated to decrease after the initial pour stops at the one-half hour point and does not exceed the concrete ablation temperature until the second debris pour (primarily oxidic debris) once again commences from the vessel.

The debris temperatures for the case without ADS actuation, as shown in Fig. 8.3.3, temporarily equilibrate to the metallic debris melting temperature and remain there until 340 min. At this point, the debris temperatures begin to surpass the metallic debris melting temperature. This is due to the large thermal power provided by the exothermic reactions of zirconium with carbon dioxide and water vapor produced from the decomposition of the drywell floor concrete. Inspection of MELCOR results at 360 min indicates typical debris total thermal heating rates of 32 MW (27 MW due to chemical power and 5 MW due to decay heating).

At 380 min, the debris temperatures begin to decrease due to the exhaustion of the zirconium inventory. The large chemical power source disappears but is somewhat offset by increasing decay power due to the continuous debris pouring of fission product

bearing UO_2 from the failed reactor vessel and the insulating effect provided by the deepening of the debris pool and the decrease in effectiveness of heat loss mechanisms. These are the reasons the debris remains above the concrete ablation temperature.

At 575 min, the metal layer develops a thick bottom crust (4 in.) and the average metal layer temperature falls below the metal solidus temperature. Heat losses are reduced by this metal layer crust formation due to the conduction resistance of the crust. Decay heating of the debris pool (which is 7 ft thick) maintains the debris temperature above the concrete ablation temperature.

Figure 8.3.4 presents the drywell floor debris cumulative gas release. Debris gas release is evident at 250 min as concrete ablation is coincident with debris pour from the reactor vessel. Hydrogen is evident first and is due to the reaction of water vapor from concrete decomposition with zirconium. No carbon monoxide is released because of the coking effect calculated by the CORCON algorithm. The carbon produced by the reaction of zirconium with the carbon dioxide from the concrete decomposition is assumed to accumulate in elemental form in the metal layer. Following depletion of the zirconium at 380 min, this carbon begins to react with carbon dioxide from concrete decomposition to produce carbon monoxide. This is a rapid release because of the doubling effect provided by this reaction (see Sect. 8.2).

Carbon dioxide and water vapor originate from concrete decomposition due to heat transfer from the light oxide layer. The light oxide layer is created at 247 min as debris pours from the vessel and concrete ablation commences. The concrete slag species, which are lighter than the metals, float on top of the metals, and form a separate layer of light oxides. This light oxide layer rapidly thickens when layer flip is calculated to occur at 255 min. In this event, the heavy oxide layer consisting of mainly UO_2 and ZrO_2 is combined with the light oxide layer to form a new light oxide layer. This new layer is less dense than the metals, and therefore, the metals are relocated to the bottom of the debris pool while the oxides lie on top of the metals. Thus a heavy oxide layer does not form. (The heavy oxide layer evident in Fig. 8.3.3 is due to the specification of a small mass of UO_2 in the MELCOR cavity input. This mass is calculated to be rapidly mixed with the light oxide layer at 255 min due to a calculated layer flip event. After this time, no heavy oxide layer is calculated.) This is in contrast to the base case (with ADS actuation) in which a heavy oxide layer does form. The light oxide layer thickness grows as UO_2 and ZrO_2 pour from the reactor vessel and as CaO and SiO_2 concrete decomposition oxides are merged with the debris pool. The resulting CO_2 and H_2O

vapors enter the debris above the metal layer and do not chemically react with the metals. *They, therefore, enter the atmosphere in unmodified form.* Once the zirconium is exhausted at 380 min, unreacted CO_2 and H_2O vapors from the metal layer also enter the atmosphere.

Maximum cavity dimensions calculated by CORCON for the drywell floor are presented in Fig. 8.3.5. The concrete floor of the drywell is 3.74 ft thick and the cavity is 9.55 ft deep. Thus the bottom (lower surface) of the drywell is located at the depth of 13.29 ft. The floor is penetrated in the axial direction at 731 min and the calculation is terminated. Radial ablation commences from the inner radius of the drywell reactor pedestal at 10.1 ft and proceeds toward the outer surface of the pedestal at 14.96 ft. By 731 min, approximately 2.4 ft of the original 4.8 ft thickness of the pedestal has been ablated.

Drywell floor debris layer thicknesses are presented in Fig. 8.3.6. The layer thicknesses are seen to increase in response to the debris pour beginning at 250 min. Metal layer thickness jumps but levels off as the initial debris pour composition changes from metallic to oxidic debris. The metallic layer thickness once again increases at 300 min as the metallic debris in the reactor vessel bottom head becomes molten and flows away.

The discontinuities in oxide layer thickness reflect events in the debris/concrete phenomenology. The break at 370 min reflects the decrease in concrete ablation and, thus, the decrease in the rate of oxide layer growth due to the exhaustion of the zirconium inventory. Debris internal heating decreases, heat transfer to the concrete decreases, and the oxide layer growth rate decreases. The break at 575 min is due to the solidification of the metal layer mentioned previously. The formation of metal layer crusts decreases heat transfer to the concrete and the rate of growth of the oxide layer due to the addition of concrete slag materials.

The results of this calculation can be summarized as follows:

- failure to actuate ADS results in more in-vessel zirconium oxidation, and debris which is much hotter at the time it leaves the reactor vessel than is the case when the reactor vessel is depressurized
- debris-concrete interactions proceed more quickly for this case than the base case
- the drywell floor is predicted to burn-through over *one hour sooner* for this case than for the base case in which the ADS was actuated (731 min vs 810 min)

- the containment pressurizes much more rapidly for this case than for the base case. The containment pressure approaches 155 psig at 700 min in this case, compared to 80 psig in the base case with ADS actuation.

8.4 SEQUENCE WITH ADS ACTUATION AND DRYWELL SPRAY ACTUATION (All Core Debris Retained In the Drywell Pedestal)

This Mark II short-term station blackout analysis involves the following conditions.

1. The ADS is actuated when the core water level reaches one-third of the core height in accordance with Revision 3 of the BWR Owners Group EPGs.
2. AC power supply systems are unavailable, hence
   - HPCI and RCIC are unavailable.
3. A small-capacity, diesel-driven pump is available to feed the existing drywell spray header.
4. Containment failure mechanisms are disabled.

The results of this calculation are compared with those of Sect. 8.2 to determine the effects of containment spray on the accident progression.

Because it is important to properly model all sources of gas that can pressurize the containment, the effect of concrete degassing has been included. It is modeled in exactly the same fashion as described in Sect. 8.3.

The drywell spray system modeled in this analysis was derived from that extant in the Susquehanna Plant. This plant has a fire protection spray system pump for the secondary containment which is powered by a dedicated independent diesel engine. The water pumped by this system can be routed by the appropriate piping from the secondary containment into the drywell. This piping is normally used for the containment spray mode of the residual heat removal system (RHR) operation. The spray discharge emanates from a spray ring header surrounding the concrete biological shield at an elevation slightly below the top head flange of the reactor vessel. There are approximately ninety, one-half inch nozzles which direct spray water into the drywell atmosphere.

The number of nozzles and the associated orifice diameter were designed for RHR containment spray operation (approximately 9000 gpm per ring header.) Because the fire pump capacity is much smaller (nominally 500 gpm), the flow per nozzle is very small. This leads to the conclusion that the water entering the drywell atmosphere will

probably be in the form of very large droplets. For this calculation, the initial spray droplet diameter was specified to be one quarter inch and corresponds to one half of the spray nozzle orifice diameter.

The water source for the spray system was assumed to be inexhaustable and of constant temperature 70°F (295 K). In addition, because the fire pump is a low pressure pump, the effect of containment back-pressure on pumping capacity was also modeled. This resulted in a table specifying pumping capacity as a function of pressure difference between the drywell and the plant external environment. The volume flow delivered by the pump decreases from a high of 571 gpm at 0.0 psid, to zero flow at a 82.5 psid. Because containment venting was assumed not to occur, and because the containment pressure leakage threshold is 135 psig, the fire pump would be ineffective in delivering water to the drywell after some point in the calculation.

Because of the assumptions imposed in this scenario, the water provided by the fire protection pump is NOT available for injection into the reactor vessel. Furthermore, this system was assumed to be activated only after the failure of the bottom head penetrations at 263.3 min after reactor scram. It should be noted that the purpose of this calculation is to ascertain whether it is possible to mitigate the effects of the debri-concrete interaction once the core debris escapes the reactor vessel. Thus, the drywell sprays are activated later in this sequence than they might be actuated under strict adherence to the BWR Owners Group EPGs (Revision 4). The EPG primary containment control guideline (DW/T-2) could lead to an attempt to activate the existing containment spray system as early as 170 minutes into the accident (based on predicted containment pressures and temperatures), when prolonged SRV actuation leads to an extremely rapid increase in containment temperature. However, if water where actually available this early in the accident, it probably would be injected into the reactor vessel in an attempt to halt the accident. Thus, the scenario for which the containment spray EPG was designed appears to be inconsistent with the fundamental definition of the station blackout sequence. (It is also not clear that the recommended EPG would be followed by all utilities or that it would be applied to the dedicated system envisioned for this analysis.)

Water accumulation on the drywell floor is limited to that corresponding to a pool of depth 1.5 ft (0.457 m). This is the height of the downcomer lip above the drywell floor at Susquehanna. All other Mark IIs utilize downcomers which do not project this far above the drywell floor. Overflow of water from the drywell to the wetwell is modeled

once the water pool depth exceeded this value. The use of the Susquehanna design thus allows for the buildup of the deepest ex-pedestal water pool possible in any Mark II plant.

Because of the placement of the spray ring headers at Susquehanna, the spray water would not fall directly onto the debris, which was assumed to reside within the drywell reactor pedestal region. Water would first accumulate in the ex-pedestal region of the floor and would then flow by gravity toward the in-pedestal region. This is implicitly represented by the current modeling approach.

MELCOR's Fuel Dispersal Interaction (FDI) Package simulates the exchange of energy between debris and a water pool through which it is falling. However, because MELCOR cannot represent the changing depth of water residing in the sump as core debris displaces water, and because the elevation of the water pool free surface changes as a function of time due to the accumulation on the drywell floor, FDI was NOT employed in the current analysis. The cavity package is driven directly by the debris pours calculated by BWRSAR. Interaction of the debris with the overlying water pool in the in-pedestal region of the drywell floor is via the pool boiling correlations employed in the CAV package at the interface between the debris and the water pool. As modeled, the debris does not exchange energy with the water as the debris falls through the pool.

The containment spray was activated upon failure of the reactor vessel bottom head penetrations at 263.3 min. Water pool overflow into the downcomers first occurred at 330 min, after one hour of spray operation. Spray injection was terminated at 715 min as the containment pressure was calculated to exceed the pump cutoff pressure. Dryout of the drywell floor water pool was calculated by 960 min. The presence of the water pool delayed, but did not prevent, rupture of the drywell floor. Rupture was calculated at 995 min after scram and is approximately 3 h later than the time of floor rupture calculated for the dry case discussed in Sect. 8.2.

The time-dependent pressure distribution within the primary containment is presented in Fig. 8.4.1. Annotations on the figure identify important events influencing the pressure response. Boiling of the water transported to the in-pedestal region of the drywell is rapid but its pressurization potential is subdued. This is because of the rapid condensation of the resulting steam onto the colder structures residing within the containment. The condensate falls from the structures into the drywell floor water pool where it once again is transported into the in-pedestal region to be boiled away. This is the reason for the subdued pressure response during the time of initial debris pour from the vessel.

The next event observed in the pressure trace is the rise associated with the second debris pour from the reactor vessel at 380 min. Water boiloff is more rapid due to the higher temperature of the debris (the second pour was oxides at 4800°F compared to the first pour of metals at 2750°F). In addition, concrete ablation commences at approximately 400 min and noncondensible hydrogen is continuously released into the drywell atmosphere. The containment pressure continues to rise and reaches the spray pump shut-off pressure of 82 psig at 715 min. After this time, no additional spray water is injected into the containment.

A pressure plateau is reached at 740 min. This corresponds to a decrease in heat transfer from the debris to the overlying water pool. The reduced heat transfer results from the formation of a stable light oxide layer on the top of the debris. A crust forms and the temperature difference driving heat transfer from the debris to the water pool decreases. Reduced heat transfer results in a reduced rate of steam injection into the containment atmosphere and, thus, a reduced rate of pressurization.

A debris layer flip occurs at 790 min. This event mixes the colder light oxide layer with the hotter heavy oxide layer to produce a much hotter light oxide layer. Heat transfer to the overlying water pool increases with a resulting increase in the rate of boiling and containment pressurization.

Containment pressures continue to increase until the end of the calculation at 995 min. Pressurization is steady even though the drywell water pool is completely boiled away by approximately 950 min. This is due to the continued release of noncondensible gases from the ongoing debris/concrete interaction after the water pool is depleted. Containment pressures are 135 and 130 psig for the drywell and wetwell respectively. This is only approximately 5 psi lower than the leakage threshold. This contrasts with the dry case of Sect. 8.2 where containment pressure at the time of floor rupture is only 120 psia in the drywell and 115 psia in the wetwell. This increased pressure is due to the decrease in free volume resulting from the injection of over 1.4 million pounds of spray water into the containment and the pressurization provided by the continuous boiling of the water overlying the hot core debris.

These results should NOT be generalized to conclude that all Mark II plants would experience drywell floor rupture in the presence of an overlying pool of water. These results indicate that the pool significantly delays (by 3 h) drywell floor burn-through for even a deep cavity. Such a cavity has limited surface area through which the debris can lose heat without ablating concrete. Debris spreading for some plants would

result in a larger surface area (compared to the deep cavity case) through which nonablative heat losses can occur.

Figure 8.4.2 depicts the primary containment atmospheric temperature distribution as a function of time. Once again, there are noticeable discontinuities in the temperature traces. At 120 and 220 min before spray initiation, the temperatures are predicted to increase rapidly in response to the SRV discharges mentioned earlier. The maximum temperature occurs in the annulus between the biological shield and the outer surface of the reactor vessel. Containment atmospheric temperatures are generally lower than those calculated for the base case discussed in Sect. 8.2. This is because of the direct atmosphere cooling provided by the spray and the cooling of the hot gases released by the debris/concrete interaction as they are equilibrated with the water pool overlying the debris. The general temperature rise that does occur is due to the heat transfer from the hot reactor vessel wall and the discharge of hot gas from the failed reactor vessel directly into the drywell atmosphere.

Even after the spray flow into the drywell is terminated at 715 min, the water pool on the drywell floor is not completely boiled away until approximately 950 min (a period of 4 h). During this time, the water pool cools the gases released by the debris/concrete interaction. In fact, the gases act to cool the containment atmosphere during the period when the drywell water pool exists. It is only after the water pool is depleted at 950 min that the containment atmosphere is rapidly heated by the debris/concrete gases.

Figure 8.4.3 shows the rate of mass injection provided by the drywell spray model used in this calculation. The spray system is turned on at the time of bottom head penetration failure at 263 min. The magnitude of the injection rate is influenced by the drywell pressure. As the drywell pressure increases, the spray injection rate decreases. By 715 min, the drywell pressure reaches the spray pump shut-off pressure and the spray flow rate decreases to zero. Since containment pressure continues to increase after 715 min, the spray flow rate remains zero.

Figure 8.4.4 presents the calculated pool levels for both the in-pedestal and ex-pedestal regions of the drywell floor as functions of time. Both the collapsed and swollen pool levels are shown. Levels are presented relative to the drywell floor surface at 0.0. As such, these levels represent pool depths. Prior to spray actuation at 263 min, the quantity of water on the drywell floor is small and is due to leakage from the reactor vessel. Following spray system initiation at 263 min, the pool level rises rapidly to reach the downcomer lip at 330 min.

Instead of stabilizing at the elevation of the downcomer lip at 1.5 ft, the pool level continues to rise until the the second debris pour commences at 380 min. By 380 min, the pool level exceeds the lip elevation by approximately 4 in.. This level is not stable and is produced because the drywell pressure is less than the wetwell pressure (see Fig. 8.4.1). The vacuum breakers have opened and gas flow is established from the wetwell airspace into the drywell. Because there is gas backflow into the drywell, interfacial drag forces act in the opposite direction of gravity and support the liquid pool at a level above the level of the downcomer lip. As soon as the second debris pour commences at 380 min, the pressure in the drywell exceeds the pressure in the wetwell and water overflow into the downcomer quickly decreases the water pool level to the level of the downcomer lip.

The swollen and collapsed liquid levels for the ex-pedestal floor are identical. This is because the pool does not boil. However, the swollen level for the in-pedestal pool exceeds the collapsed level due to the existence of vapor bubbles rising through the pool. These bubbles are produced by boiling at the debris/pool interface. The pool levels begin to decrease once spray injection is precluded due to high drywell pressure at 715 min. The levels continue to decrease until approximately 950 min when the pools have essentially boiled away.

Figure 8.4.5 indicates that the in-pedestal water pool is saturated while the ex-pedestal pool remains subcooled. Comparison of the pool temperatures against the saturation temperature corresponding to the total pressure indicates that the in-pedestal pool becomes saturated shortly after the initiation of the drywell spray at 263 min. This pool boils continuously as the debris transfers energy to it. The ex-pedestal pool does not saturate because there is no heating of the pool. The pool temperatures are set by MELCOR to the atmosphere temperatures after pool boiloff and the temperatures begin to increase.

Figure 8.4.6 presents calculated debris temperatures for the deep in-pedestal sump assumed for this analysis. Temperatures rapidly escalate as debris pours from the failed reactor vessel at 270 min but decrease once the pour stops at 300 min. A comparison with Fig. 8.2.4 indicates the effect of the overlying water pool. Temperatures at 300 min are much lower than those of the dry case due to enhanced heat transfer. Debris temperatures once again escalate upward as the second debris pour commences at 380 min.

Formation of a stable light oxide layer is delayed until around 740 min compared to the 460 min of the dry case (Sect. 8.2). This delay is due to the lower metal layer temperature and the corresponding delay in concrete ablation by the metal layer. Concrete slag products are lighter than the metals and, therefore, any concrete ablation by the metal layer results in the concrete slag floating to the top metal layer and forming a layer of light oxides. Once the light oxide layer is formed, however, it acts to insulate the underlying metals so that the metals can become completely molten. Complete metal layer melting occurs by 790 min for the wet case compared to 540 min for the dry case.

Layer flip occurs at 790 min as the underlying heavy oxide layer is sufficiently diluted by concrete ablation by-products to become less dense than the overlying metal layer. Again, this is delayed with respect to the dry case when layer flip is calculated to occur at 590 min. At the time of layer flip, the light oxide layer temperature is approximately 500°F lower than the underlying metal layer temperature which is, in turn, 300°F lower than the underlying heavy oxide layer. This contrasts with the dry case where all debris layers exist at approximately the same temperature at the time of layer flip. Thus one effect of the overlying water pool is to cause a severe temperature gradient in the debris.

This temperature distribution is consistent with the formation of thick debris crusts that act to insulate the underlying debris from the water pool. The insulation provided by the overlying crust combined with the volumetric heat source due to decay heat results in a highly elevated heavy oxide layer temperature. The maximum heavy oxide layer temperature of 3807°F occurs at 530 min and is comparable to the maximum calculated for the dry case at 490 min. Even after layer flip at 790 min, the debris temperatures remain elevated and only gradually approach the metal layer melting temperature.

Cumulative debris gas releases are presented in Fig. 8.4.7. The first gas to be released (at 400 min) is hydrogen. This release is due to zirconium oxidation by water vapor originating from the decomposition of concrete. Zirconium oxidation by carbon dioxide results in elemental carbon production and retention of the carbon in the metal layer. This is the reason for the absence of an early CO and CO_2 release.

After debris layer flip (at 790 min), the metal layer is relocated downward adjacent to the concrete and all oxidic debris is located above the metals. As a result, all concrete ablation by the oxide layer releases gas into the debris above the metal layer. Reduction of this gas to hydrogen and carbon is precluded and these gases are transported

directly to the overlying atmosphere in unconverted form. This is the reason for the appearance of carbon dioxide and water vapor shortly after layer flip at 790 min. Only small quantities of carbon dioxide and water vapor are calculated to be released when compared to the dry case discussed in Sect. 8.2. Again, this is due to limited radial concrete ablation by the light oxide layer. This in turn is due to the thicker radial crusts resulting from heat transfer to the overlying water pool.

The appearance of carbon monoxide at 940 min is due to zirconium depletion and the reaction of the accumulated carbon in the metal layer with carbon dioxide to produce carbon monoxide. The release is rapid due to the doubling effect discussed in Sect. 8.2.

Drywell floor concrete ablation histories are presented in Fig. 8.4.8. Radial ablation is significant but not as pronounced as that calculated in the dry case. Ablation proceeds from the inner radius of the reactor pedestal at 10.1 ft to a radius of 11.9 ft. The outer radius of the reactor pedestal is 14.96 ft, so 1.8 ft of the 4.8 ft-thick reactor pedestal is consumed by concrete ablation. This compares to 3.1 ft of radial ablation calculated in the dry case. Once again, this can be attributed to the overlying water pool. Increased debris heat losses result in thicker radial crusts that reduce radial heat transferred to the concrete.

Debris layer thicknesses are presented in Fig. 8.4.9. The thicknesses of the layers increase directly in response to the debris pours at 270 and 380 min. The heavy oxide layer is created only after the initiation of the second debris pour at 380 min. It is composed mainly of UO_2 and ZrO_2. These materials are calculated to sink through the metal layer that is composed primarily of iron, chromium, nickel, and zirconium.

Following layer flip at 790 min, the heavy oxide layer disappears and the light oxide layer thickness continues to increase. This is an artifact of the continued ablation of concrete and the incorporation of the concrete slag into the light oxide layer.

The results of this analysis can be summarized as follows:

- The drywell floor is predicted to fail due to ablation at 995 min into the transient. This is approximately 3 h later than floor failure is predicted to occur in the dry case.
- The containment does not reach the 135 psig level required for wetwell failure prior to drywell floor failure. However, the predicted wetwell pressure is within 5 psi of this value at the time of drywell floor failure.

- The containment pressure would reach the shutoff head of the diesel-driven spray pump (82 psig) at 715 min into the transient. No additional water would be injected into the containment after this time.

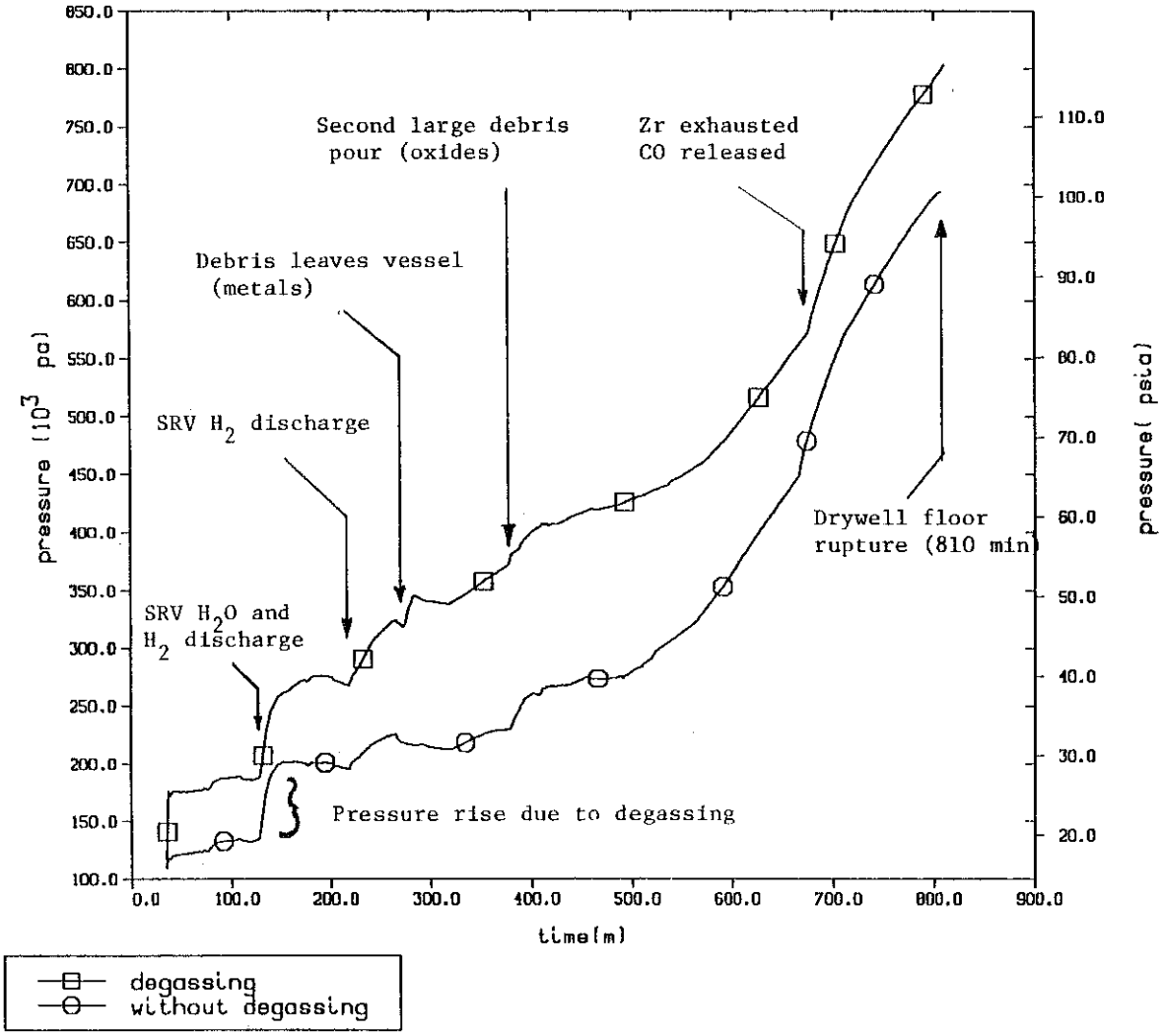

Fig. 8.2.1. Effect of concrete structure degassing on ex-pedestal wetwell pressure for the single cavity Mark II short-term station blackout sequence with ADS actuation.

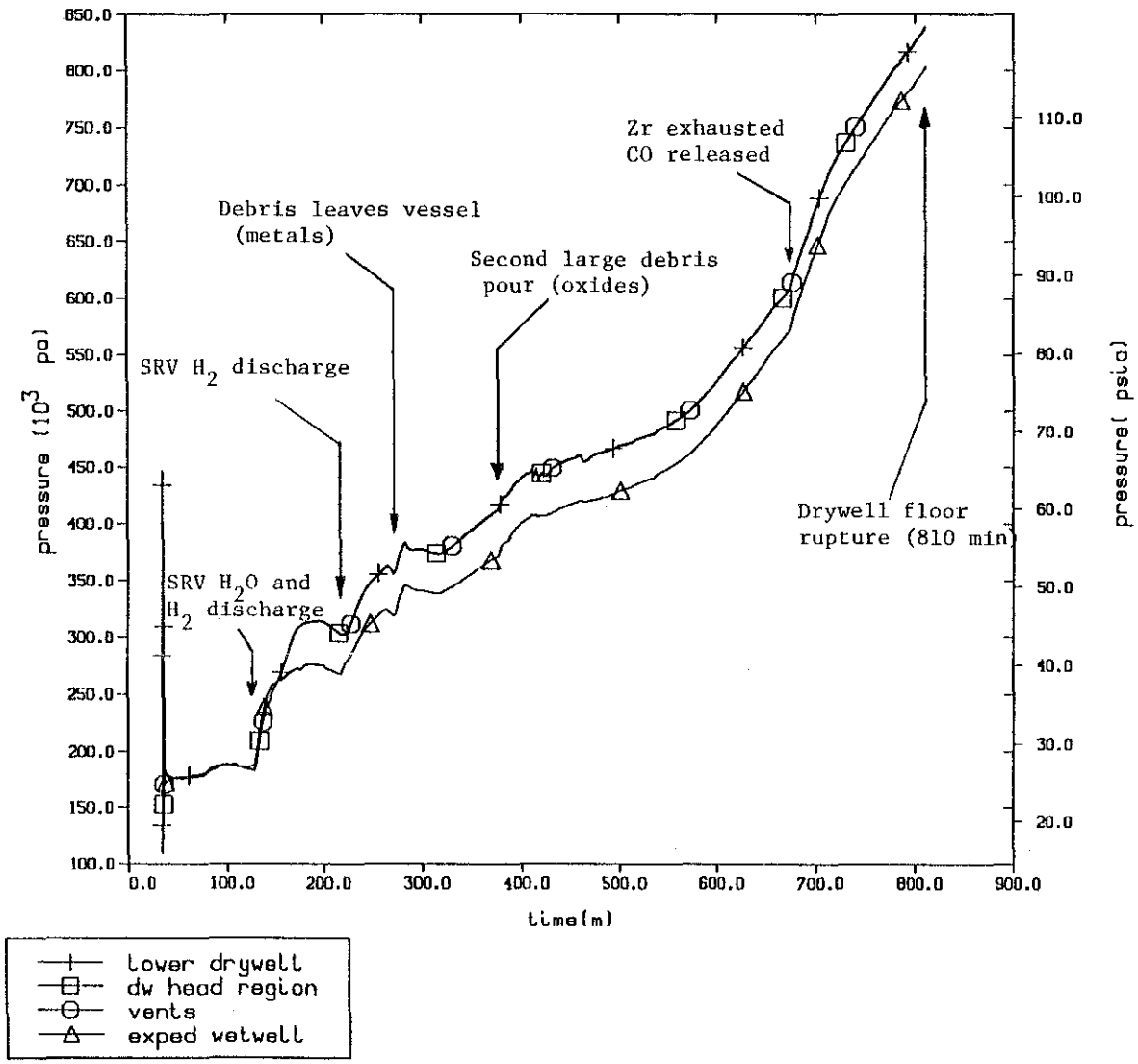

Fig. 8.2.2. Primary containment pressure distribution for the single cavity Mark II short-term station blackout sequence with ADS actuation.

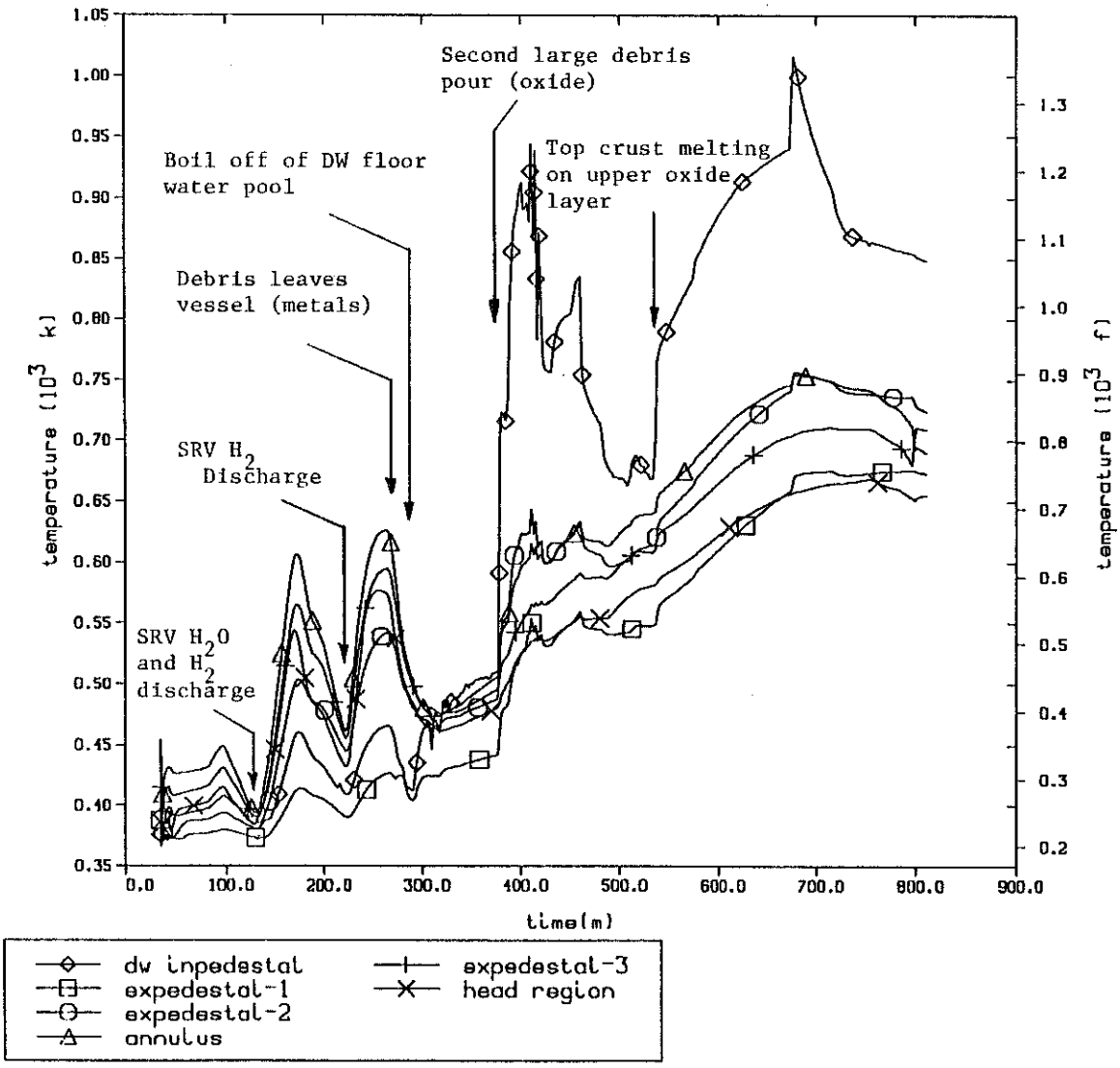

Fig. 8.2.3. Primary containment temperature distribution for the single cavity Mark II short-term station blackout sequence with ADS actuation.

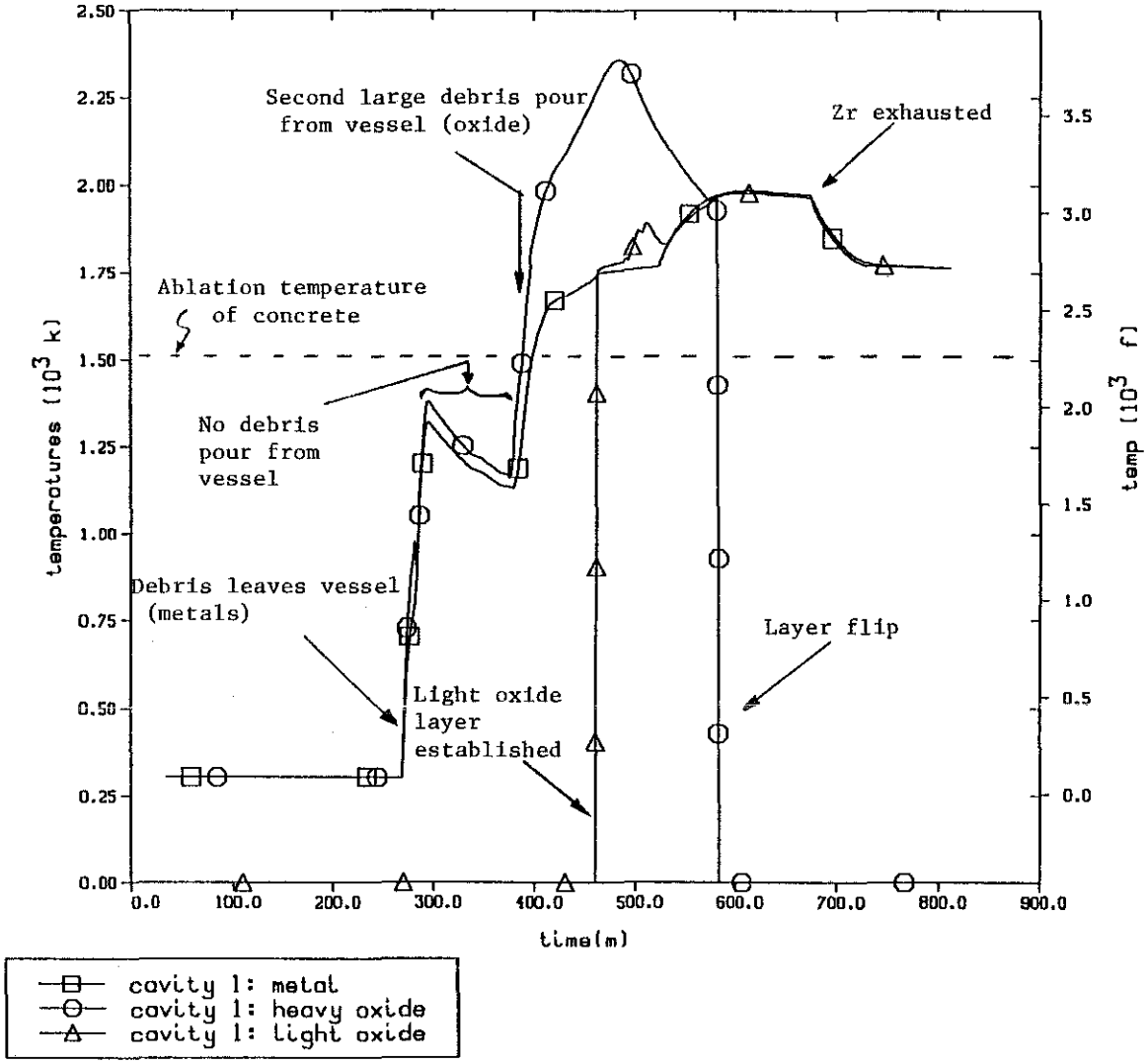

Fig. 8.2.4. Debris layer temperatures for the single cavity Mark II short-term station blackout sequence with ADS actuation.

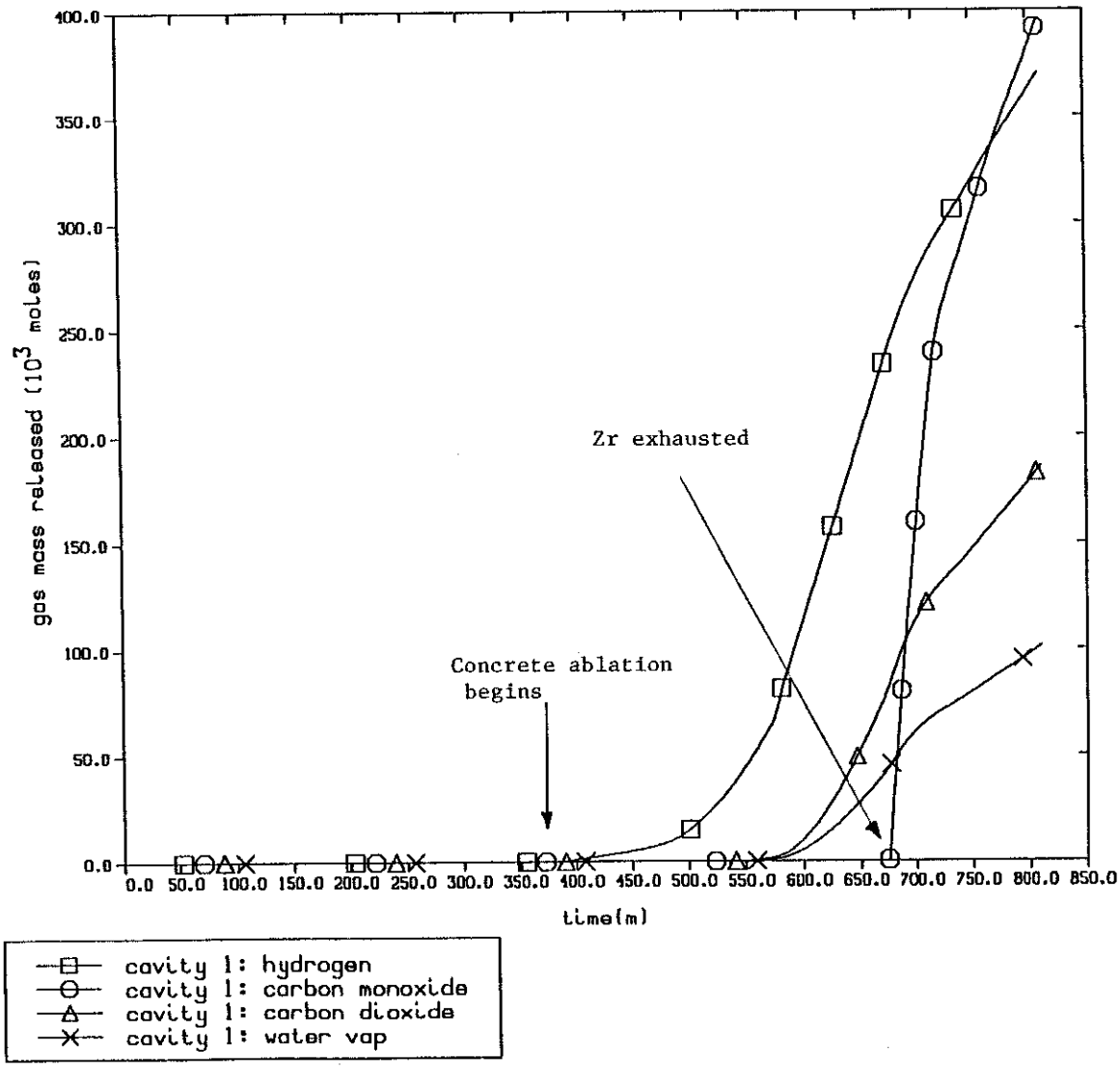

Fig. 8.2.5. Debris gas releases for the single cavity Mark II short-term station blackout sequence with ADS actuation.

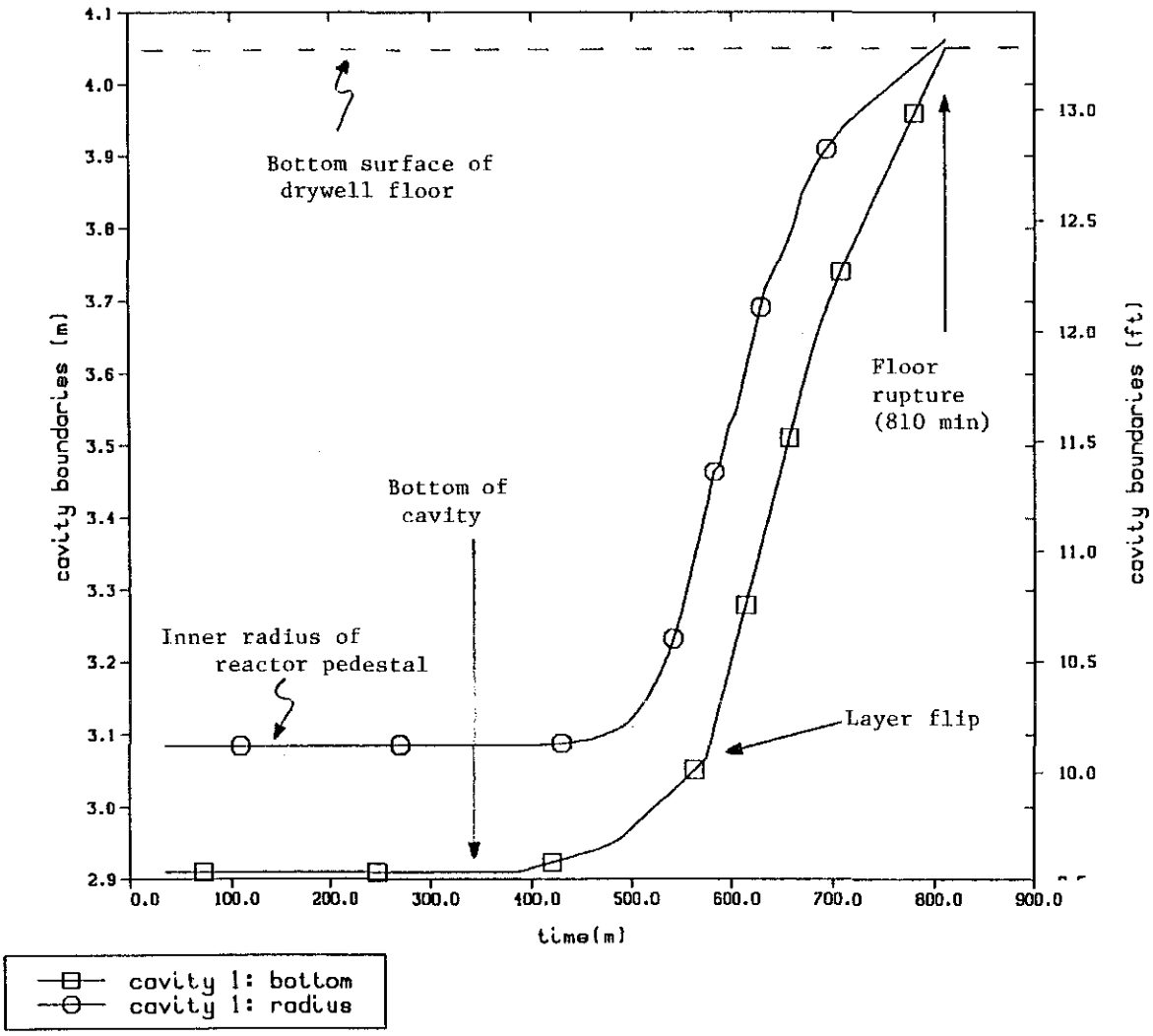

Fig. 8.2.6. Maximum cavity dimensions for the single cavity Mark II short-term station blackout sequence with ADS actuation.

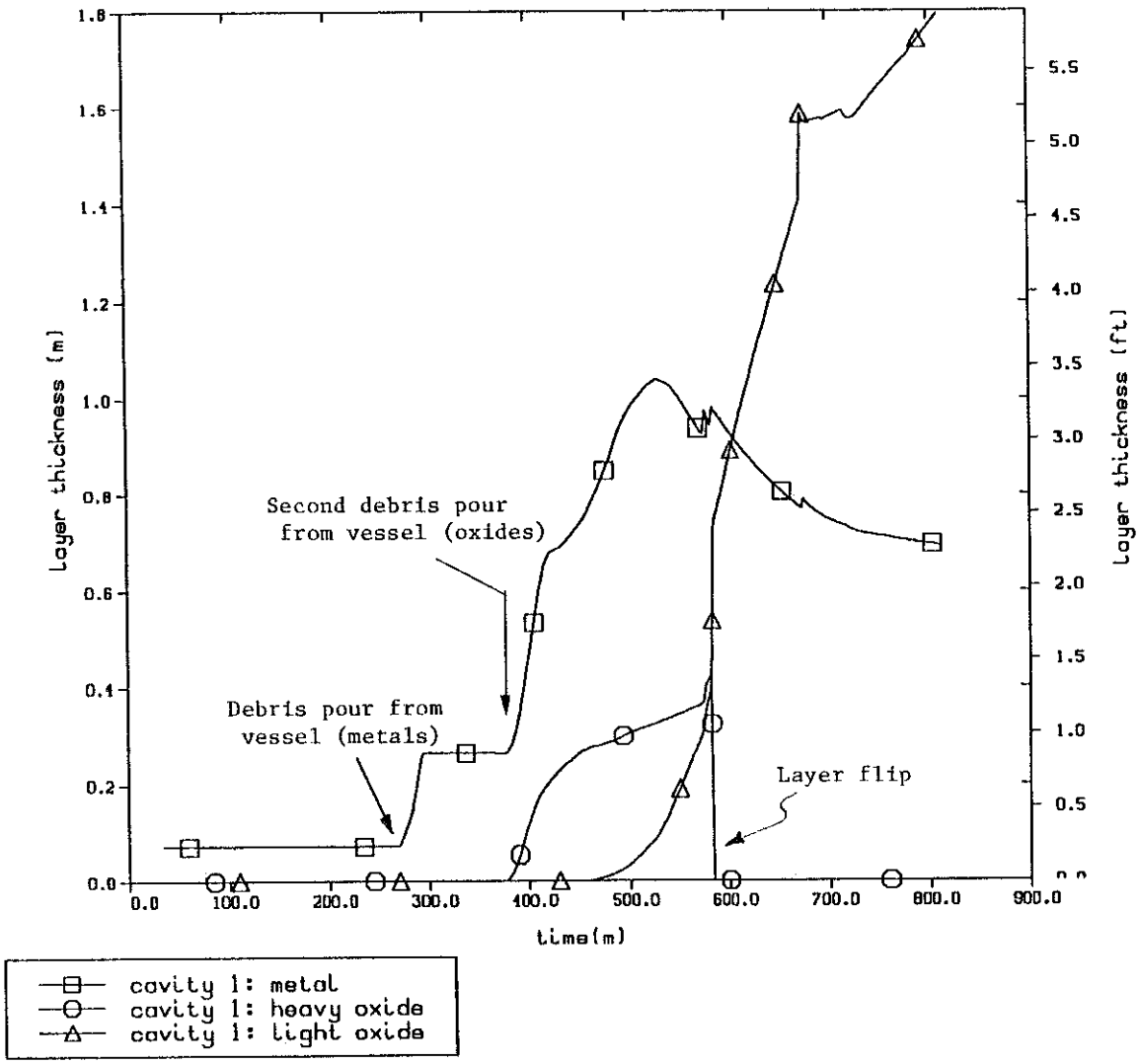

Fig. 8.2.7. Debris layer thicknesses for the single cavity Mark II short-term station blackout sequence with ADS actuation.

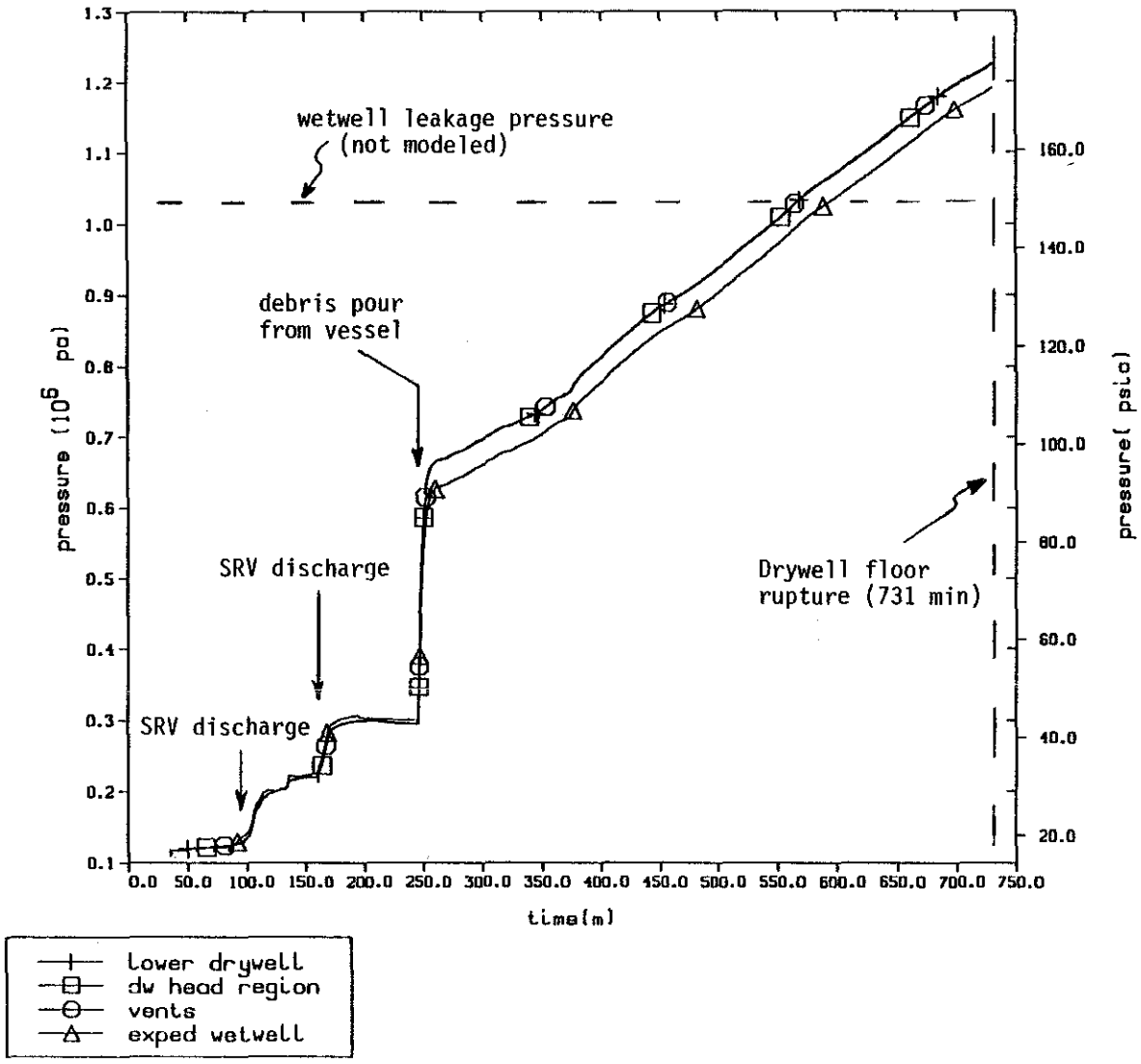

Fig. 8.3.1. Primary containment pressure distribution for the single cavity Mark II short-term station blackout sequence without ADS actuation.

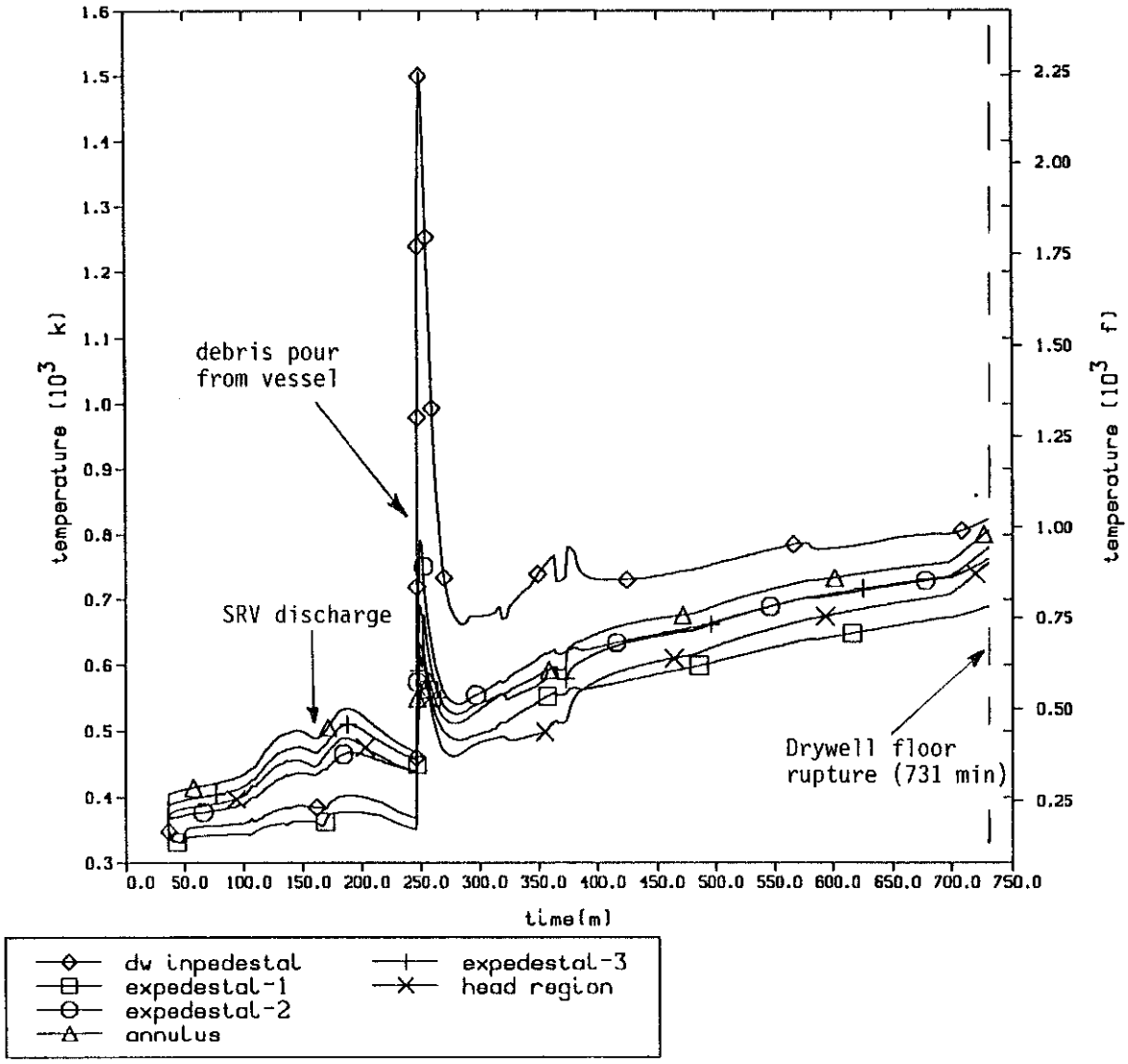

Fig. 8.3.2. Primary containment temperature distribution for the single cavity Mark II short-term station blackout sequence without ADS actuation.

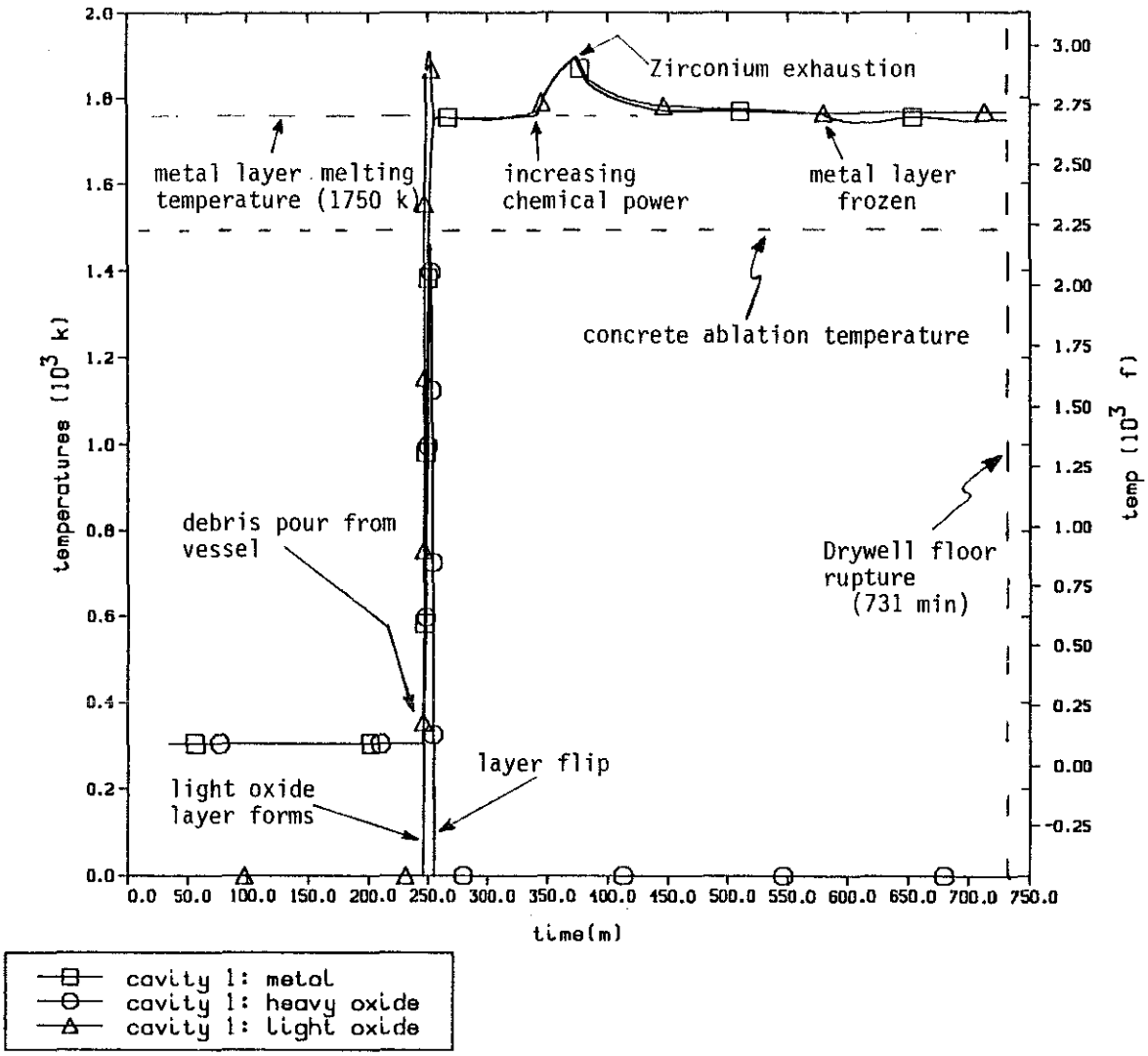

Fig. 8.3.3. Debris layer temperatures for the single cavity Mark II short-term station blackout sequence without ADS actuation.

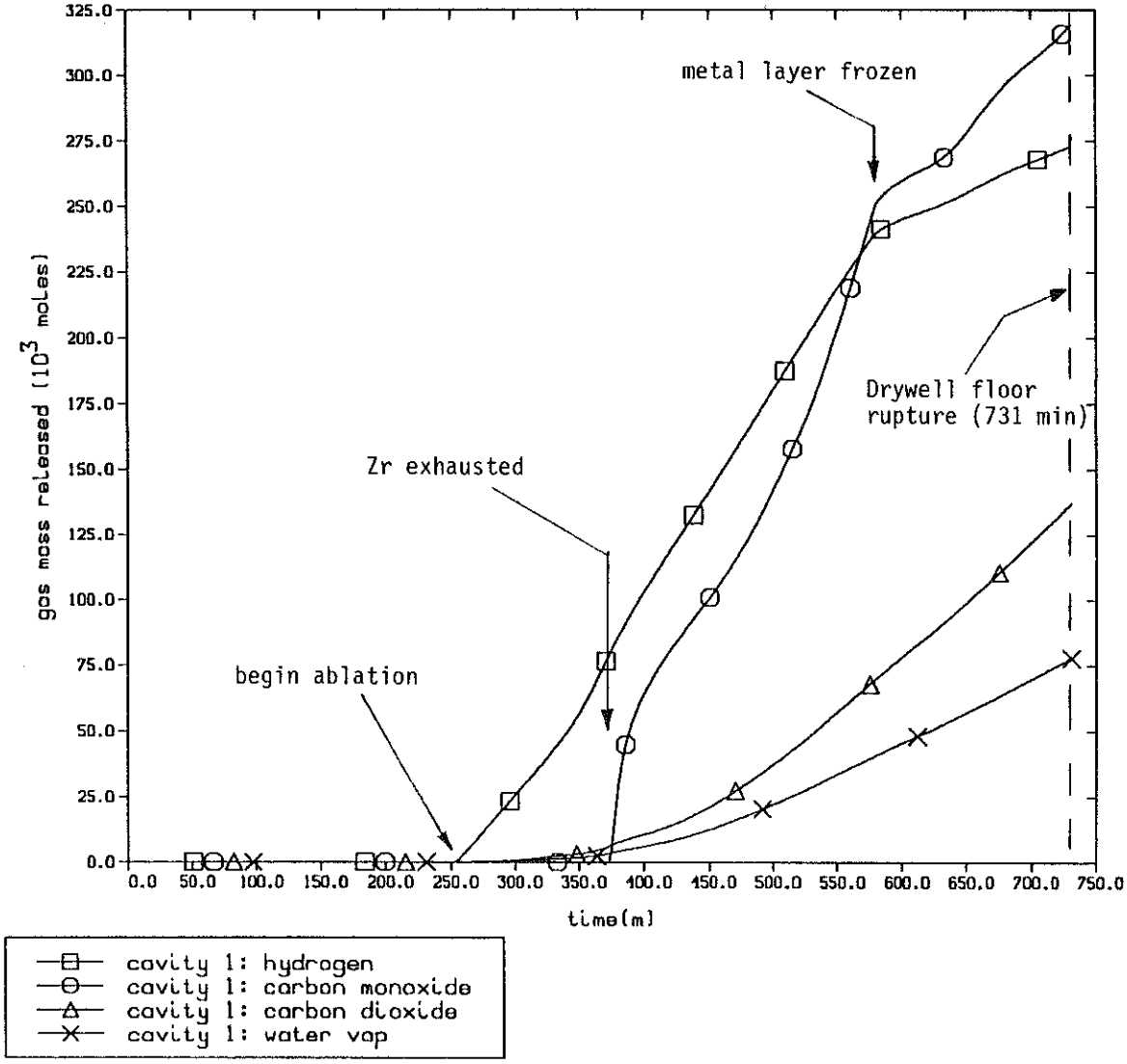

Fig. 8.3.4. Debris gas releases for the single cavity Mark II short-term station blackout sequence without ADS actuation.

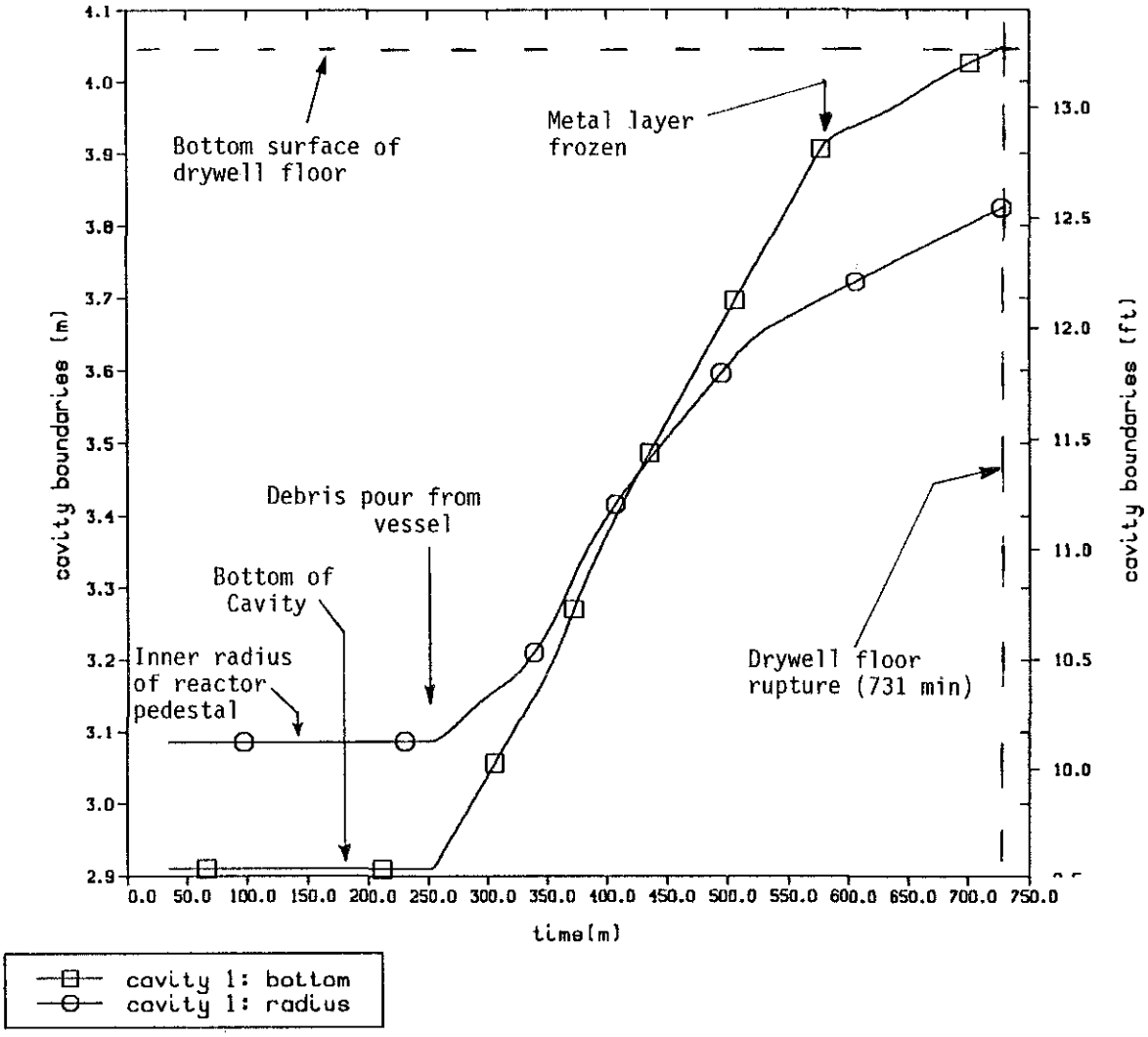

Fig. 8.3.5. Maximum cavity dimensions for the single cavity Mark II short-term station blackout sequence without ADS actuation.

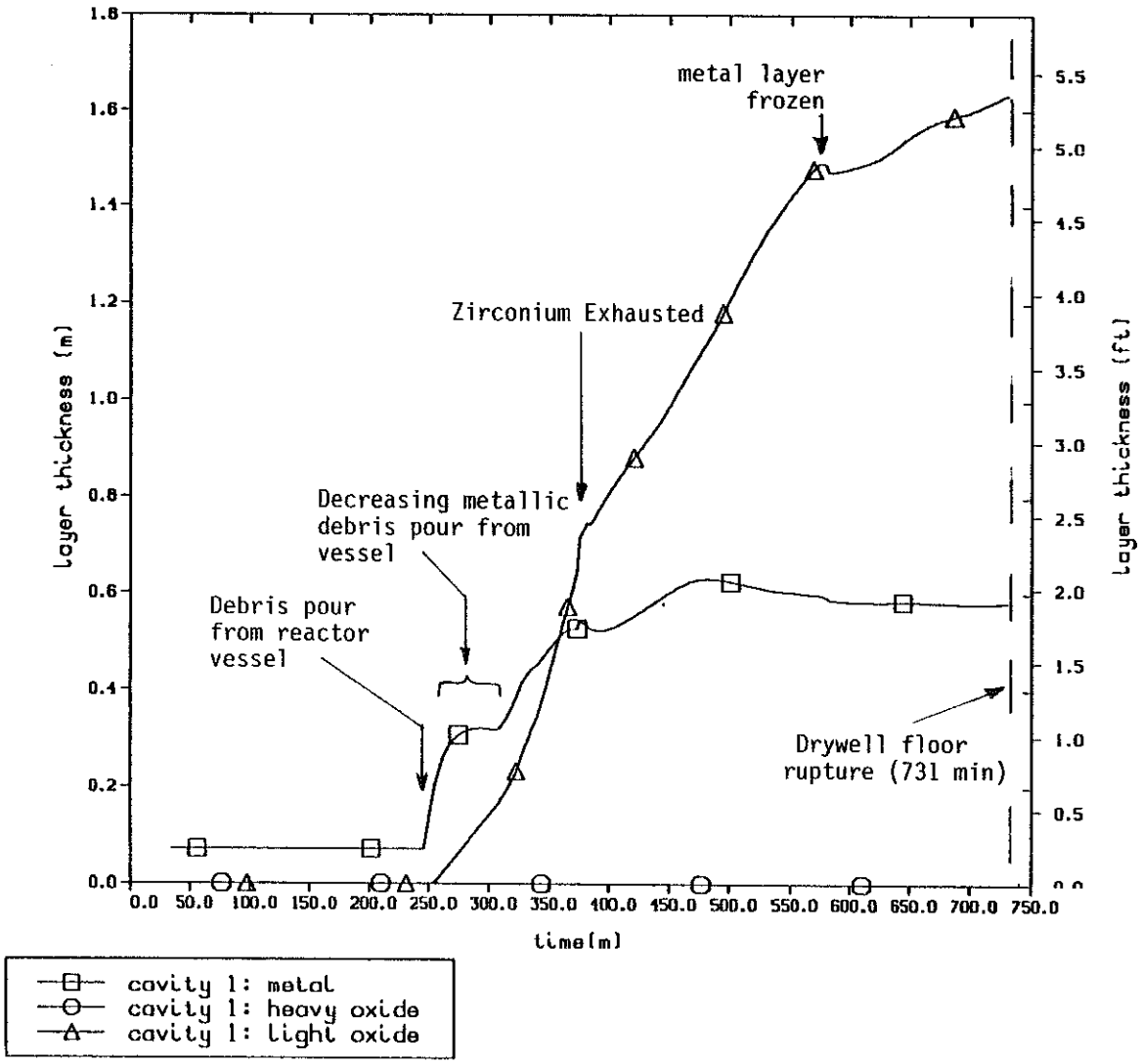

Fig. 8.3.6. Debris layer thicknesses for the single cavity Mark II short-term station blackout sequence without ADS actuation.

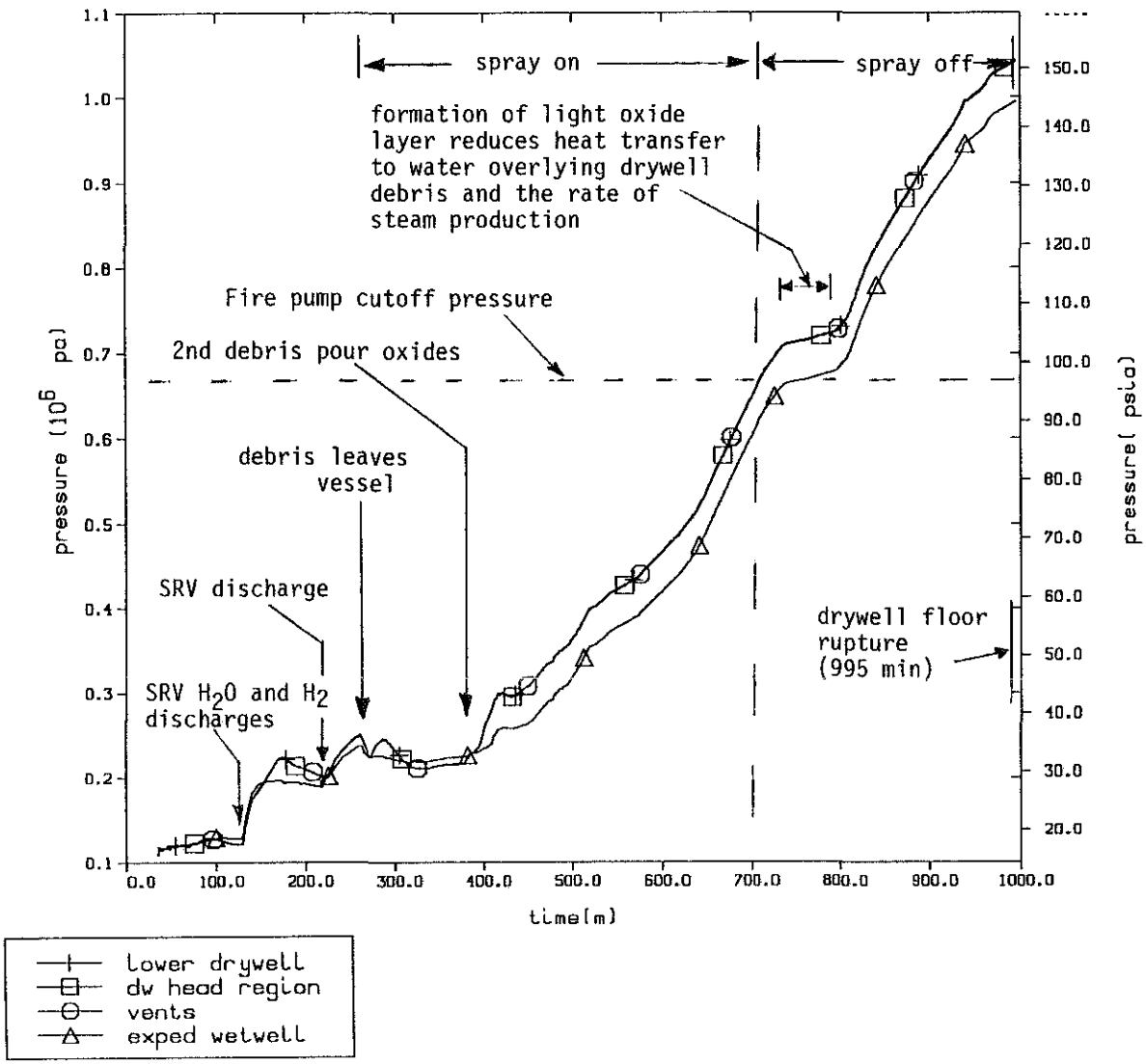

Fig. 8.4.1. Primary containment pressure distribution for the single cavity Mark II short-term station blackout sequence with ADS and drywell spray actuation.

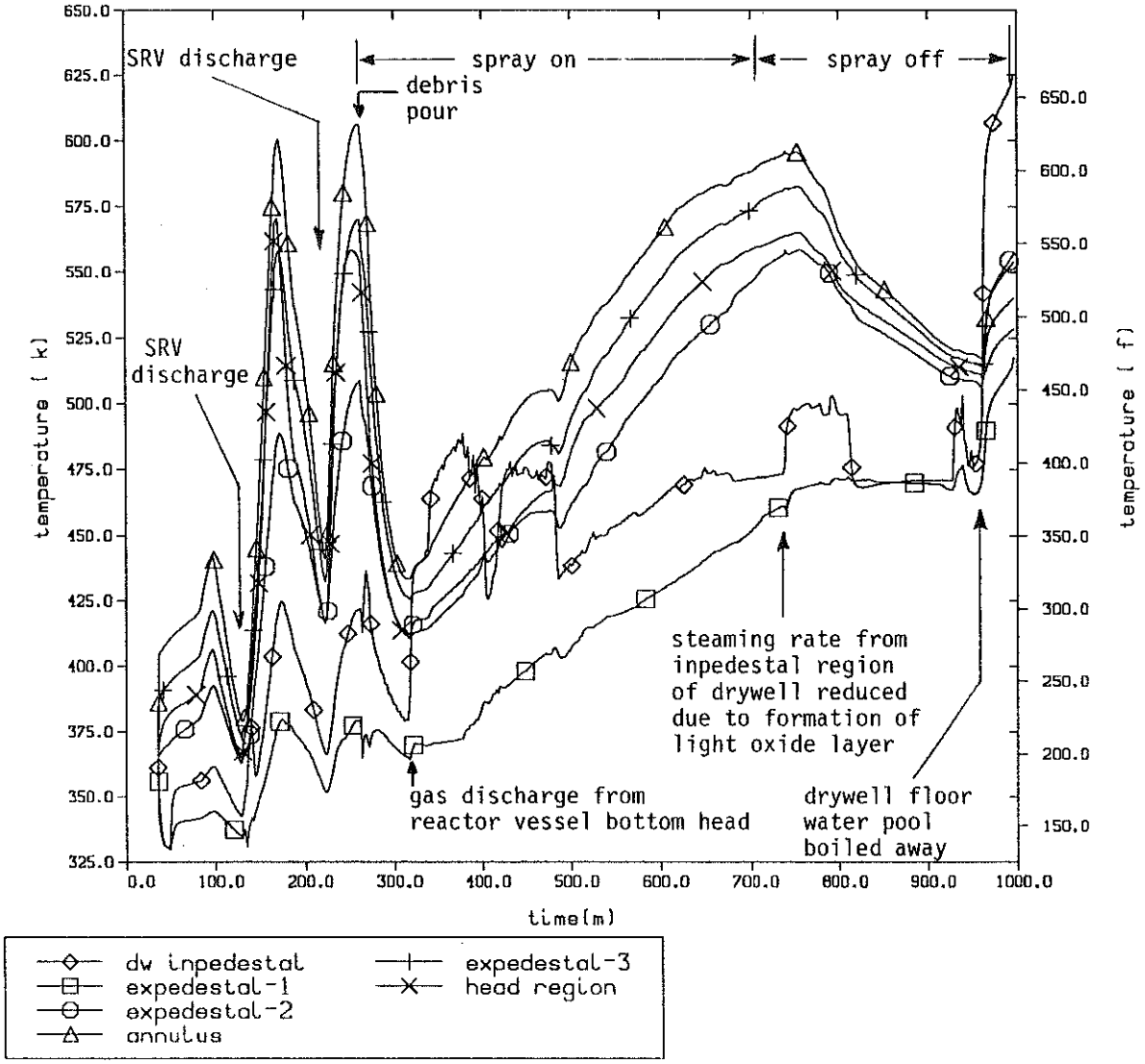

Fig. 8.4.2. Primary containment atmospheric temperature distribution for the single cavity Mark II short-term station blackout sequence with ADS and drywell spray activation.

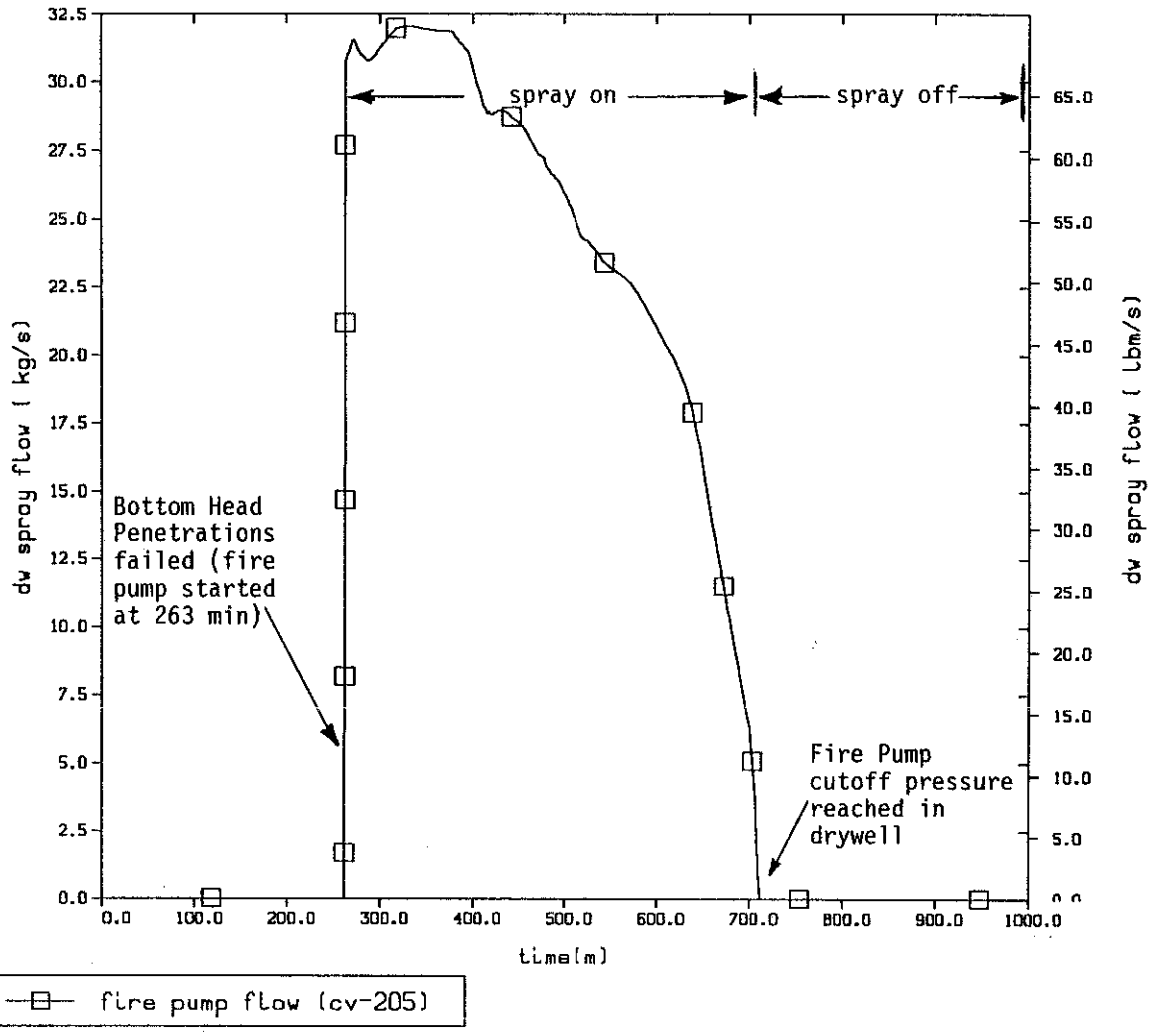

Fig. 8.4.3. Drywell spray flow rate for the single cavity Mark II short-term station blackout sequence with ADS and drywell spray actuation.

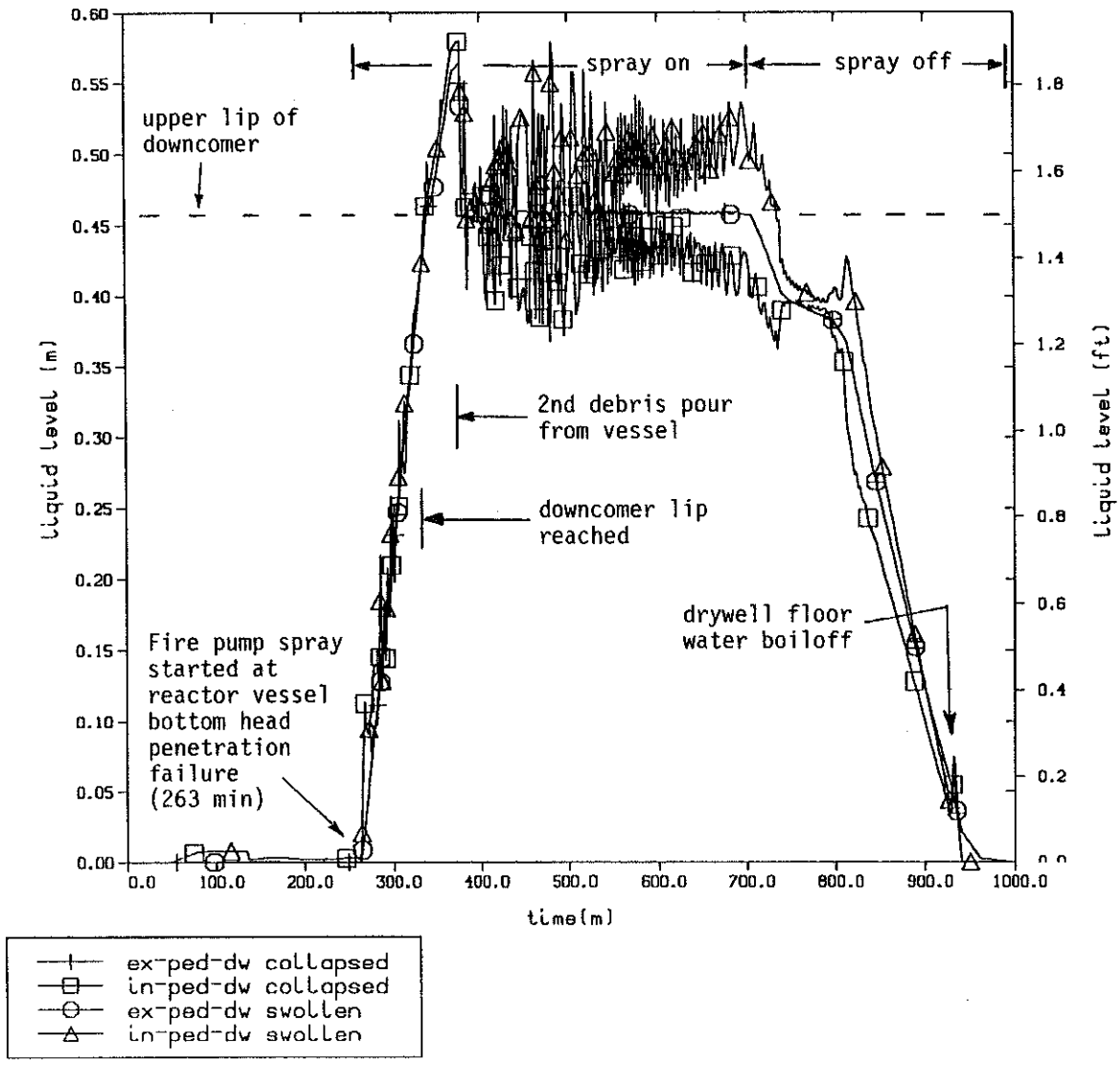

Fig. 8.4.4. Drywell floor (in-pedestal and ex-pedestal) pool elevations (swollen and collapsed) for the single cavity Mark II short-term station blackout sequence with ADS and drywell spray actuation.

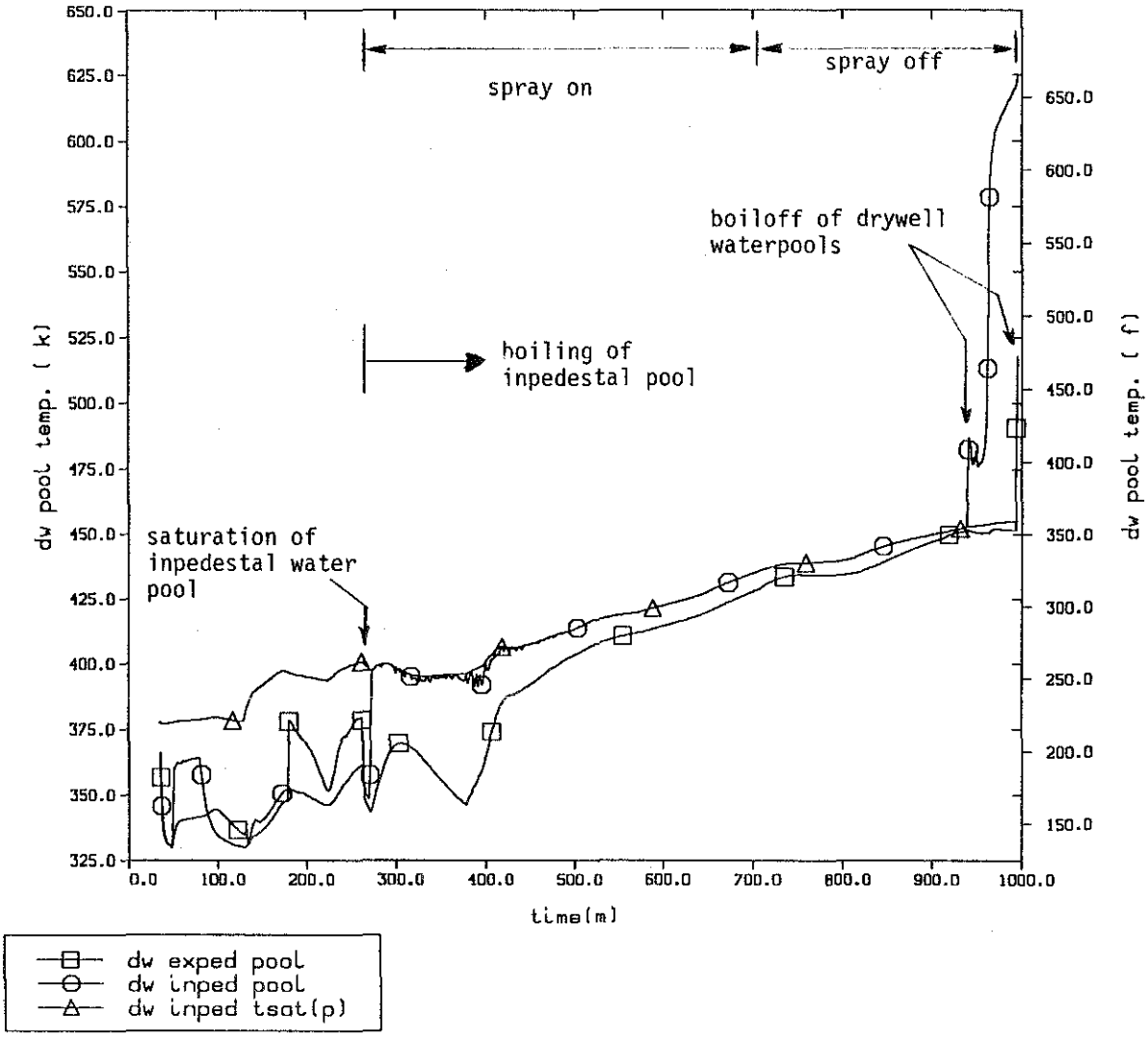

Fig. 8.4.5. Drywell floor (in-pedestal and ex-pedestal) pool temperatures for the single cavity Mark II short-term station blackout sequence with ADS and drywell spray actuation.

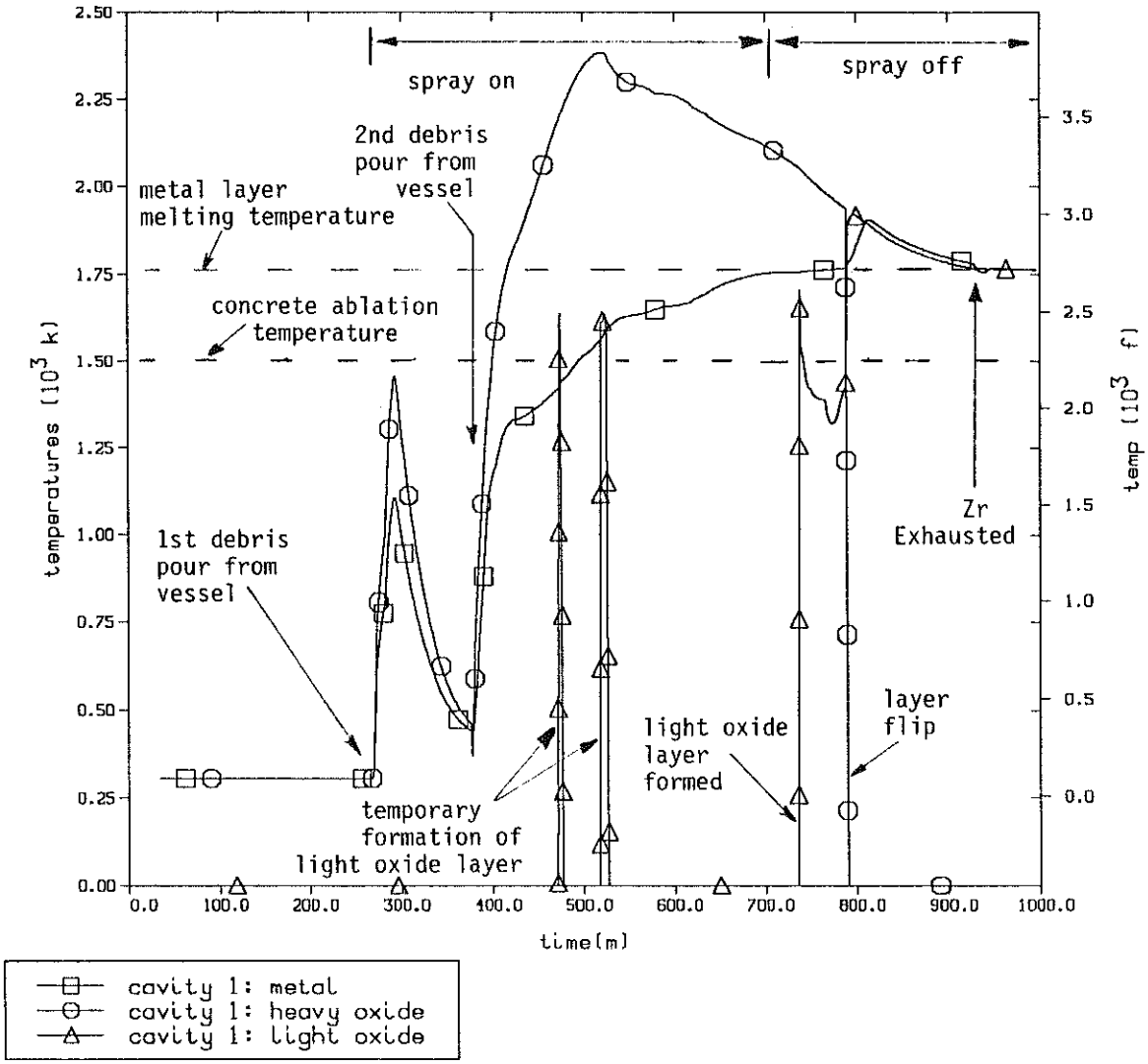

Fig. 8.4.6. Drywell floor debris temperatures for the single cavity Mark II short-term station blackout sequence with ADS and drywell spray actuation.

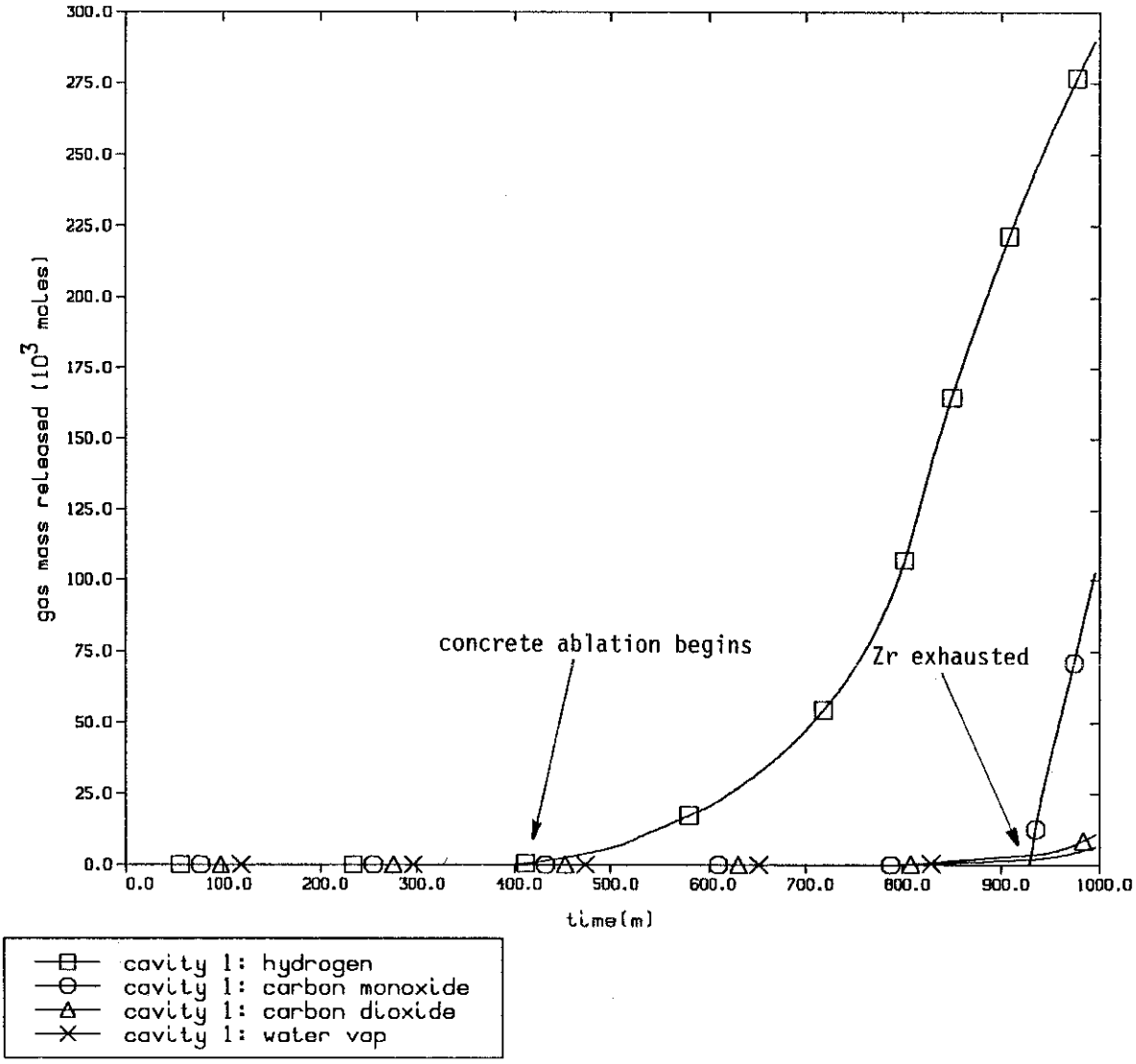

Fig. 8.4.7. Drywell floor debris gas releases for the single cavity Mark II short-term station blackout sequence with ADS and drywell spray actuation.

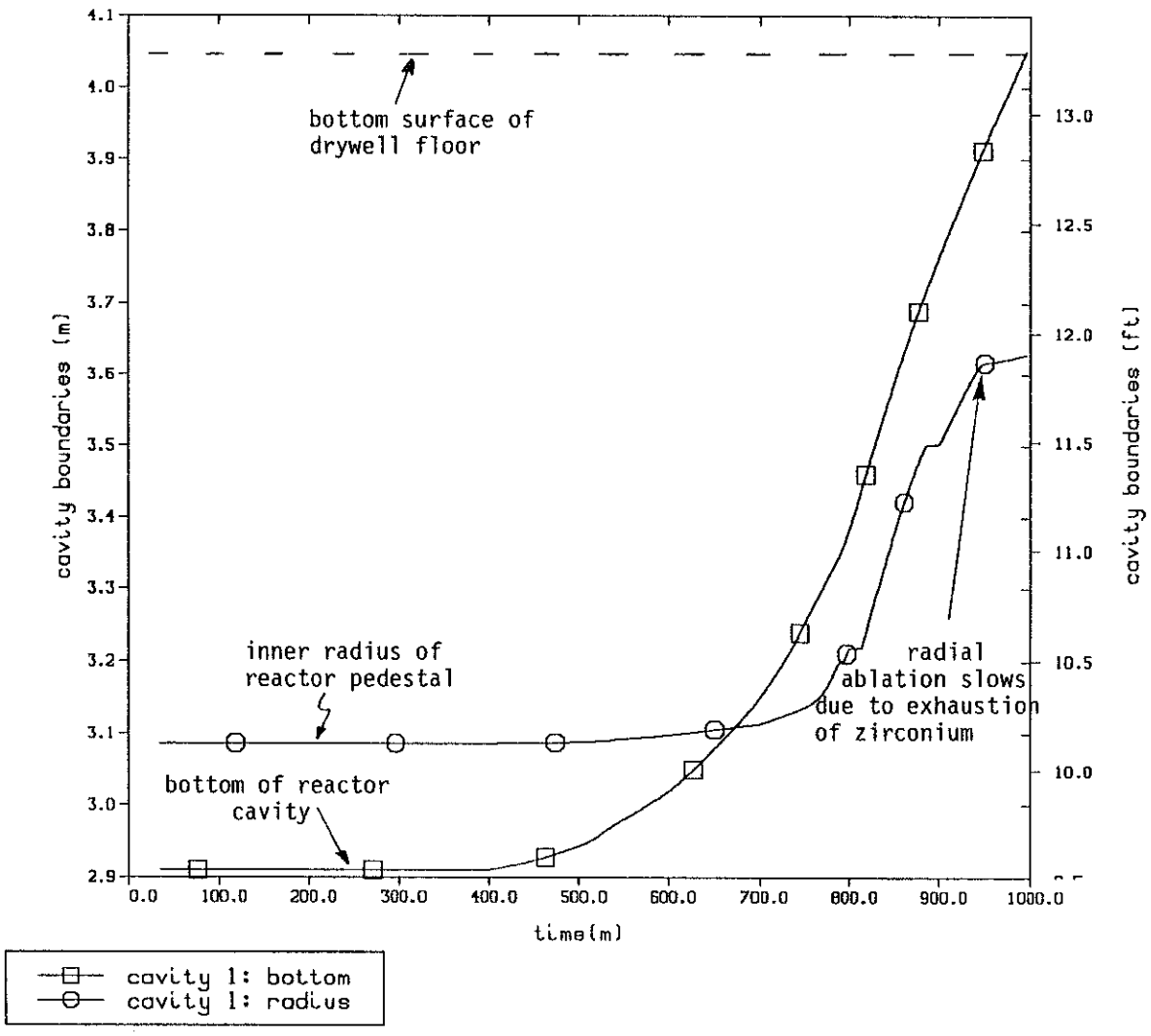

Fig. 8.4.8. Maximum cavity boundaries for the single cavity Mark II short-term station blackout sequence with ADS and drywell spray actuation.

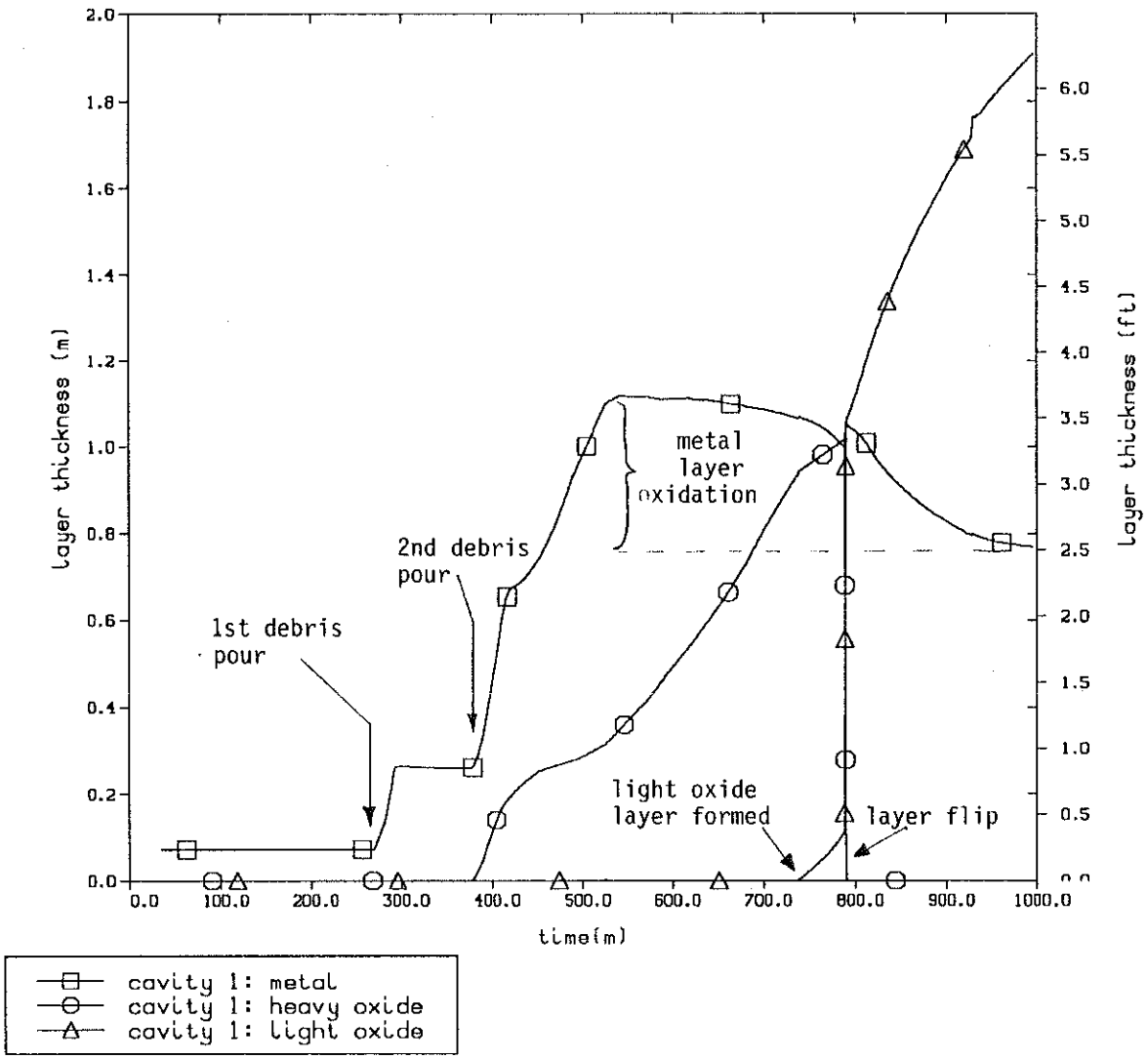

Fig. 8.4.9. Debris layer thicknesses for the single cavity Mark II short-term station blackout sequence with ADS and drywell spray actuation.

9. MARK II CONTAINMENT RESPONSE: SHORT-TERM STATION BLACKOUT WITH ADS ACTUATION AND WETWELL POOL-DEBRIS INTERACTION

9.1 INTRODUCTION

This chapter presents containment response results obtained by MELCOR analysis of the short-term station blackout scenario assuming operation of the ADS system and entrance of some core debris into the pressure suppression pool. The transient addressed is identical to the one discussed in Sect. 8.2 except that it is further assumed that a fraction of the core debris leaving the reactor vessel is immediately transferred into the water pool of the wetwell. This is an important consideration because most Mark II containments have in-pedestal drywell floor drains (and some have in-pedestal downcomers) which could provide an avenue for early entry of core debris into the wetwell pool.

It is important to note that MELCOR does not have the capability to directly model the flow of molten debris from above the drywell floor through openings (downcomers or failed drain pipes) in the drywell floor, the subsequent acceleration of the debris as it falls through the wetwell airspace, the debris-coolant interaction as the debris then falls through water, the debris bed formation as the quenched material accumulates on the wetwell floor, or the debris-concrete interaction at the bed-floor interface. What can and has been done by manipulation of code input is to direct part of the debris pour *from the reactor vessel* directly into the wetwell pool.

The debris/pool interaction is calculated by the Fuel Dispersal Interactions (FDI) package within MELCOR. The documentation of the package is incomplete. The package was used in a manner consistent with the approach which would have been employed if the MELCOR COR package had generated the debris transfers to FDI. Since the COR package was not used to calculate the debris pours leaving the reactor vessel, additional information that is not normally required from BWRSAR was needed as input to the MELCOR FDI calculation. This information consists of the hole diameter through which the debris leaves the drywell, the debris speed through the hole (assuming the hole is completely filled with flowing debris), and the time-integrated total enthalpy of the debris which has passed through the hole.

For the current application, it was desired that the debris speed be small. It was decided that the area of the hole in the drywell floor through which the debris is assumed

to pass would be specified to be the same fraction of the in-pedestal floor area as the fraction of debris mass assumed to flow into the wetwell from the reactor vessel. Thus, the speed of the debris as it leaves the drywell floor is the same for all cases. This approach also limits variation of FDI input information between the different analyses so that differences in results could be attributed mainly to the differences in debris partitioning between the drywell and wetwell.

A second cavity was specified in order to calculate the debris/concrete interaction occurring once the debris settles to the bottom of the wetwell inpedestal water pool. The geometric characteristics of the CORCON cavity representing the wetwell in-pedestal region were assumed identical to that employed in the drywell CORCON cavity.

Because the extent of debris relocation to the wetwell is highly uncertain, a parametric analysis approach was employed. Calculations were performed for cases in which 5%, 20%, 40%, and 100% of the pour is assumed to directly enter the wetwell pool. (The case in which none of the pour is assumed to directly enter the wetwell was discussed in Section 8.2)

A further distinction between this analysis and that reported in Chapter 8 consisted of the provision to allow the containment to fail. The two failure modes modeled are direct overpressurization wetwell failure at a wetwell pressure of 135 psig and drywell head flange seal leakage. Head flange leakage is assumed to occur once the drywell head seals have thermally degraded (temperature of 700°F) and the drywell-to-refueling bay pressure difference has reached 82 psi.

9.2 SEQUENCE WITH 95% DRYWELL/5% WETWELL DEBRIS SPLIT

This section presents results of the first case, in which 5% (by mass) of the time-dependent debris pour is directed into the wetwell pool while the remaining 95% of the debris pour is assumed to remain on the in-pedestal floor of the drywell. The conservative approach (described in Section 8.2) for assigning initial structural temperature distributions was used.

Figure 9.2.1 presents the time-dependent pressure distribution calculated for the Mark II primary containment. As can be seen, the pressure does not reach the 135 psig level required for wetwell failure. The calculation is terminated when the drywell concrete floor is calculated to have been ruptured by axial concrete ablation at 846 min. (This is 36 min later than for the case in which all debris is represented to remain within

the drywell in-pedestal region.) Because the pressure is continuing to rise at the time of floor rupture, it should not be assumed that the maximum pressure had been reached or that the containment would not fail due to the steam spike generated when the drywell debris dumps into the wetwell pool.

There are distinct discontinuities exhibited by the pressure trace of Fig. 9.2.1. These are caused by significant events in the progression of the transient. At times 130 and 220 min, the pressure increases markedly due to the discharge of steam and hydrogen gases through the SRVs into the wetwell pool. At 270 min, another rise occurs as the reactor vessel bottom head fails and debris begins to pour into the drywell and wetwell. Another discontinuity occurs as the second debris pour commences at 380 min. A final pressure increase is noted at 675 min. This corresponds to the rapid release of carbon monoxide from the debris as the carbon from the coking reaction begins to burn with the carbon dioxide and water vapor released from the concrete.

Figure 9.2.2 depicts the primary containment atmospheric temperature distribution as a function of time. Once again there are noticeable discontinuities in the temperature traces. At times 130 and 220 min, the temperatures are predicted to increase rapidly in response to the SRV discharges mentioned earlier. As noted in previous calculations, the maximum temperature occurs in the annulus between the biological shield and the outer surface of the reactor vessel.

There is no obvious increase in the in-pedestal air temperature at the time of reactor vessel bottom head failure (270 min). This is because the debris falls into a shallow pool of water created by primary coolant system water leakage prior to failure of the bottom head. At 290 min, however, this water has been vaporized and the debris immediately begins to heat the in-pedestal atmosphere and the temperature increases. At 380 min, the second major debris pour commences and the in-pedestal air temperature increases rapidly. At approximately 550 min, the upper oxide layer top crust melts and heat transfer to the in-pedestal atmosphere increases.

As shown in Fig. 9.2.2, the drywell head region atmosphere temperature reaches approximately 700°F by the end of the calculation at 846 min. The results also indicate that the drywell head flange reaches only 590°F. This is because the head flange is bounded on the inner surface by the drywell head atmosphere, but on the outside it is bounded by the cooler surrounding atmosphere in the reactor pit. Thus the head failure criteria described earlier are not satisfied and the head does not leak.

There is a substantial temperature difference (350°F at 846 min) between the hottest and coldest regions of the primary containment. This is calculated as a result of the detailed nodalization scheme employed for the Mark II containment and would not be calculated if simpler nodalizations were used.

Figure 9.2.3 reports the calculated debris temperatures for the drywell floor in-pedestal cavity. Both the heavy oxide and metal layer temperatures rapidly increase as the debris begins pouring from the failed reactor vessel at 270 min. The layer temperatures reach a local peak of approximately 1900°F at 300 min due to the termination of the pour from the reactor vessel. Because there is no additional pour from 300-380 min, the debris cools and the temperatures decrease. The debris temperatures once again begin to increase as the second massive debris pour commences at 380 min.

At approximately 400 min, the debris reaches the ablation temperature of the limestone common sand concrete (2245°F) and concrete ablation begins. The pouring debris contains a mixture of low melting temperature metals (2750°F) and higher melting temperature oxides (4800°F). The debris pour temperature is between the two melting temperatures and the cavity debris temperatures continue to rise. The heavy oxide layer is at the bottom of the debris pool and has a much higher melting temperature than the overlying metal layer. Thick crusts initially form which insulate the bulk of the oxide layer. The oxide layer temperature therefore increases more rapidly than that of the overlying metals. This is the reason for the diverging layer temperatures between 400-490 min.

A light oxide layer forms on top of the metal layer at approximately 460 min. This is due to the small content of UO_2 in the debris pour after 460 min. Because UO_2 is extremely dense, and because it constitutes a large fraction of the earlier (380-460 min) portion of the second pour, all of the oxide pouring from the reactor vessel from 380-460 min settles to the bottom of the debris pool and no upper oxide layer can form. After 460 min, the UO_2 content of the debris pour is small, and, when the debris pour oxide combines with the concrete oxide rising through the metal layer, a buoyantly stable upper oxide layer is formed.

After 490 min, the heavy oxide layer temperature begins to decrease due to the increased heat losses. The increased heat losses stem from the melting of the heavy oxide and metal layer crusts, resulting in large intralayer convective heat transfer coefficients. This results in effective homogenization of the debris - decreasing the heavy oxide layer temperature while increasing the metal and light oxide layer temperatures. The melting

of the heavy oxide layer is due to the increasing concentration of the concrete oxides in the heavy oxide layer. Since the concrete oxides (SiO_2 and CaO) melt at lower temperatures than the core debris oxides (UO_2 and ZrO_2), mixing the two oxides results in a lowering of the heavy oxide layer solidus temperature. Thus, the heavy oxide layer experiences thinning of its crusts which lowers the thermal resistance to conduction heat transfer at the boundaries of the layer and the layer temperature begins to decrease.

Concrete oxide dilution of the heavy oxide layer continues until approximately 585 min. At this time, the heavy oxide layer density is calculated to be less than the overlying metal layer density and the code performs a "layer flip" of the metal and heavy oxide layers. In addition, the material of the formerly heavy oxide layer is combined with that of the light oxide layer so that the resulting mixture of light oxides is placed on top of the metal layer.

At 675 min, the debris temperatures drop due to depletion of the unoxidized zirconium and the reduction of the chemical power supplied to the debris. The carbon inventory which has been accumulating in the metal layer begins to react with the CO_2 released by the ablation of concrete. This process produces large quantities of CO by the process described in Sect. 8.2.

Figure 9.2.4 shows the cumulative debris gas releases for CO, CO_2, H_2, and H_2O. The CO release is very rapid and occurs only after the oxidation of all of the zirconium. This is the reason for the increased rate of pressure rise at 675 min as shown in Fig. 9.2.1.

Figure 9.2.5 depicts the axial and radial concrete ablation distances calculated for this transient. The concrete floor of the drywell is 3.74 ft thick and the cavity is 9.55 ft deep. Thus, the bottom of the cavity is located at a depth of 13.3 ft. It is seen that the floor is penetrated at 846 min and the calculation is terminated.

These results should not be generalized to conclude that all Mark II drywell floors will be completely ablated for a depressurized short-term station blackout scenario. The main reason for this limitation is that the current calculation assumes a deep cavity retains the core debris in a crucible geometry. In the current calculation, Fig. 9.2.6 shows that the total debris thickness is approximately 7.9 ft at 846 min and is well below the 13.3 ft thickness required before overflow onto the remaining drywell floor can occur. In this configuration, the debris has limited surface area through which it can lose heat to the atmosphere. Thus, more heat is transferred downward into the underlying concrete and more concrete is ablated. The core debris would spread into a configuration having a much larger surface area in Mark II drywell floor geometries that do not incorporate a

deep cavity. Thus, less heat would be transferred into the concrete and less ablation would result.

Figure 9.2.7 exhibits the time-dependent cumulative steam generation by the falling debris as it interacts with the water pool. Only 18,739 lb of steam are predicted to be produced as a result of this interaction. The conclusion to be made is that a 5% debris relocation to the wetwell in-pedestal pool does not result in pressures that threaten the containment (in the absence of a steam explosion). Figure 9.2.8 shows the calculated temperatures of the debris on the wetwell floor. The debris temperature is predicted to remain very low and there is no calculated debris-concrete interaction.

9.3 SEQUENCE WITH 80% DRYWELL/20% WETWELL DEBRIS SPLIT

This section presents containment response results obtained by MELCOR analysis of the short-term station blackout scenario assuming operation of the ADS system and entrance of 20% of the core debris into the pressure suppression pool. The transient addressed is identical to that described in Sect. 9.2 except for the assumption that 20% of the debris leaving the failed reactor vessel is deposited directly into the wetwell water pool.

Since the fraction of debris pouring from the failed reactor vessel is 20%, it is expected that the debris water pool interaction may be quite significant, and that large quantities of steam may be released into the containment atmosphere. It, therefore, becomes very important to properly model all sources of gas that can pressurize the containment. For the current case, realistic initial structural temperature profiles were explicitly specified. These profiles were based on the results of BWR-LTAS and BWRSAR calculations.

Because earlier analyses of the 100% drywell and the 95% drywell/5% wetwell cases resulted in the drywell floor being completely ablated in the axial direction, an effort was made to ascertain if the drywell floor would rupture with only 80% of the total debris mass interacting with the floor. This calculation continued until 1223 min without calculated floor rupture nor containment leakage due to overpressurization beyond 135 psig. This time frame is well beyond the 800-850 min period when floor rupture was predicted for the earlier cases and is also well beyond the end of the BWRSAR analysis of this scenario. The calculation was terminated due to a MELCOR floating point interrupt in subroutine MHTRAN.

The calculated containment pressure distribution is presented in Fig. 9.3.1. Annotations on the figure identify important events influencing the pressure response. The calculation begins at 35 min, with the first significant event being a pressure rise due to a SRV discharge of steam and hydrogen into the wetwell pool at approximately 120 min, with a second SRV discharge at approximately 220 min. Reactor vessel debris pouring first occurs at 270 min into the accident, and is accompanied by a simultaneous pressure rise due to steam production in the wetwell pool as a result of debris-water pool interaction in the wetwell. The debris pour lasts until approximately 300 min with the attendant steam production being rapidly condensed on the cold containment structures - thus, the subdued pressure response at this time.

A sharp pressure rise is calculated when a second very large debris pour commences at 380 min. The debris is primarily oxidic and its temperature as it exits the failed reactor vessel is higher than that of the earlier primarily metallic debris pour at 270 min. Thus, the debris energy exchange with the wetwell pool is quite vigorous. Large quantities of steam are produced and the containment pressure increases rapidly.

The pressure plateau between 530-570 min corresponds to a period when a significant fraction of the drywell debris internal heating is consumed by melting of the large quantity of metals lying on the floor. Once fully molten at 550 min, rapid radial ablation of the reactor pedestal ensues, the metal layer temperature rises to the overlying oxide layer temperature, hydrogen gas is rapidly released into the drywell atmosphere, and the pressure continues its upward track.

At approximately 700 min, the zirconium metal on the in-pedestal drywell floor is completely oxidized and a large debris release of hot carbon monoxide is calculated. Another inflection in the pressure response is observed at 800 min and is due to the refreezing of the thick metal layer adjacent to the drywell concrete floor. Freezing introduces a large conduction resistance to heat transfer between the debris and the underlying concrete so that concrete ablation and debris gas release decrease with an associated decrease in rate of containment pressurization.

Figure 9.3.2 depicts the primary containment atmospheric temperature distribution as a function of time. Once again there are noticeable discontinuities in the temperature traces. At times 130 and 220 min, the temperatures are predicted to increase rapidly in response to the SRV discharges mentioned earlier. The maximum temperature (with the exception of the in-pedestal airspace) occurs in the annulus between the biological shield and the outer surface of the reactor vessel. There is no general increase

in containment temperatures at the time of reactor vessel bottom head failure (270 min). Indeed, the drywell atmosphere temperatures actually decrease as debris begins to pour into the wetwell water pool. This is because the steam released into the airspace above the wetwell pool exists at the saturation temperature corresponding to the total pressure. At 270 min, this temperature is approximately 260°F. This steam is partially transported (via vacuum breakers) into the drywell and mixes with thermally stratified air that varies in temperature from 200°F in the lower ex-pedestal region to 600°F in the biological shield region. Thus drywell air temperatures generally decline immediately after the debris pour commences.

There is a noticeable increase in the temperature of the containment atmosphere at 380 min as the second debris pour from the reactor vessel begins and heat is transferred to the atmosphere. The drywell floor metal layer is fully molten by 550 min, so that the rate of heat transfer to the containment gas increases significantly and the in-pedestal gas temperature again increases. At approximately 690 min, the drywell floor zirconium content is completely oxidized and oxidation of the metal layer carbon accumulation begins to release significant quantities of carbon monoxide into the atmosphere. This gas is very hot and its effect is to temporarily raise the overall in-pedestal gas temperature. By approximately 800 min, the drywell floor metal layer once again is completely frozen so that heat transfer to the overlying in-pedestal atmosphere is reduced and the atmosphere temperature begins to drop. It should be noted that the drywell head region atmosphere does not exceed 700°F during the entire calculation. The drywell head seals are not expected to lose their integrity.

Figure 9.3.3 depicts the calculated drywell floor debris layer temperatures. Temperatures rapidly escalate as debris pours from the failed reactor vessel at 270 min but decrease once the pour stops at 300 min. They once again accelerate upward as the second debris pour commences at 380 min. The light oxide layer vanishes at 380 min due to combination with the heavy UO_2 and ZrO_2 pouring out of the failed reactor vessel. The new layer subsequently settles through the metallic layer into the heavy oxidic. The underlying heavy oxides accumulate decay heat because of the assumed association of the radionuclides with the UO_2 fuel. As a result, the heavy oxide layer temperature rises faster than the overlying frozen metals during the 380-470 min period.

The frozen metal layer temperature also rises and reaches its solidus temperature at approximately 470 min. At this time, the metal layer begins to melt and the thick radial crust thins. This enhances radial heat transfer to the reactor pedestal so that radial

ablation commences at 470 min. Since the metals overlay the heavy oxides, the oxides produced concrete ablation, rise through the metal layer and form a slag layer of light oxides on top of the metals. This is the reason for the appearance of the light oxide layer temperature at 470 min.

By 495 min, the heavy oxide layer temperature has peaked. This is due to the increasing heat transfer to the overlying metals, the gradual melting of the heavy oxide layer itself, and the temporary cessation of UO_2 pour from the failed reactor vessel. The UO_2 pour commences again at approximately 510 min and quickly drives the light oxide layer temperature upward such that the metal layer is heated by both the overlying and underlying oxide layers. The metal layer is completely molten by approximately 550 min and its temperature reaches the overlying oxide layer temperature by approximately 580 min.

By approximately 595 min, all three layer temperatures have converged. In addition, the heavy oxide layer has been sufficiently diluted by concrete slag oxides that its density is less than the overlying metal layer. MELCOR then performs a layer flip so that the metal layer is located adjacent to the concrete. The previous heavy oxide material is combined with the previous light oxide material so that the resulting mixture of oxides resides as a new light oxide layer.

At 690 min, the drywell zirconium inventory is depleted and the debris temperatures begin to decrease. By 710 min, the debris temperature has fallen to the metal layer freezing temperature and metal layer crusts begin to develop. By 790 min, the metal layer is completely frozen so that the metal and oxide layer temperatures begin to diverge. From this time forward, the debris temperature slowly decreases with decay heat but still remains continuously above the concrete ablation temperature of 2246°F.

Cumulative debris gas release from the debris on the drywell floor is shown in Fig. 9.3.4. The first gas to be released in significant quantities is hydrogen at 400 min, and is due to zirconium oxidation by water vapor originating from the decomposition of concrete produced by concrete ablation. Zirconium oxidation by carbon dioxide results in carbon being produced and retained in the metal layer. As mentioned earlier, drywell debris layer flip is calculated at 595 min. Following this event, the metal layer is relocated downward, adjacent to the concrete, and all oxidic debris is located above the metals. As a result, all concrete ablation by the oxide layer releases gas into the debris above the metal layer. Reduction of this gas to hydrogen and carbon is precluded and it

is transported directly to the overlying atmosphere in unconverted form. This is the reason for the appearance of carbon dioxide and water vapor at 595 min.

By 690 min, the zirconium inventory is completely oxidized. The carbon inventory accumulated in the metal layer during the oxidation of the zirconium begins to oxidize with the carbon dioxide originating from concrete ablation. A very rapid release of carbon monoxide is calculated so that by 800 minutes, the release of carbon monoxide surpasses that of hydrogen. After this time, the rate of release of each gas appears approximately linear.

Drywell floor concrete ablation histories are presented in Fig. 9.3.5. The upper surface of the basemat is eroded to the point almost reaching the lower surface of the drywell floor. The difference at the end of the calculation is approximately 0.5 in. Since axial concrete ablation is still occurring at 1223 min, it is expected that the drywell floor would be ruptured shortly thereafter. By 1223 min, approximately 0.98 ft of pedestal thickness (or approximately 20% of the initial pedestal thickness) remains, so that pedestal integrity in the radial direction is also in question.

It is observed that rapid concrete ablation occurs between approximately 500-800 min. This is well after the onset of the second debris pour at 380 min from the failed reactor vessel. The delay is caused by the heatup and melting of the frozen metallic debris poured from the vessel during the initial debris pour from 270-300 min. The rapid ablation continues as unoxidized zirconium exothermically reacts with H_2O and CO_2 gas released from concrete decomposition. After zirconium exhaustion at 690 min and complete metal layer freezing at 790 min, ablation rates slow significantly. The slow ablation rates observed after 790 min are due to the continuously decreasing debris decay heat.

In-pedestal drywell debris layer thicknesses are presented in Fig. 9.3.6. The thickness of the layers are seen to increase directly in response to the debris pours at 270 and 380 min. The heavy oxide layer is created only after the initiation of the second debris pour at 380 min. It is composed mainly of UO_2 and ZrO_2 pouring from the reactor vessel bottom head. These materials are calculated to sink through the metal layer which is composed primarily of iron, chromium, nickel, and zirconium. Following layer flip at 595 min, the heavy oxide layer disappears and the light oxide layer thickness ratchets upward. The metal layer thickness decreases between 500 and 800 min. This is due to the oxidation of metals and the relocation of their masses in oxide form to the overlying oxide layer. After 800 min, the layers are almost unchanging in thickness. This is due to

the very slow debris pour from the reactor vessel and the very slow rate of concrete ablation.

Figure 9.3.7 presents the calculated thermal history of the debris transferred onto the wetwell floor after having interacted with the water pool and losing much of its thermal energy. As mentioned previously, the interaction with the water pool is calculated via the FDI package and it should be recognized that no accounting is made for concrete decomposition products in the debris or the possible occurrence of steam explosions. Figure 9.3.7 indicates that the thermal response of the debris is benign when compared to that of the drywell floor debris. Significant temperature excursions occur only after the second debris pour commences at 400 min.

A heavy oxide layer forms at the bottom of the debris pile. The temperature of the heavy oxide layer slowly increases as decay heat accumulates in the layer, and the debris in general becomes insulated from the overlying pool of water. The average temperature of the heavy oxide layer reaches the concrete ablation temperature of 2246°F (1503 K) at 900 min. Prior to this at 730 min, the temperature profile in the heavy oxide layer is such that ablation of the underlying concrete begins, even though the average layer temperature is below the concrete ablation temperature. By 850 min, a layer of light oxides is calculated to form on top of the metal layer. The light oxide layer acts to insulate the frozen metal layer and the metal layer temperature begins to escalate. By 1150 min, the heavy oxide layer has been sufficiently diluted that layer flip is predicted to occur. This places relatively cold, frozen metal adjacent to the concrete and concrete ablation stops.

It is possible that the wetwell debris temperatures would have continued to rise after 1223 min if the error had not been encountered in subroutine MHTRAN. The reason for this is the existence of 13200 lb of unoxidized zirconium in the metal layer at the time the run aborted. As can be seen in Fig. 9.3.7, the metal layer temperature is approaching the concrete ablation temperature and it is conceivable that concrete ablation could be sufficient to release enough gas to cause runaway zirconium oxidation. The temperature excursion would be short-lived however, because of the small zirconium mass. In any event, the calculation would be terminated by the impending rupture of the drywell floor overlying the wetwell.

Wetwell debris cumulative gas releases are shown in Fig. 9.3.8. The only significant gas release is the hydrogen produced by the chemical reaction of water vapor with zirconium. This reaction begins at the onset of concrete ablation at 720 min.

Chemical reaction of the carbon dioxide with zirconium does not directly release carbon monoxide but produces condensed carbon which is assumed to be retained in the metal layer. As mentioned above, the zirconium inventory remaining at the end of the calculation (at 1223 min) is 13,200 lb. This mass of zirconium would have to be oxidized before there is any conversion of the condensed carbon to carbon monoxide. The release of hydrogen ceases at 1150 min due to the layer flip described above. The layer flip causes frozen metals to be located adjacent to the concrete basemat. Concrete ablation ceases, and the gas supply feeding the zirconium-steam reaction is terminated.

The wetwell cavity ablation characteristics are shown in Fig. 9.3.9. The geometrical configuration of the wetwell cavity is assumed to be exactly as described above for the drywell cavity. Thus, cavity penetration occurs if the bottom of the cavity reaches 13.3 ft or the radius of the cavity reaches 14.96 ft. As described above, axial ablation of the wetwell cavity begins when the temperature of the concrete interface of the heavy oxide layer exceeds the concrete ablation temperature of 2246°F (1503 K). By the time of layer flip at 1150 min, only approximately 4 in. of concrete have been ablated. Radial ablation is calculated to be insignificant.

Wetwell debris layer thicknesses are shown in Fig. 9.3.10. The metal layer thickness increases directly with the debris pours leaving the reactor vessel at 270 and 380 min. The heavy oxide layer is created only after the initiation of the second debris pour at 380 min. The heavy oxide layer is composed mainly of UO_2 and ZrO_2 pouring from the reactor vessel bottom head. These materials are calculated to sink through the metal layer which is composed primarily of iron, chromium, nickel, and zirconium. The heavy oxide layer disappears at 1150 min because layer flip causes the heavy oxide layer to mix with light oxide materials so that a new light oxide layer is formed. This is the reason for the jump in light oxide layer thickness at 1150 min. The cold metal layer is relocated to the bottom of the debris pile where, as explained previously, concrete ablation and chemical reactions cease.

Figure 9.3.11 presents the cumulative steam production due to the debris-wetwell water pool interaction as the debris falls through the pool (as calculated by FDI). The steam production corresponds directly with the debris pours from the failed reactor vessel. Cumulative steam production is approximately 74,956 lb, a factor of four higher than the 18,739 lb produced in the 95% drywell/5% wetwell case reported in Sect. 9.2. This is consistent with the fact that four times as much debris is relocated to the wetwell in the 80%/20% case as in the 95%/5% case analyzed earlier.

9.4 SEQUENCE WITH 60% DRYWELL/40% WETWELL DEBRIS SPLIT

This section presents containment results obtained by MELCOR analysis of the short-term station blackout scenario assuming operation of the ADS system and entrance of 40% of the core debris into the pressure suppression pool. The transient addressed is identical to those of Sect. 9.2 and 9.3 except for the assumption that 40% of the debris leaving the failed reactor vessel is deposited directly into the wetwell water pool.

As expected, the drywell floor ablation was decreased for this case and floor rupture was not calculated during the time frame investigated (35-1600 min). At 1600 min (27 h), the drywell floor thickness remaining to be ablated is 5.3 in. Assuming a constant concrete ablation rate, the extrapolated time of floor burn-through is 2380 min (40 hr).

The calculated wetwell containment pressure remains below the leakage threshold of 135 psig, even at time 1600 min. This is a result of the very slow gas evolution rate from the debris-concrete interactions in the drywell and the wetwell. At 1600 min, the drywell pressure is calculated to be 130 psig while wetwell pressure is 125 psig. Extrapolation of the containment pressurization rate indicates that the wetwell would reach the leakage pressure of 135 psig at 2037 min (34 h) - six hours before the time predicted for drywell floor burn-through.

Because of the very slow rate of change of the containment response at 1600 min, the MELCOR analysis of this scenario was terminated at this time. No thermal-hydraulic forcing functions remain to be investigated with the exception of a slowly decreasing decay heat that causes a slow rate of concrete ablation. BWRSAR analysis was terminated at 900 min because of the expulsion of all the debris residing in the failed reactor vessel bottom head.

The time-dependent containment pressure distribution is presented in Fig. 9.4.1. A sharp pressure rise is calculated when a second very large debris pour commences at 380 min. The debris pour is primarily oxidic and its temperature as it exits the failed reactor vessel is higher than that of the earlier primarily metallic pour at 270 min. Thus, at 380 min, the debris energy exchange with the wetwell pool is quite vigorous, large quantities of steam are produced, and containment pressure increases rapidly.

The pressure peak at 530 min and the subsequent pressure decrease until 570 min corresponds to a period when a significant fraction of the drywell debris internal heating is consumed by melting of the large quantity of metals lying on the drywell floor. At

570 min, the drywell floor metals are fully molten and the temperatures of both the metal and overlying oxide layers begin to rise due to heat transfer from the underlying heavy oxide layer. The containment pressure stabilizes due to the increasing drywell debris gas release.

At 600 min, the drywell debris metal and heavy oxide layers experience layer flip. This event results in a fully molten metal layer being relocated adjacent to the concrete floor and a vigorous interaction with the concrete. Large quantities of hydrogen are released from the debris into the drywell atmosphere and the containment pressure once again increases.

At approximately 680 min, the drywell debris zirconium inventory is exhausted and the accumulated inventory of carbon begins to react with the carbon dioxide and water vapor originating from concrete decomposition of the drywell floor. This oxidation of carbon results in two moles of gas produced for every mole of gas reacted so that the molar gas flow leaving the debris is effectively double that entering the debris from the concrete. The containment pressure experiences another step upward.

At 1099 min, the wetwell inventory of zirconium is exhausted and the inventory of carbon in that cavity begins to react with the carbon dioxide from the concrete to produce a significant quantity of carbon monoxide that enters the wetwell airspace. This is the reason for the step increase in wetwell pressure at this time.

At 1600 min, the gas release rate from the drywell and the wetwell debris-concrete interactions sums to 5.3 moles. Thus the containment pressurization rate is very slow and the extrapolated time of containment overpressurization is 2037 min (34 h).

Figure 9.4.2 depicts the primary containment atmospheric temperature distribution as a function of time. Once again there are noticeable discontinuities in the temperature traces. At times 130 and 220 min, the temperatures are predicted to increase rapidly in response to the SRV discharges mentioned earlier. There is no general increase in containment temperatures at the time of reactor vessel bottom head failure and debris discharge (270 min). Indeed, the drywell atmosphere temperatures actually decrease as debris begins to pour into the wetwell water pool. This is because the steam released into the airspace above the wetwell pool exits at the saturation temperature corresponding to the total wetwell pressure. At 270 min, this temperature is approximately 260°F. This steam is partially transported (via vacuum breakers) into the drywell and mixes with thermally stratified air that varies in temperature from 200°F in the lower ex-pedestal region to 600°F in the biological shield region. Thus the drywell air temperatures

generally decline immediately after the debris pour commences, due to mixing with the cold saturated steam flowing from the wetwell.

At 380 min, there is a noticeable increase in the temperature of the containment atmosphere as the second debris pour from the reactor vessel begins and heat is transferred to the atmosphere. As mentioned earlier, layer flip occurs at 600 min for the drywell debris. This places very hot oxide on top of the molten metal and concrete ablation accelerates, thus accelerating the debris gas release into the drywell atmosphere. This gas is very hot and therefore the drywell atmosphere, especially that of the in-pedestal region adjacent to the debris, rapidly heats. Again at 680 min, gas release into the drywell atmosphere is enhanced as the drywell inventory of zirconium is exhausted and carbon monoxide is released from the debris.

At 760 min, the drywell metallic debris becomes frozen so that a large conduction resistance to heat transfer to the underlying concrete drywell floor develops. This slows concrete ablation, gas release into the debris, and gas release from the debris into the in-pedestal drywell region. Thus the drywell atmospheric temperatures begin to experience a general decline as the heating source provided by the debris gas release is outweighed by the cooling source provided by the cold water vapor entering the drywell from the wetwell airspace. Again the water vapor is produced by the interaction of the 40% of the debris falling through and interacting with the wetwell water pool.

Figure 9.4.3 compares the calculated drywell floor debris layer temperatures. Temperatures rapidly escalate as debris pours from the failed reactor vessel at 270 min, but decrease once the pour stops at 300 min. They once again accelerate upward as the second debris pour commences at 380 min. The light oxide layer appears at 460 min as the metal layer temperature exceeds the concrete ablation temperature and concrete slag accumulates on top of the debris. From 530-570 min, the metal layer undergoes melting and is fully molten at 570 min. Metal and light oxide layer temperatures increase after 570 min and converge to the heavy oxide layer temperature at 600 min.

By 600 min, all drywell debris temperatures are uniform at approximately 3014°F. This is well above the concrete ablation temperature and so concrete ablation is vigorous. Gas release into the debris rapidly oxidizes the zirconium inventory and produces a chemical power approximately seven times that of the decay power. By 680 min, the zirconium inventory has been exhausted, the chemical power source disappears, and the drywell debris temperatures begin to decrease.

By 760 min, the metal layer has completely frozen and its temperature falls below that of the decay energy-bearing overlying oxide layer. From this time forward, the drywell debris temperatures slowly decrease (but remain above the concrete ablation temperature). Thus even though the debris temperatures are less than they were earlier, concrete ablation continues, albeit at a slower rate. Thus, there is a continuous gas source into the drywell atmosphere and containment pressure continues to increase.

Cumulative debris gas release from the debris on the drywell floor is shown in Fig. 9.4.4. The first gas to be released in significant quantities is hydrogen at 400 min and is due to zirconium oxidation by water vapor originating from the ablation of concrete. Zirconium oxidation by carbon dioxide results in carbon being produced and retained in the metal layer. Drywell debris layer flip is predicted to occur at 600 min. Following this event, the metal layer is relocated downward adjacent to the concrete and all oxidic debris is located above the metals. As a result, all concrete ablation by the oxide layer releases gas into the debris above the metal layer. Reduction of this gas to hydrogen and carbon is precluded and it is transported directly to the overlying atmosphere in unconverted form. This is the reason for the appearance of carbon dioxide and water vapor at 600 min.

By 680 min, the zirconium inventory is completely oxidized. The carbon inventory that had accumulated in the metal layer during zirconium reaction begins to oxidize with the carbon dioxide originating from the concrete ablation. A very rapid release of carbon monoxide is calculated until 760 min. At this time the metal layer has become completely frozen so that a large conduction resistance develops to inhibit heat transfer to the underlying concrete. Concrete ablation slows and so does the gas release rate into the debris and from the debris. After 760 min, gases are slowly released from the debris consistent with the reduced concrete ablation rate and the associated chemistry of the oxidation of remaining metallic species such as chromium and iron.

Drywell floor concrete ablation histories are presented in Fig. 9.4.5. The upper surface of the basemat is 9.55 ft. The lower surface of the drywell floor is located at 3.74 + 9.55 = 13.29 ft and, as can be seen in Fig. 5, the upper surface of the basemat is eroded to a depth of approximately 12.8 ft by 1600 min. The remaining thickness of the drywell floor is 5.3 in. and the corresponding concrete erosion rate is 0.4 in./h. Extrapolation of this ablation rate leads to the estimation that the drywell floor would burnthrough at 2380 min (40 h), some 13 h after the point of termination of this calculation.

It is observed that rapid concrete ablation occurs between approximately 500 and 700 min. After zirconium exhaustion at 680 min and complete metal layer freezing at 760 min, ablation slows significantly. The slow ablation rate of 0.4 in./h observed at 1600 min as mentioned above is due to the slowly decreasing decay heat.

In-pedestal drywell debris layer thicknesses are presented in Fig. 9.4.6. Following layer flip at 600 min, the heavy oxide layer disappears and the light oxide layer thickness increases. The metal layer thickness decreases between 500 and 760 min, due to the oxidation of metals and the relocation of their masses in oxide form to the overlying oxide layer. After 760 min, layer thicknesses change very slowly and are indicative of the slow debris pour from the reactor vessel and the very slow rate of concrete ablation.

Figure 9.4.7 presents the calculated thermal history of the debris transferred onto the wetwell floor after having interacted with the water pool and losing much of its thermal energy. As mentioned previously, the interaction with the water pool is calculated via the FDI Package which does not account for the presence of concrete decomposition products or the possible occurrence of steam explosions. The debris-concrete interaction at the bottom of the wetwell pool is calculated via the CORCON portion of the CAV module of MELCOR.

The heavy oxide layer temperature rapidly increases at the onset of the second debris pour at 380 min. The average temperature of the heavy oxide layer reaches the concrete ablation temperature of 2246°F (1503 K) at 650 min. Prior to this at 550 min, the temperature profile in the heavy oxide layer is such that ablation of the underlying concrete begins even though the the average layer temperature is below the concrete ablation temperature.

By 850 min, a layer of light oxides is calculated to form on top of the metal layer. The light layer of oxides acts to insulate the frozen metal layer from the overlying water pool and the metal layer temperature begins to escalate. By 1000 min, the heavy oxide layer has been sufficiently diluted that layer flip is predicted to occur. By this time, the metal layer temperature has reached its melting temperature. When layer flip occurs partially molten metallic debris is located adjacent to the underlying concrete. The ensuing rapid concrete ablation releases gas so that the resulting chemical power produced by metal oxidation combined with heat transfer from the overlying oxide layer is sufficient to completely melt the metallic debris by 1050 min. Slight superheating of the metal layer is observed shortly thereafter, and the metal and oxide layer temperatures are calculated to converge.

By 1100 min, the wetwell zirconium inventory is exhausted, the chemical power is reduced, and the metal layer rapidly freezes. From this point forward, the metal layer is slightly cooler than the overlying layer of decay energy-bearing oxides. At all times after 1100 min, however, both the oxide and the metal layer temperatures remain above the concrete ablation temperature. As a result, concrete ablation and the associated gas release continue (at a slower pace).

Wetwell debris cumulative gas releases are shown in Fig. 9.4.8. The predominant gas release is hydrogen produced as a result of chemical reaction of zirconium with water vapor originating from concrete decomposition. The generation of carbon monoxide is due to the exhaustion of zirconium at 1100 min and the subsequent oxidation of carbon that had accumulated during the period of zirconium oxidation. Insignificant quantities of carbon dioxide and water vapor are released from the debris. This is because the metal layer rapidly freezes and concrete ablation slows significantly once the zirconium is completely oxidized (at 1100 min). Thus, there is little gas that enters or leaves the debris.

The wetwell cavity ablation characteristics are shown in Fig. 9.4.9. As described above, axial ablation of the wetwell cavity begins when the temperature of the concrete interface of the heavy oxide layer exceeds the concrete ablation temperature of 2246°F (1503 K). This occurs at 550 min and the bottom surface of the wetwell cavity begins to recede.

The axial ablation rate escalates as the heavy oxide layer accumulates mass and a thick upper crust forms at the interface with the overlying metal layer. It escalates even further at 1000 min when layer flip occurs and partially molten metals are located adjacent to the underlying concrete. Ablation rates slow when the wetwell zirconium inventory is exhausted at 1100 min and the metal layer layer rapidly freezes. The formation of a frozen metal layer creates a significant resistance to heat transfer to the underlying concrete thus providing the mechanism for the slowdown in concrete ablation. After 1100 min, concrete ablation proceeds slowly as the temperature of the debris continues to exceed the concrete ablation temperature of 2246°F (1503 K).

Wetwell debris layer thicknesses are shown in Fig. 9.4.10. The appearance of a light oxide layer at 850 min occurs near the end of the debris pour from the reactor vessel at 900 min as calculated by BWRSAR. This light oxide layer forms as concrete ablation by the metal layer generates concrete slag products such as SiO_2 and CaO. These species are lighter than the metals and therefore float on the metals and form a separate layer.

By 1000 min, the heavy oxides have been sufficiently diluted that layer flip is calculated to occur. The metal layer is relocated adjacent to the concrete while the heavy and light oxide layer materials are combined into a single new layer of light oxides overlying the metals. As a result, the thickness of the light oxide layer increases significantly and the thickness of the heavy oxide layer is reduced to zero. The decrease in metal layer thickness after 1000 min is due to the oxidation of the significant inventory of zirconium and the relocation of its mass in oxide form to the overlying light oxide layer. Following zirconium exhaustion at 1100 min, the metal layer thickness changes very little while the light oxide layer thickness continues to grow, but at a much reduced rate.

Figure 9.4.11 presents the cumulative steam production due to the debris/wetwell water pool interaction as the debris falls through the pool (as calculated by FDI). The steam production corresponds directly with the debris pours from the failed reactor vessel. Cumulative steam production is approximately 148,000 lb, a factor of two greater than the 75,000 lb generated in the 20% wetwell debris split case described in Sect. 9.3. This is consistent with the fact that twice as much of the debris is directed into the wetwell pool for the current calculation.

9.5 SEQUENCE WITH 0% DRYWELL/100% WETWELL DEBRIS SPLIT

This section presents containment response results obtained by MELCOR analysis of the short-term station blackout scenario assuming operation of the ADS system and entrance of all core debris into the pressure suppression pool. The transient addressed is identical to those in Sects. 9.2-9.4 except for the assumption that all debris leaving the failed reactor vessel is deposited directly into the wetwell water pool. In this sense, this calculation represents one of the extreme debris partitionings possible.

The calculation terminated abnormally in subroutine VSCRIT at 774 min while attempting to determine the square root of a negative number. It is believed that this error does not affect the credibility of the results presented here. Although there are several important phenomenological aspects of the problem remaining to be calculated after 774 min, the critical question of determining maximum containment pressure has been answered; no further analysis is required for this purpose.

Figure 9.5.1 presents the time-dependent primary containment pressure distribution for this sequence. As can be seen, the pressure reaches the 135 psig level

required for wetwell failure at 510 min. A permanently-open leakage area of 0.1 ft^2 is assumed to occur at this time.

Figure 9.5.2 depicts the primary containment atmospheric temperature distribution as a function of time. By 300 min, the initial debris pour has terminated and hot hydrogen and steam begin to stream into the in-pedestal region of the drywell from the failed reactor vessel and atmosphere temperatures begin to increase. When the second debris pour commences at 380 min, drywell atmospheric temperatures decrease slightly due to the mixing process described above. After approximately 420 min, drywell temperatures resume their slow rate of increase due to atmospheric heating from the hot reactor vessel wall and the streaming of hot hydrogen and water vapor from the failed bottom head. It should be noted that the drywell head flange seals are not sufficiently heated to threaten their integrity.

Figure 9.5.3 presents the cumulative mass leakage for each of the hydrodynamic materials considered by MELCOR. Most of the mass that has left the containment is water vapor with nitrogen being a distant second. By 750 min, approximately 95% of the initial nitrogen has left the containment which implies that the predominant containment atmospheric gas is water vapor. Noncondensible gases such as carbon monoxide, hydrogen, and carbon dioxide constitute such a small fraction of the containment atmosphere that their egress from the containment is not noticeable relative to the nitrogen and water vapor.

Figure 9.5.4 depicts the calculated debris temperatures for the debris lying on the wetwell floor. Significant excursions are noticed only after the second debris pour at 380 min. By 750 min, debris temperatures are such that the oxide layer has only thin top and bottom crusts while the metal layer is mostly frozen with the only molten portion being located adjacent to the heavy oxide layer. Debris decay heat amounts to 13.3 MW while chemical power is 8.96 MW.

The debris gas releases of hydrogen, carbon monoxide, carbon dioxide, and water vapor are shown in Fig. 9.5.5. The only significant gas release is hydrogen that is produced as a result of the chemical reaction of water vapor with zirconium. Chemical reaction of the carbon dioxide with zirconium does not directly release carbon monoxide but produces solid carbon which is assumed to be retained in the metal layer. By 750 min, 102,177 lb of zirconium remain (total inventory not oxidized within the reactor vessel is 113,869 lb) to be oxidized and 1217 lb of carbon has accumulated in the metal layer. The carbon will continue to accumulate in the metal layer until all the zirconium is

oxidized. Once the zirconium is exhausted, the carbon will react with any carbon dioxide or water vapor flowing through the metal layer to produce large quantities of carbon monoxide. Given the zirconium inventory at 750 min, complete zirconium oxidation may require an additional significant period of time.

CORCON's calculated maximum cavity boundaries are shown in Fig. 9.5.6. Axial concrete ablation commences around 470 min and coincides with the debris temperature reaching the concrete ablation temperature of 2246°F (Fig. 9.5.4). The axial ablation rate at 750 min is 0.36 ft/h with a total of approximately 0.6 ft having been ablated at that time. It is anticipated that this rate of ablation would continue (or may even escalate) at least until the time of zirconium exhaustion. Radial ablation is insignificant during the period of this calculation but might accelerate following layer flip caused by dilution of the heavy oxide layer by concrete slag products.

Wetwell debris layer thicknesses are shown in Fig. 9.5.7. The heavy oxide layer is created only after the initiation of the second debris pour at 380 min. It is believed that the oxide layer thickness would continue to increase after the termination of debris pour from the reactor vessel at 900 min. This is because of the continued concrete ablation driven by debris decay heat and chemical power.

Cumulative steam generation calculated by the FDI module of MELCOR is shown in Fig. 9.5.8. Steam production directly corresponds to the timing (270 and 380 min) and magnitude of debris pours from the failed reactor vessel. It is interesting to note that the steam production at 750 min amounts to 3.38×10^5 lb while for the 80%/20% case studied in Sect 9.3 cumulative steam production amounts to 7.21×10^4 lb. This converts to a factor of 4.7 greater steam production in the 100% wetwell case compared to the 20% wetwell case. Since the cumulative wetwell debris mass ratio is 5.0, this suggests that FDI calculated less energy transfer per unit debris mass for the 100% case than the 20% case, a fact confirmed by study of FDI output.

This result is also consistent with the specified FDI input hole diameter of 20.25 ft in the 100% wetwell case compared to the 9.06 ft diameter specified in the 20% case. Since the initial debris jet diameter is larger for the 100% wetwell case, it appears likely that the jet breakup droplet size is larger for the 100% case than the 20% case. Because the droplet surface area to volume ratio directly depends on the reciprocal of the drop diameter, it is reasonable that heat transfer is more efficient for smaller drops than for larger drops; thus, the greater energy transfer per unit mass for the 20% wetwell case. It appears however that entry of large fractions of the core debris into the wetwell results in

sufficient heat transfer and steam generation to pressurize the wetwell to the leakage threshold. This observed sensitivity of calculated results to the arbitrary FDI input specification chosen for this calculation demonstrates the need for further exploration of FDI modeling.

9.6 SUMMARY OF MARK II DUAL CAVITY CALCULATIONS

Five calculations in this series (100% drywell/0% wetwell, 95% drywell/5% wetwell, 80% drywell/20% wetwell, 60% drywell/40% wetwell, and 0% drywell/100% wetwell) have been completed. The fundamental results of these calculations are summarized in Fig. 9.6.1, which depicts the time required to reach various containment pressures as a function of the percentage of the reactor vessel debris pour that is assumed to enter the wetwell.

The first noteworthy observation from Fig. 9.6.1 is that pressures above 100 psig were not reached prior to gross in-pedestal drywell floor failure in the 0% wetwell and 5% wetwell debris split cases. Second, while containment pressures rise very gradually for cases in which a relatively minor fraction of the debris enters the pool (9.2 h is required to raise the containment pressure from 30 psig to 100 psig in the 5% wetwell split fraction case), the time required to raise containment pressure from 30 psig to the estimated failure pressure (135 psig) is only 2.2 h for the case in which all of the debris enters the wetwell. The final (and perhaps the most interesting) observation is that the time required to reach highly-elevated pressures (100-120 psig) is maximized for some intermediate debris splits. While not completely understood at the present time, this phenomenon appears to be due to competition between steam and non condensible gas generation from the core-concrete and debris-coolant interactions, and steam condensation on the containment structures.

These analyses indicated that the containment would fail if the fraction of debris residing on the floor of the drywell floor equaled or exceeded 80% of the total BWRSAR calculated debris mass pouring from the failed reactor vessel. Containment failure was predicted to occur by drywell floor rupture due to extensive concrete ablation. Containment pressurization due to the steam production created as a result of the debris-wetwell water interaction was limited by rapid steam condensation onto the relatively cold containment structures. In these calculations, the drywell floor was not covered by a pool of water.

Containment failure via overpressurization past the leakage threshold of 135 psig was calculated for the case of 100% debris entering the wetwell pool. In this case, steam condensation could not prevent overpressurization of the containment.

Several important modeling uncertainties and limitations should be considered while reviewing Fig. 9.6.1. First, the effects of steam explosions are not considered in the present analysis. Second, the reactor vessel debris is assumed to instantaneously transport to the wetwell, without dilution or mixing with drywell floor concrete decomposition products. Third, the opening in the drywell floor which could provide the pathway for transport of the debris into the wetwell was not modeled as a hydraulic flowpath. Therefore, the applicability of these calculations for cases in which failed in-pedestal drainlines or downcomers provide the debris flowpath is somewhat uncertain. No provision for a drywell-to-wetwell airspace flowpath was made. The predicted behavior of the drywell vacuum breakers and drywell water pools (formed from reactor vessel leakage and steam condensation) is subject to great uncertainty. Fourth, the FDI package was exercised as a "black box". No effort has been made to investigate the sensitivity of these results to some basic FDI modeling parameters such as debris particle size and the velocity of the debris as it falls through the water. Fifth, these results are relevant only to that portion of the sequence prior to gross in-pedestal drywell floor or reactor pedestal failure (due to ablation). Since the containment was assumed to fail at 135 psig in these calculations, no pressures in excess of this value are predicted. Finally, it should be noted that the fundamental pedestal design of the various Mark II plants would tend to drive debris split fractions to opposite extremes. Plants such as Nine Mile Point-2, with a deep drywell in-pedestal cavity and in-pedestal downcomers, would tend to transport very large fractions of the debris into the pool, while plants such as Susquenhanna, which have no in-pedestal cavity, drains, or downcomers, would tend to delay the entrance of any debris into the pool. The remaining plants (which all have through-the-floor in-pedestal drains) could allow some amount of debris to enter the pool via melt-through and failure of the drain lines. All of these limitations act together to limit the applicability of the results depicted in Fig. 9.6.1. Nevertheless, Fig. 9.6.1 does present an interesting look at the potential impact of debris-pool interactions on Mark II severe accident containment performance.

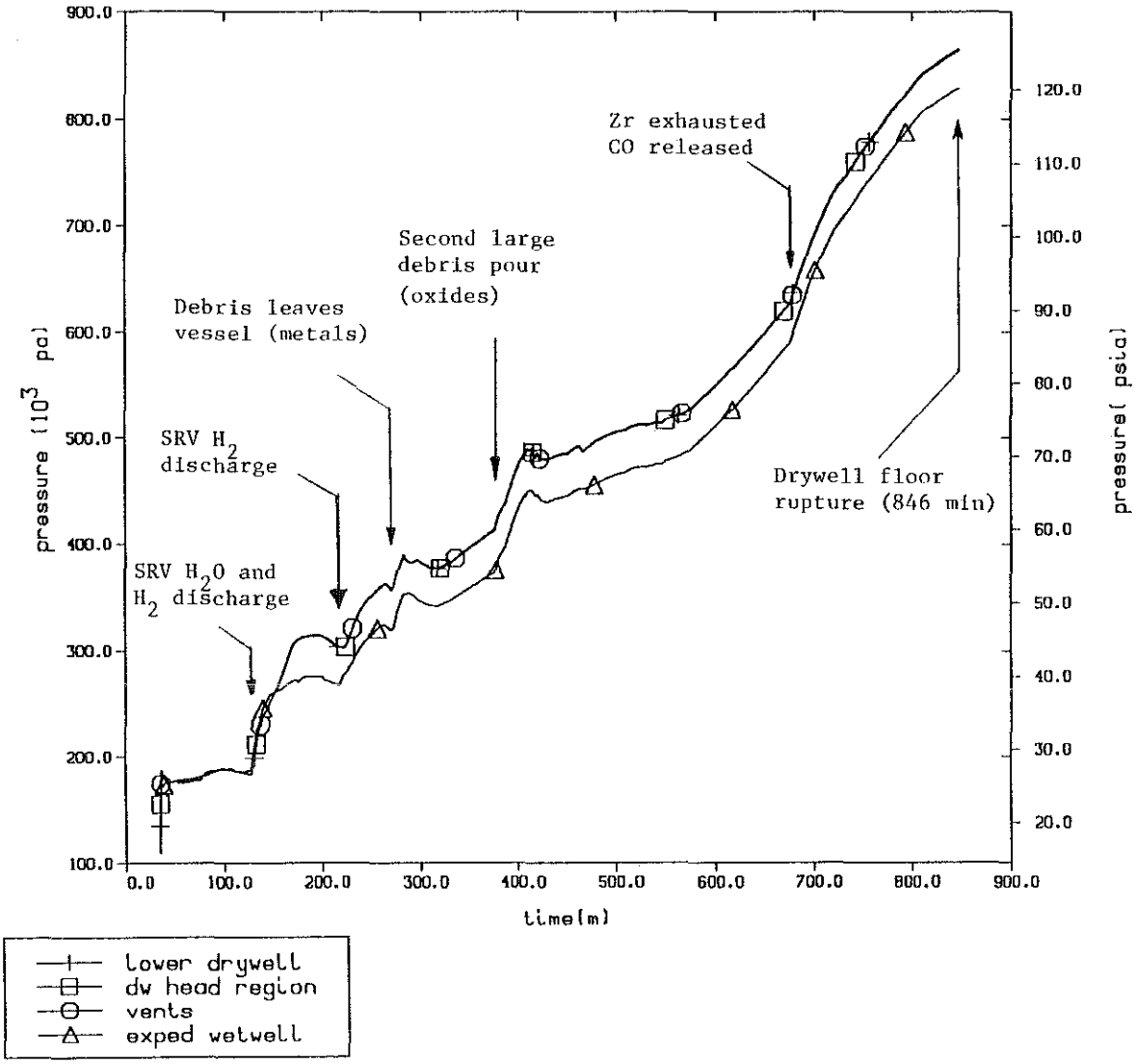

Fig. 9.2.1. Primary containment pressure distribution for the dual cavity (95% drywell/5% wetwell) Mark II short-term station blackout with ADS actuation.

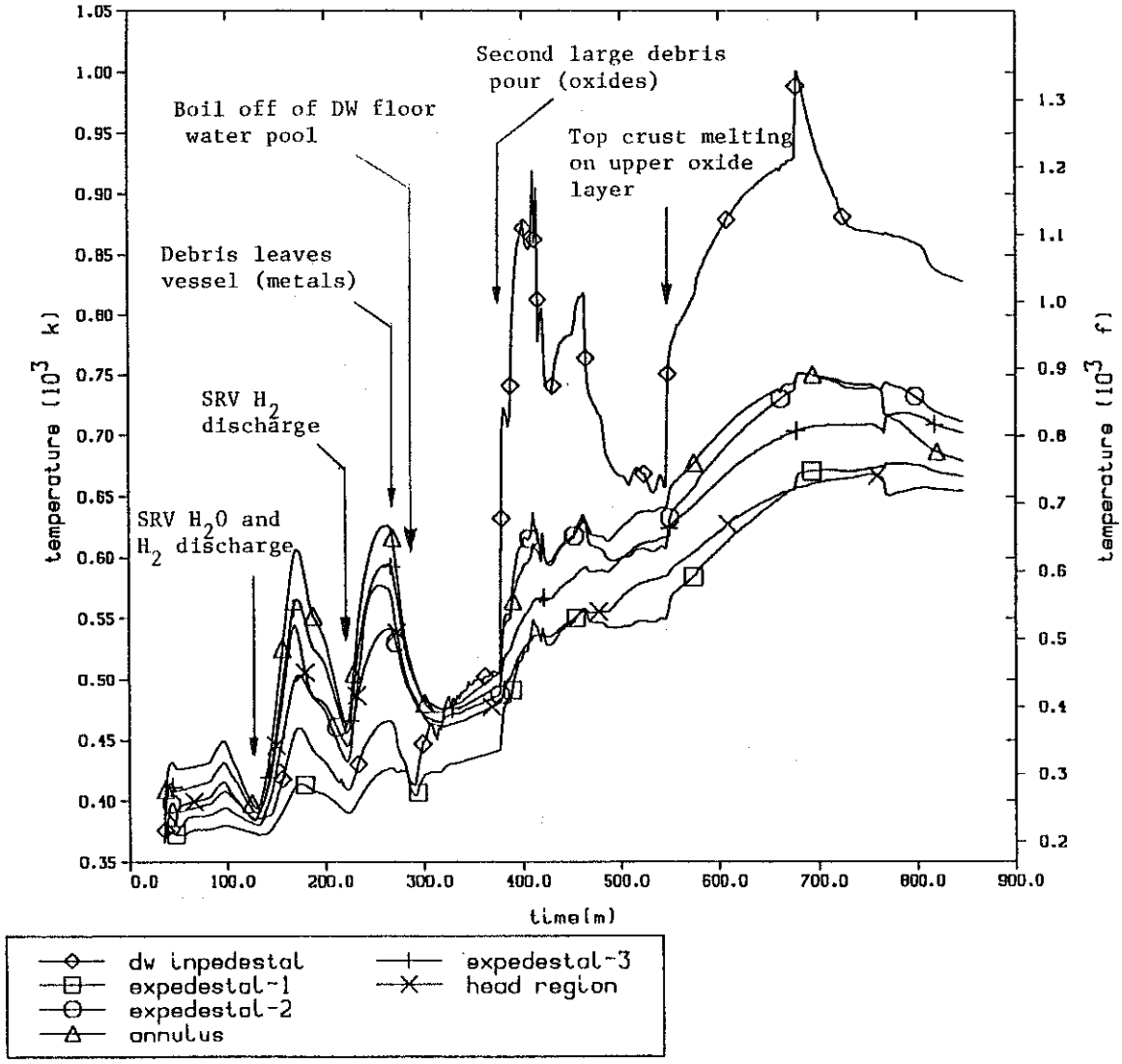

Fig. 9.2.2. Primary containment temperature distribution for the dual cavity (95% drywell/5% wetwell) Mark II short-term station blackout with ADS actuation.

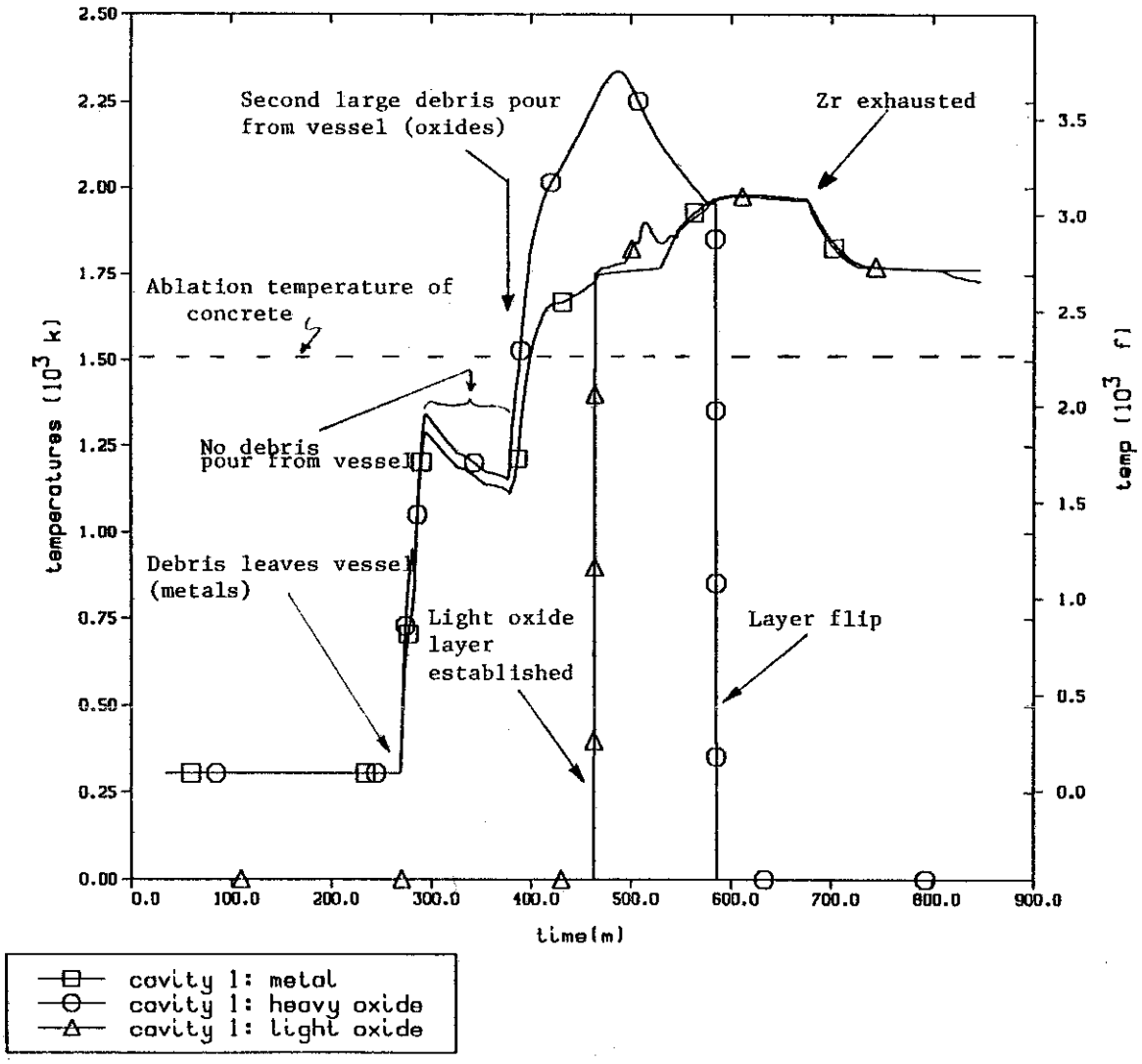

Fig. 9.2.3. In-pedestal drywell debris layer temperatures for the dual cavity (95% drywell/5% wetwell) Mark II short-term station blackout with ADS actuation.

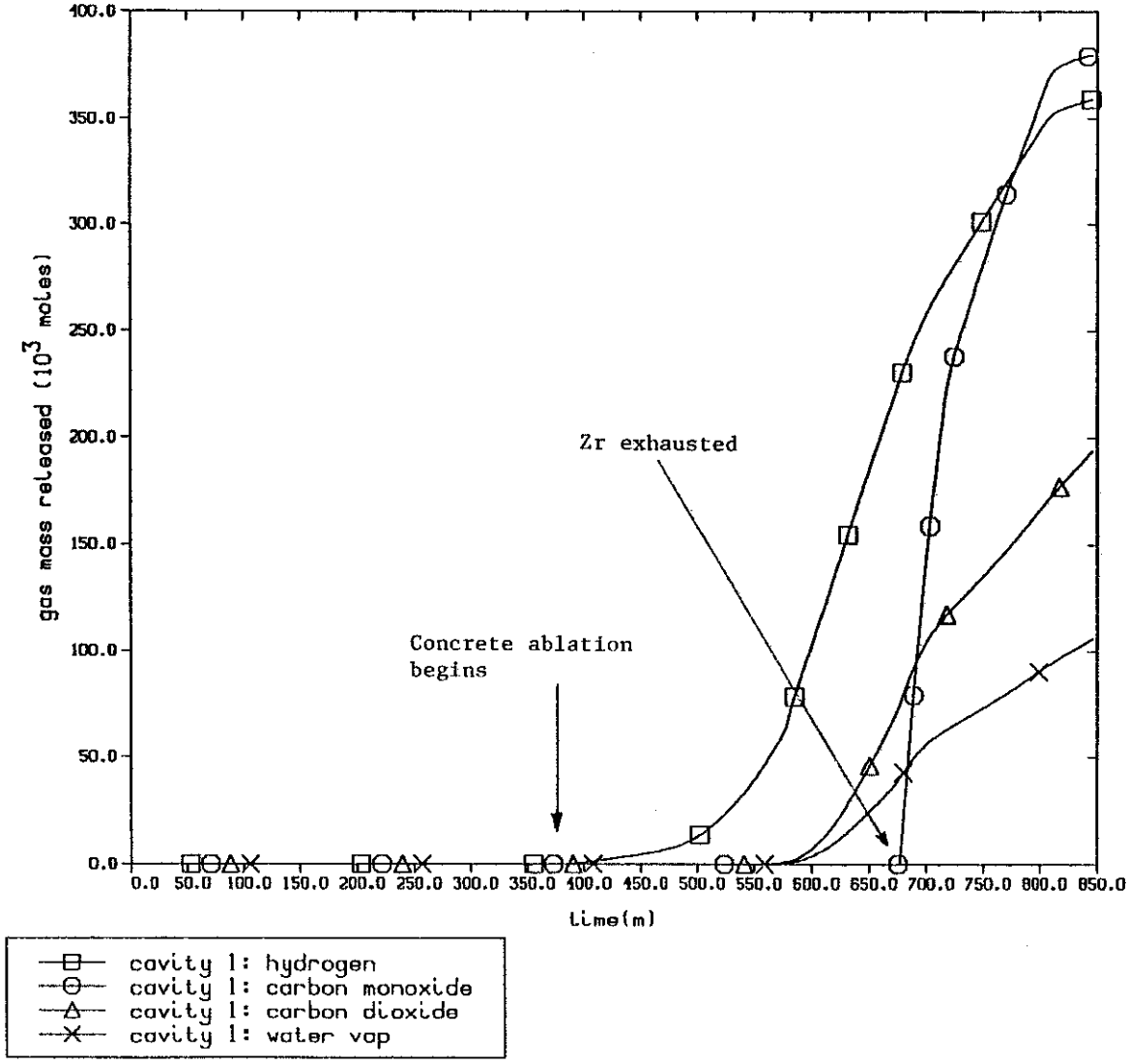

Fig. 9.2.4. In-pedestal drywell debris gas releases for the dual cavity (95% drywell/5% wetwell) Mark II short-term station blackout with ADS actuation.

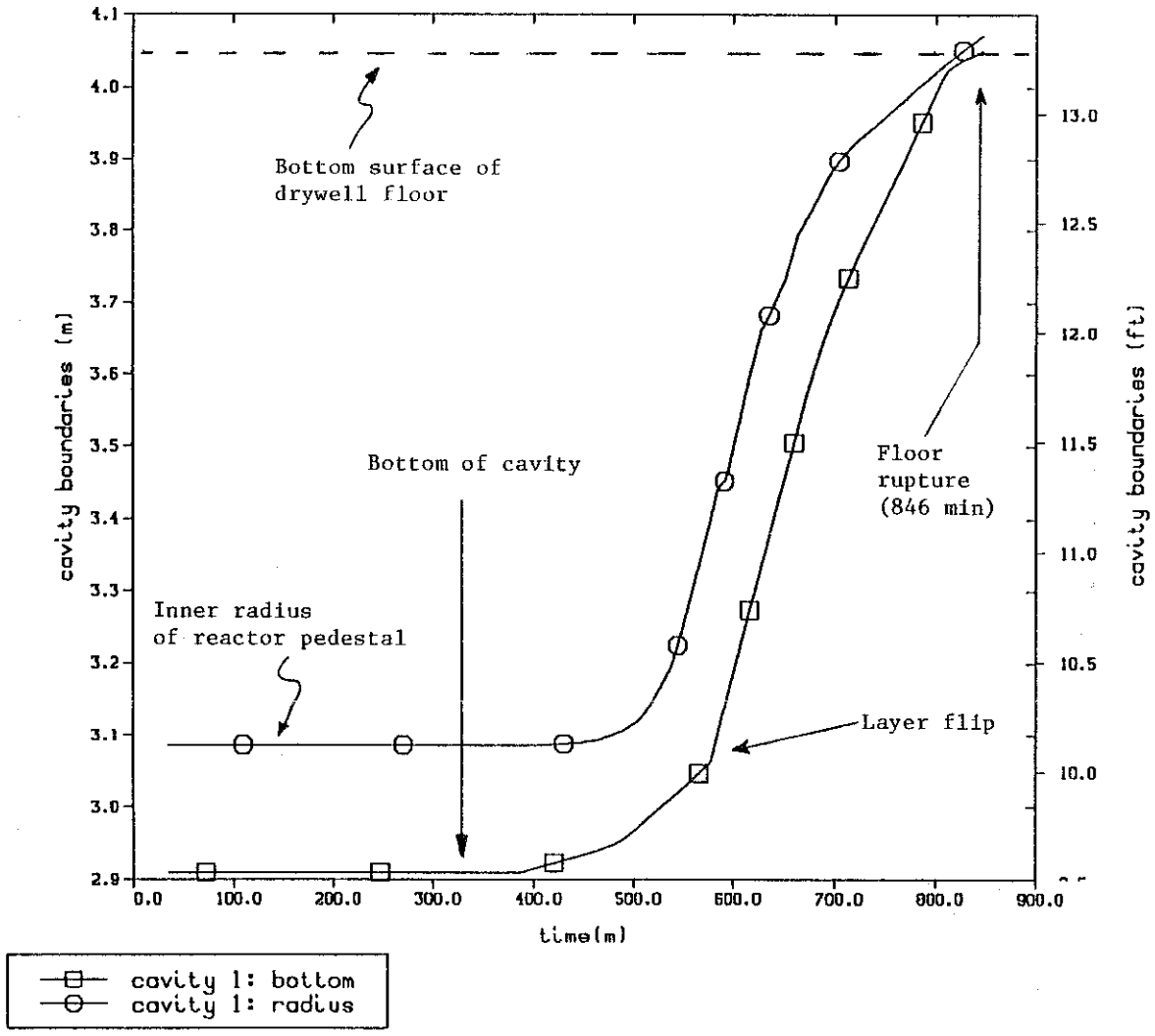

Fig. 9.2.5. In-pedestal drywell maximum cavity dimensions for the dual cavity (95% drywell/5% wetwell) Mark II short-term station blackout with ADS actuation.

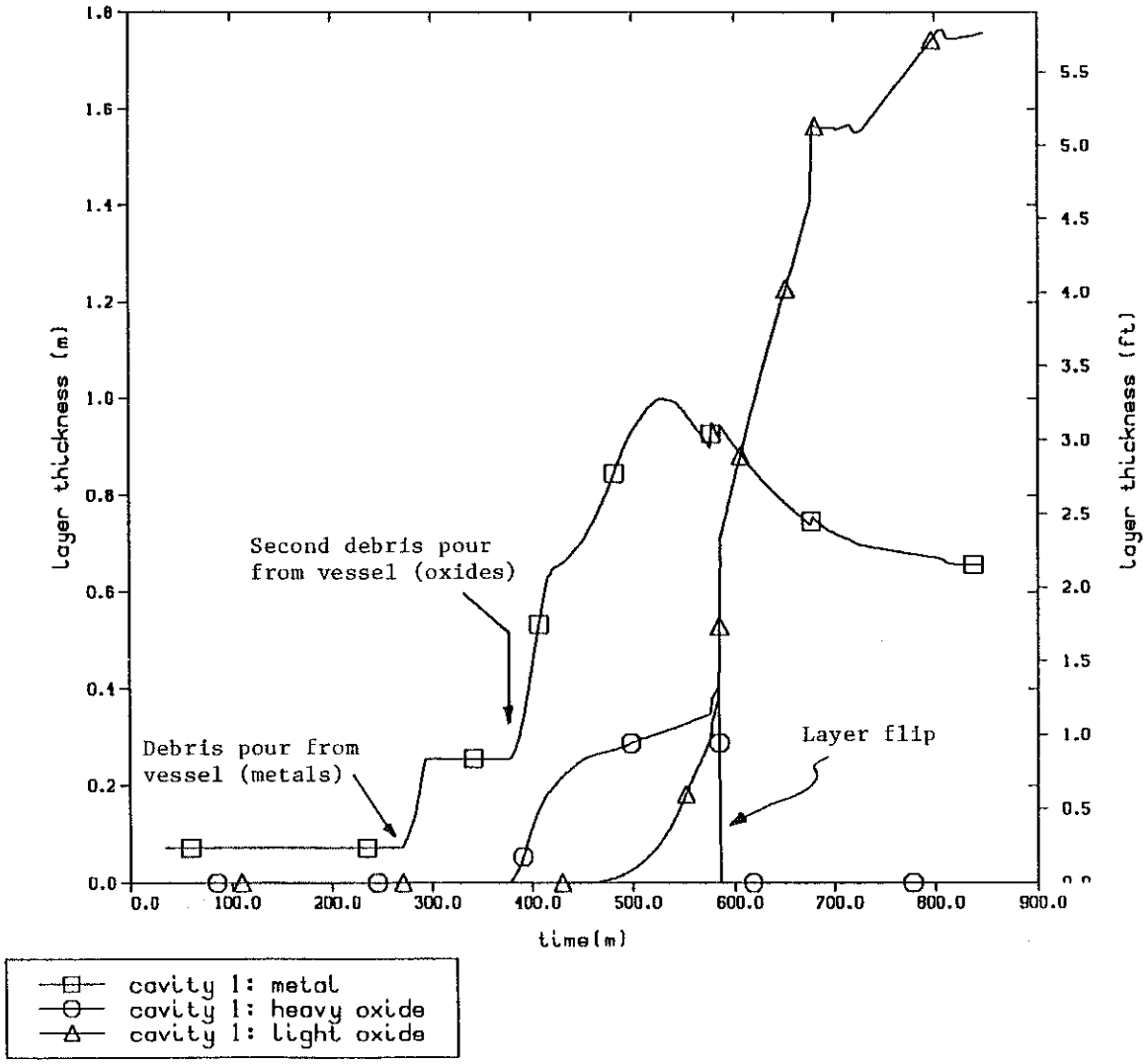

Fig. 9.2.6. In-pedestal drywell debris layer thicknesses for the dual cavity (95% drywell/5% wetwell) Mark II short-term station blackout with ADS actuation.

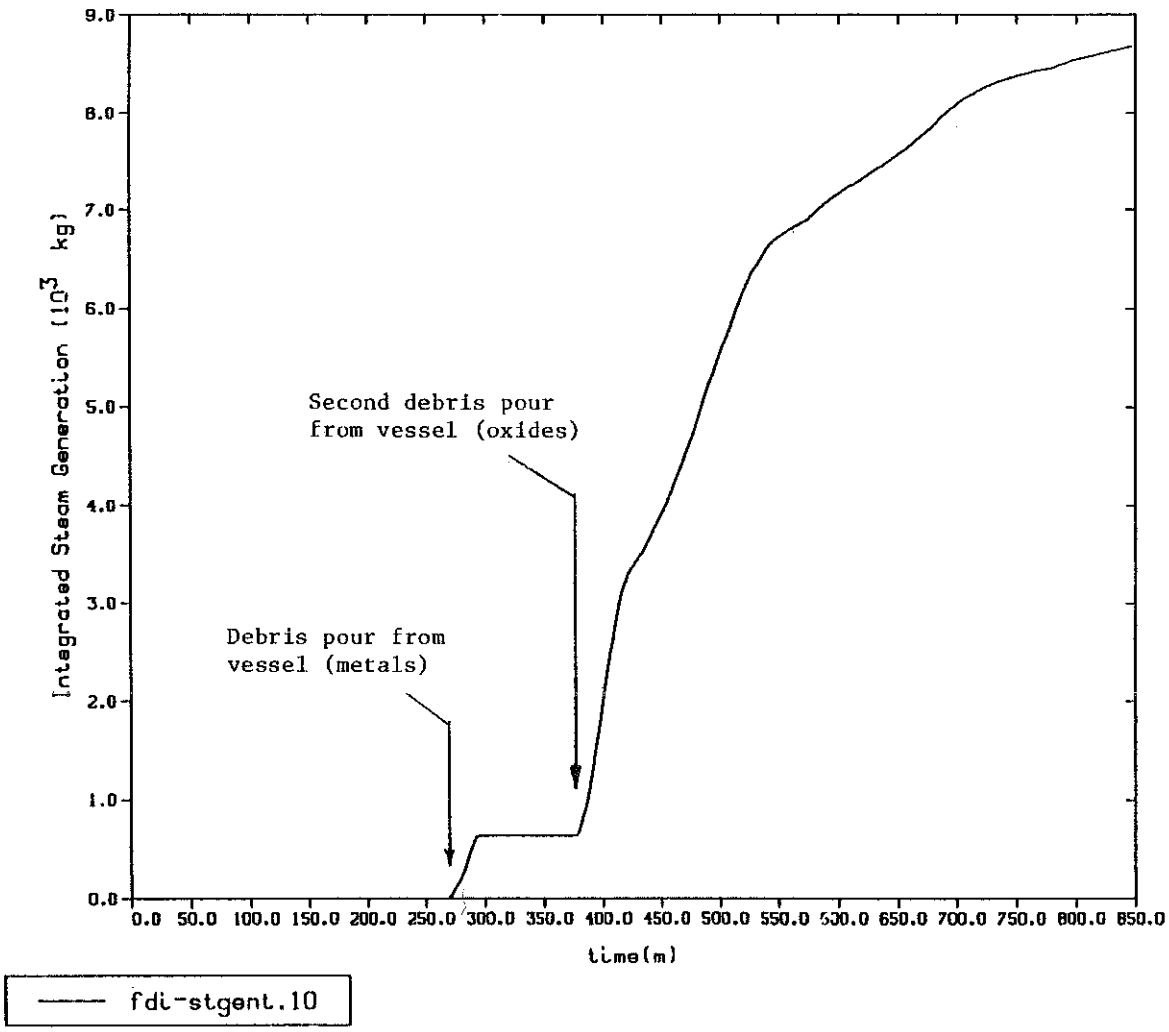

Fig. 9.2.7. Integrated steam generation from debris/wetwell pool interaction for the dual cavity (95% drywell/5% wetwell) Mark II short-term station blackout with ADS actuation.

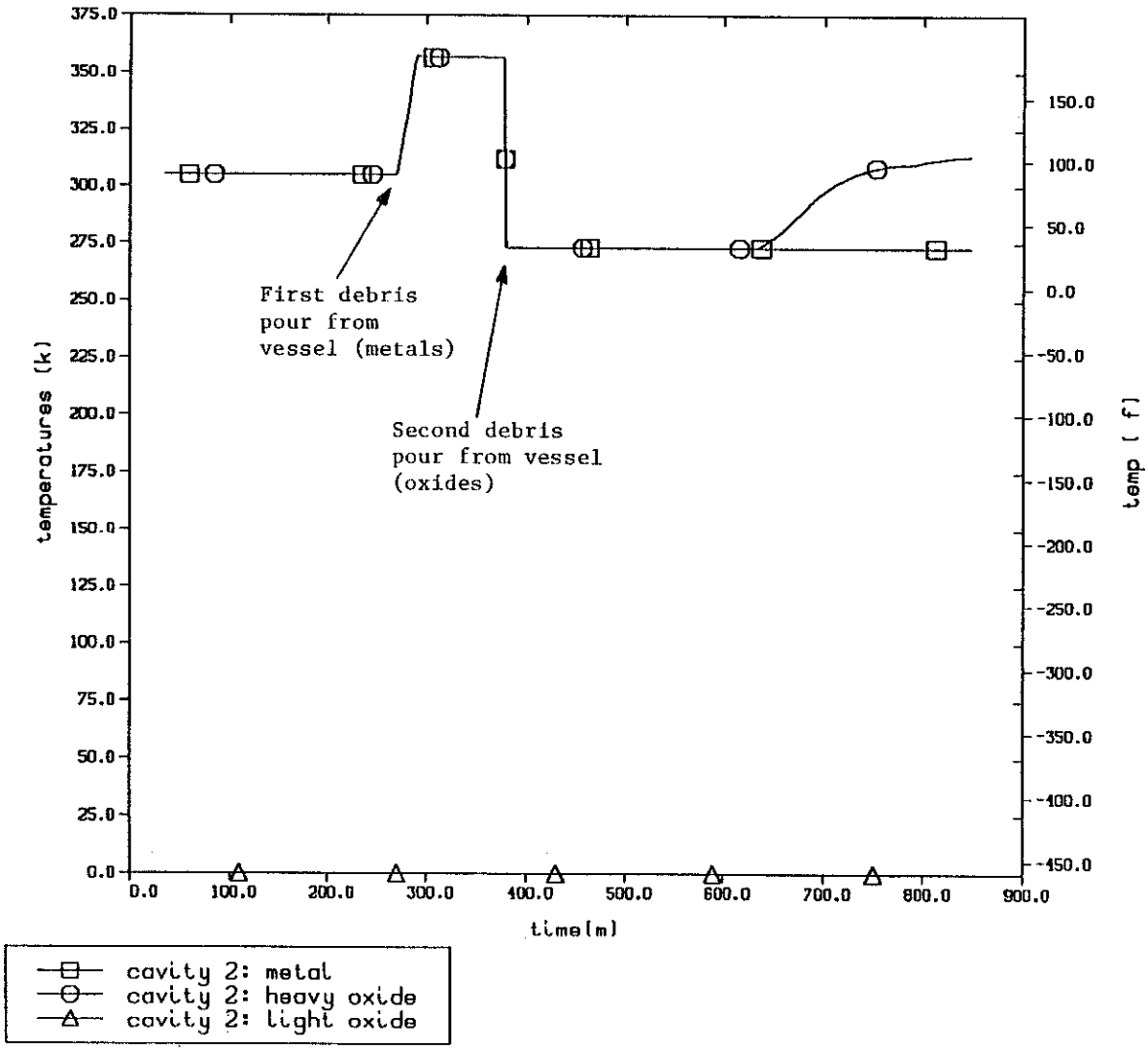

Fig. 9.2.8. In-pedestal wetwell debris layer temperatures for the dual cavity (95% drywell/5% wetwell) Mark II short-term station blackout with ADS actuation.

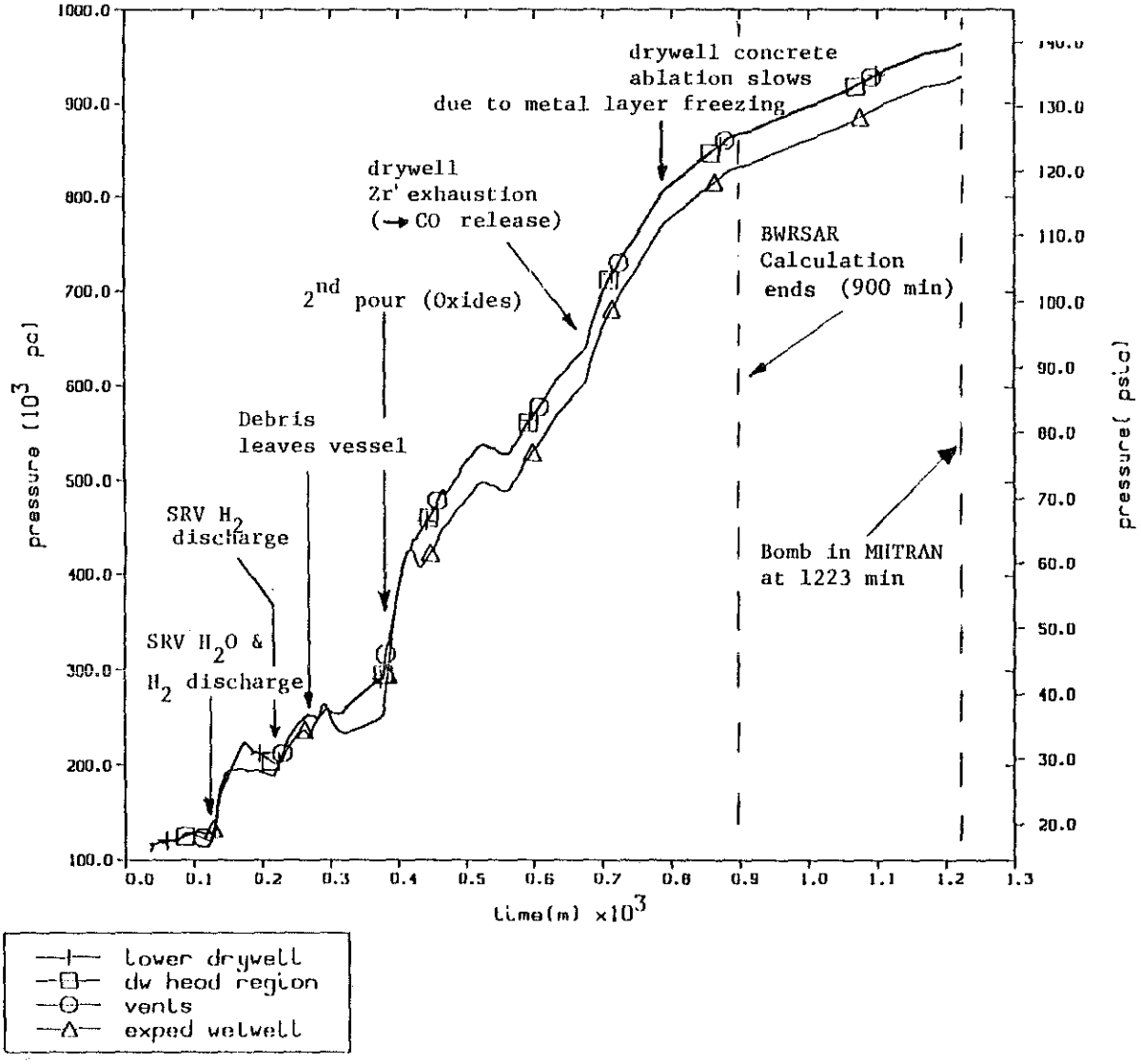

Fig. 9.3.1. Primary containment pressure distribution for the dual cavity (80% drywell/20% wetwell) Mark II short-term station blackout with ADS actuation.

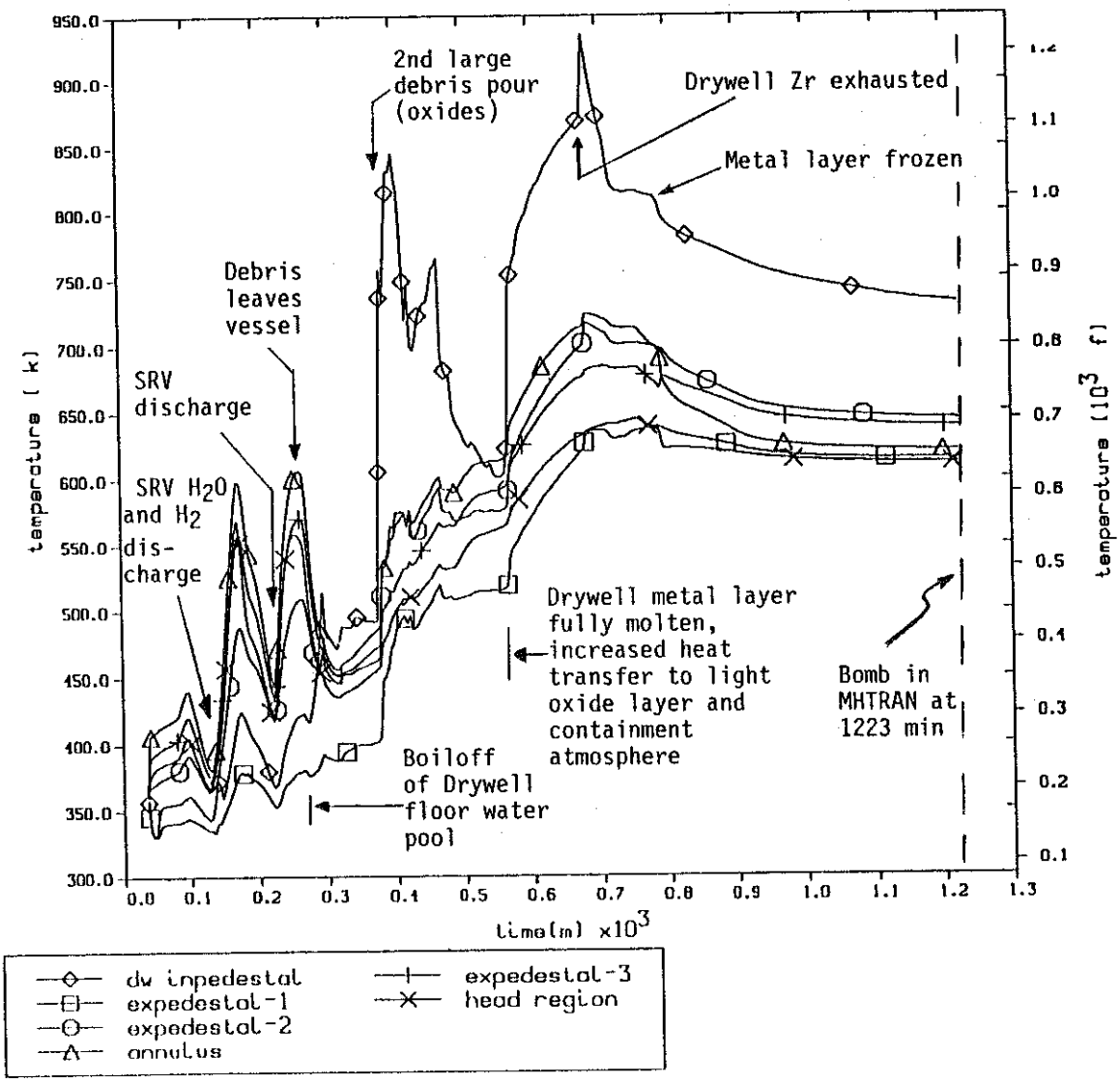

Fig. 9.3.2. Primary containment temperature distribution for the dual cavity (80% drywell/20% wetwell) Mark II short-term station blackout with ADS actuation.

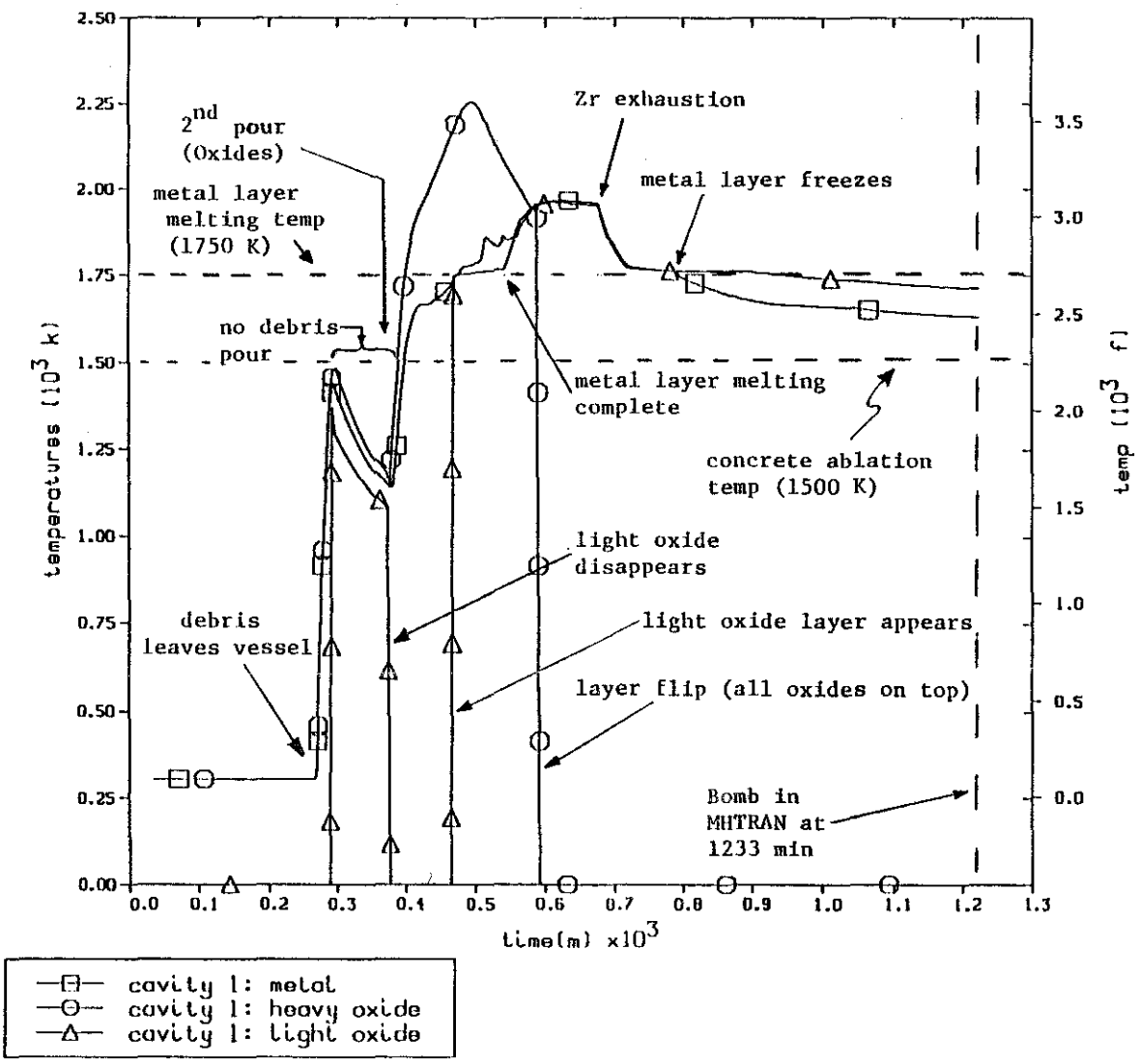

Fig. 9.3.3. In-pedestal drywell debris layer temperatures for the dual cavity (80% drywell/20% wetwell) Mark II short-term station blackout with ADS actuation.

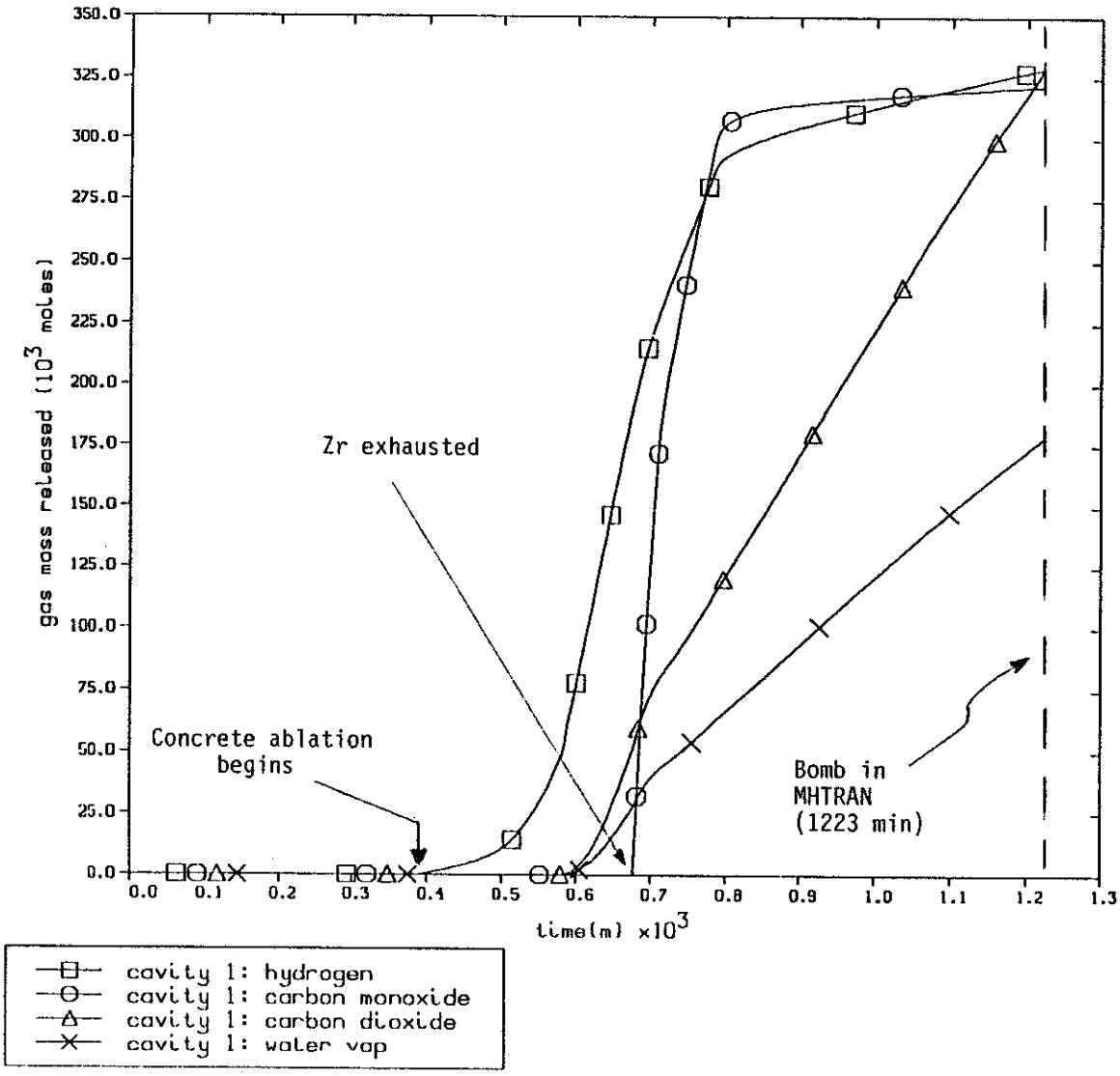

Fig. 9.3.4. In-pedestal drywell debris gas releases for the dual cavity (80% drywell/20% wetwell) Mark II short-term station blackout with ADS actuation.

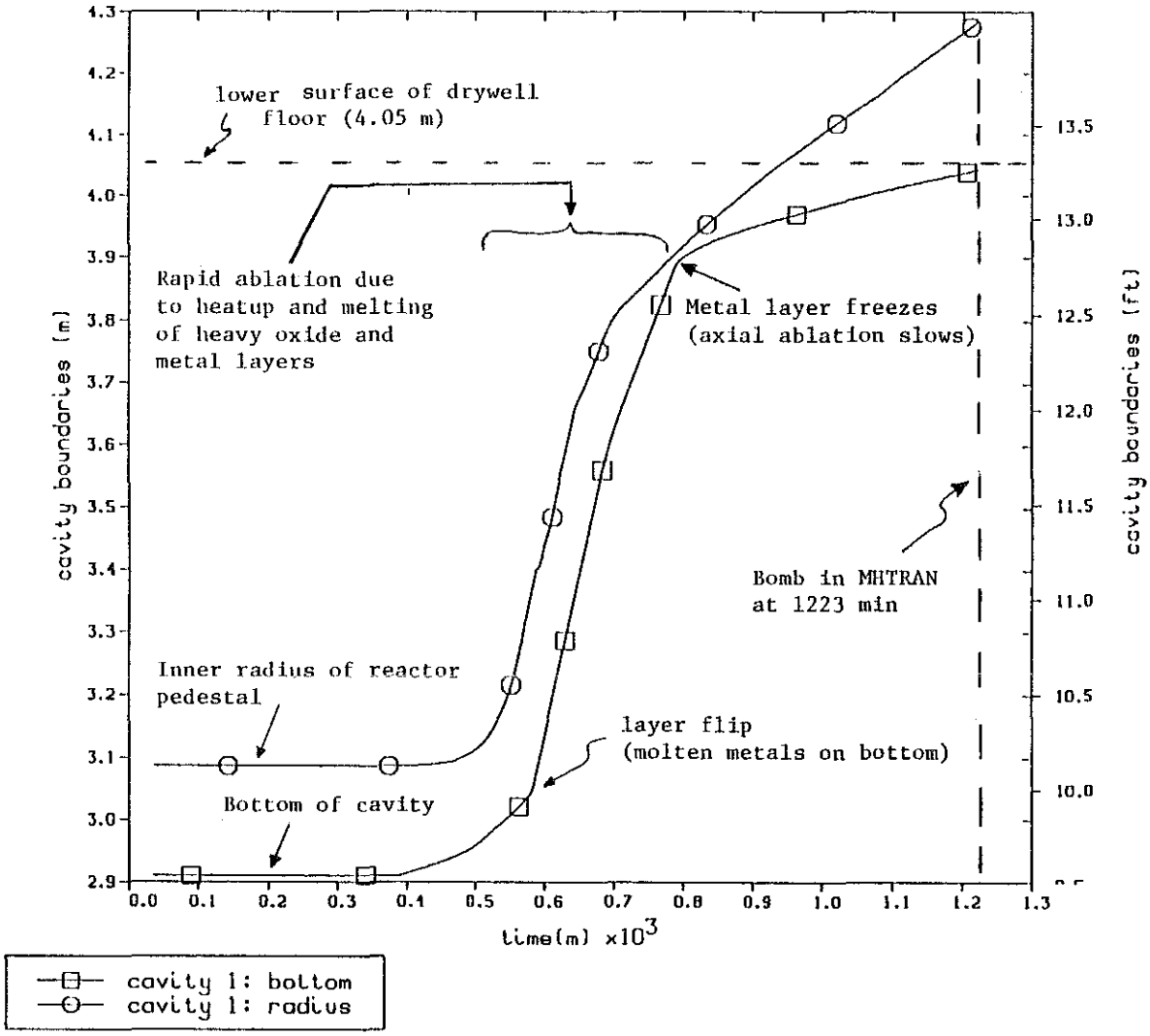

Fig. 9.3.5. In-pedestal drywell maximum cavity dimensions for the dual cavity (80% drywell/20% wetwell) Mark II short-term station blackout with ADS actuation.

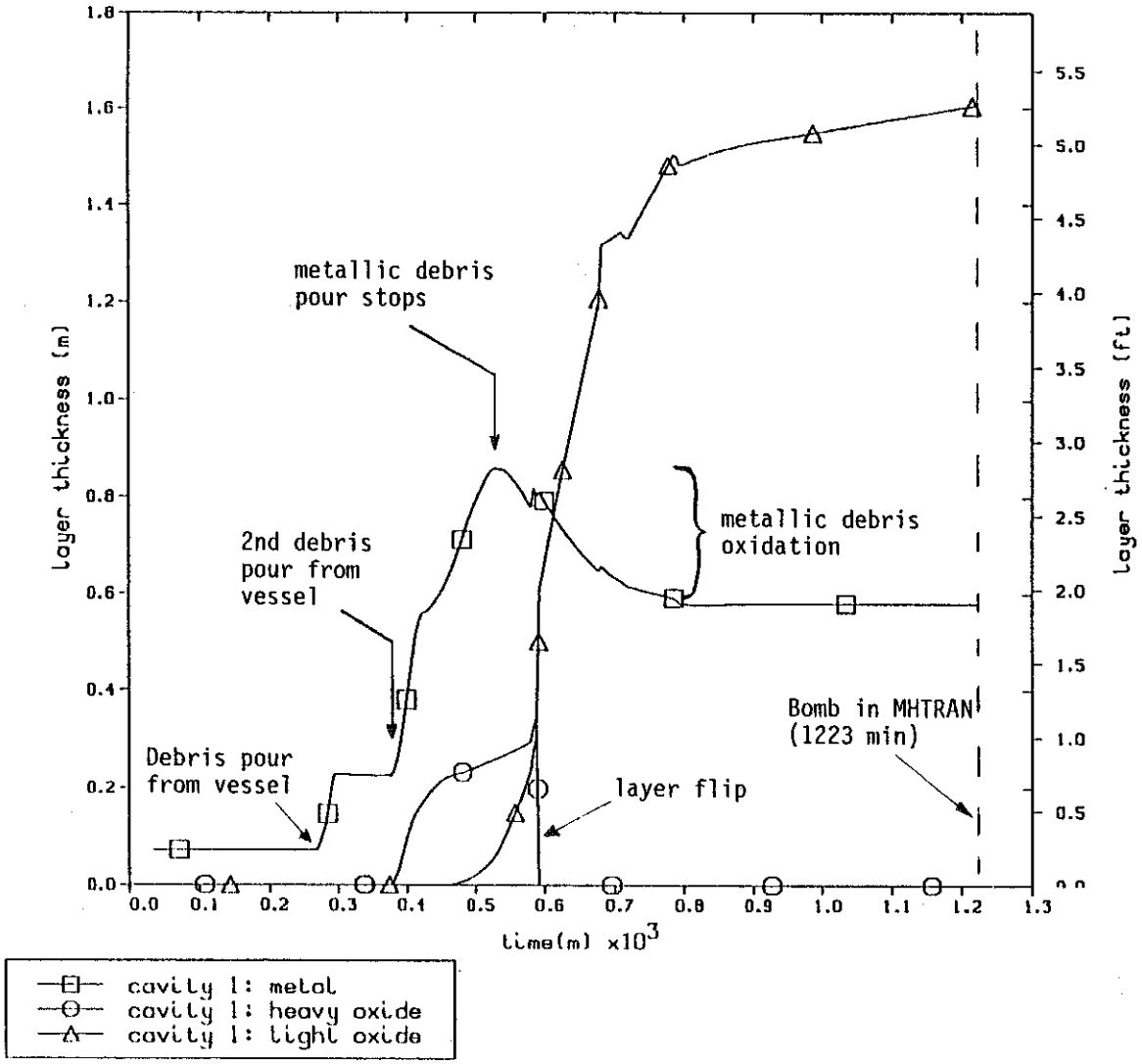

Fig. 9.3.6. In-pedestal drywell debris layer thicknesses for the dual cavity (80% drywell/20% wetwell) Mark II short-term station blackout with ADS actuation.

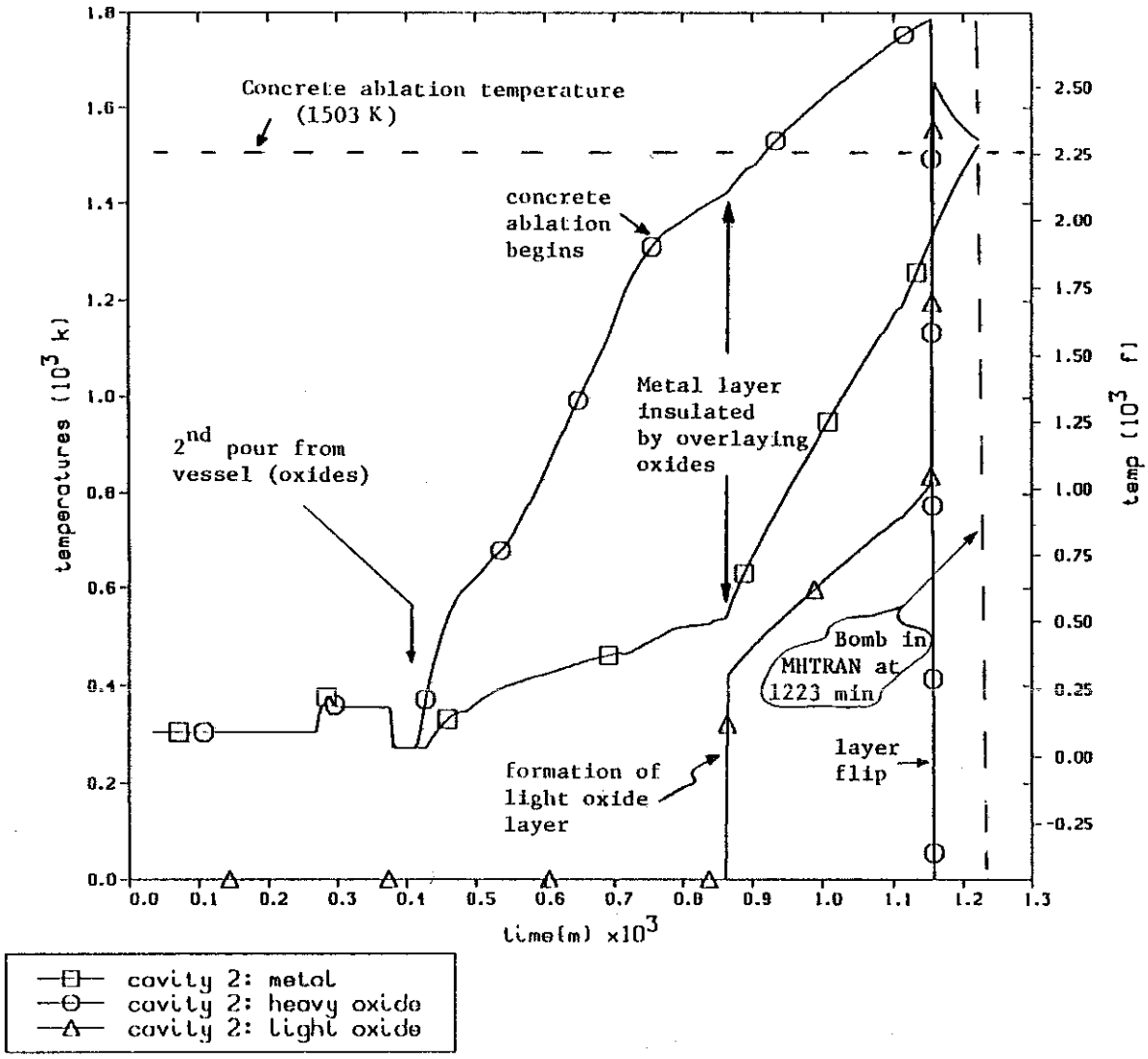

Fig. 9.3.7. In-pedestal wetwell debris layer temperatures for the dual cavity (80% drywell/20% wetwell) Mark II short-term station blackout with ADS actuation.

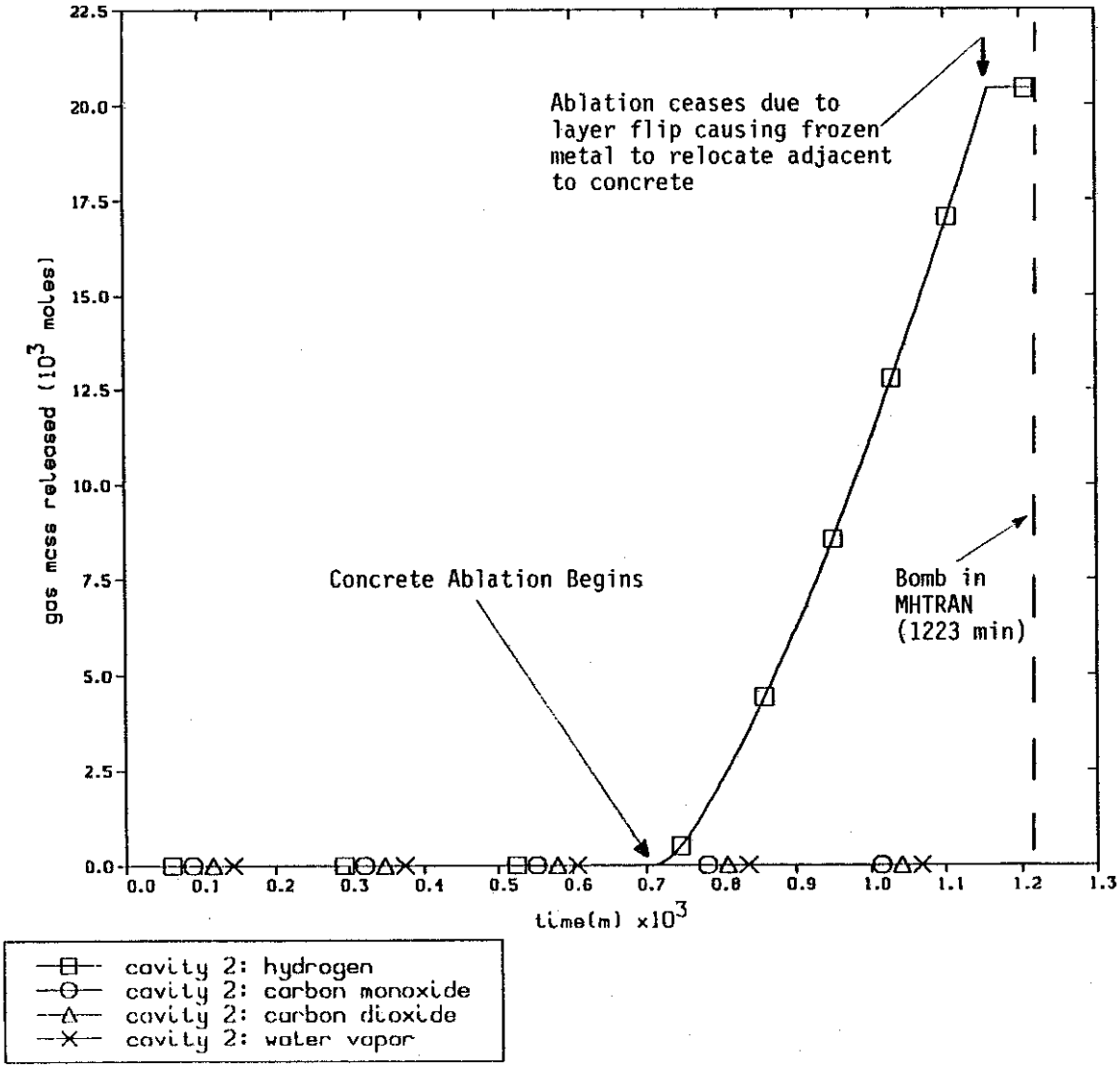

Fig. 9.3.8. In-pedestal wetwell debris gas releases for the dual cavity (80% drywell/20% wetwell) Mark II short-term station blackout with ADS actuation.

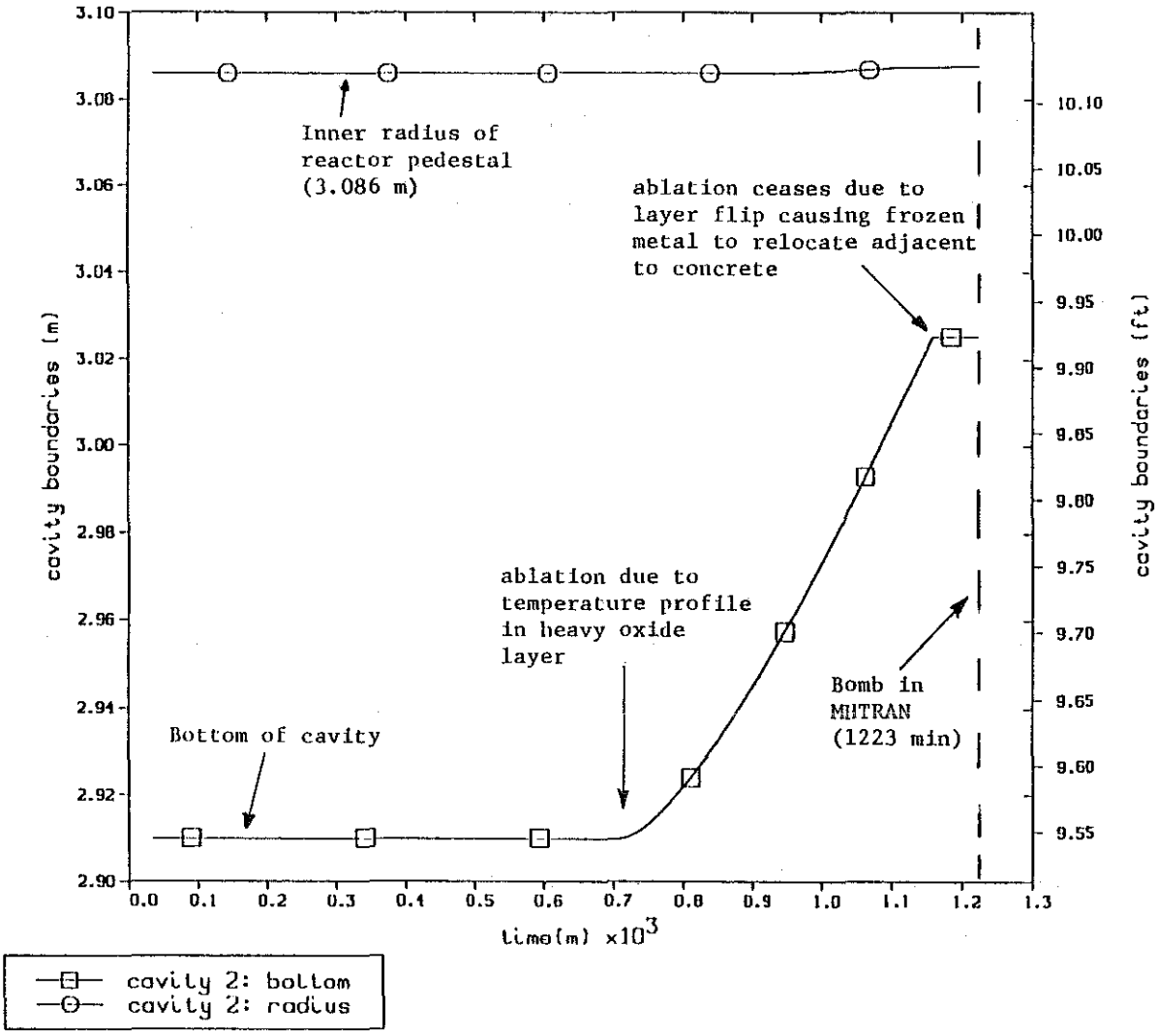

Fig. 9.3.9. In-pedestal wetwell maximum cavity dimensions for the dual cavity (80% drywell/20% wetwell) Mark II short-term station blackout with ADS actuation.

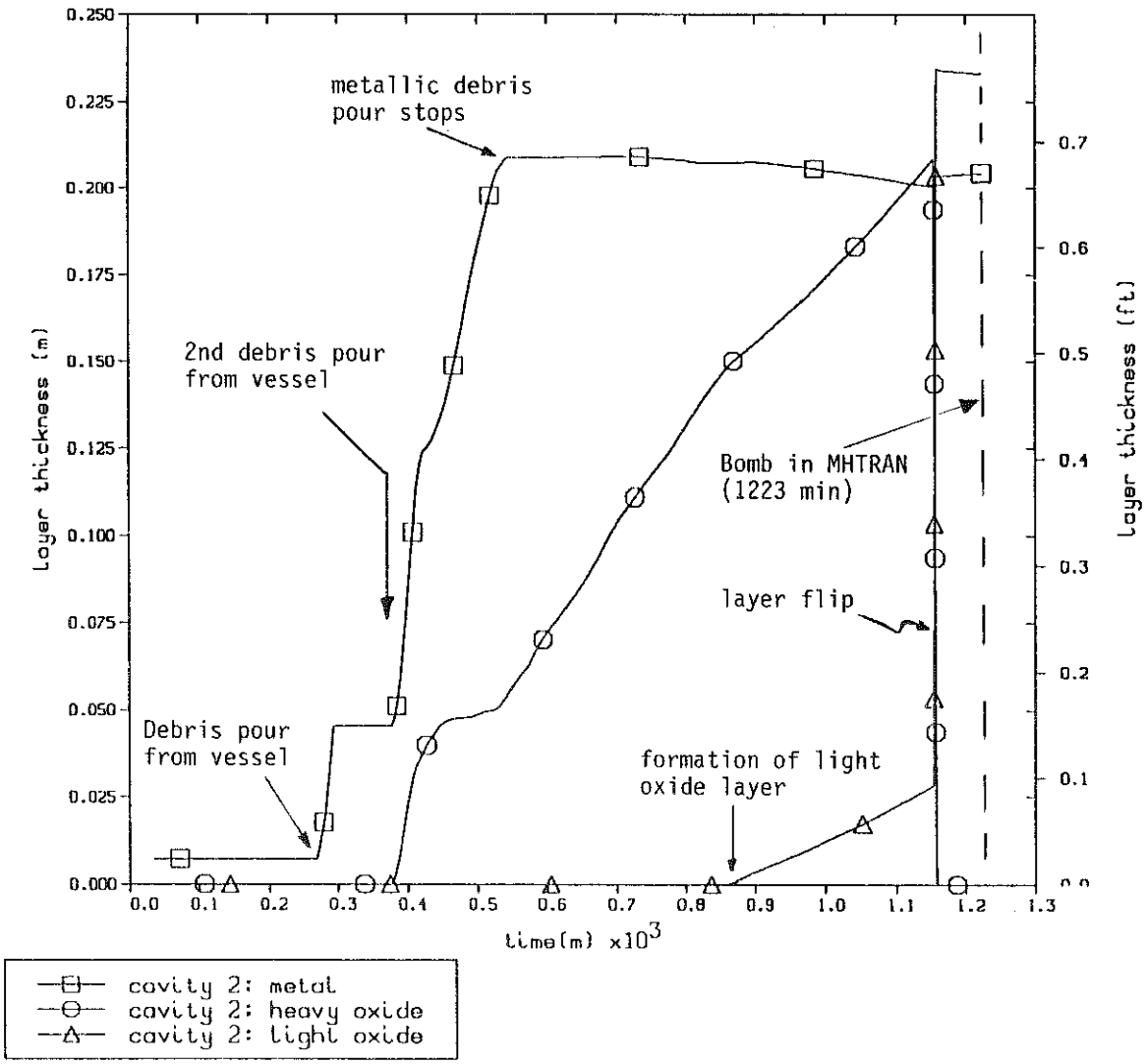

Fig. 9.3.10. In-pedestal wetwell debris layer thicknesses for the dual cavity (80% drywell/20% wetwell) Mark II short-term station blackout with ADS actuation.

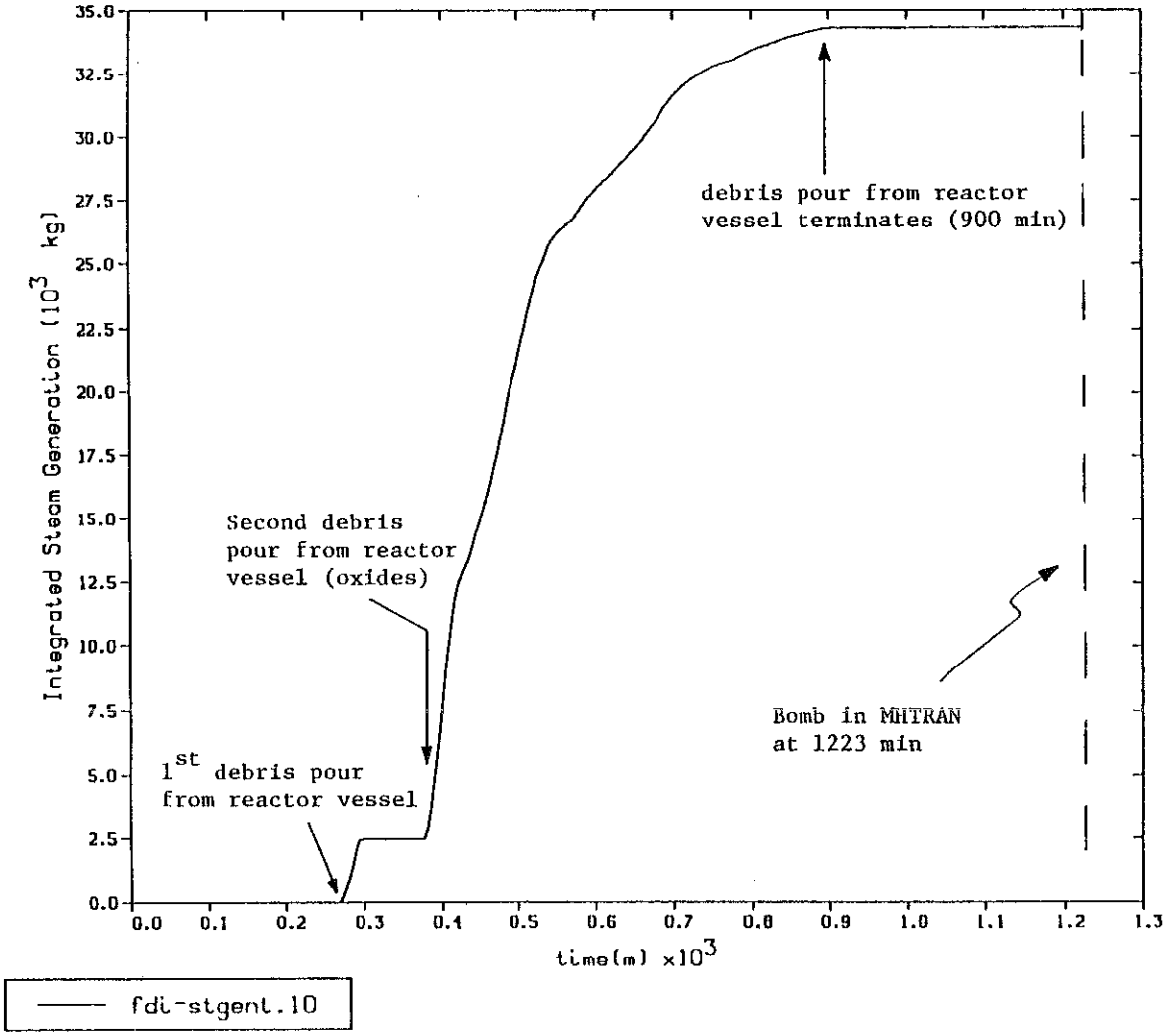

Fig. 9.3.11. Integrated steam generation from debris/wetwell pool interaction for the dual cavity (80% drywell/20% wetwell) Mark II short-term station blackout with ADS actuation.

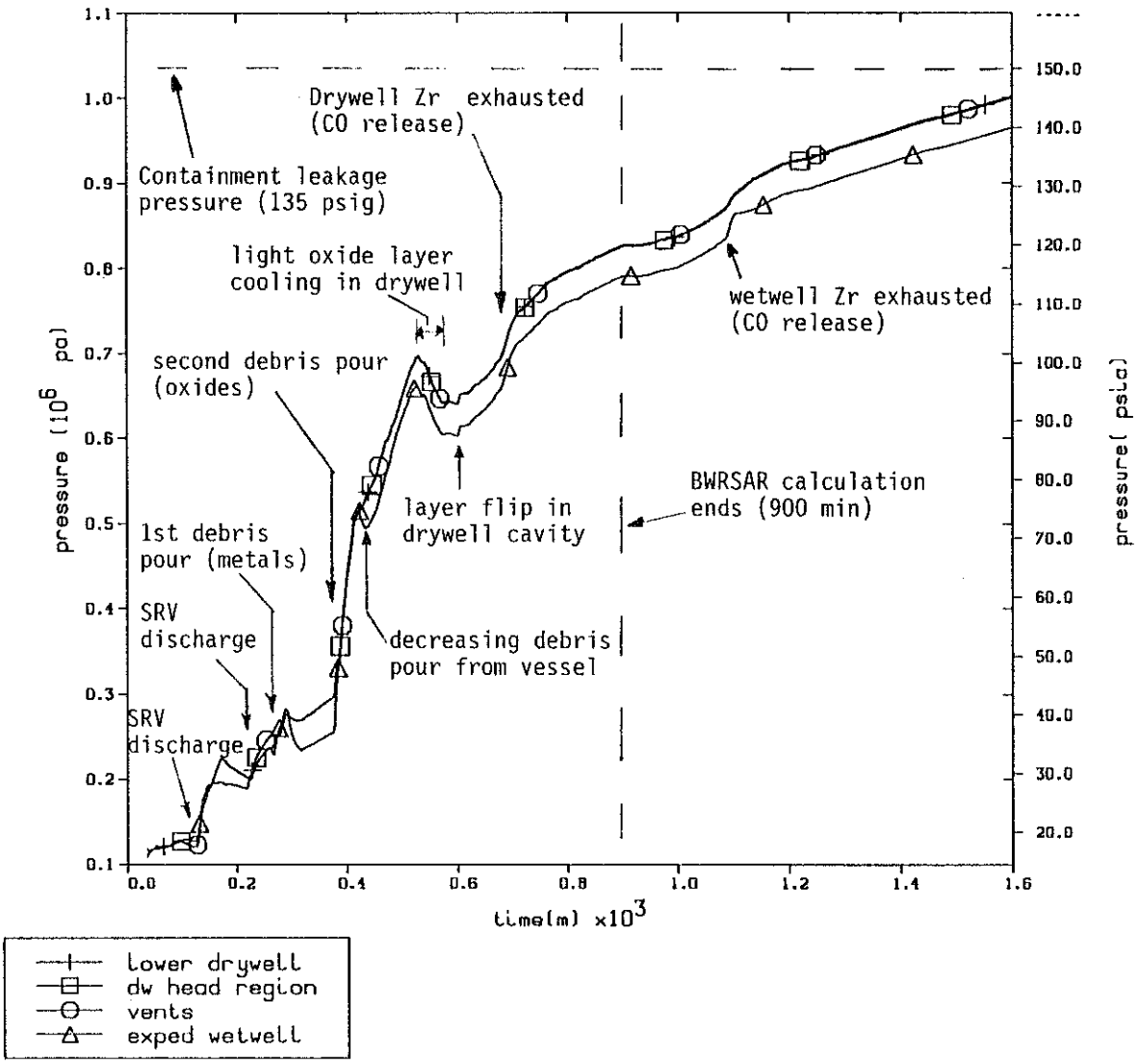

Fig. 9.4.1. Primary containment pressure distribution for the dual cavity (60% drywell/40% wetwell) Mark II analysis of short-term station blackout with ADS actuation.

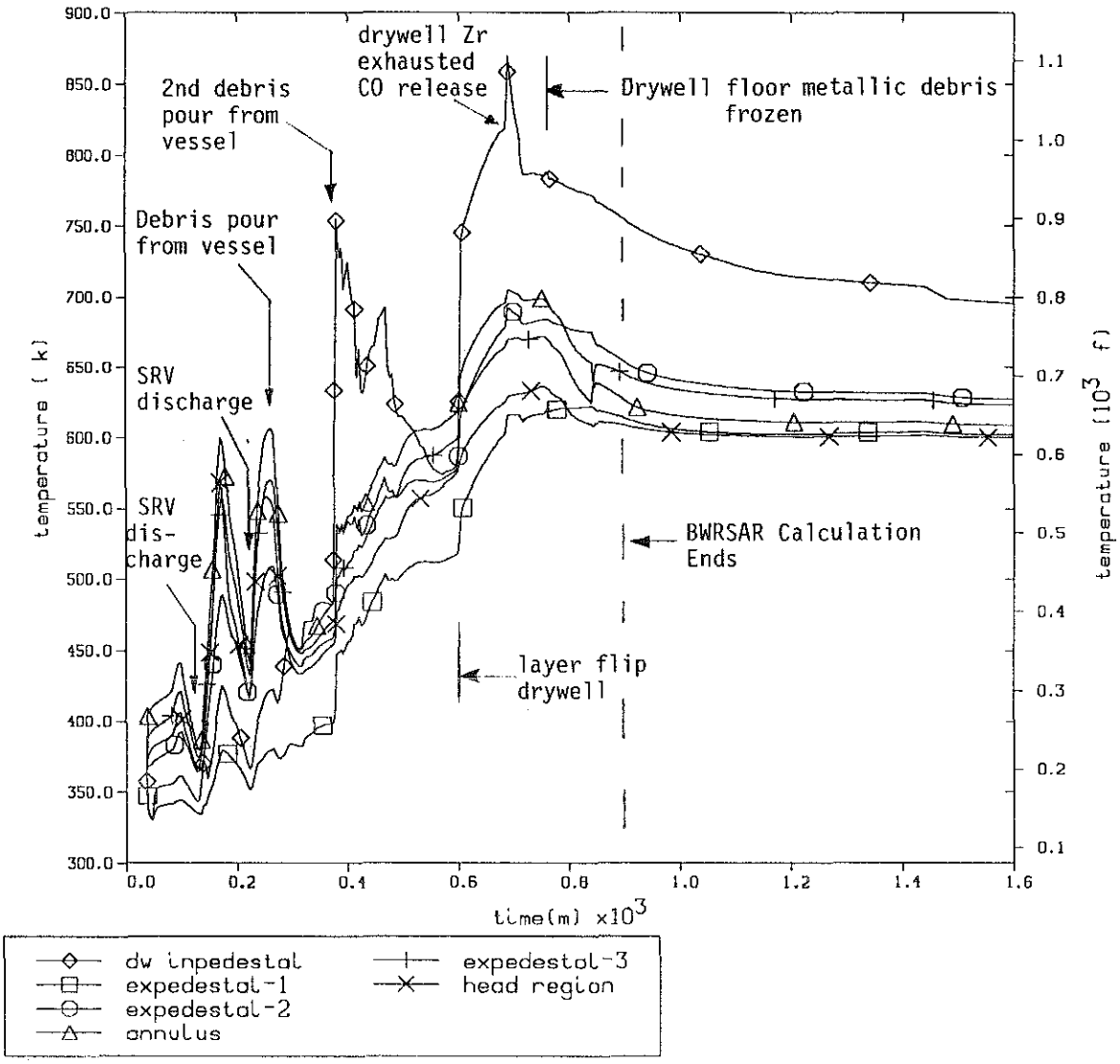

Fig. 9.4.2. Primary containment temperature distribution for the dual cavity (60% drywell/40% wetwell) Mark II short-term station blackout with ADS actuation.

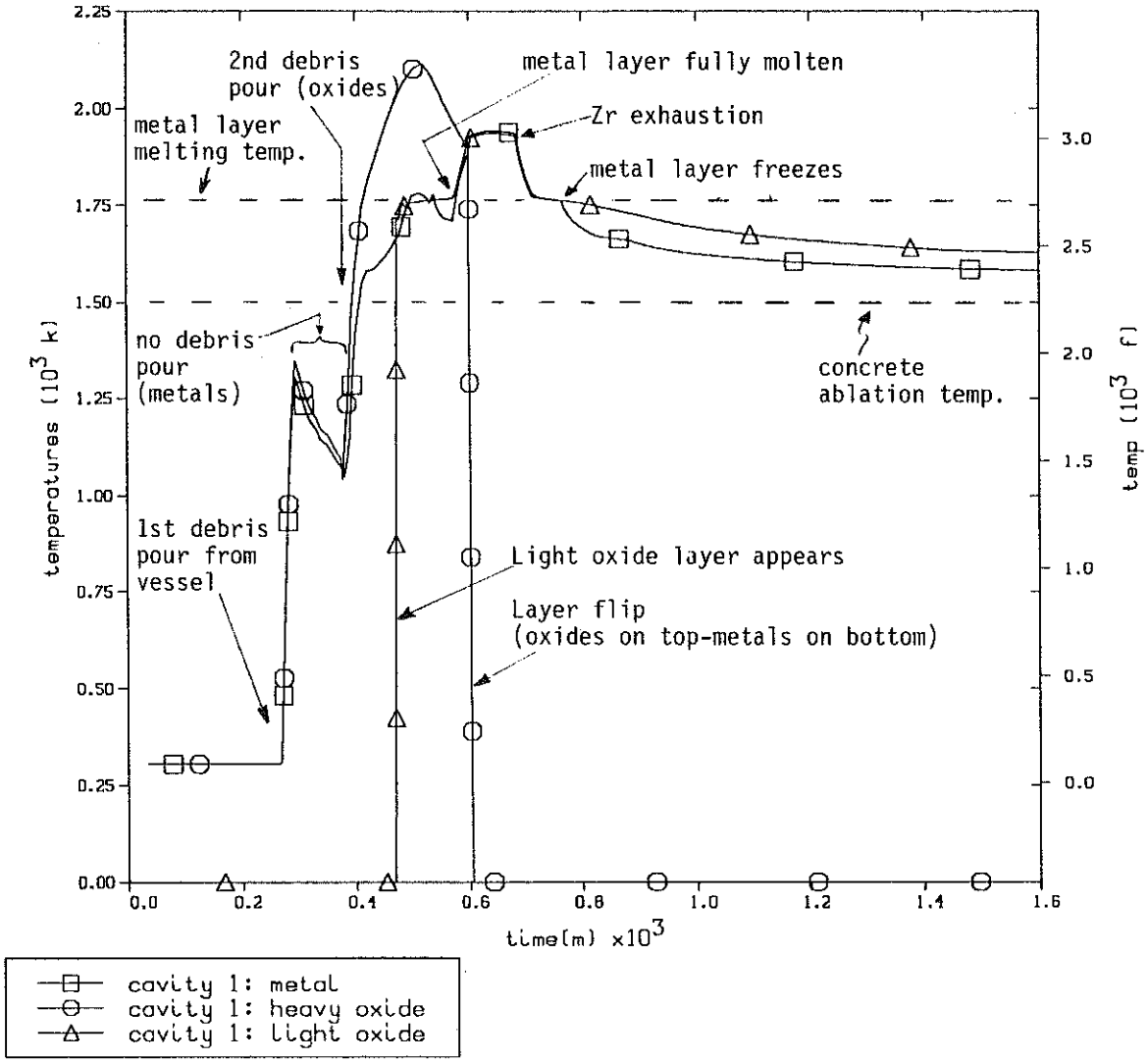

Fig. 9.4.3. In-pedestal drywell debris layer temperatures for the dual cavity (60% drywell/40% wetwell) Mark II short-term station blackout with ADS actuation.

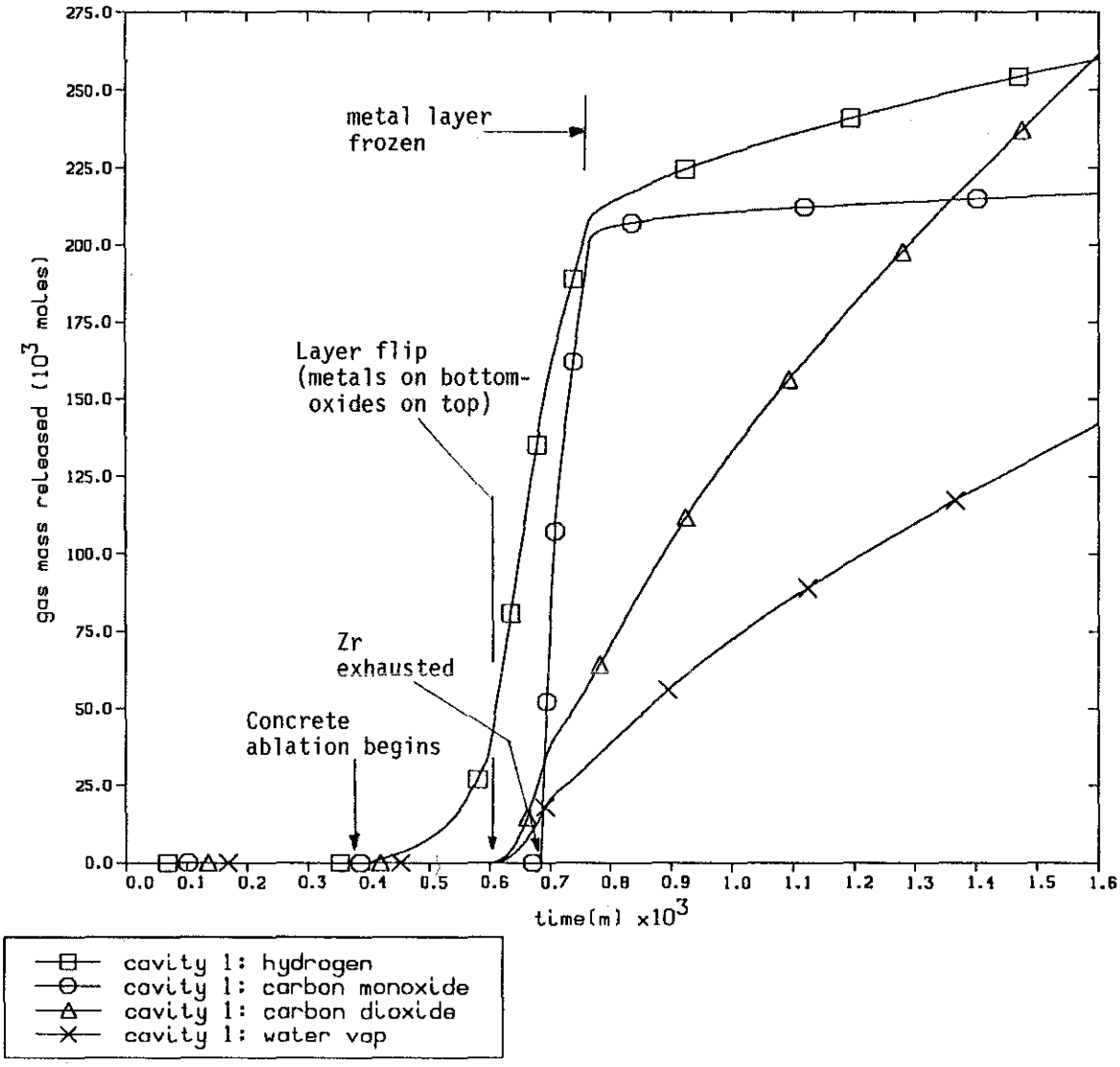

Fig. 9.4.4. In-pedestal drywell debris gas releases for the dual cavity (60% drywell/40% wetwell) Mark II short-term station blackout with ADS actuation.

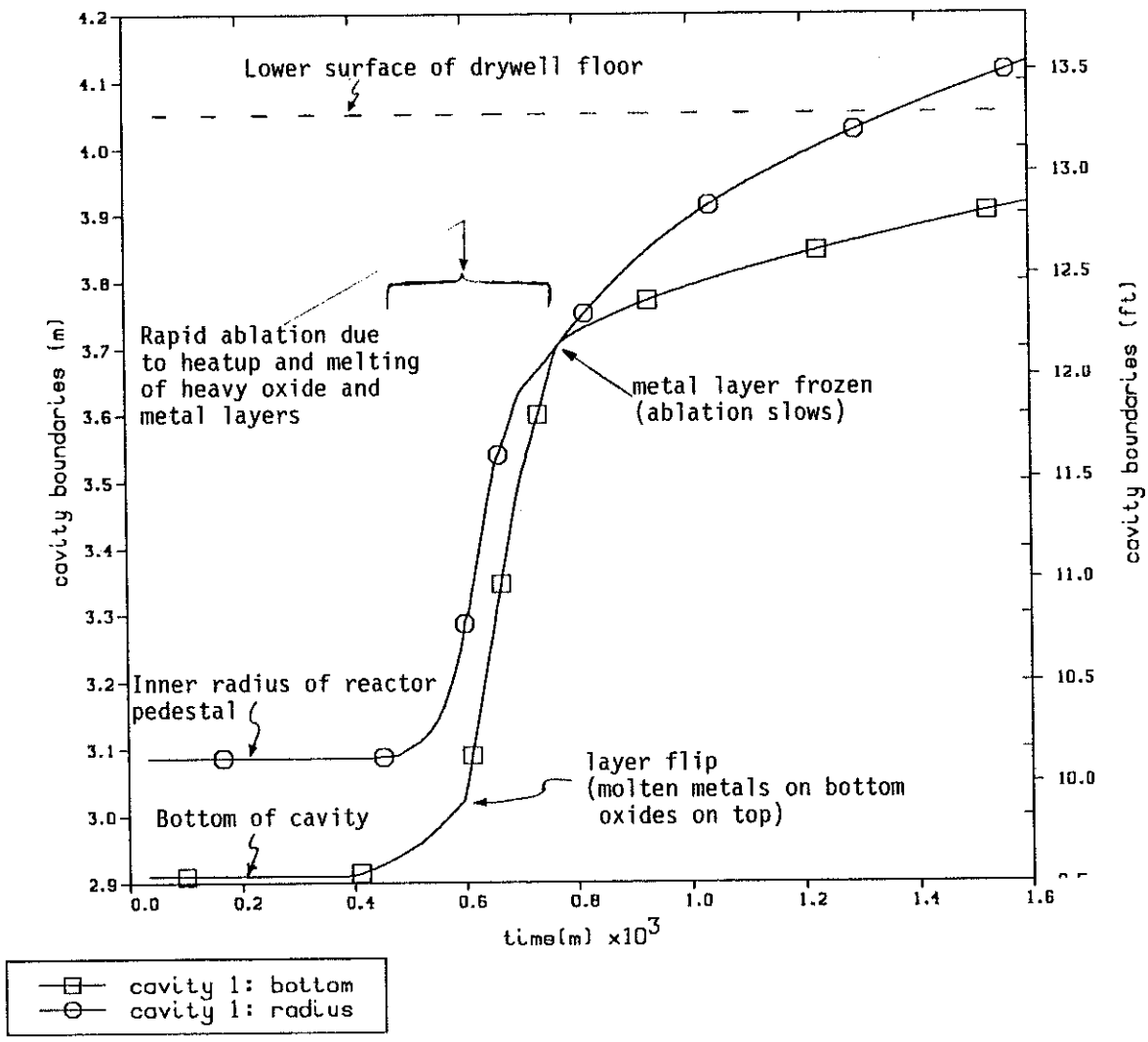

Fig. 9.4.5. In-pedestal drywell maximum cavity dimensions for the dual cavity (60% drywell/40% wetwell) Mark II short-term station blackout with ADS actuation.

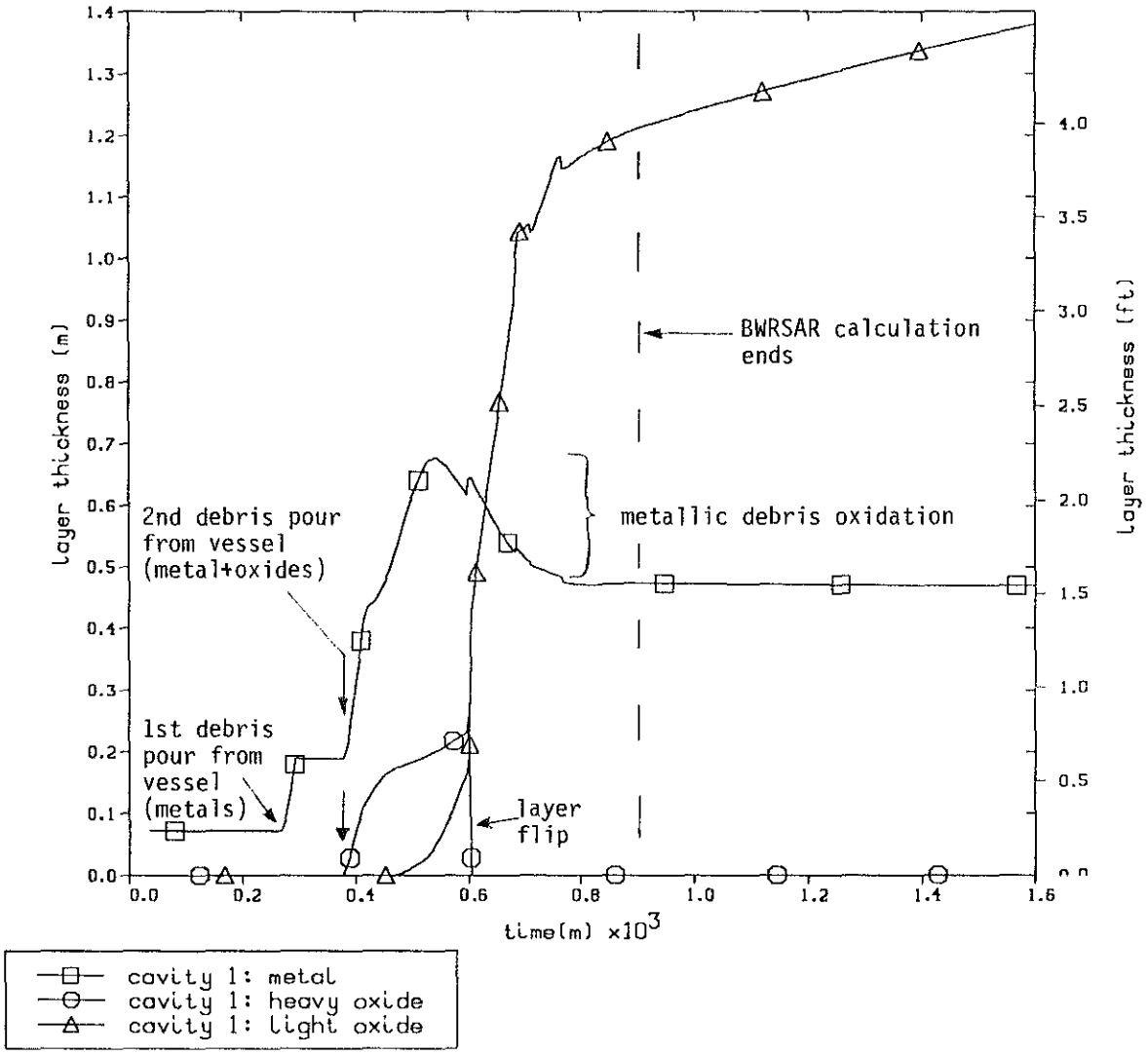

Fig. 9.4.6. In-pedestal drywell debris layer thicknesses for the dual cavity (60% drywell/40% wetwell) Mark II short-term station blackout with ADS actuation.

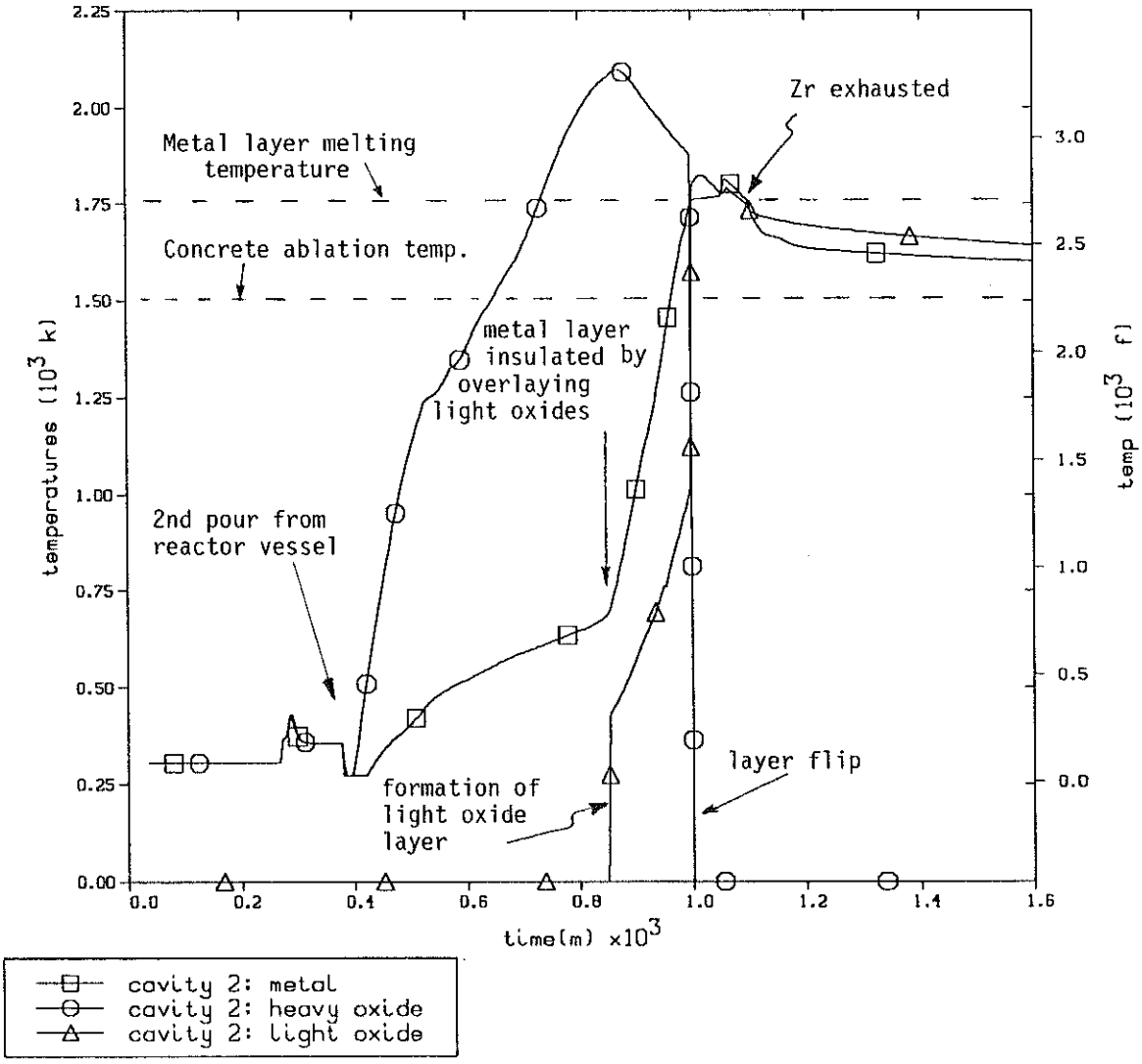

Fig. 9.4.7. In-pedestal wetwell debris layer temperatures for the dual cavity (60% drywell/40% wetwell) Mark II short-term station blackout with ADS actuation.

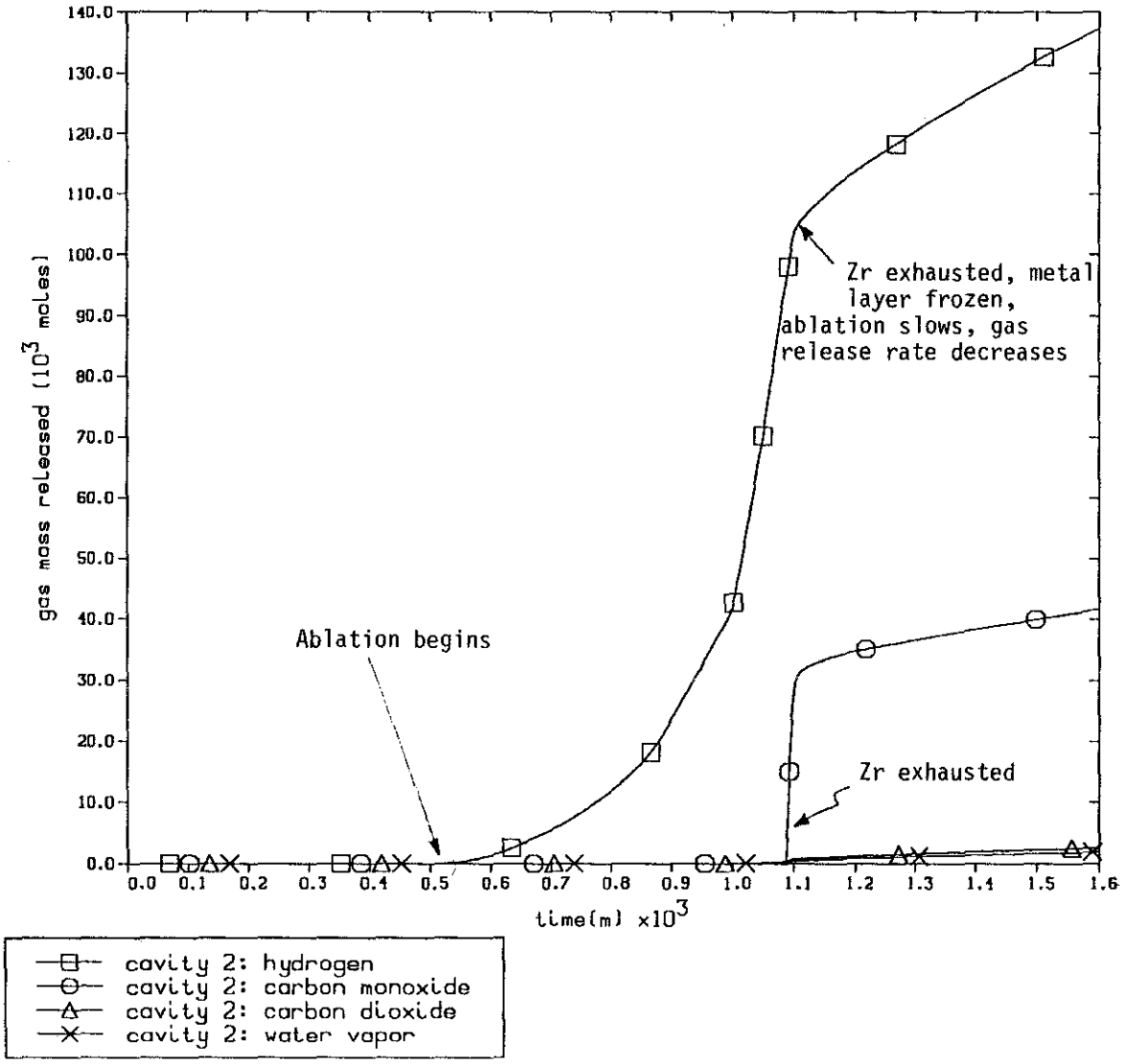

Fig. 9.4.8. In-pedestal wetwell debris gas releases for the dual cavity (60% drywell/40% wetwell) Mark II short-term station blackout with ADS actuation.

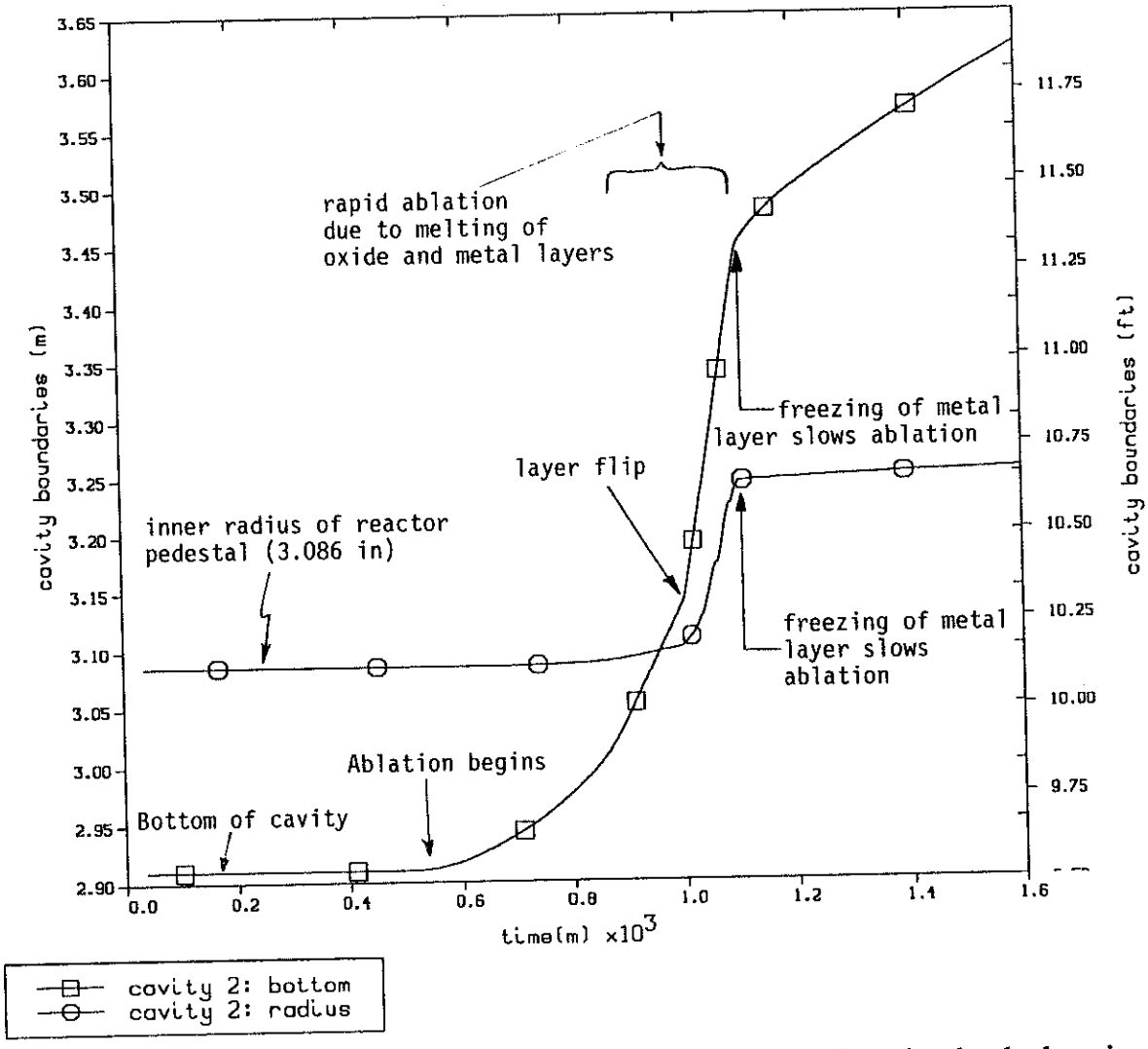

Fig. 9.4.9. In-pedestal wetwell maximum cavity dimensions for the dual cavity (60% drywell/40% wetwell) Mark II short-term station blackout with ADS actuation.

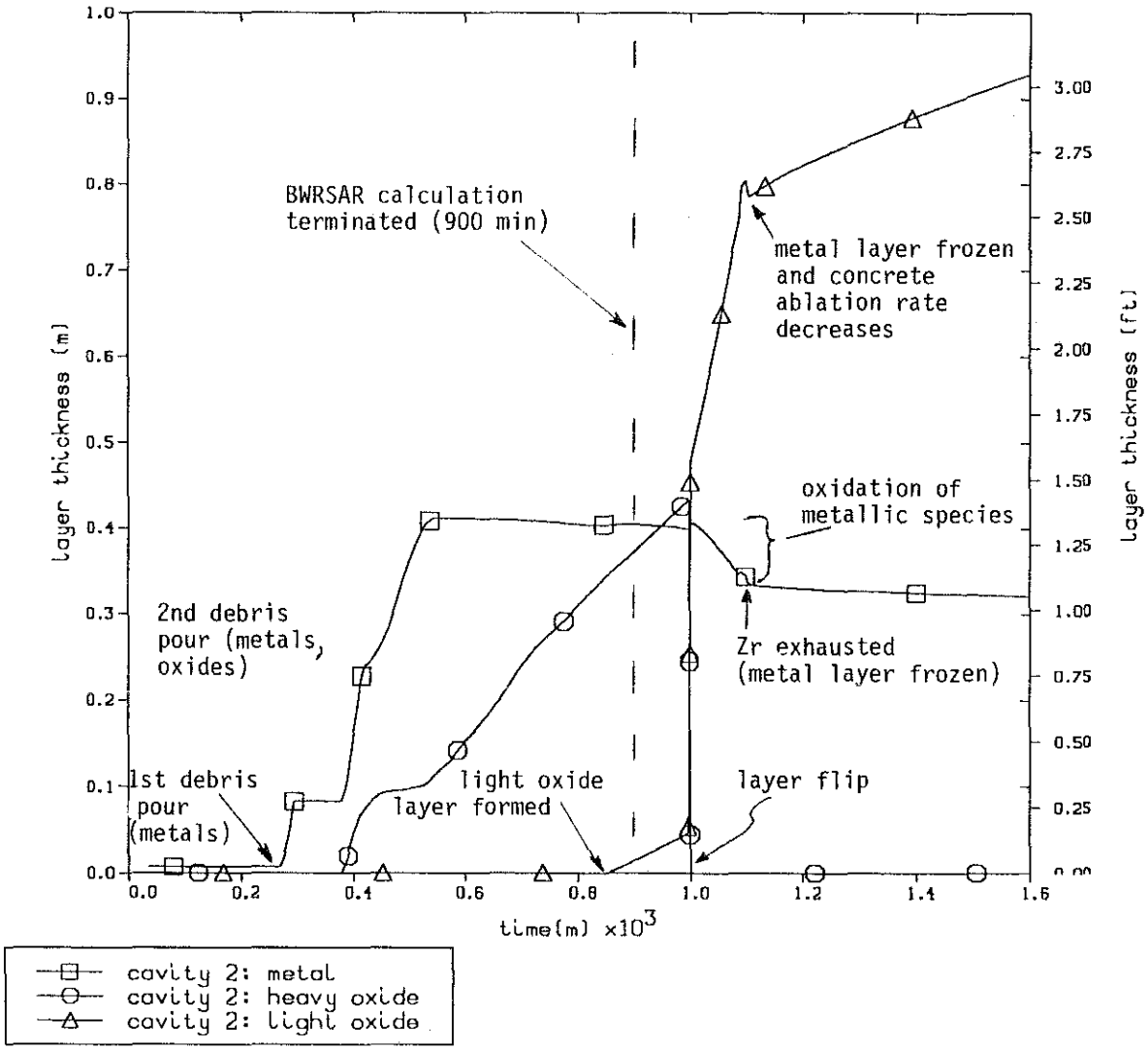

Fig. 9.4.10. In-pedestal wetwell debris layer thicknesses for the dual cavity (60% drywell/40% wetwell) Mark II short-term station blackout with ADS actuation.

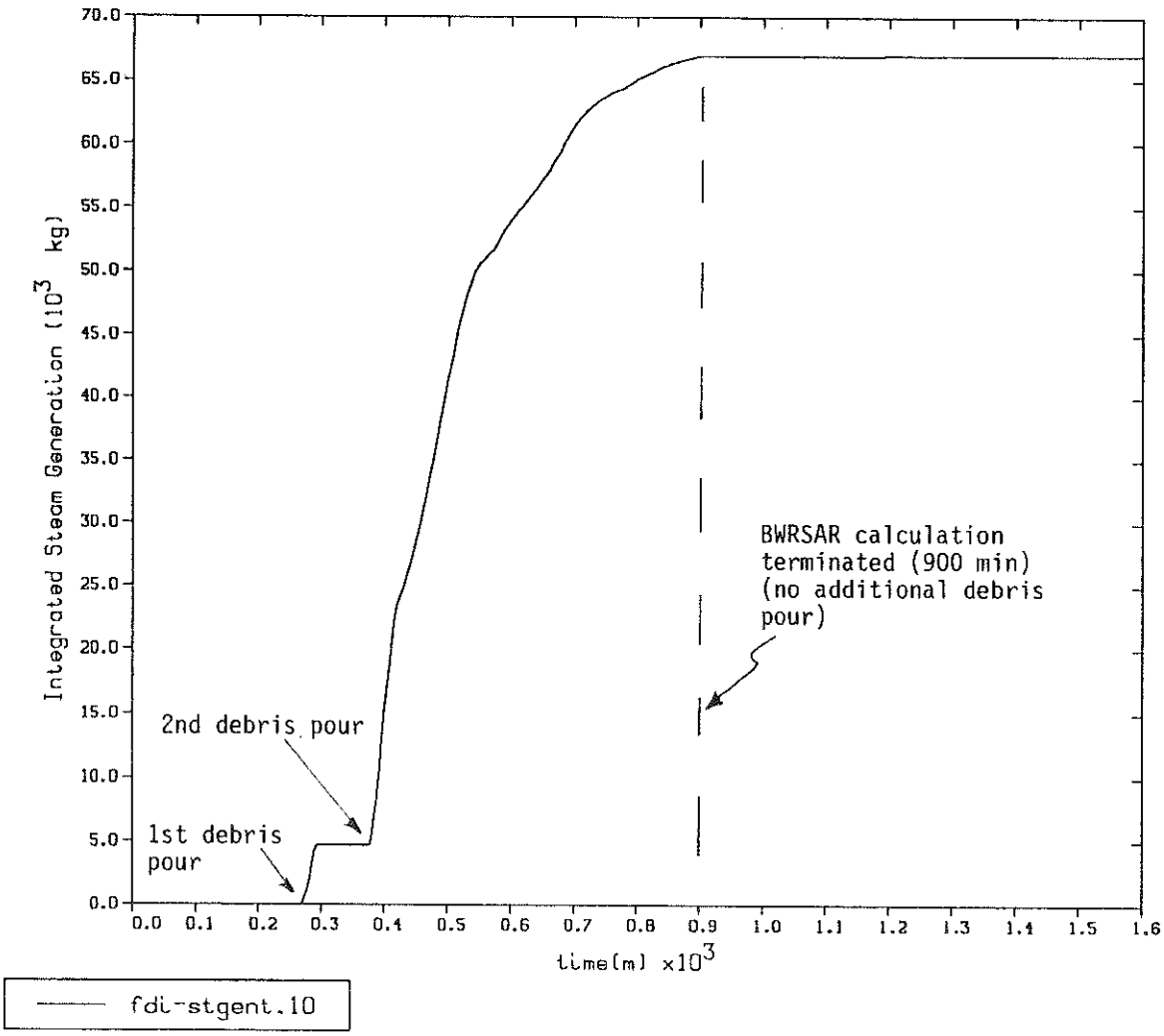

Fig. 9.4.11. Integrated steam generation from debris/wetwell pool interaction for the dual cavity (60% drywell/40% wetwell) Mark II short-term station blackout with ADS actuation.

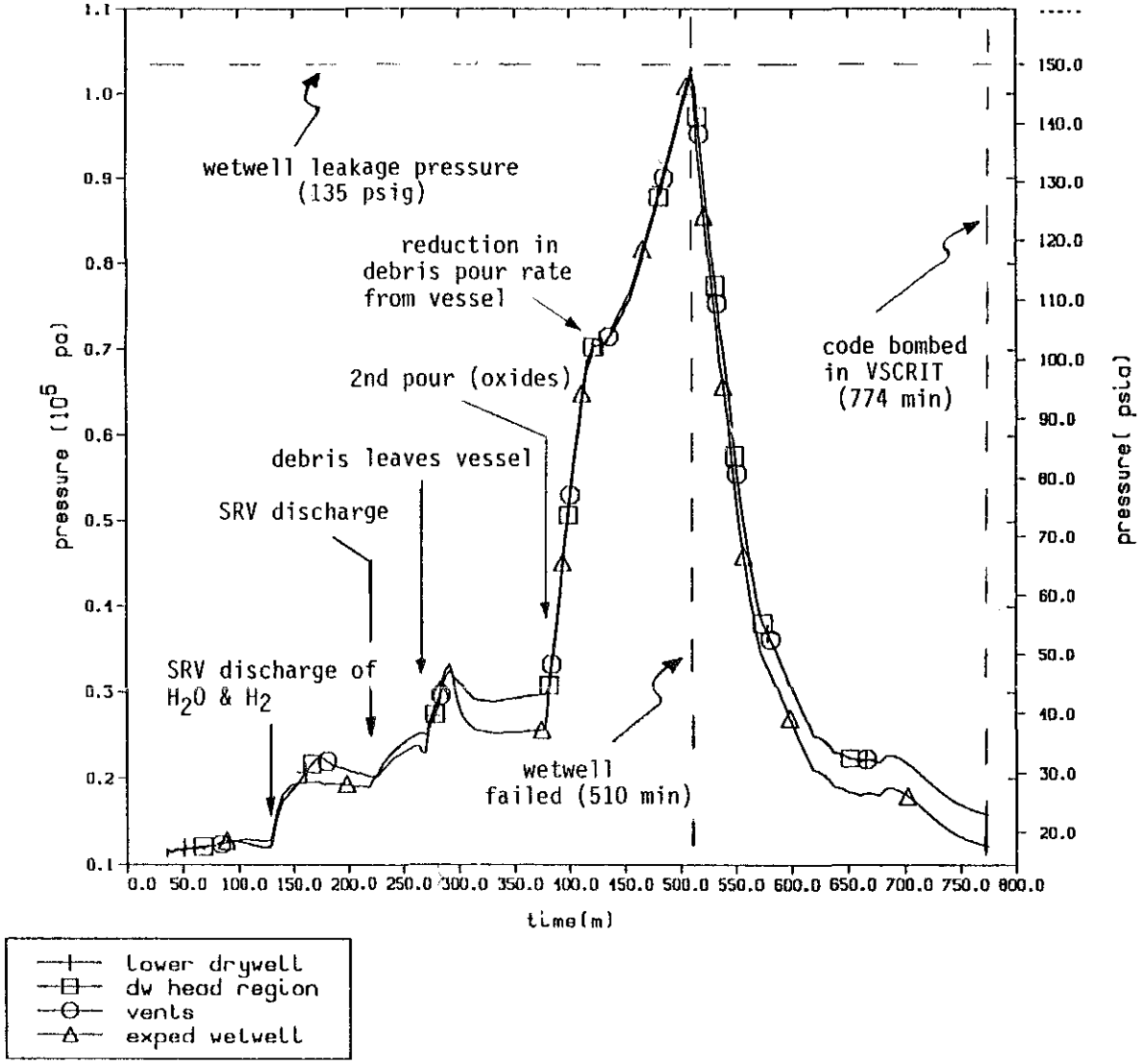

Fig. 9.5.1. Primary containment pressure distribution for the dual cavity (0% drywell/100% wetwell) Mark II analysis of short-term station blackout with ADS actuation.

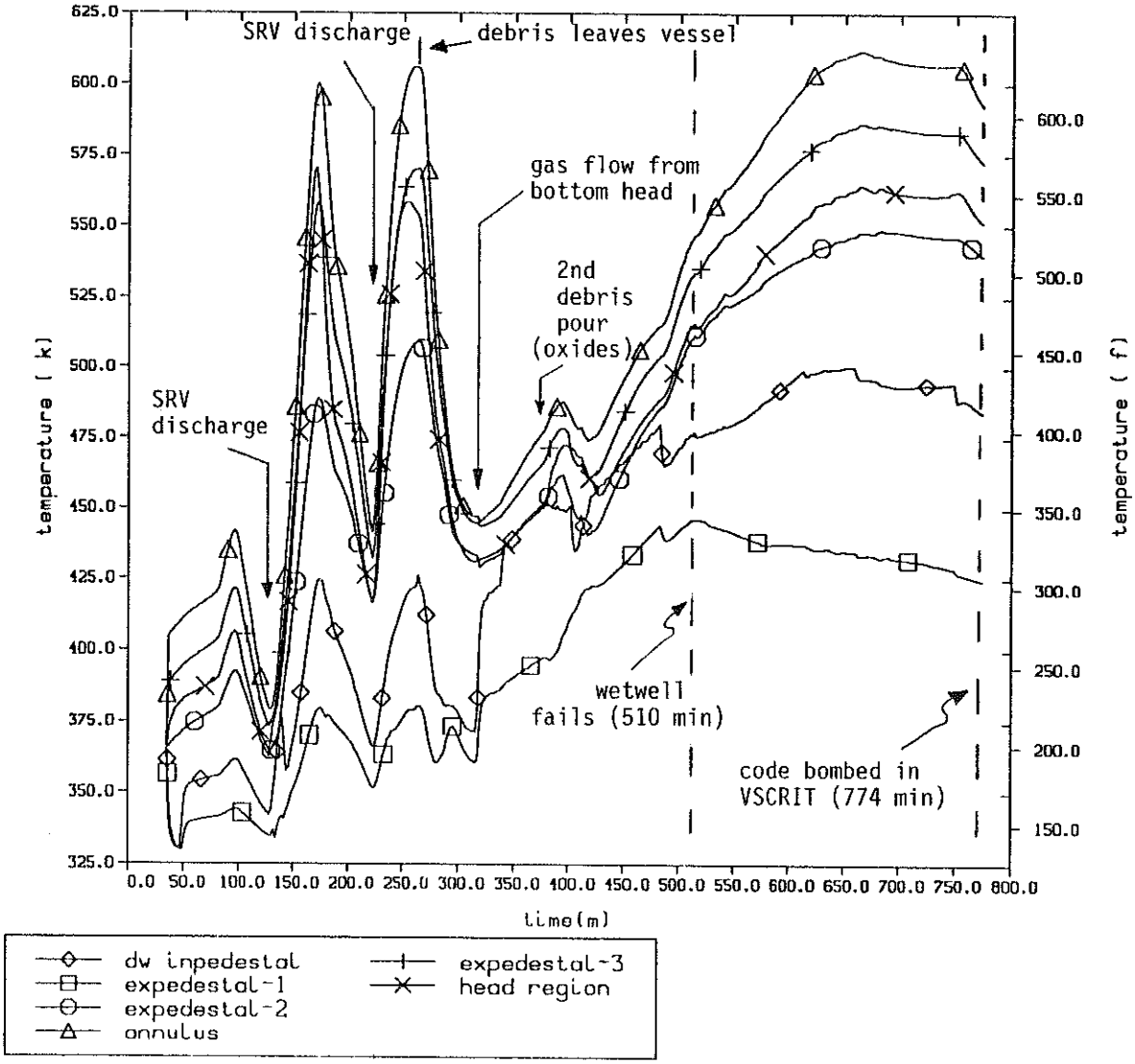

Fig. 9.5.2. Primary containment temperature distribution for the dual cavity (0% drywell/100% wetwell) Mark II short-term station blackout with ADS actuation.

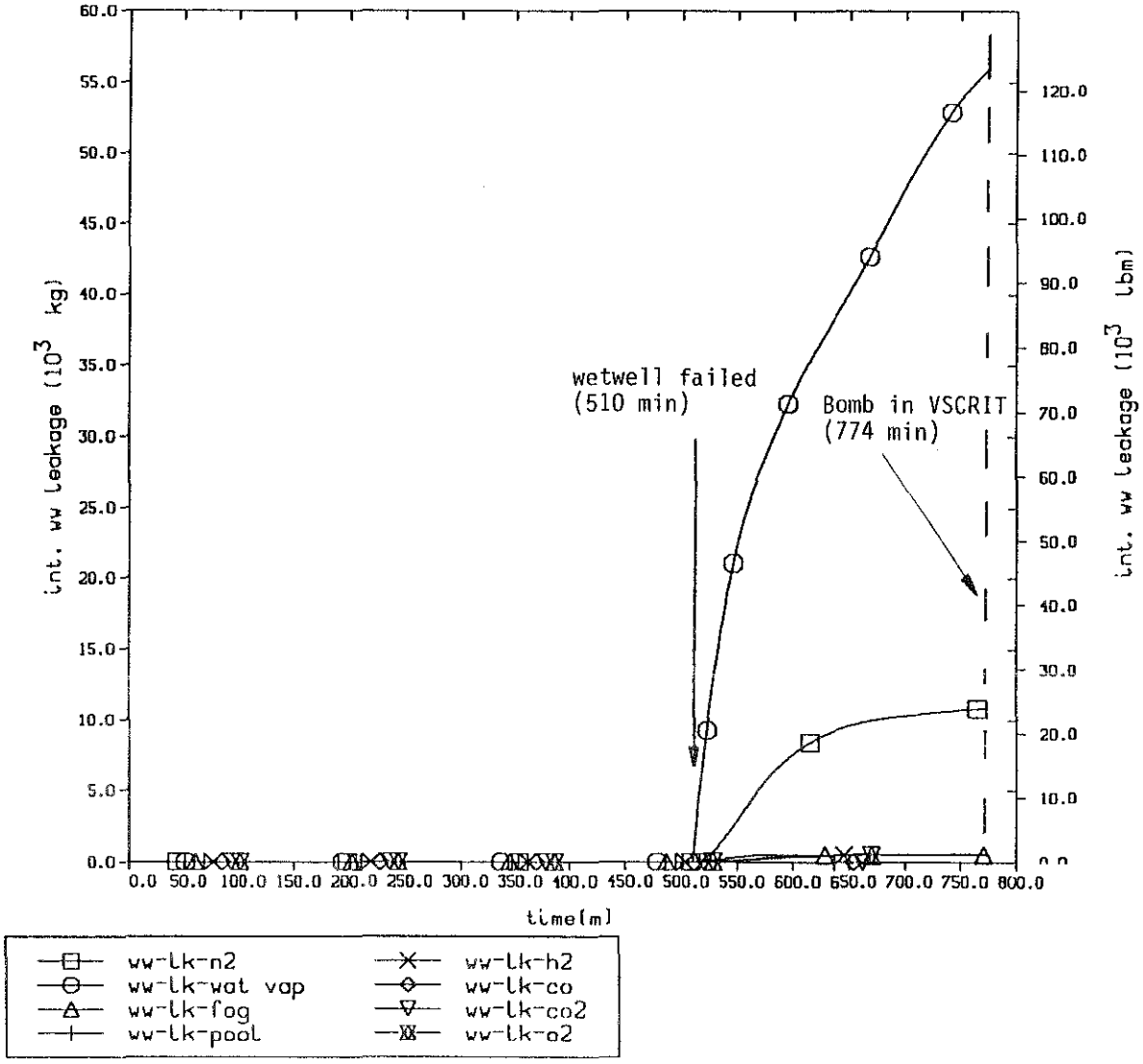

Fig. 9.5.3. Cumulative wetwell leakage for the dual-cavity (0% drywell/100%wetwell) Mark II short-term station blackout with ADS actuation.

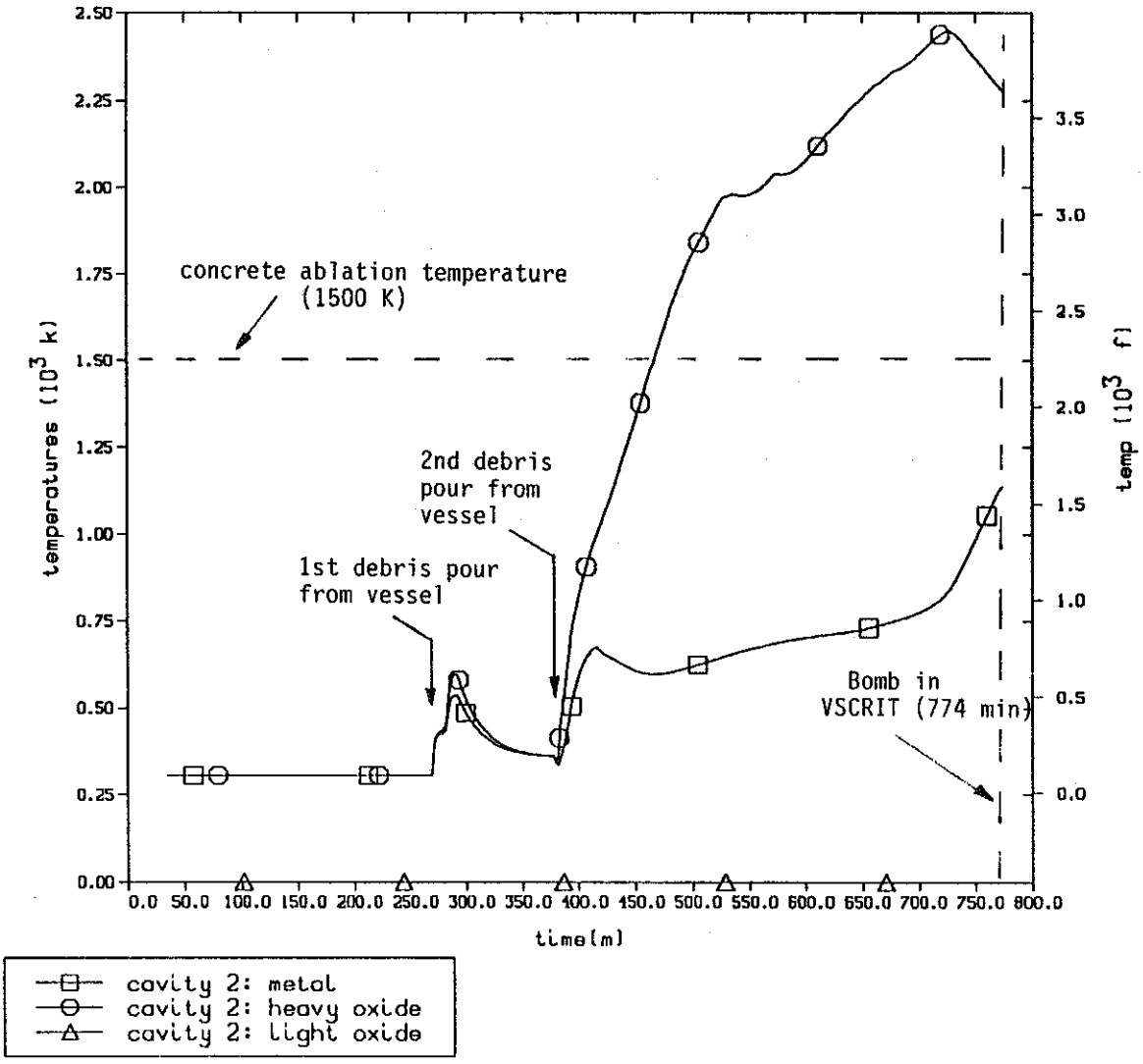

Fig. 9.5.4. In-pedestal wetwell debris layer temperatures for the dual cavity (0% drywell/100% wetwell) Mark II short-term station blackout with ADS actuation.

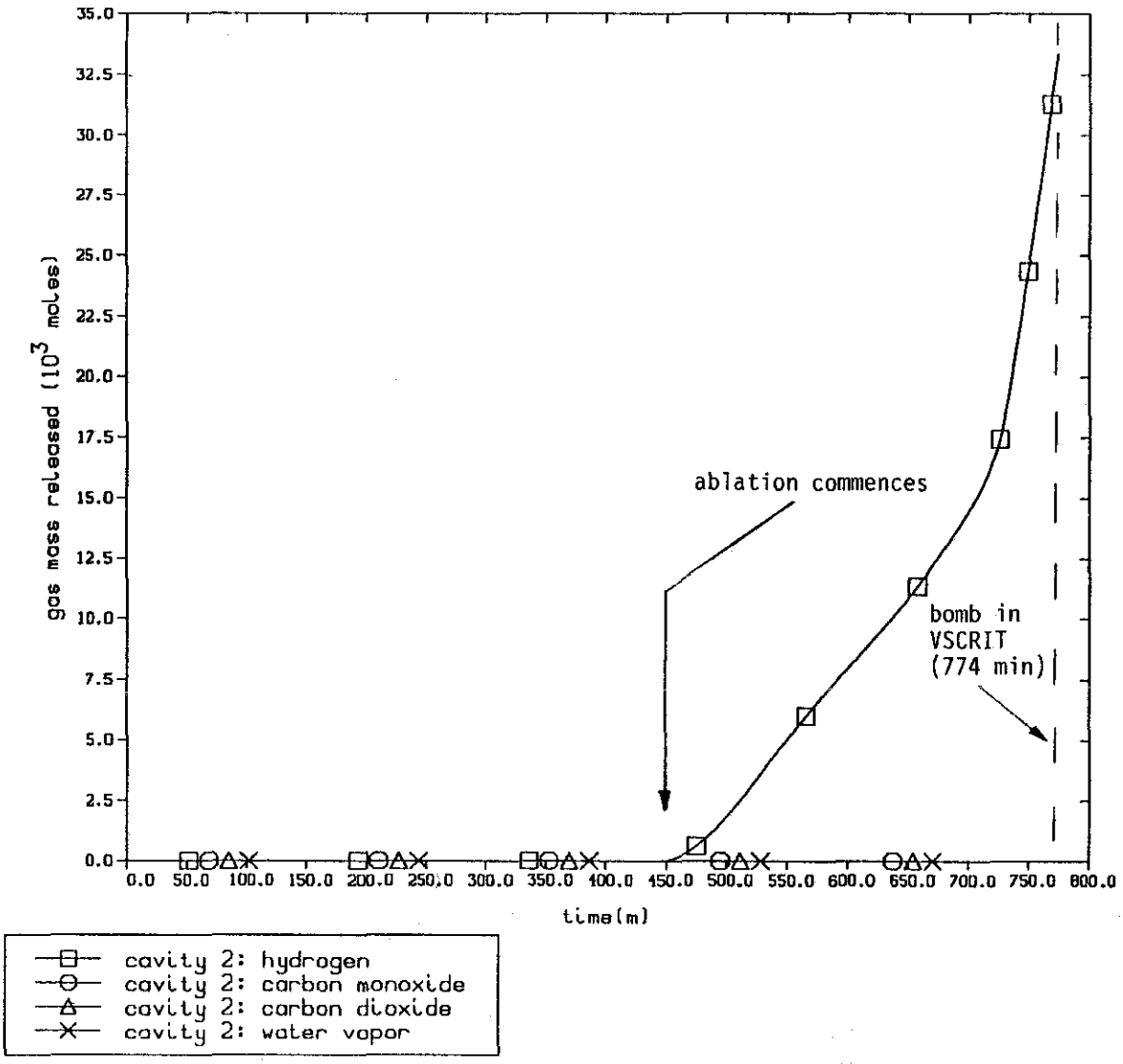

Fig. 9.5.5. In-pedestal wetwell debris gas releases for the dual cavity (0% drywell/100% wetwell) Mark II short-term station blackout with ADS actuation.

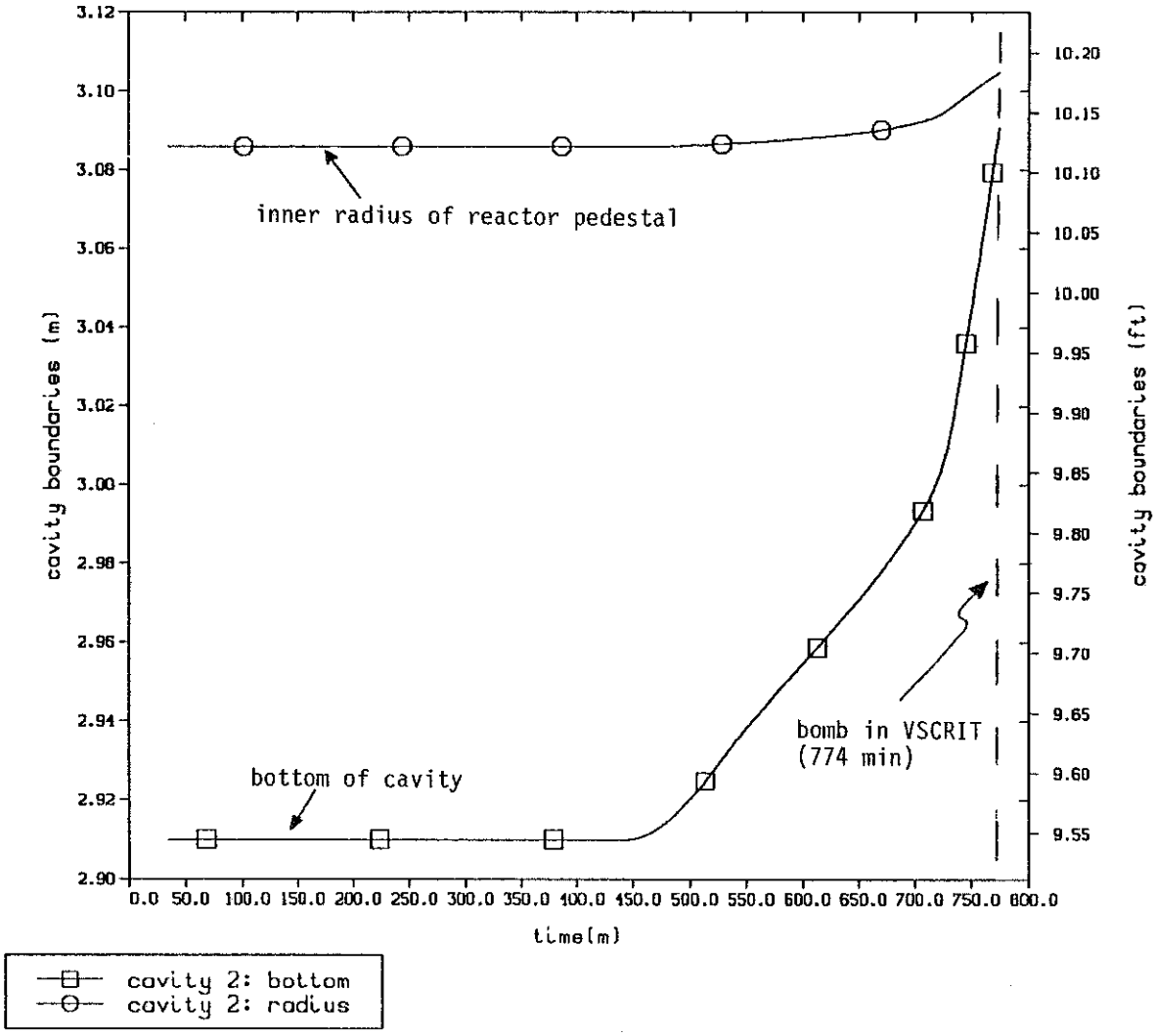

Fig. 9.5.6. In-pedestal wetwell maximum cavity dimensions for the dual cavity (0% drywell/100% wetwell) Mark II short-term station blackout with ADS actuation.

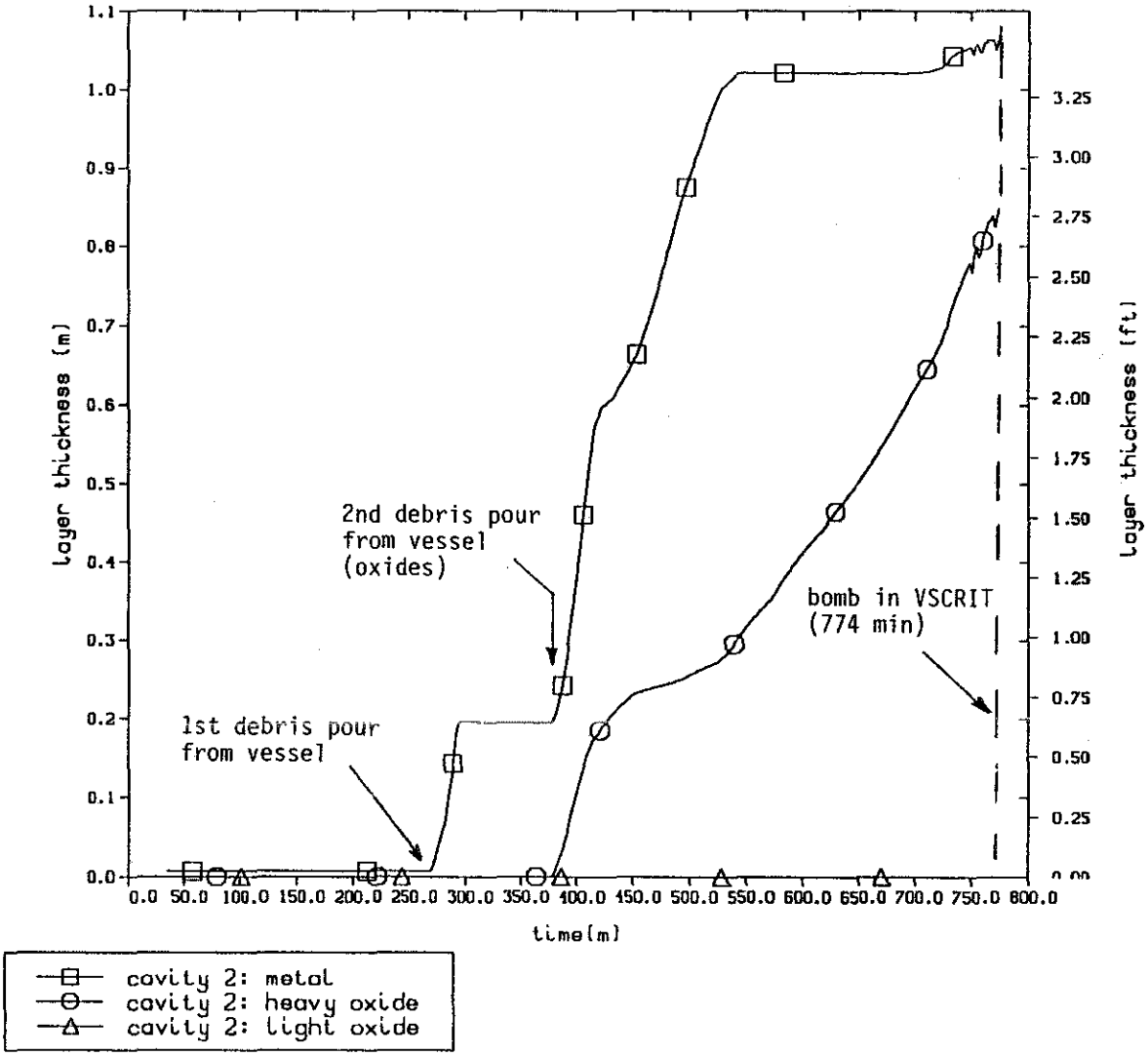

Fig. 9.5.7. In-pedestal wetwell debris layer thicknesses for the dual cavity (0% drywell/100% wetwell) Mark II short-term station blackout with ADS actuation.

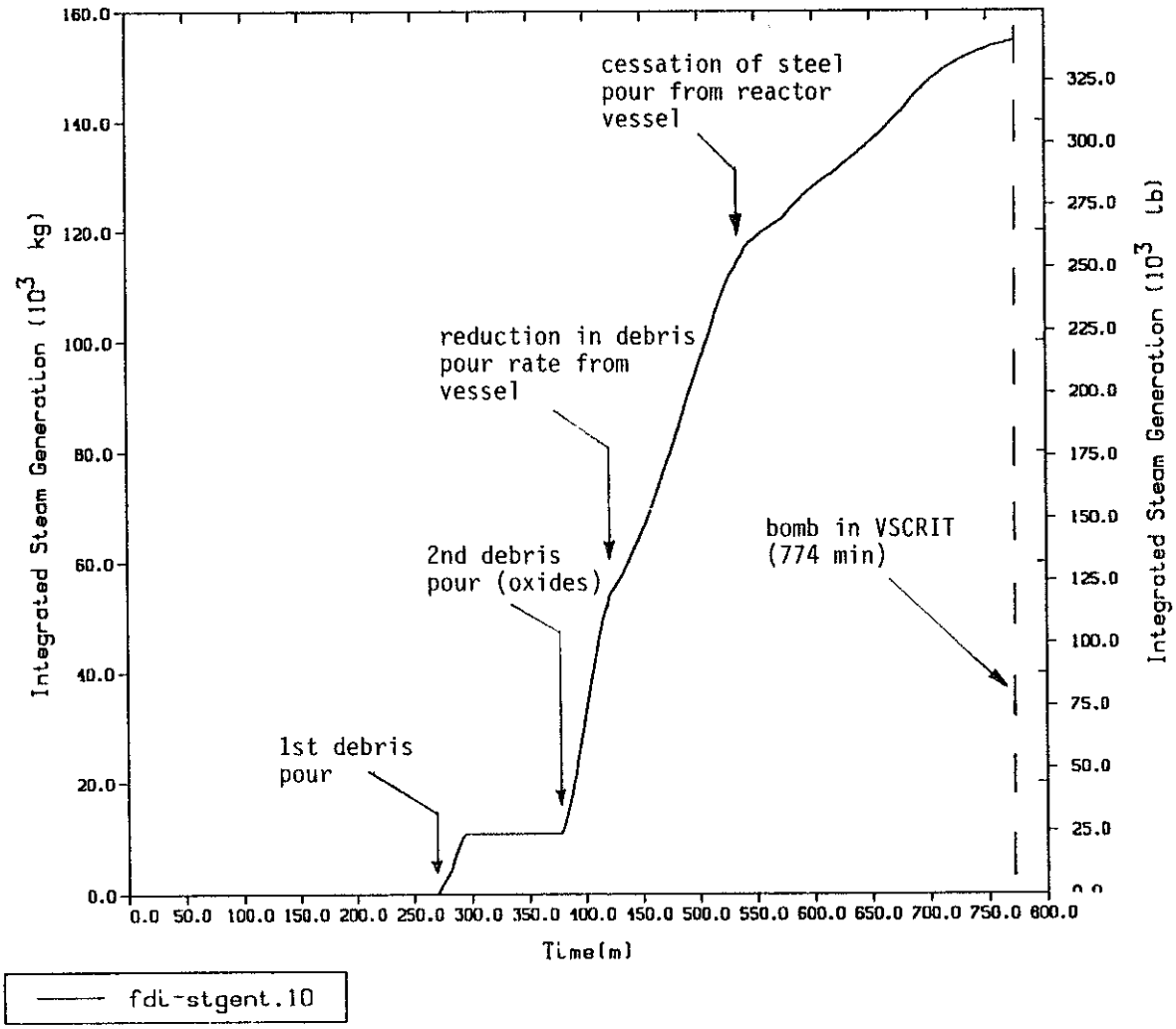

Fig. 9.5.8. Integrated steam generation from debris/wetwell pool interaction for the dual cavity (0% drywell/100% wetwell) Mark II short-term station blackout with ADS actuation.

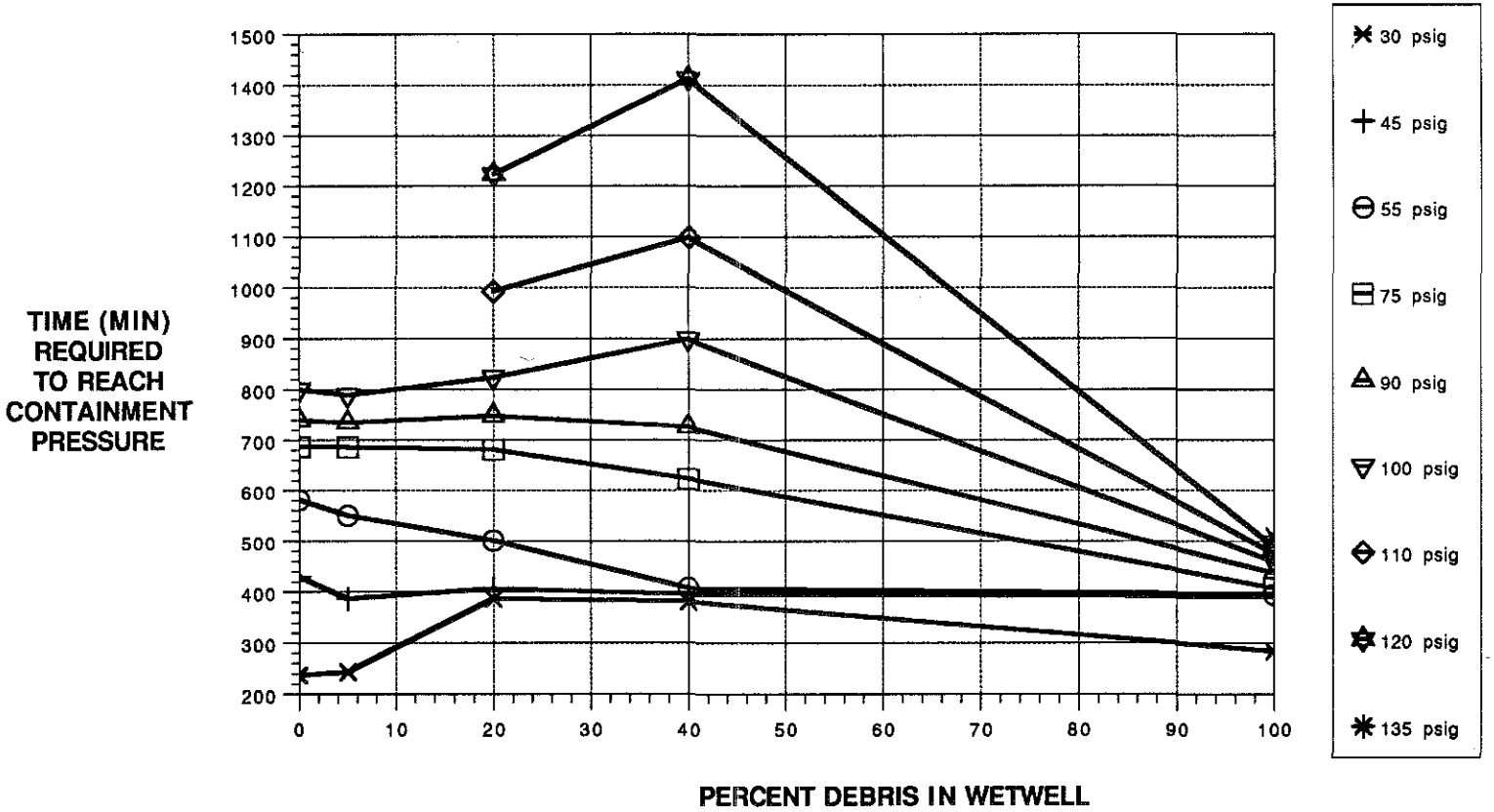

Fig. 9.6.1. Effect of debris-wetwell pool interactions on Mark II primary containment (wetwell) pressure response.

10. MARK II CONTAINMENT RESPONSE FOR UNMITIGATED LONG-TERM STATION BLACKOUT

10.1 INTRODUCTION

This chapter presents containment results obtained by MELCOR analysis of the long-term station blackout scenario assuming that all debris leaving the failed reactor vessel is maintained within the in-pedestal portion of the drywell floor. The scenario and its development is described in Chapter 3 as are the in-vessel BWRSAR analysis and results. The primary containment model is described in Chapter 7. The containment failure models described in Chapter 7 were disabled for this calculation.

The MELCOR analysis of the containment response was performed subsequent to completion of the BWRSAR calculations and represents the same period of the accident sequence. The containment atmosphere and containment structure initial conditions for MELCOR were specified to be consistent with those used by BWRSAR and the time-dependent containment conditions were calculated in response to the mass and energy sources generated by BWRSAR. These sources consisted of SRV discharges of steam and hydrogen into the wetwell pool, leakage of water from the reactor coolant system, discharge of steam and hydrogen from the bottom head of the reactor vessel after the head penetrations fail, and core and bottom head structural material debris pours from the failed reactor vessel.

Both BWRSAR and MELCOR were initiated at 630 min. This time is shortly before the core uncovers at 637 min. The calculation proceeded through the timing of core degradation, relocation, debris-bottom head interactions, and core-concrete interactions. The analysis was terminated at 1324 min because the wetwell reached the user-defined pressure limit of 150 psig. This corresponds to the wetwell condition in which the pressure exceeds by one atmosphere the estimated leakage threshold.

10.2 ANALYSIS RESULTS

This scenario is very similar to the short-term station blackout without ADS actuation. The main difference is the reduction in decay heating due to the delay of events afforded by the availability of unit batteries. Also there is a distinctive difference between the debris pours of the two scenarios. The debris pour for the short-term scenario with no ADS is almost continuous. The debris pour for the long-term case is

initially metallic but then approximately 1.5 h transpires with no pour from the vessel. The debris on the drywell floor during this time cools significantly so that concrete ablation is delayed until approximately 2 h after bottom head failure. Concrete ablation is coincident with the initial debris pour from the failed reactor vessel for the short-term station blackout without ADS actuation.

Drywell floor burn-through was not predicted to occur during the time frame addressed in the long-term blackout. At 1324 min (22 h), the axial concrete erosion rate was calculated to be 7 in./h and approximately 19 in. of concrete remained to be ablated. The extrapolated time of drywell floor burn-through is estimated to be 1487 min (24.8 h).

The time-dependent containment pressure distribution is presented in Fig. 10.2.1. Annotations on the figure identify important events influencing the pressure response. The calculation begins at 630 min, with the first significant event being a pressure rise due to a SRV discharge of steam and hydrogen into the wetwell pool occurring at 760 min with a second discharge at 870 min. Reactor vessel debris pouring first occurs at 986 min into the transient.

The containment pressure rise due to the blowdown from the reactor vessel bottom head is approximately 60 psi and closely corresponds to that calculated for the short-term blackout/no ADS scenario. The magnitude of this pressure rise is due to the large inventory of hydrogen created as steam is reacted with the zirconium in the vessel bottom head during primary system blowdown. Containment pressure at the end of the blowdown is approximately 105 psig for the long-term blackout and is only 75 psig for the short-term/no ADS blackout. The pressure is higher in the long-term case because the initial containment pressure is higher. Initial pressure is higher because the containment has preheated for over 10 h in the long-term case as compared to only 0.5 hour in the short-term case.

The containment leakage pressure of 135 psig is reached in the wetwell at approximately 1250 min (20.8 h) and the containment pressures at the end of the calculation (at 22 h) are 156 and 150 psig for the drywell and wetwell, respectively.

Between 10.5 h and the end of the calculation at 22 h, the containment pressure generally increases with a slight decrease during the period immediately prior to reactor vessel bottom head failure at 986 min (16.4 h). This long-term pressure rise occurs as noncondensible gases are released into the containment atmosphere and as the atmosphere is heated. The sources of the gases are the previously mentioned SRV discharges and the gases released from the hot core debris as a result of the molten core

concrete interaction on the drywell floor. Although the containment is not allowed to leak in the current calculation, it should be recognized that it would have leaked had the option been enabled via input. At 22 h, the drywell pressure is 156 psig while the wetwell pressure is slightly above 150 psig.

Atmosphere heating is most evident in Fig. 10.2.2 which presents the calculated atmospheric temperature distribution. There are small temperature rises at 760 and 870 min due to the SRV discharges. The striking rise at 986 min occurs at reactor vessel bottom head failure. After this time, hot debris and gas exit from the failed reactor vessel and flow into the drywell. The atmosphere temperature increases as hot debris both directly heats the drywell atmosphere and as hot gas is released from the core-concrete interaction and mixes with the cooler drywell atmosphere. At 1070 min, the atmosphere temperatures begin to increase in response to a second debris pour from the reactor vessel. The temperature rise is most pronounced for the in-pedestal region of the drywell floor where the core-concrete reaction is proceeding.

At the end of the calculation (1324 min), the gas temperature near the drywell head is less than the estimated drywell head flange failure threshold of 700°F. It is therefore probable that the containment would fail due to overpressurization before it would fail due to drywell head flange seal degradation in this scenario.

Drywell floor debris temperatures are presented in Fig. 10.2.3. The debris temperatures immediately rise in response to the debris pour from the reactor vessel at 986 min but fall once the initial debris pour stops at 995 min. The debris temperature only momentarily reaches the concrete ablation temperature of 2246°F (1503 K) so that no concrete ablation is calculated. Debris temperatures rise after the second debris pour at 1070 min and concrete ablation is calculated to begin shortly thereafter at 1120 min.

Concrete ablation releases CO_2 and H_2O into the debris so that a large chemically-derived thermal power begins to be generated within the debris. This chemical power combines with the UO_2 pouring from the reactor vessel at 1130 min to produce a mild temperature excursion for the light oxide layer of approximately 50°F. The temperature increase at 1200 min is due to an increase in the debris pour temperature from the reactor vessel and results in the complete melting of the metal layer radial crust at this time. By 1250 min, the zirconium inventory lying on the drywell floor has been completely exhausted, the chemical power source decreases, and the debris layer temperatures begin to fall.

It is interesting to note that CORCON does not calculate the formation of a stable heavy oxide layer. This is characteristic of the core-concrete reaction associated with debris pours of BWR transients involving high pressure blowdowns through debris beds in the reactor vessel bottom head. For both the short-term station blackout without ADS (discussed in Section 8.3) and the long-term station blackout currently under discussion, significant quantities of zirconium are converted to ZrO_2 in the reactor vessel bottom head during the blowdown. Thus the oxide portion of the debris leaving the reactor vessel is enriched with ZrO_2 compared to that calculated for low pressure debris pour. Because the density of ZrO_2 (350 lb/ft^3) is less than steel (495 lb/ft^3)and UO_2 (684 lb/ft^3), the oxidic portion of the debris pour is less dense than the metallic portion. CORCON therefore calculates that the oxidic debris remains on top of the metallic and no heavy oxide layer is formed.

This contrasts with the low pressure debris pours where the oxidic debris pours are more dense than the metallic and the oxides are calculated to settle through the metals and to form a heavy oxide layer. For these transients, the occurrence of a light oxide layer is calculated only after layer flip. This event is calculated when the heavy oxide layer density falls below that of the metal layer density. In turn the heavy layer density is reduced by the continuous influx of light concrete slag originating from concrete ablation.

Calculated debris layer thicknesses are presented in Fig. 10.2.4. Like the debris temperatures discussed above, the layer thicknesses increase in response to the debris pours from the reactor vessel. The metal layer thickness jumps at the initiation of debris pour at 986 min but quickly levels off as the debris pour stops at 995 min. No oxide pours from the vessel during the initial phase of the accident and thus no oxide layers are calculated during this time.

The second pour from the vessel commences at 1100 min, but once again, it is initially metallic with the only oxides pouring being ZrO_2. At around 1130 min, UO_2 is evident in the debris pour and the light oxide layer thickness rapidly increases. As mentioned above, MELCOR does not calculate the formation of a heavy oxide layer. The reduction in metal layer thickness after 1200 min corresponds to the oxidation and removal of metallic mass from the metal layer and its relocation in oxide form to the light oxide layer.

Figure 10.2.5 reports the cumulative releases of gas from the debris into the drywell atmosphere. The gas release is primarily hydrogen that results from the oxidation of zirconium with the water vapor released from concrete ablation. Little carbon bearing

gas is evident until approximately 1260 min when a rapid release of carbon monoxide is calculated. This release is due to the oxidation of carbon that had accumulated in the metal layer. This carbon accumulation is due to CORCON's assumption of complete reduction of the CO_2 by zirconium into carbon. Once the zirconium is exhausted, however, the carbon begins to oxidize with the CO_2 from the concrete ablation and large amounts of carbon monoxide are produced.

Small quantities of carbon dioxide and water vapor are evident by the end of the calculation at 1324 min. These gases are due to concrete ablation by the light oxide layer. The light oxide layer overlies the metal layer and, therefore, physical contact and chemical reactions of the concrete gases with the metal layer are avoided. Had the calculation been continued further in time, it is expected that significantly more gas would be released from the debris. This is because of the continued high debris temperature (2750°F) and concrete ablation rate (7 in./h).

Maximum cavity dimensions calculated by CORCON for the drywell floor are presented in Fig. 10.2.6. The drywell floor ablation is substantial (2.1 ft) by the end of the calculation. Nineteen inches of the concrete floor remains to be ablated and the ablation rate is 7 in./h. The extrapolated time of drywell floor burn-through is 1487 min (24.8 h). As explained earlier, the calculation was terminated at 1324 min (22 h) because the wetwell pressure (150 psig) was well beyond the leakage threshold of 135 psig.

Radial ablation is calculated to erode 1.5 ft of the original 4.8 ft of pedestal thickness by the end of the calculation. The drop in the rate of radial erosion at 1260 min is due to the reduction in chemical thermal power supplied to the debris after exhaustion of zirconium at 1250 min. Conversion of the carbon to carbon monoxide is endothermic and this reaction competes with oxidation of chromium with the CO_2 and H_2O produced from concrete ablation. Thus, the overall chemical power drops significantly after the exhaustion of the zirconium. The resumption of the radial ablation rate is due to the developing chemical reaction of chromium with CO_2 and H_2O and the increase in chemical power. Chromium oxidation at this time generates approximately the same power as fission product decay.

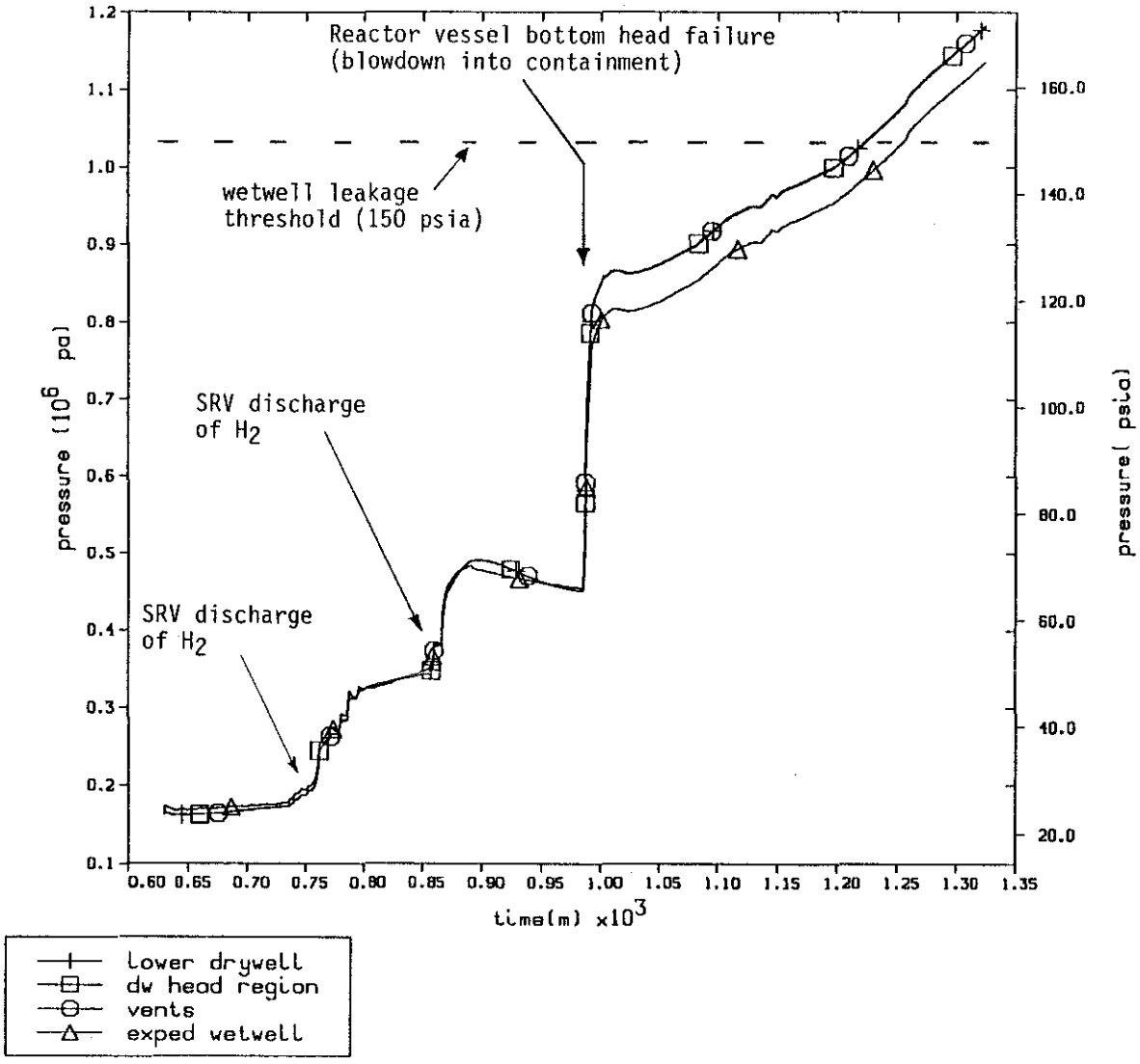

Fig. 10.2.1. Primary containment pressure distribution for the single cavity Mark II long-term station blackout sequence with ADS actuation.

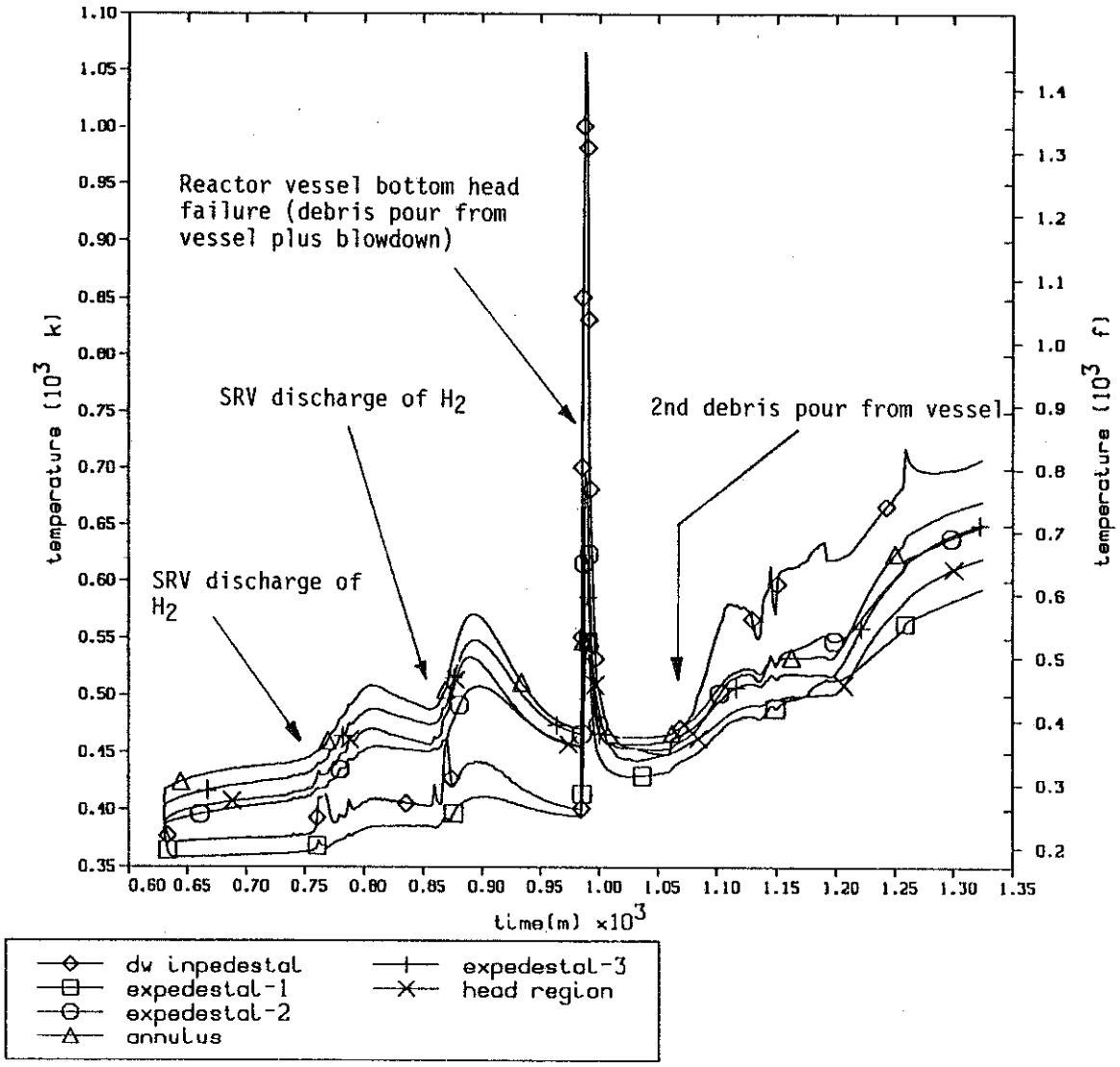

Fig. 10.2.2. Primary containment temperature distribution for the single cavity Mark II long-term station blackout sequence.

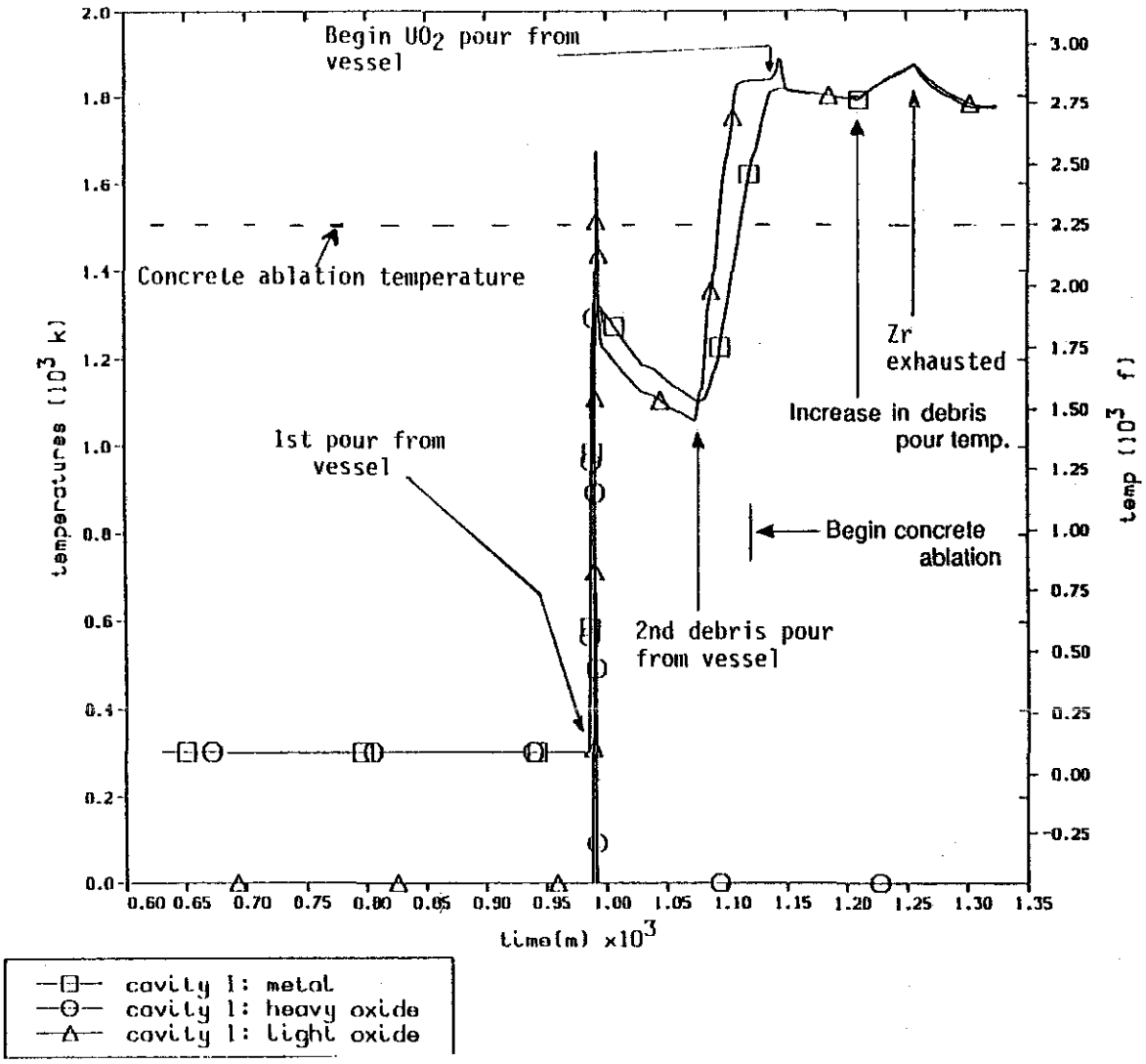

Fig. 10.2.3. Debris layer temperatures for the single cavity Mark II long-term station blackout sequence.

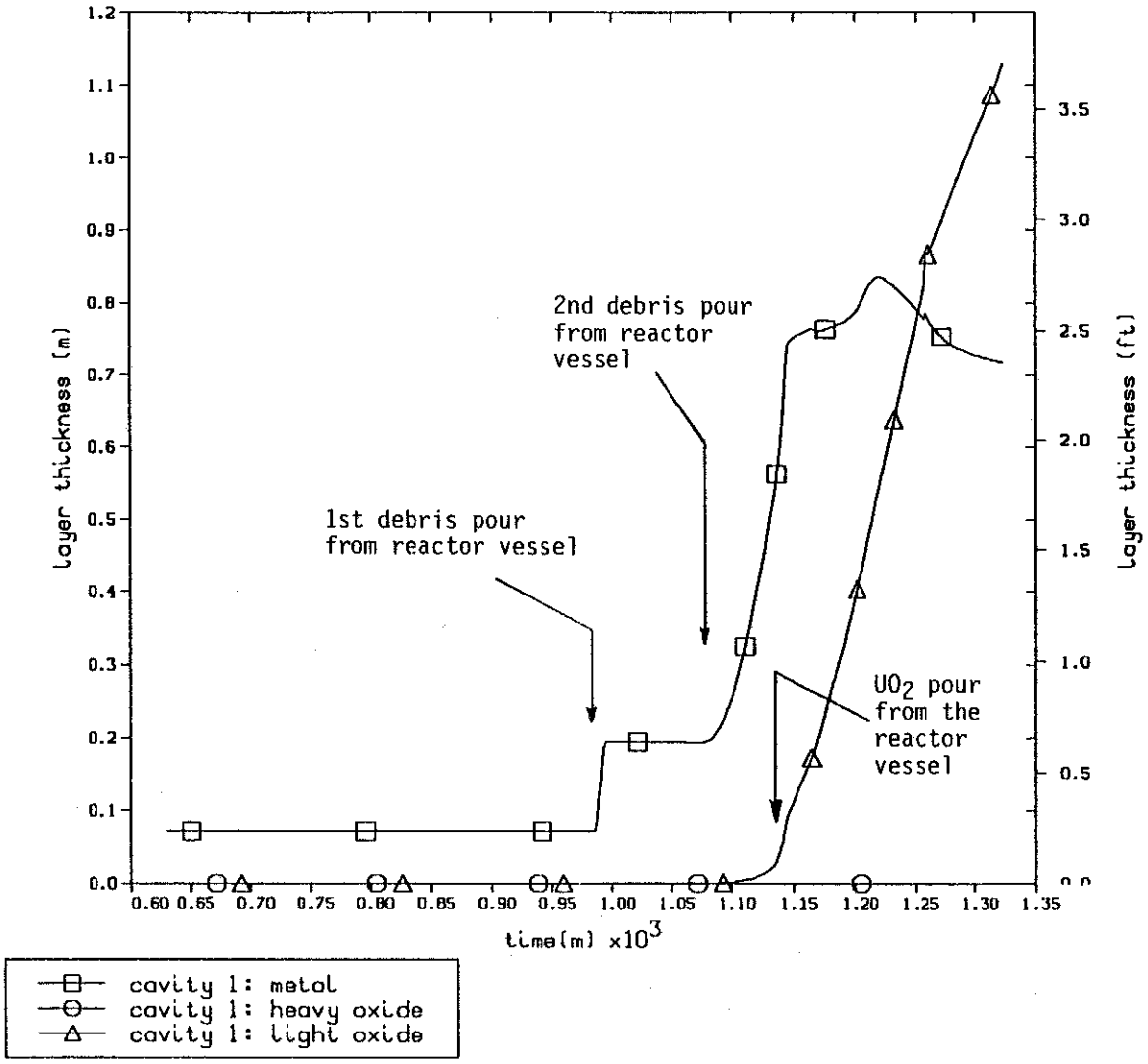

Fig. 10.2.4. Debris layer thicknesses for the single cavity Mark II long-term station blackout sequence.

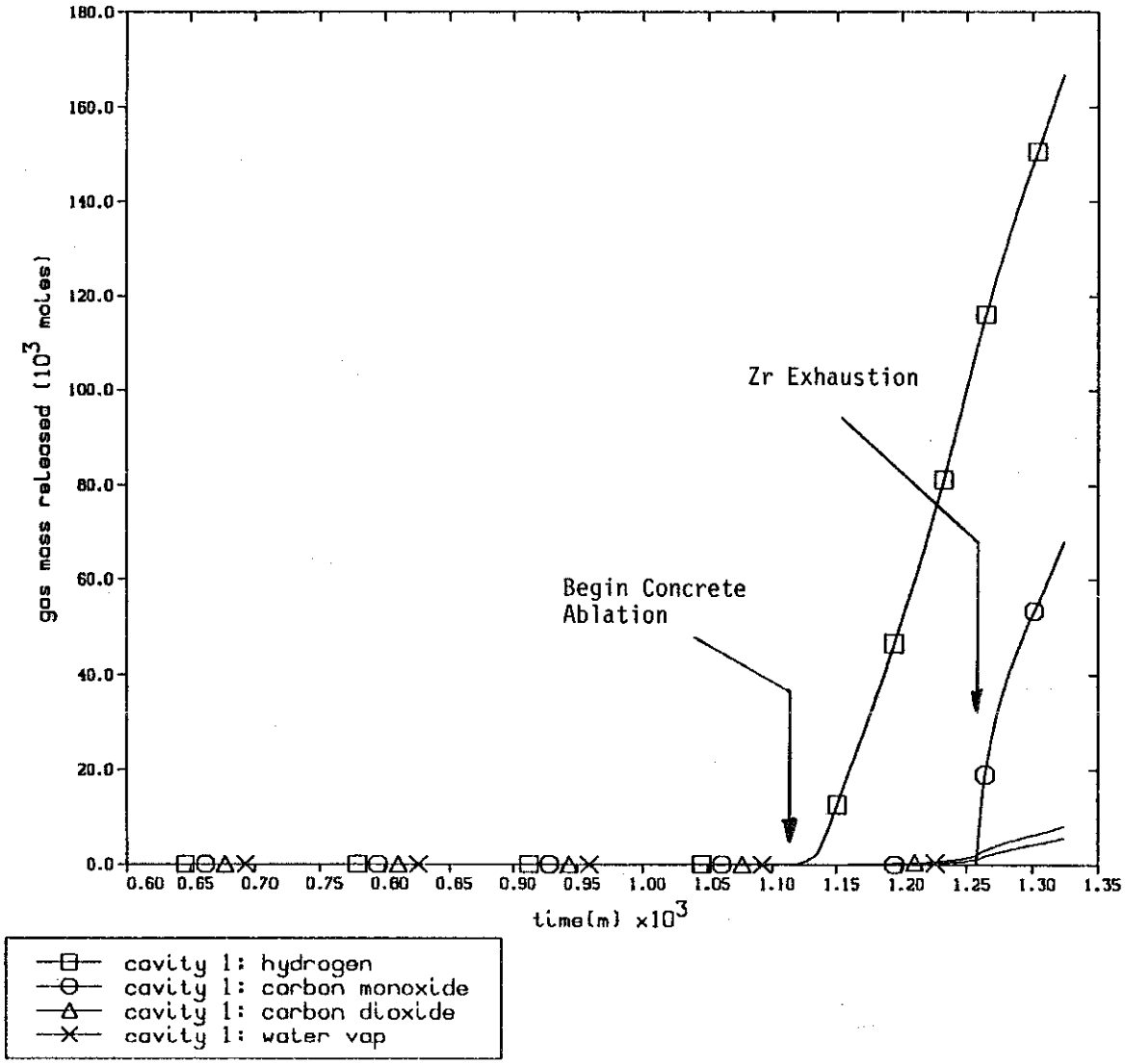

Fig. 10.2.5. Debris gas releases for the single cavity Mark II long-term station blackout sequence.

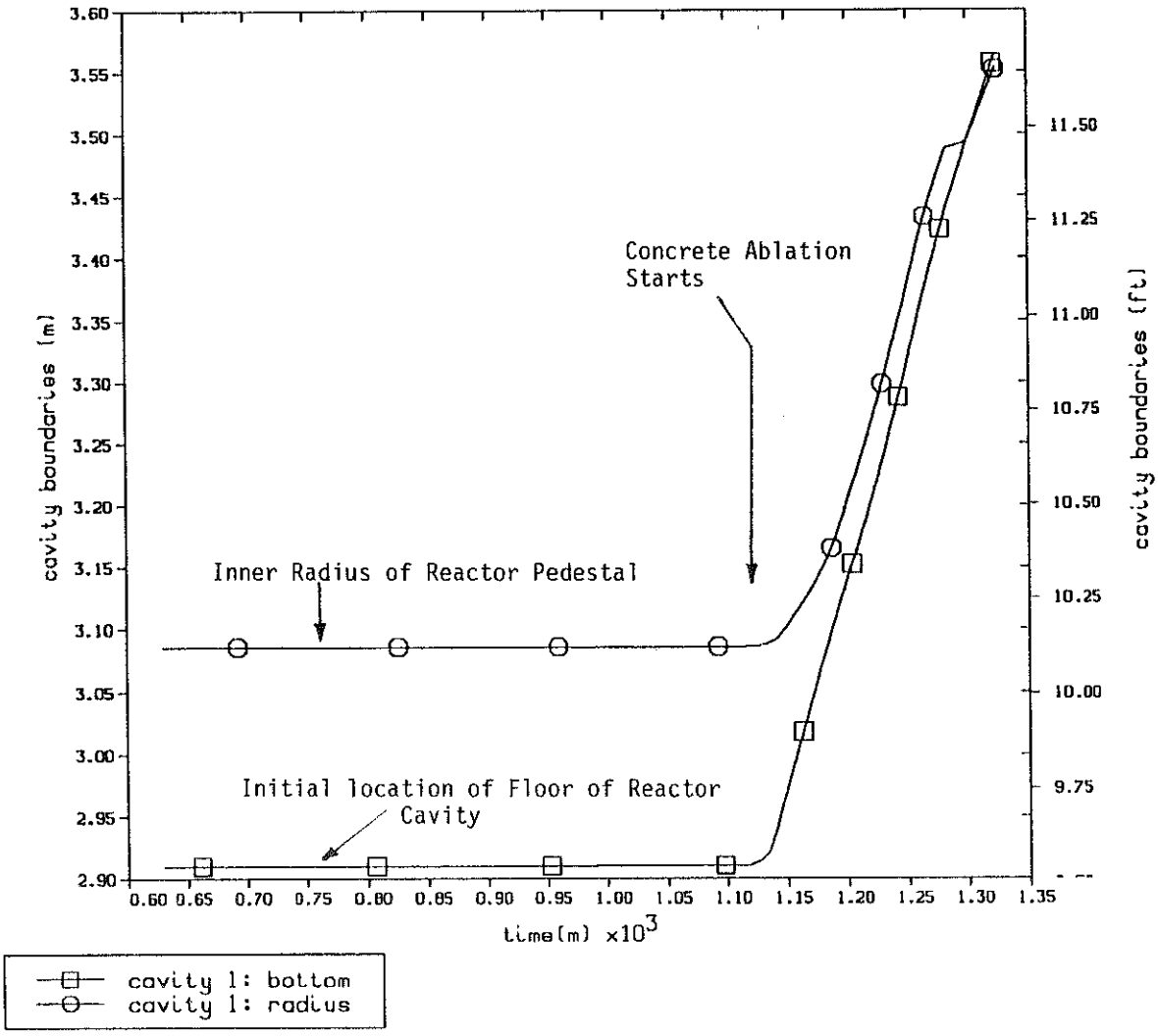

Fig. 10.2.6. Maximum cavity dimensions for the single cavity Mark II long-term station blackout sequence.

11. UNCERTAINTIES

11.1 INTRODUCTION

The major uncertainties in the analyses presented in this report are in the areas of (a) in-vessel phenomenology, (b) ex-vessel phenomenology, (c) the impact of plant-specific design characteristics on the applicability of the analyses, and (d) the impact of plant-specific emergency operating procedures on accident progression. Each of these areas of uncertainty are briefly discussed below in a qualitative manner.

11.2 IN-VESSEL PHENOMENOLOGY

There are many areas of uncertainty associated with modeling in-vessel BWR severe accident phenomena. Two of the most important involve the treatment of eutectic formation during the debris melting process, and the simulation of debris relocation from the core region into the vessel lower plenum.

As noted in Chapter 3, BWRSAR is the only BWR core degradation code which currently has the potential to model formation of the eutectic species actually observed in the Parker experiments. Use of the "Parker eutectics" model results in different debris pour timings and temperatures. However, it is not possible to assess the actual implications of these differences, since CORCON will not accept the Parker eutectics.

The BWR core plate does not support the core, but rather provides lateral alignment for the upper portion of the control rod guide tubes, which do support the fuel assemblies of the core. Under severe accident conditions, however, the peripherally supported stainless steel core plate would be exposed to vertical loading by the relocating core and structural debris that would accumulate over its upper surface. If the core plate remains in place, then the resulting debris bed would form in the core region. If, however, local plate failures permit the accumulating debris to fall into the vessel lower plenum, the debris bed would form there. Thus, the fate of the core plate determines the progression of BWR accident sequences for times beyond the onset of significant material relocation.

A recent study (Ref. 18) has addressed the modeling of core plate failure in the severe accident analysis codes APRIL, BWRSAR, MELCOR, MELPROG, and SCDAP/RELAP. None of the existing core plate models are capable of reliably

predicting how much of the relocating material would actually reach the plate, the rate of plate heatup, chemical reactions between the plate stainless steel and the overlying debris, or failure of local core plate regions by creep rupture. The models currently employed in the codes are based upon engineering judgment and conceptualization of the material relocation and core plate failure mechanisms rather than upon observation of these phenomena in the appropriate experimental settings.

A related issue with great uncertainty is the mode of reactor vessel bottom head failure. If a debris bed is formed above the core plate, it is probable that the vessel would fail via melt-through of one or more instrument tubes, while the majority of the debris is still in solid form. This is the mode of vessel failure modeled in the current analyses. If, however, the debris bed forms in the lower plenum of the reactor, a molten, superheated mass of debris could be formed, and the vessel could fail via gross rupture of the bottom head. Such a rupture could spill superheated debris onto the floor of the drywell (or into the wetwell pool). The potential for direct containment heating and steam explosions would be greatly increased in this case.

11.3 EX-VESSEL PHENOMENOLOGY

There are a variety of major uncertainties associated with ex-vessel debris transport and material/structural interactions. The CORCON code employed in these calculations does not have the capacity to model the flow of molten debris or the interaction of debris with downcomers and in-pedestal drains. This issue was addressed in the present analyses by parameterizing on the fraction of the debris pour assumed to enter the wetwell cavity. Several other important limitations of CORCON are described in Ref. 27.

The flooded-drywell case described in Sect. 8.4 probably underestimates the cooling effect of the overlying water pool generated by the drywell sprays. This uncertainty is related to the use of a traditional plate-type boiling curve for specification of the heat transfer coefficient between the surface of the debris and the water pool. Since this approach does not account for the heat transfer enhancement associated with sparging of the debris and the water from the core-concrete reaction off-gases, the model may overestimate the debris temperature, ablation rate, and non-condensable gas generation rates. This could translate to biased (excessively-high) predictions for containment pressure *if* the higher non-condensible gas generation rates in the present approach are not

counteracted (in reality) by the expected enhancement in pool steaming rate associated with the gas sparging.

The dual cavity calculations described in Chapter 9 were facilitated via a somewhat novel use of MELCOR's Transfer Process Package, along with multiple core-concrete interaction cavities. This approach makes it possible to direct various portions of the reactor vessel debris pour directly into the wetwell pool, but does not automatically account for the presence of the implied flow path in the thermalhydraulic modeling of the containment's performance. While the implied flow path (between the in-pedestal regions of the drywell and wetwell) can be explicitly modeled via other existing options, this was not done for these calculations due to the large uncertainty in the time-dependent size of the open area. (The present calculations basically assume that the hole is completely filled with flowing debris at all times.) It is not clear what, if any, impact this limitation has on the results of these calculations. The presence of an open "suppression pool bypass" flow path in the floor of the in-pedestal drywell would prevent the buildup of water pools in the in-pedestal drywell region, affect the magnitude of gas transfers between the drywell and the wetwell, and probably impact the drywell temperature. It certainly would lead to increased fission product releases should containment failure occur in the wetwell region.

Little information exists concerning the characteristics of core-concrete debris-water interactions. The calculations conducted for this study assumed that no explosive debris-water interactions occur, and, furthermore, model the debris-water interactions with a simplistic approach which does not acknowledge the presence of the large amount of concrete and concrete decomposition products which would be present in the debris should an actual event occur. Due to viscosity and thermal conductivity considerations, it is likely the probability of a steam explosion would be lowered by the presence of concrete decomposition products in the debris. The energy yield (*per unit mass of debris*) of non-explosive debris-water reactions would probably also be reduced (due to the lower thermal conductivity of the concrete decomposition products). However, since the *total* debris mass would be increased by the concrete decomposition products, the *total* non-explosive energy yield calculated by the present method may not be an upper bound.

11.4 PLANT-SPECIFIC DESIGN CHARACTERISTICS

As described in Chapter 3, the timing to core uncovery in the long-term station blackout is directly related to the lifetime of the station batteries under blackout conditions. The performance of the station batteries would, in turn, be related to both the design capacity of the batteries, and the plant-specific, load-shedding procedures executed by the operators. A 6-h battery lifetime was employed in these analyses. This lifetime estimate is based upon information supplied by PP&L for the Susquehanna Steam Electric Station. This value should not be applied to other plants without prior validation.

BWR Mark II primary containments exhibit highly-variable design features and are much less standardized than either Mark I or Mark III designs. As described in Chapter 5, the reactor pedestal configuration (in-pedestal/ex-pedestal floor elevations, in-pedestal downcomer and drain architecture, etc) is unique in each of the six domestic Mark IIs. These features will directly affect all important ex-vessel phenomena. The extent to which core debris spreads into the ex-pedestal region of the drywell; the mode, timing, and amount of debris entry into the wetwell pool; the probability and timing of pool bypass, the containment pressurization and heatup rate; the importance of ADS actuation; the effectiveness of containment sprays in cooling the debris; the probability of explosive core-concrete-coolant interactions; and the timing to containment failure are but a few of the critical phenomena and events which are *very* sensitive to the pedestal design. The "deep-cavity" pedestal design utilized in this study is similar to that employed in WNP-2 and La Salle. The timing of significant ex-vessel events for other designs could be significantly different than those described in this report.

A brief description of the various BWR Mark II drywell head closure designs was given in Chapter 5. It is clear that the failure criteria (temperature history, pressure, etc) for these components would be highly plant-specific. The failure pressure/temperature history criterion employed in this analysis is based on detailed analyses for the Peach Bottom Mark I plant, and may not be applicable for any plant other than Peach Bottom. It is possible that the design employed at some Mark II plants would result in failures for cases in which no failure was predicted in these analyses.

The 135 psig ultimate pressure capability (i.e., containment over-pressure failure criterion) employed in these analyses is based on the lowest value available from a limited number of detailed Mark II structural analyses. It does not account for early

leakage around containment penetrations. Since the containment liner/wall, and penetration configurations are highly plant-specific, a generic pressure criterion for the onset of significant containment leakage cannot be specified. These factors could significantly effect the calculated time to containment failure for some sequences.

The results of the calculations documented in this report can and do provide interesting and useful generic insights to Mark II severe accident behavior. However, the factors mentioned above suggest that the results of these analyses should not be applied to specific plants without explicit consideration of the many plant-specific design differences which exist in domestic BWR Mark II facilities.

11.5 EMERGENCY OPERATING PROCEDURE IMPLEMENTATION

While the BWR Owners Group has promulgated a detailed set of symptom-based emergency procedure guidelines, the actual implementation of these procedures is a voluntary action by each utility. It is known that various utilities have implemented different versions of the EPGs, and that the extent to which the EPGs have been and are being implemented varies. Chapter 3 of this report provided a brief discussion of the differing impacts of reactor vessel depressurization via Revision 3 and 4 of the EPGs. The analyses conducted in this study were based on the Revision 3 procedures for ADS actuation.

The sensitivity of the time of station battery depletion (and the resulting core uncovery) to load shedding procedures was noted above. There are, no doubt, many such examples in which utility-developed emergency procedures, and the utilities' interpretation and implementation of the BWR Owners Group's Emergency Procedure Guidelines differ from those assumed in this study.

12. SUMMARY OF TECHNICAL FINDINGS

12.1 INTRODUCTION

Detailed analyses of seven BWR Mark II short-term station blackout scenarios, and one long-term station blackout scenario were conducted. The BWR-LTAS, BWRSAR, and MELCOR codes were employed to provide analyses of the accident sequences from their inception until several hours after reactor vessel failure. Four of the calculations were halted at the time of drywell floor burn-through (due to the core-concrete interaction), because MELCOR does not have the capability to model the prompt debris-pool interactions (and containment pressure increase) that would occur following this event. Two of the calculations aborted due to code bugs. In both of these cases, however, the aborts occurred very near or after the time of containment failure. It is unlikely that the problems which caused the aborts affect the results or conclusions of the analyses.

12.2 CONTAINMENT DESIGN DIFFERENCES

The nine existing domestic Mark II containments (six sites) each employ unique design features which significantly limit the applicability of analytical results and experimental databases to plant configurations other than those for which the results are obtained. This is particularly true in relation to ex-vessel containment phenomena such as core-concrete interactions, fuel-coolant interactions, and containment liner failure modes and mechanisms. The designs differ in terms of depth of the in-pedestal floor relative to the ex-pedestal drywell floor (i.e. the presence and depth of an in-pedestal cavity), the thickness of the in-pedestal drywell floor, and the presence of penetrations (downcomers and floor drains) in the in-pedestal floor. Drywell head closure designs and head flange bolt preload are also highly variable, plant-specific characteristics.

Since it was not feasible to perform plant-specific evaluations for each of the six pedestal/cavity designs during the course of this project, a single deep-cavity design (somewhat representative of La Salle and WNP-2) was selected. The choice of this design was dictated by current modeling limitations in the CORCON and MELCOR codes, which preclude credible analyses of designs in which debris would be allowed to spread or flow outward from the in-pedestal to the ex-pedestal region of the drywell floor.

12.3 MARK II CONTAINMENT FAILURE MECHANISMS AND CRITERIA

Failure pressures for Mark II containments have been predicted to range between 120-160 psig. The model employed in these analyses incorporated two primary containment failure modes. The first failure mode is a simple over-pressure failure which opens a 0.1 ft^2 hole in the wetwell airspace region when the pressure in that region exceeds 135 psig. The second failure mode simulates the combined over-pressure/over-temperature failure of the drywell head flange seals (see Chapter 6). This failure model is consistent with available analytical results for the Peach Bottom Mark I drywell head closure design and available experimental results which relate seal resiliency to the gasket temperature history. The drywell head flange seals were modeled to begin leaking when the drywell pressure is greater than 82 psig if the head flange temperature has ever exceeded 700°F at any previous time in the transient. It is possible that these failure criteria would not apply at any facility other than Peach Bottom.

12.4 IMPACT OF ADS ACTUATION TIMING ON SHORT-TERM BLACKOUT ACCIDENT PROGRESSION

BWRSAR calculations indicate that the timing of ADS actuation significantly impacts the rate of core degradation in the short-term blackout sequence. Relocation of core debris begins 25-30 minutes later when Revision 3 of the BWR Owners Group Emergency Procedure Guidelines (EPGs) are utilized than when the Revision 4 procedures are employed. This delay could increase the probability of halting the accident prior to reactor vessel failure because additional time is provided for connection of alternate water sources for use by in-vessel injection systems.

12.5 IMPACT OF IN-VESSEL DEBRIS EUTECTIC FORMATION ASSUMPTIONS ON SHORT-TERM BLACKOUT ACCIDENT PROGRESSION

The potential impact of the most recent experimental findings regarding BWR debris eutectic formation in the lower head of the reactor vessel has been examined. These calculations indicate that more unoxidized zirconium would be expected to enter the containment early in the accident than is predicted by traditional modeling methods. This unoxidized zirconium would oxidize on the containment floor, heating the debris and providing a direct source of hydrogen to the drywell atmosphere. However, the

calculations also indicate that any significant differences in the predicted containment response would be limited to the first 2 h after initial reactor vessel penetration failure.

12.6 TIME REQUIRED TO EXCEED CONTAINMENT DESIGN PRESSURE FOR STATION BLACKOUT SEQUENCES

Table 12.1 summarizes the results of the calculations performed during this study. The containment pressure response histories for all cases are summarized in Figure 12.6.1. Existing Mark II containment design pressures range from 45-55 psig. This pressure is exceeded within 4 h for the short-term blackout case in which the reactor is not depressurized. The time required to exceed the containment design pressure ranges from approximately 6.5 to 10 hours for short-term blackout cases in which the ADS is actuated. Over 15 h is required to exceed the containment design pressure for the single long-term blackout sequence analyzed. These timings are significant because containment design pressures are utilized as criterion for initiation of emergency operator actions (such as venting) at some plants. Containment pressurization rates of 5-10 psi/h are typically predicted during the period in which robust core-concrete reactions are underway.

12.7 IMPACT OF ADS ACTUATION ON CONTAINMENT FAILURE TIMING

The first two short-term blackout calculations investigated the role of automatic depressurization system (ADS) activation on Mark II severe accident containment performance. The results of these two calculations are shown in Figure 12.7.1. The base case analysis (which assumes the reactor vessel *is* depressurized by the operators prior to the onset of significant core damage) indicated that gross containment failure might be avoided until approximately 13 h after the onset of the accident. By 13.5 h, however, the in-pedestal drywell floor would be completely ablated and a mixture of hot core-concrete debris would fall into the in-pedestal region o the wetwell. It is quite possible that the containment would fail when this occurs, due either to the structural weakening associated with drywell floor erosion, or due to a steam spike which would occur coincident with entry of the debris into the in-pedestal wetwell region. (The in-pedestal wetwell regions of all Mark II plants except La Salle are flooded.) The results of the second calculation indicate the primary containment would fail via the over-pressure

mode in approximately 10 h, if the reactor pressure vessel is not depressurized prior to the onset of core degradation.

12.8 IMPACT OF DRYWELL SPRAY ACTUATION ON CONTAINMENT FAILURE TIMING

The third short-term blackout calculation investigated the impact of drywell spray activation (a dedicated alternate power supply system is assumed) on Mark II severe accident containment performance. Flooding of the drywell floor via operation of the existing containment spray system reduces the ablation rate of the concrete drywell floor and (the spray system employed in these calculations) produces a 3-h delay (i.e., 16.6 h vs 13.5 h) in the time of drywell floor burn-through for the short-term blackout case in which the reactor is depressurized. However, this retardation in floor ablation is gained at the expense of higher ultimate containment pressures associated with the vaporization of the spray water as it interacts with the hot core-concrete debris (Figure 12.8.1). The containment was predicted to be very near its failure pressure at the time of drywell floor burn-through. The overall effectiveness of existing systems can also be limited because they often utilize low-head pumps (an 82.5 psid shut-off head was employed for this analysis). The drywell pressure exceeded the cutoff head of these pumps at 12 h into the accident. The existing pool of water generated by the pumps was depleted via boiling within 4 h after pump cutoff, and drywell floor burn-through was calculated to occur 0.6 h after the drywell pool water is exhausted.

12.9 IMPACT OF SUPPRESSION POOL-DEBRIS INTERACTIONS ON CONTAINMENT FAILURE TIMING

All domestic BWR Mark II containments except Susquehanna utilize a reactor pedestal design which incorporates either in-pedestal drains or downcomers that penetrate the drywell floor in the region beneath the reactor vessel bottom head. Following reactor vessel failure and debris discharge, it is, therefore, possible that hot debris (a mixture of reactor fuel, cladding, control blade, core plate, and reactor vessel materials, and concrete decomposition products) would enter the pressure suppression pool (*except* in LaSalle, which does not employ a flooded wetwell pedestal). The fraction of the debris which would enter the suppression pool would be both sequence- and plant-specific. Existing severe accident analysis tools cannot simulate this phenomenon.

A simple parametric study was conducted to evaluate the impact of the non-explosive interaction of various amounts (fractions) of the *reactor* debris (no concrete decomposition products included) with the pressure suppression pool. The results of this series of calculations are presented in Figure 12.9.1, where the time to reach various primary containment pressures is plotted as a function of the fraction of the debris assumed to enter the wetwell. As seen in Figure 12.9.1, containment pressures above 100 psig were not reached prior to gross in-pedestal drywell floor failure in the 0% wetwell and 5% wetwell cases. Second, while containment pressures rise very gradually for cases in which a relatively minor fraction of the debris enters the pool, the time required to raise containment pressure from 30 psig to the estimated failure pressure (135 psig) is only 2.2 h for the case in which all of the debris enters the wetwell. The time required to reach highly-elevated pressures (above 100 psig) is maximized for some intermediate debris splits (Fig. 12.9.2). This interesting observation appears to be an artifact of competition between steam and non-condensible gas generation from the core-concrete and debris-coolant interactions, and steam condensation on the containment structures.

12.10 CONTAINMENT FAILURE TIMING FOR LONG-TERM STATION BLACKOUT

Containment failure via over-pressurization is predicted to occur at 20.8 h in the long-term station blackout sequence compared to 10 h for the short-term blackout case in which the ADS system is not actuated. (The long-term station blackout scenario is very similar to the short-term station blackout scenario in which the ADS is not actuated, except that the sequence is delayed due to the early availability of reactor vessel injection.)

Table 12.1. Mark II short-term station blackout scenario summary

Case	ADS actuated?	Drywell sprays activated?	Debris split fraction % drywell	Debris split fraction % wetwell	Time to containment failure (h)	Time to drywell floor failure (h)	Wetwell pressure at time of floor failure (psia)
ST-1	yes	no	100	0	N/A	13.5	117
ST-2	no	no	100	0	10.0	12.2	173
ST-3	yes	yes	100	0	N/A	16.6	145
ST-4	yes	no	95	5	N/A	14.1	120
ST-5	yes	no	80	20	>20.4	>20.4	134[a]
ST-6	yes	no	60	40	>26.7	>26.7	140[b]
ST-7	yes	no	0	100	8.5	>12.9	145
LT-1	no	no	100	0	20.8	>22.1	165[c,d]

[a]Wetwell pressure at 20.4 h.

[b]Wetwell pressure at 26.7 h.

[c]Wetwell pressure at 22.1 h.

[d]Note: All containment failure mechanisms were disabled for the long-term station blackout calculation.

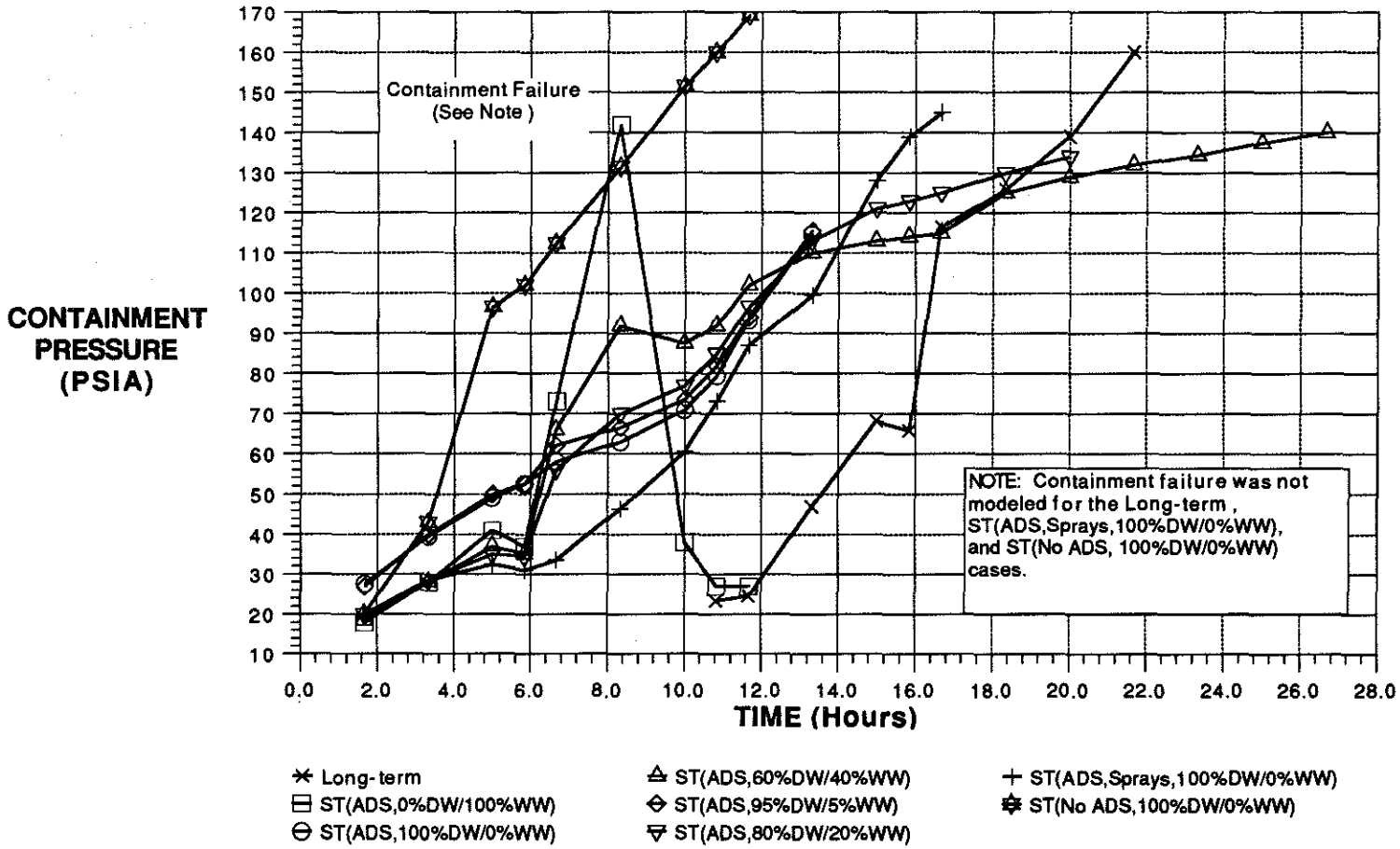

Fig. 12.6.1. Predicted containment pressurization histories for Mark II station blackout sequences.

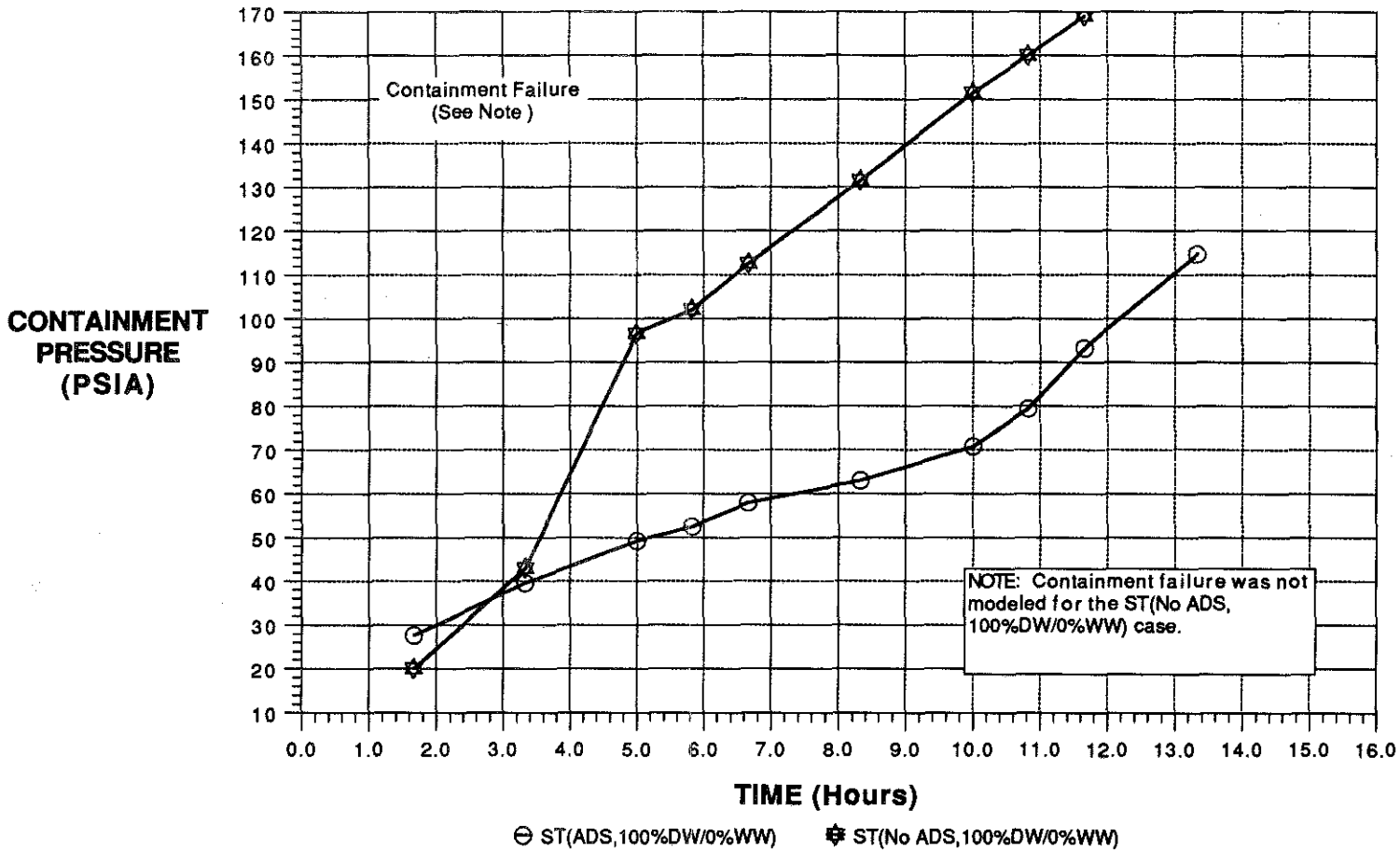

Fig. 12.7.1. Impact of ADS actuation on containment pressurization history for short-term station blackout sequence.

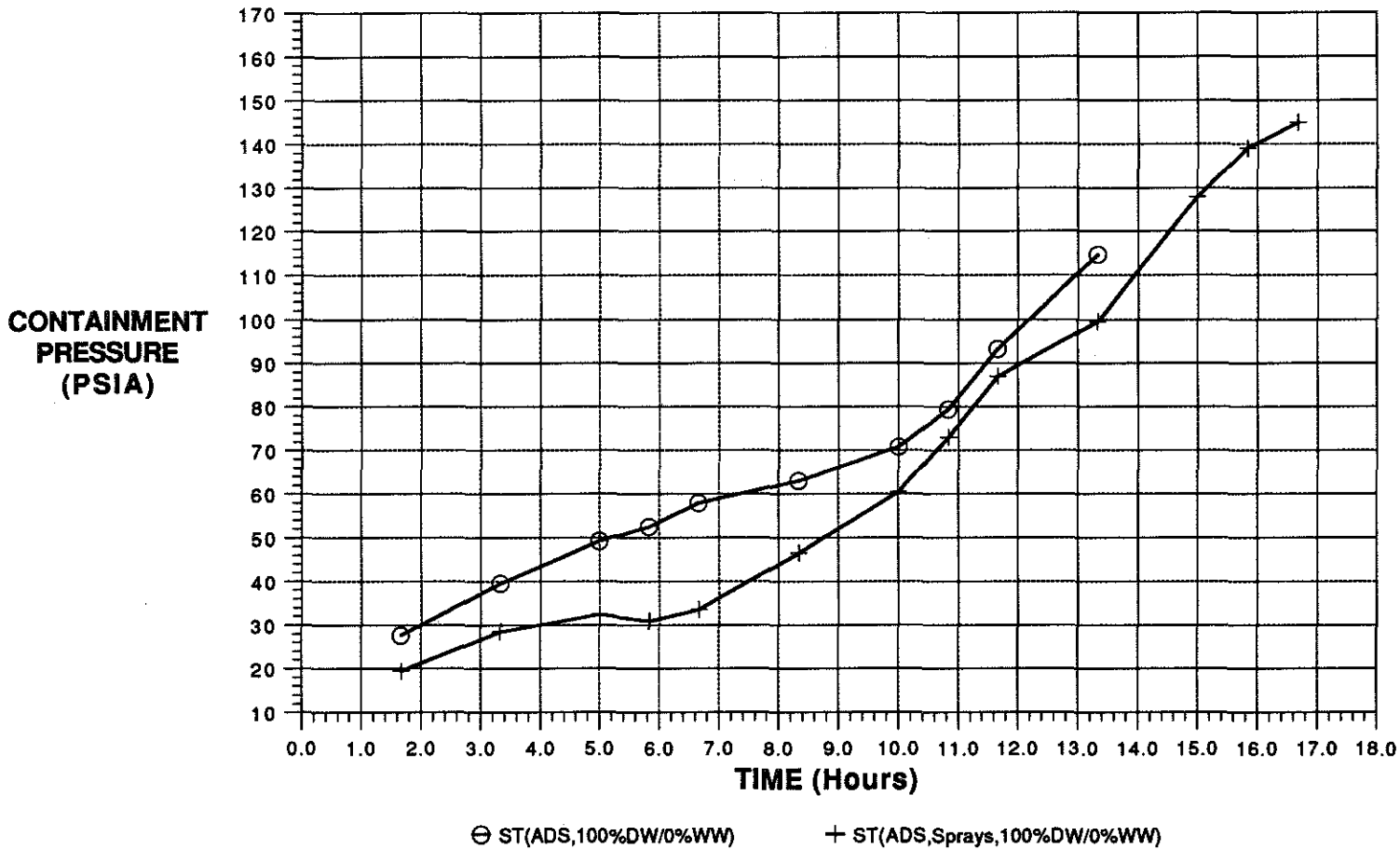

Fig. 12.8.1. Impact of drywell spray activation on short-term station blackout sequence with ADS actuation.

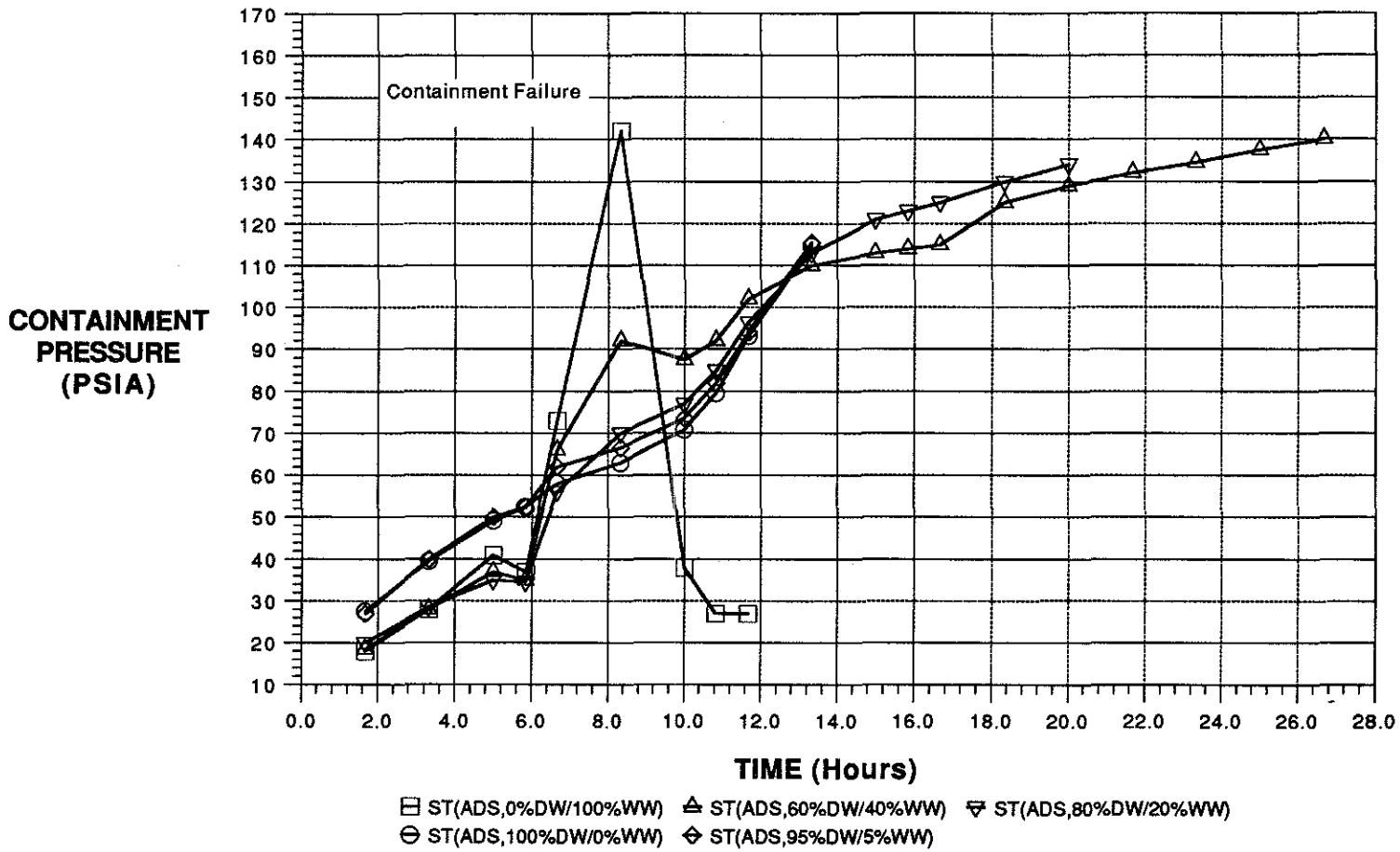

Fig. 12.9.1. Containment pressurization histories for dual cavity short-term station blackout sequences with ADS actuation.

13. REFERENCES

1. USNRC, Reactor Safety Study, WASH-1400 (NUREG-75/014), October, 1975.
2. U.S. Nuclear Regulatory Commission, *Severe Accident Risks: An Assessment for Five U.S. Nuclear Power Plants, Summary Report Second Draft for Peer Review*, NUREG-1150, Vol. 1, May 1989.
3. R. M. Harrington and L. C. Fuller, *BWR-LTAS: A Boiling Water Reactor Long-Term Accident Simulation Code*, NUREG/CR-3764 (ORNL/TM-9163), February 1985.
4. S. A. Hodge and L. J. Ott, *Boiling Water Reactor Severe Accident Response (BWRSAR) Code Description and Assessment*, Oak Ridge National Laboratory.
5. F. E. Haskin et al., "Development and Status of MELCOR," presented at the Fourteenth Water Reactor Safety Information Meeting, Gaithersburg, MD, October 1988.
6. C. A. Kukielka, S. Seyedhosseini, and M. P. Carr, "Feedwater Coast-Down Measurement of a BWR," *Proceedings of the U.S. NRC Sixteenth Water Reactor Safety Information Meeting, Gaithersburg, MD*, NUREG/CP-0097, Vol. 6, February 1989.
7. L. J. Ott, "Advanced Severe Accident Response Models for BWR Application," *Nuclear Engineering and Design*, 115, pp. 289-303, North-Holland, Amsterdam, 1989.
8. G. W. Parker, L. J. Ott, and S. A. Hodge, "Small-Scale BWR Core Debris Eutectics Formation and Melting Experiment," *Nuclear Engineering and Design*, 121, pp. 341–347, North-Holland, Amsterdam (1990).
9. BWR Owner's Group, "Emergency Procedure Guidelines," Revision 3.
10. BWR Owners' Group Emergency Procedure Guidelines, Revision 4, General Electric Topical Report NEDO-31331, March 1987.
11. D. H. Cook, S. R. Greene, R. M. Harrington, S. A. Hodge, and D. D. Yue, *Station Blackout at Browns Ferry Unit One - Accident Sequence Analysis*, NUREG/CR-2182, (ORNL/NUREG/TM-455/V1), November 1981.
12. Susquehanna Steam Electric Station (SSES) Final Safety Analysis Report (FSAR), Chap. 6, Figure 6.3-2., Pennsylvania Power and Light Co.
13. Ibid, Figure 5.4-10.

14. S. R. Greene, *Realistic Simulation of Severe Accidents in BWRs - Computer Modeling Requirements*, NUREG/CR-2940, April 1984.
15. Reactor Safety Study, WASH-1400, Appendix VII, U.S. Nuclear Regulatory Commission, October 1975.
16. L. G. Greimann et al., *Reliability Analysis of Steel Containment Strength,* NUREG/CR-2442, Ames Laboratory, Iowa State University, June 1, 1982.
17. Ultimate Pressure Capability of Limerick Primary Containment, Appendix J, Limerick Generating Station Probabilistic Risk Assessment, Bechtel Power Corporation, September 1982.
18. Request For Authorization to Increase Power to 25%, (Shoreham Nuclear Power Station, Unit 1), Long Island Lighting Company, Docket No. 50-322-0L, Appendix 3, April 1987.
19. S. A. Hodge, C. R. Hyman, and L. J. Ott, "Primary Containment Response Calculations for Unmitigated Short-term Blackout at Peach Bottom," letter report to Dr. Thomas J. Walker, Accident Evaluation Branch, Division of Reactor Accident Analysis, Office of Nuclear Regulatory Research, USNRC, November 28, 1988. Published as Appendix A to NUREG/CR-5528 (EGG-2593), July, 1990.
20. "Mark I Containment Severe Accident Analysis," CBI NA-CON, Inc. for the BWR Mark I Owners' Group, April 1987.
21. T. L. Bridges, "Containment Penetration Elastomer Seal Leak Rate Tests," NUREG/CR-4944, Idaho National Engineering Laboratory, July 1987.
22. D. A. Brinson and G. H. Graves, *Evaluation of Seals for Mechanical Penetrations of Containment Buildings*, NUREG/CR-5096, ERC International, August 1988.
23. R. F. Kulak et al., *Structural Response of Large Penetrations and Closures for Containment Vessels Subjected to Loading Beyond Design Basis*, NUREG/CR-4064, Argonne National Laboratory, February 1985.
24. David B. Clauss, "Failure Mechanism of LWR Steel Containment Buildings Subject to Severe Accident Loadings," *Proceedings of the Third Workshop on Containment Integrity*, NUREG/CP-0076, August 1986.
25. C. A. Kukielka, (Pennsylvania Power and Light Co.) personal communication with S. R. Greene (ORNL), Feb. 15, 1989.
26. *Reactor Safety Research Semi-Annual Report - July-December 1986*, NUREG/CR-4805 (2 of 2), SAND86-2752 (2 of 2), November 1987.

27. C. R. Hyman, "Current Limitations in the Application of CONTAIN/CORCON to BWR Mark I Severe Accident Analyses," ORNL Letter Report to Dr. Thomas J. Walker, Accident Evaluation Branch, Division of Reactor Accident Analysis, Office of Nuclear Regulator Research, USNRC, January 27, 1989.

Appendix A: BWRSAR/MELCOR INTERFACE

BWRSAR was used for simulation of the in-vessel phase of the severe accident scenarios discussed in this report. The use of BWRSAR for these analyses presented a code interface problem. The BWRSAR SRV discharge, vessel leakage, and debris pour results are needed as input for the MELCOR containment model. The interface between the BWRSAR and MELCOR codes is provided by the External Data File (EDF) option in MELCOR. This approach required a modification of an existing BWRSAR post processor code and the addition of an "interface" control volume in the primary containment model.

The EDF Package serves as a MELCOR utility to allow the code to communicate with external data files. These files may define sources or boundary conditions which vary with time. The EDF Package has the capability to both read and write data files. The addition of the EDF Package to MELCOR was in response to an ORNL request originally submitted to SNL on March 20, 1987.

There are four external data files to interface BWRSAR and MELCOR codes. The first file consists of five parameters: time, integrated SRV flows (water, steam, and hydrogen), and instantaneous SRV gas temperature at monotonically increasing times. The second file consists of five parameters: time, integrated reactor vessel and recirculation loop leakage (water, steam, and hydrogen), and instantaneous leakage temperature at monotonically increasing times.

The third external data file contains all of the information necessary to characterize the debris pours entering the containment. This file contains seventeen parameters related to the debris at monotonically-increasing times throughout the accident.

1. Time
2. Integrated mass of: UO_2
   zirconium (Zr)
   steel
   ZrO_2
   steel oxide
   control rod poison (B_4C)
3. Integrated enthalpy of the debris
4. Debris temperature

5. Debris pour column diameter (equivalent to the reactor vessel failure hole size in a normal MELCOR calculation)
6. Debris velocity as it enters the containment cavity (normally calculated by MELCOR as the debris ejection velocity from the reactor vessel)
7. The steel mass fractions of: iron (Fe)
   chromium (Cr)
   nickel (Ni)
   iron oxide (FeO)
   chromium oxide (Cr_2O_3)
   nickel oxide (NiO).

The integrated flows of successive time steps are multiplied by 1.000001) during the period when the integrated flow is constant. This ensures that the flows always increase slightly and avoids a bug in MELCOR which results in abnormal run termination for cases in which the integrated flows do not monotonically increase.

The fourth external data file contains the total ex-vessel debris decay heat history. This file contains only two parameters: time and total ex-vessel debris decay heat at monotonically increasing times.

Two separate BWRSAR post processor codes generate the four external data files. The first post processor reads the BWRSAR-generated data files. This post processor generates both SRV and vessel leakage flow plots and the MELCOR SRV and vessel leakage external data files. BWRSAR generates this information directly and no other manipulation or modification is needed.

The second BWRSAR post processor (SARCON2) also reads the BWRSAR generated data files. SARCON2 generates the MELCOR external data files for the debris pour characteristics and pour decay heat. The debris pour characteristics file contains zeros in the data fields for the integrated debris enthalpy, debris pour column diameter, and the debris pour velocity. The FDI package requires these parameters to determine the amount of steam generated by the debris as it falls through a pool of water.

To complete this file, a third code (MELCOR EDF pre-processor) was written. This code calculates the debris enthalpy using the material properties functions of the MELCOR code. (The necessary property correlations were obtained from the Material Properties User's Guide for Version 1.8.0 of the MELCOR code.) The data is in the form of tables of temperature vs enthalpy per unit mass. The values of enthalpy at intermediate temperatures were obtained by linear interpolation between the tabulated values as is done in the MELCOR code itself.

The file generated by SARCON2 contains values of the integrated flow of each material up to time t_i. At time t_i, the temperature of the pour is T_i. $M_{j,i}$ is the integrated flow of material j up to time t_i. The code calculates the enthalpy, $h_{j,i}$, per unit mass of each material j at temperature T_i. The total enthalpy at particular time, t_k, is the sum of all enthalpy additions up to time t_k.

$$\text{Total Enthalpy} = \Sigma_i \Sigma_j h_{j,i}\left[M_{j,i} - M_{j,i-1}\right] \tag{1}$$

The summation over j is over all materials. The summation over i is from i=2 to i=k. For the initial time, t_i, the enthalpy value is the sum of $h_{j,1}M_{j,1}$ for all the materials j. This value is actually zero since at the first time in the SARCON2 file, the $M_{j,1}$ values are all zero. If it should happen that values of $M_{j,i}$ are the same for successive values of i, $M_{j,i+1}$ is set to 1.000001 $M_{j,i}$) to prevent an interruption of the calculation, as previously discussed.

The EDF pre-processor code also provides for a constant value of the flow diameter. The flow diameter is the diameter of a circle whose area is a user-determined percent of the total in-pedestal drywell floor area, A. The velocity of the flow at time t_i is a function of the integrated mass flows and the component densities, d_j.

$$\text{Flow Velocity} = \frac{\Sigma_i \Sigma_j\left[M_{j,i} - M_{j,i-1}\right] / \left(Ad_j\right)}{t_i - t_{i-1}} \tag{2}$$

The values for the densities were also obtained from the Material Properties User's Guide. Hand calculations verified the code results for enthalpies, velocities, and debris pour column diameter.

Several short MELCOR calculations verified the new external data files generated by the code. A base case was first run for 2400 seconds of problem time. The integrated enthalpy was set to zero for the second case. The answers were identical except the listings of the values in the external data file. (The inserted value appears to be for checking purposes.)

The routines in the MELCOR EDF pre-processor code will be implemented directly into SARCON2. This will end the need for post-processing the external data files generated by SARCON2.

MELCOR 1.8.0 does not possess the capability to model the injection of externally-sourced hydrogen into a pool of water. Therefore an additional "interface cell" was added in the MELCOR model to provide this link. The interface cell is partially flooded and is connected to the pressure suppression pool via a flow path. This is undesirable because the use of this interface volume results in small code time steps and long computational times. The use of a large volume causes a distortion of the pool's response due to the time delay associated with material and energy transport through the volume. Thus, it is not possible to provide a realistic treatment of the impact of externally calculated SRV hydrogen flows on pressure suppression pool temperature or wetwell pressure. Nevertheless, the volume is in the model to provide the necessary interface between BWRSAR and MELCOR.

Appendix B: BWR-LTAS INPUT DECK FOR BWR-4

This appendix provides representative code input for the Boiling Water Reactor Long-Term Accident Simulation (BWR-LTAS) code. This input was used to generate the first 35 min of the short-term station blackout accident sequence for the Mark II containment calculations. The BWRSAR severe accident response calculation was initiated at accident time 35 min from the results of the BWR-LTAS calculation.

input data after modifications

```
&NAM1  ACOP = 191.993,  ACOR = 144.939,  ACPF = 1.0,  ADMET = 16570.0,  ADSOVR = 1.0,  ADVENT = 0.0,  AWVENT = 1.75,
 ALEAKO = 0.0,  APMET = 7847.7,  ART = 42.332,  ASSPW = 5277.0,  ATWSF = 0.0,  AOCP = 975.8,  A1CP = 3.025E-03,
 A2CP = -1.72304E-06,  BDWCO = 2800.0,  BDWSPO = 1250.0,  BC100 = 27000.0,  BHOT10 = 0.0,  BHOT04 = 430.0,  BLPMIN = 8500.0,
 BM = 20.0,  BRDPC = 2.5,  BRHRP = 22.2,  BRHRPO = 22.2,  BSPDWO = 2000.0,  BSUMP = 50.0,  CDMET = 19346.9,  CPMET = 9075.6,
 CPREF = 3293.0,  CPST = 0.1259,  CPO = 3293.0,  CVVENT = 0.833,  DALEAK = 0.0,  DELT = 0.5,  DKDTCR = -1.0E-05,  DM = 80000.0,
 DMIN = 0.2,  DPHP = 190.0,  DPLP = 75.0,  DTRVHL = 423.0,  DZS = 21.2,  DZV = 35.0,  ERHRR = 0.375,  EWSDC = 234.0,
 FCSTSP = 0.7,  FFLASH = 5.0E-04,  FFREC = 2.0E-02,  FINTIM = 2103.0,  FLDWG = 3.12E-08,  FLSPG = 1.0E-08,  FTSTAB = 2000.0,
 HBOAF = 18.025,  HCIO = 539.0,  HCST = 58.0,  HPCIMX = 694.167,  HPCIPC = 0.0,  HREF = 522.0,  HSCSF = 16.2,  HSRHRF = 15.6,
 HUDWCI = 20.0,  HUMDWO = 50.0,  HUMSPO = 99.0,  H0 = 3816.0,  H1 = 1.552,  H2 = -2.517E-02,  JETPMP = 0.0,  KCRDCH = 4.47E-02,
 KCRDTV = 5.07E-02,  KPTB = 1.0E-02,  KSU = 5.157E-04,  LBASE = 0.0,  LBOT = 26.392,  LCORE = 12.5,  LCSTSS = 0.0,
 LCSTUV = 8.266E-05,  LDCR = 27.58,  LDCSET = 560.0,  LDCO = 28.32,  LHEDER = 23.4,  LHPIN = 476.0,  LHPMIN = 490.0,
 LHPMT = 540.0,  LHPT = 582.0,  LLPI = 413.5,  LLPIT = 575.0,  LOP = 5.167,  LRCIN = 476.5,  LRCMIN = 550.0,  LRCMT = 582.0,
 LRCT = 582.0,  LRT = 11.033,  LRVADS = 397.0,  LSPSS = 12.0,  LTCRD = 581.0,  LTRDWC = 99.0,  LTRJP = 490.0,  MINT = 477000.0,
 MRVST = 1500000.0,  NCS = 4.0,  NLPCI = 4.0,  NSORV = 0.0,  NTRHR = 4.0,  NTRHRD = 4.0,  OBRVD = 120.0,  OCBPC = 60.0,
 ODCS = 1000000.0,  ODLPCI = 1000000.0,  OERVD = 720.0,  OHPMAN = 1000000.0,  OHPT = 0.0,  OHPTR = 1000000.0,  OOCBP = 1000000.0,
 OOPTB = 1000000.0,  OOTV = 1000000.0,  OPCHRC = 60.0,  OPCHSV = 30.0,  ORCMAN = 1000000.0,  ORCT = 0.0,  ORCTR = 1000000.0,
 ORDWC = 1000000.0,  OSBOR = 300.0,  OSCRI = 300.0,  OSCS = 1000000.0,  OSDLEV = 1000000.0,  OSDPC = 1000000.0,
 OSLPCI = 1000000.0,  OSSCRD = 1000000.0,  OSSDC = 1000000.0,  OSSUBP = 1000000.0,  OSVMAN = 120.0,  OTCBP = 0.0,
 OTCRDP = 1000000.0,  OTDWC = 1000000.0,  PC = 1015.7,  1017.7,  1025.7,  1027.7,  1029.7,  1031.7,  1035.7,  1036.7,  1037.7,
 1038.7,  1045.7,  1046.7,  1047.7,  PCDWV = 15.0,  PCOR = 6693.37,  PDCVP = 5.05,  PDHOSV = 1.0E-02,  PDLPI = 16.95,
 PDOCSV = 2.0E-02,  PDWADS = 16.42,  PEHPIS = 165.0,  PERCT = 40.0,  PFMOSV = 110.0,  PFODP = 765.0,  PHCOVR = 1.0,
 PHPIN = 16.42,  PHPIS = 115.0,  PIDWV = 1000000.0,  PLDWCA = 1.389E-03,  PMXDPC = 1.35,  PMNDPC = 1.1,  PO = 1090.7,  1092.7,
 1100.7,  1102.7,  1104.7,  1106.7,  1110.7,  1111.7,  1112.7,  1113.7,  1120.7,  1121.7,  1122.7,  PRATED = 1196.0,
 PRCIS = 65.0,  PRELR = 0.32,  PRR = 1020.0,  PTDWGO = 14.95,  PTRDWC = 16.95,  PTSPGO = 14.95,  PVLPI = 480.0,  PVLPIV = 480.0,
 PVTDWC = 465.0,  PO = 1034.7,  QDWCR = 1389.0,  QOPHLO = 298.3,  QRVHLO = 1583.3,  RCICMX = 83.3,  SBOFLG = 2.0,  SDVFLG = 0.0,
 TADWCI = 145.0,  TAULEN = 2.5,  TAUOHL = 600.0,  TBASE = 85.0,  TBGRHR = 1800.0,  TDGRHR = 1000000.0,  TRERHR = 2000000.0,
 TBLEIN = 0.0,  &END
&NAM11  TCFAIL = 2.5,  TDIESL = 1000000.0,  TDHETO = 126.0,  TFDWC = 200.0,  TFDWCA = 1000000.0,  TGDWO = 126.0,  TGSPO = 85.0,
 THPIS = 194.0,  TPAIR = 90.0,  TPMETO = 85.0,  TRCF = 200.0,  TRCIS = 194.0,  TSLC = 1000000.0,  TSLEIN = 1000000.0,
 TSORV = 1000000.0,  TSQUEN = 10.0,  TSTRAT = 0.0,  TSW = 90.0,  TSWD = 90.0,  TWDWCI = 100.0,  TO = 36.0,  UAIRV = 33.0,
 VANN = 1177.51,  VCSTO = 362000.0,  VCSTMX = 375000.0,  VCSTSP = 135000.0,  VHOTMU = 97000.0,  VHOTWO = 113000.0,
 VDIFF = 189.076,  VFREE = 14580.074,  VGDW = 239600.0,  VJET = 95.195,  VOJP = 1535.473,  VOLP = 2428.636,  VREC = 1150.0,
 VSL = 2100.907,  VSSOP = 3864.149,  VTSP = 276831.4,  VUV1 = 1061.371,  VUV2 = 2042.338,  WBSLC = 0.1826,  WDLEAK = 0.24,
 WGUESS = 5139.0,  WRATED = 239.6,  WREF = 9111.0,  WRHRR = 1389.0,  WRHRSD = 625.0,  WRHRSW = 625.0,  WSWR = 625.0,
 WTEHPO = 47.85,  WTERCO = 9.167,  WWDWC = 143.4,  XL1 = 0.0,  XL2 = 8.483,  XL3 = 18.858,  XL4 = 32.6,  XL5 = 35.85,
 XL6 = 37.85,  XL7 = 44.058,  XREF = 0.133,  &END
&NAM2  ABIO = 4207.6,  ADFLR = 4715.8,  ADMM = 60080.0,  APED = 1998.6,  AWMM = 28969.6,  CBIOL = 20119.0,  CDMM = 288277.0,
 CWMM = 109739.1,  DXBIO = 1.75,  DXGDW = 1.0E-04,  DXGWW = 1.0E-04,  DXS = 1.0E-02,  KCON = 1.917E-04,  MK = 2.0,
 RHOCON = 140.8,  &END
```

Appendix C: BWRSAR INPUT DECK FOR BWR-4

This appendix provides representative code input for the Mark II calculations performed with the Boiling Water Reactor Severe Accident Response (BWRSAR) code. This input was used to calculate the events of the short-term station blackout accident sequence (with ADS actuation) from accident time 35 to 905 min. The MELCOR containment response calculation was driven by the results of this BWRSAR calculation.

```
susquehanna stsb with ads actuation, parker eutectics, 01/06/90
steel      concrete
dwliner    dwfloor    dwpdstl    sldwall    dwsteel    wwliner    wwpedst    wwspclm
wwvnpip    wwroof     qdot-ps
 &change
       check=0,    cpstp=300.0,    trst=905.01,
 &end
 &nlmar
  atime= 35.00,    fptmon=2000.0,    tap=5.256e5,
       ibrk= 0,         icbrk= 0,     iecoxx=  0,
      ifpsm= 2,         ipdtl= 0,       ispra= 0,
 &end
 &nlslab
  den(1)=489.0,140.8,3*0.0,
  dtdx(1)=0.0,0.0,0.0,0.0,0.0,0.0,0.0,0.0,0.0,0.0,5*0.0,
  fc1xxx=0.458,  fc2xxx=0.105,  fc4xxx=0.049,
  fract1=0.0, fract2=0.96,
  hc(1)=0.1124,0.3107,3*0.0,
  hif(1)=1000.,1000.,0.,1000.,0.,1000.,1000.,0.,0.,1000.,5*0.0,
  iblat1=2, iblat2=3, igas=2,
  ivl(1)=1,1,1,1,1,2,2,2,2,2,1,4*0,
  ivr(1)=1,1,1,1,1,2,2,2,2,2,1,4*0,
  mat1(1)=1,1,2,1,1,1,1,1,1,1,1,4*0,
  mat2(1)=2,2,2,2,1,2,2,1,1,2,1,4*0,
  nmat=2,
   nno1(1)=2,2,9,3,3,2,2,4,3,2,5*0,
  nno2(1)=13,9,0,7,0,13,9,0,0,9,5*0,
  nod(1)=1,16,36,27,49,46,64,75,79,82,
  nodes=10,   nslab=11,
  sarea(1)=17571.6,5227.0,3997.1,8415.3,60080.,7331.,4111.7,3500.6,
  sarea(9)=14502.3,5290.4,0.01,4*0.0,
  tc(1)=8.0,1.05,3*0.0,
  tchi=1472., tclo=1022.,
 temp(1)=2*131.80,
 temp(3)=131.2,130.3,128.8,127.0,126.1,124.0,121.2,116.2,110.8,103.2,
 temp(13)=95.5,87.8,80.0,
 temp(16)=2*129.6,
 temp(18)=129.3,128.8,127.8,126.7,126.1,123.4,118.6,111.1,105.5,
 temp(27)=132.3,131.3,129.5,127.3,126.1,4*126.0,
 temp(36)=129.6,129.5,129.4,129.2,128.6,127.6,126.5,126.0,2*126.0,
 temp(46)=132.22,132.15,132.08,
 temp(49)=2*87.27,
 temp(51)=87.0,86.5,85.9,85.2,85.0,84.7,84.5,83.9,83.35,
 temp(60)=82.5,81.7,80.85,80.0,
 temp(64)=87.3,87.2,87.0,86.5,85.9,85.2,5*85.0,
 temp(75)=87.6,87.5,87.4,87.2,
 temp(79)=3*87.6,
 temp(82)=87.3,87.3,87.0,86.5,85.9,85.9,86.8,88.65,92.4,99.9,105.5,
 temp(93)=108*0.0,
  twhi=968.0, twlo=190.0,
 x(1)=0.000,0.0208,
 x(3)=.022,.032,.052,.092,.172,.332,.652,1.292,2.0,3.0,4.0,5.0,6.021,
 x(16)=0.000,0.0208,
 x(18)=.022,.032,.052,.092,.172,.332,.652,1.292,1.771,
 x(27)=0.000,0.010,0.030,0.070,0.15,0.31,0.63,1.27,2.250,
 x(36)=0.00,0.040,0.086,0.087,0.100,0.120,0.160,0.260,0.500,0.961,
 x(46)=0.00,0.040,0.0863,
 x(49)=0.000,0.0208,
 x(51)=.022,.032,.052,.092,.172,.332,.652,1.292,2.0,3.0,4.0,5.0,6.021,
 x(64)=0.00,0.021,0.022,0.032,0.052,0.092,0.172,0.332,0.652,1.292,2.542,
 x(75)=0.00,0.035,0.070,0.10417,
 x(79)=0.00,0.040,0.089,
 x(82)=0.000,0.00625,
 x(84)=.010,.020,.040,.080,.160,.320,.640,1.280,1.760,108*0.0,
  uarv=13604.0,
```

```
&end
&nlecc
 csprc=0.0,
 dtsubx=-100.0,
 eccrc=.01,
 rwstm=1870438.,
 trwstx=85.0,
 wtcavx=1.0,
 npump=7,
 ivolec(1)=    2,       3,       3,       1,       1,       1,       2,
  npsuc(1)=    2,       2,       3,       3,       3,       3,       3,
  nptyp(1)=    3,       3,       3,       3,       1,       1,       3,
      p(1)=  289.0,  289.0,  1250.0, 403.0,  1250.0,  1250.0, 131.5,
    plo(1)=   0.1,    0.1,    0.0,    0.1,    115.0,    65.0,   0.0,
    stp(1)=  1.0e8,  1.1e8,  1.2e8,  1.3e8,   1.4e8,  1.5e8, 1.6e6,
     tm(1)=  1.0e8,  1.1e8,  1.2e8,  1.3e8,   1.4e8,  1.5e8, 1.6e6,
    wec(1)=    0.0,    0.0,    0.0,    0.0,  5000.0,   600.0,   0.0,
 pgpm(1,1)= 41148., 40000., 38200., 36000., 32000., 28000., 24000.,
 phead(1,1)=    0.,    20.,   46.9,   81.1,  133.7,  182.1,  222.1,
 pgpm(8,1)= 18000., 10000.,     0.,
 phead(8,1)= 263.5,  309.8,  331.5,
 pgpm(1,2)= 15240., 14000., 12500., 12000., 10000.,  8000.,  6000.,
 phead(1,2)=    0.,   57.8,   120.,  137.3,  200.9,  254.1,  292.6,
 pgpm(8,2)=  4000.,  2000.,    0.0,
 phead(8,2)= 319.5,  336.3,  343.6,
 pgpm(1,3)=  180.0,  168.4,  156.2,  143.0,  128.5,  112.0,   92.6,
 phead(1,3)=   0.0,  215.0,  415.0,  615.0,  815.0, 1015.0, 1215.0,
 pgpm(8,3)=   67.6,   21.7,    0.0,
 phead(8,3)= 1415.,  1615.,  1635.,
 pgpm(1,4)= 30347., 29399., 28023., 26730., 21385., 16033., 10689.,
 phead(1,4)=   0.0,    27.,    60.,    91.,   202.,   288.,   351.,
 pgpm(8,4)=  5345.,  2672.,    0.0,
 phead(8,4)=  389.,   396.,   403.,
 pgpm(1,7)=  580.0,  450.0,  350.0,  300.0,  250.0,  200.0,  150.0,
 phead(1,7)=   0.0,   30.5,   50.0,   58.5,   65.1,   71.0,   76.0,
 pgpm(8,7)=  100.0,   50.0,    0.0,
 phead(8,7)=  79.0,   80.5,   81.0,
 wshpci= 3368.0,   wsrcic=  444.0,   zjl=470.0,   zjh=583.0,
&end
lpci    cs      crd     cbp     hpci    rcic    fire
 &nlecx
      eqr=0.0,     etplr=0.0,     etslr=0.0,     ewpr=0.0,     ewsr=0.0,
 &end
 &nlcsx
      sqr=0.0,     stplr=0.0,     stslr=0.0,     swpr=0.0,     swsr=0.0,
 &end
 &nlcool
  cqr=7.28e6,    ctpr=135.0,    ctsr=50.0,    cvap=0.693,
 cwpr=112000.0,   cwsr=6190.3,       jcool=0,   tcool=1.0e8,
 &end
 &nlleak
  nlc=1,   ilkp=1,   ilkt=0,   kleak=1,
  dpleak(1)=126.,128.0,130.0,133.0,136.0,140.0,145.0,152.5,160.0,200.0,
   aleak(1)=000.,0.007,0.015,0.026,0.037,0.054,0.070,0.097,0.124,0.271,
  a1=0.0,   a2=0.0,   t1=0.0,   t2=0.0,   test=0.0,
  clk=0.583,   nhyst=1,   indx=10,   fctr(1)=10*0.0,
 &end
 &nlmace
  area(1)=5227.2,5572.65,
  c1(1)=500.0,174.0,8*0.0,
  c2(1)=0.593,0.593,8*0.0,
  c3(1)=0.196,1.10,8*0.0,
  c4(1)=0.0,0.0,8*0.0,
  dcf=1000.0,  dto=0.05,  dtpnt=19.99,  tpntm=155.01,  dtpnt2=29.99,
   hmaxx=280.0,
   hum(1)=0.1234,0.9262,
```

```
  kt(1,1)=0,kt(2,1)=2,
  kt(1,2)=2,kt(2,2)=0,
  n=2,    nc(1)=2,2,8*0,
  ns(1)=2,2,8*0,    nt(1)=7,7,8*0,
  po(1)=17.09,15.81,
  press(1,1)=0.0,press(2,1)=0.5,
  press(1,2)=5.293,press(2,2)=0.0,
  sumpa=256.0,  tdwsmp=110.0,  tempo(1)=199.13,94.70,
  tpool=124.17, vc(1)=239600.0,143709.07,0.0,
  vcav=24.06, vflr=7345.0, wdwsmp=327.43, wflash=2000.0, wpool=8192443.8,
   wcdo(1)=0.0,0.0,
   wcmo(1)=0.0,0.0,
   whyd(1)=0.0,0.0,
   wntr(1)=-.965,-.965,
   woxy(1)=-.035,-.035,
 &end
 &nlboil
  abr(1)=-1.0,-1.0,-1.0,-1.0,-1.0,-1.0,-1.0,-1.0,-1.0,-1.0,
         -1.0,-1.0,-1.0,-1.0,-1.0,0.1091,
  abrk=2.29e-5,
  ah(1)=651.0,8230.2,673.5,4*0.0,
  ahu(1)=1620.0,426.0,1270.0,1270.0,1270.0,1270.0,19010.8,13*0.0,
  arstr(1)=0.0,-7.87,-12.22,4*0.0,
  arstru(1)=148.04,148.04,42.33,42.33,42.33,42.33,128.4,13*0.0,
  clad=0.0025,  cladwr=0.00254,
  cm(1)=2337.0,15310.2,21653.6,4*0.0,
  cmu(1)=29280.0,37973.0,26486.0,26486.0,26486.0,26486.0,78000.0,13*0.0,
  conb=4.7,        d=0.0353,       dcrdod=0.8958,
  dd(1)=0.125,0.0208,0.635,4*0.0,
  ddu(1)=0.160,1.00,0.5054,0.5054,0.5054,0.5054,0.071,13*0.0,
  df=0.0297,       dh=0.0423,    dpart=.01177,     drgap=3.125e-4,
    tpn(1)=20.0,40.1,280.1,1.0e6,2.0e6,3.0e6,4.0e6,5.0e6,
   dtpn(1)=5.00,10.0,20.00,100.0,101.0,102.0,103.0,104.0,
  drxid=20.91667,     dshdid=16.96,    fcfail=0.75,
  duo2=0.0297,  dwrod=0.0354,     fcol=0.250,    fdfuel=0.92,
  fld=0.0, fpv(1)=0.00,0.50,0.10,0.05,0.03,0.02,0.30,13*0.0,
  fwsscr=0.18,    fwssfe=0.74,    fwssni=0.08,    fwuzr(1)=0.20,19*0.0,
  fz(1)=0.66006,0.9004,0.96607,1.02072,1.07198,1.12138,1.1816,1.22818,
  fz(9)=1.22008,1.15622,0.97839,0.49386,13*0.0,
  f12=0.01,    hz=12.500,    hnf=0.814,
  hfss=114.7,    hfuo2=118.0,    hfzirc=108.0,    htmtoc=600.0,
         iaxxx=1,      ibedc=2,       ibeds=3,
         ifp=2,        imwa=2,
         ipower=1,     ir1=1,ir2=2,ir3=3,
         istr=3,       istru=7,       mwornl=1,
         ndzf=12,      nnt=61884,       nr=60356,     ndzn=1,
  pf(1)=1.14375,1.14375,1.072,1.072,0.853,0.853,0.382,0.382,
  pitch=0.0477,  porb=0.4,  pvsl=980.4,  q235u=193.0, qzerox=1.1236e10,
  rhocld=408.9,    rhoful=646.7,  r1=1, r2=8,  r239u=0.8,    sfactr=2.0,
    tb(1)=1.0e8,15*1.0e8,
     tcormb=1.e4, tfailx=2100.0, tfail2=2100.0, tfus=4600.0,
  tfpcld=1800.0,    thkrx=0.5417,    thkshd=0.166667,
  thku(1)=0.042,0.166667,0.025,0.025,0.025,0.025,0.01,13*0.0,
    tmeltt=4900.0,  tmybk=1.0e6,  tpm=1.0,
   tsb(1)=.050,.025,0.100,.020,0.050,0.020,0.100,0.200,
  tsct(1)=10.0,77.50,100.0,124.,180.0,220.0,265.0,280.0,
  ttu(1)=542.2,542.2,542.2,542.2,542.2,542.2,542.2,13*0.0,
  vf(1)=.311515,.311515,.062825,.062825,.06021,.06021,.065445,.065445,
  xoo=6.233e-6,
 ybr(1)=-1.0,-1.0,-1.0,-1.0,-1.0,-1.0,-1.0,-1.0,
        -1.0,-1.0,-1.0,-1.0,-1.0,-1.0,-1.0,20.00,
   ybrk=-100.0,  ybrk2=1000.0,
 &end
t.guide shr.heads/spip 1s/spip 2s/spip 3s/spip 4dryers
 &nbwrin
 farin=86.48, farout=61.56, pbox=1.7543,xbox=0.006667,xboxzi=8.333e-6,
```

```
xboxzo=8.333e-6, f12bx=0.010,   f22bx=0.010,   f22rd=0.010,  frdbx=0.25,
 fbxcb=0.25, dhbxcb=0.016583, tmelbx=3365.0,
   nboxs=764,       imwbox=1,   thkcb=0.0217,
 iocb(1,1)=1,1,1,1,1,1,1,1,1,1,1,1,1,
 iocb(1,2)=0,0,0,0,0,0,0,0,0,0,0,0,0,
 iocb(1,3)=1,1,1,1,1,1,1,1,1,1,1,1,1,
 iocb(1,4)=0,0,0,0,0,0,0,0,0,0,0,0,0,
 iocb(1,5)=1,1,1,1,1,1,1,1,1,1,1,1,1,
 iocb(1,6)=0,0,0,0,0,0,0,0,0,0,0,0,0,
 iocb(1,7)=1,1,1,1,1,1,1,1,1,1,1,1,1,
 iocb(1,8)=0,0,0,0,0,0,0,0,0,0,0,0,0,
 xlcb=.40625, thksso=0.00467, xcbdo=3.33e-6,  ncblad=185,   f12cb=0.010,
 f22cb=0.010,  tmelcb=2450.0,  imwss=1,
 xlcpst=0.065083,  thkssi=0.002083,  diab4c=0.0115,  thkgap=0.0005,
 rhob4c=110.0,  rhoss=496.0,  nabrod=76,  imwb4c=2,    fb4cmx=0.03,
&end
&nbwrlv
   hbaf=216.3125,  hbsb=121.5,  hdead=205.3125
 hinitl=367.68, hllsl=646.5,
  hsjjp=205.3125,  htaf=366.3125,  htjp=317.1875,
   htop=876.0,   hts=607.5,    na=50,
hh(1)=0.0,6.0,11.0,16.0,21.0,26.0,32.0,37.0,42.0,48.0,
hh(11)=51.0,58.0,64.0,69.0,74.0,79.0,85.0,90.0,95.0,101.0,
hh(21)=106.,111.,116.,121.5,127.5,191.125,216.312,317.187,360.125,379.125,
hh(31)=411.625,414.,417.,420.,423.,426.,429.,431.,434.,437.,
hh(41)=440.,442.625,514.,533.5,564.,577.87,607.5,635.,749.,876.,
vcore(1)=0.0,7.95,26.36,55.02,93.48,
vcore(6)=141.3,210.42,277.29,352.1,451.74,
vcore(11)=505.38,633.48,753.11,859.14,970.43,
vcore(16)=1086.55,1231.61,1352.72,1485.2,1643.17,
vcore(21)=1777.45,1913.64,2051.28,2203.82,2296.69,
vcore(26)=3334.98,3712.77,4924.898,5440.199,5671.609,
vcore(31)=6347.52,6393.289,6446.238,6493.691,6535.551
vcore(36)=6571.719,6602.129,6619.160,6639.762,6654.328,
vcore(41)=6662.871,6665.262,6933.539,7117.27,7470.629
vcore(46)=7613.559,7789.031,0.0,0.0,0.0,
vshrd(1)=20*0.0,
vshrd(21)=0.0,0.0,0.0,0.0,58.72,
vshrd(26)=743.37,982.48,1946.08,2367.92,2507.09,
vshrd(31)=2745.15,2762.74,2790.40,2824.23,2864.32,
vshrd(36)=2910.77,2963.68,3002.59,3066.48,3173.92,
vshrd(41)=3214.52,3287.95,4784.512,5193.379,5832.891,
vshrd(46)=6113.609,6713.301,0.0,0.0,0.0,
vtot(1)=0.0,7.95,26.36,55.02,93.48,
vtot(6)=141.3,210.42,277.29,352.1,451.74,
vtot(11)=505.38,633.48,753.11,859.14,970.43,
vtot(16)=1086.55,1231.61,1352.72,1485.2,1643.17,
vtot(21)=1777.45,1913.64,2051.28,2203.82,2355.41,
vtot(26)=4078.35,4695.25,6870.98,7808.121,8178.699,
vtot(31)=9092.672,9156.031,9236.641,9317.922,9399.871,
vtot(36)=9482.488,9565.809,9621.750,9706.238,9828.250,
vtot(41)=9877.391,9953.211,11718.051,12310.648,13303.520,
vtot(46)=13727.172,14502.328,15308.719,18651.578,21134.289,
&end
&nbwrrv
   dpvdyc=20.0,   dpvdyo=50.0,
   iads(1)=0,0,0,0,0,0,0,0,0,0,1,1,1,1,1,0,4*0,
     nvalve=17,       ntpsrv=1,      pdwca=100.0,
 psrvo(1)=1090.7,1092.7,1100.7,1102.7,1104.7,1106.7,1110.7,1112.7,
 psrvo(9)=1114.7,1116.7,1120.7,1122.7,1124.7,1130.7,1132.7,1134.7,
 psrvo(17)=25.0,
 psrvc(1)=1015.7,1017.7,1025.7,1027.7,1029.7,1031.7,1035.5,1037.7,
 psrvc(9)=1039.7,1041.7,1045.7,1047.7,1049.7,1055.7,1057.7,1059.7,
 psrvc(17)=20.0,
 ratflo(1)=2*862400.0,
 ratflo(3)=4*883950.0,
```

```
 ratflo(7)=4*891380.0,
 ratflo(11)=3*898800.0,
 ratflo(14)=3*906250.0,
 ratflo(17)=8000.0,
 ratprs(1)=2*1196.0,
 ratprs(3)=4*1225.3,
 ratprs(7)=4*1235.7,
 ratprs(11)=1246.0,1246.0,1246.0,
 ratprs(14)=1256.3,1256.3,1256.3,
 ratprs(17)=1050.0,
 ratrho(1)=2*2.75,
 ratrho(3)=4*2.83,
 ratrho(7)=4*2.86,
 ratrho(11)=2.88,2.88,2.88,2.90,2.90,2.90,
 ratrho(17)=2.35,
  tmsvlk=60.0,
 manval=1,  pmnset=1005.0,  pmnban=70.0,  topchk=0.10,  tmanon=35.0,
 tmanof=77.99,  tadson=79.49,  nsorv=1,  tsorvo=77.99,
&end
&nbwrqb
  h23=207.4,   h35=380.6,   djp=11.86,   ajp=20,
 tmasso(1)=500.39,
 tmasso(2)=505.00,
 tmasso(3)=542.21,
 tmasso(4)=542.21,
 tmasso(5)=542.21,
 tmasso(6)=542.21,
&end
&nlhead
 dbh=0.10,  fhead=0.068,  fopen=0.932,  dthead=10.0,  h1max=2.50,
 condox=2.02,  condss=11.3,  hdld2=3.64,  hrvdw=0.625,  hskirt=6.02,
 nmeltx=0,  sfcrdb=2.0,   thkcrs=0.500,
 thkhd1=0.708,   thkhd2=0.505,   nps=26,
 hpipes=180.0,  thk6=2250.0,  thk60=2050.0,  tablat=2660.0,
 amtmel(1)=2920.,2920.,2920.,2920.,
 amtmel(10)=4172.,4172.,4172.,4172.,4172.,4172.,4172.,4172.,4800.,
 ieutec=4
 frckey(1)=0.631,0.1902,0.300,0.750,6*0.0,
 ieukey(1)=2,3,1,11,6*0,
 tmlieu(1)=2642.,2660.,2912.,4172.,6*0.,
 ieu(1,1)=1,1,1,0,0,0,0,0,0,0,0,0,0,0,0,0,0,0,0,0,
 ieu(1,2)=0,1,1,1,0,0,0,0,0,0,0,0,0,0,0,0,0,0,0,0,
 ieu(1,3)=1,1,0,1,0,0,0,0,0,0,0,0,0,0,0,0,0,1,0,0,
 ieu(1,4)=0,0,0,0,0,0,0,0,0,0,1,0,0,0,0,0,0,1,0,0,
 ieutyp(1)=2,2,2,2,6*0,
 xrnkey(1,1)=0.193,0.631,0.176,
 xrnkey(1,2)=0.0,0.7306,0.1902,0.0792,
 xrnkey(1,3)=0.300,0.008,0.0,0.592,
 xrnkey(18,3)=0.100,
 xrnkey(11,4)=0.750,
 xrnkey(18,4)=0.250,
&end
```

Appendix D: MELCOR INPUT DECK FOR BWR MARK II CONTAINMENT

This appendix provides representative code input as processed by the MELGEN package of MELCOR for the Mark II Containment response calculations. This MELCOR input was used for the short-term station blackout accident sequence with ADS actuation. It provides a single drywell cavity for the representation of debris-concrete interactions. This is the basic code input deck to which variations were made as required to perform the MELCOR calculations discussed in Chapters 8 through 10.

```
*********************************************************************
*********************************************************************
*
* CPI Plant primary containment model
*
* Case 1 - STSB w/ADS, no vent, no sprays, no sovb, no head flooding &
*          NO PRIMARY CONTAINMENT FAILURE ALLOWED
*
* Updated to incorporate PPL's comments of 7/6/89,7/13/89,7/18/89
*   and 9/14/89--should be final CPI deck
*
*  added degassing 10/25/89
*  properly initialized all structure temperatures (20-jan-90).
*
*********************************************************************
*********************************************************************
title     s1
jobid     s1
*
tstart   2100.  *  35 min, end of bwrltas
*
restartf s1rst
outputf  s1gout
diagf    s1gdia
plotf    s1ptf
crtout
dttime    0.1
*
*sc0000 10 1.     1  * cpu weighting factor
*sc0001 10 0.22   2  * i/o weighting factor
*sc0002 10 0.223  3  * memory weighting factor
*
*
*************************************************************************
*************************************************************************
***                                                                   ***
***                                                                   ***
***                CPI Primary Containment Model                      ***
***                                                                   ***
***                                                                   ***
***         Total Drywell Volume =  228627 ft**3 =  6474 m**3         ***
***         Total Downcomer Volume = 11675 ft**3 =   331 m**3         ***
***         Total Wetwell Volume =  280141 ft**3 =  7933 m**3         ***
***            Total P. C. Volume = 520443 ft**3 = 14738 m**3         ***
***                                                                   ***
***                                                                   ***
***                                                                   ***
*************************************************************************
*************************************************************************
*  cont.    cont. volume    connects
* vol. #       name        via FL#  to cont. volume   (#)
* ------  ----------------  ----  ----------------  ----
*
*   200   drywell inpedestal   201   drywell 705-723      (201)
```

```
*                                   202   drywell 705-723       (201)
*                                   203   drywell 723-758       (202)

*   201   drywell 705-723           210   drywell 723-758       (202)
*                                   250   downcomers            (300)
*                                   290   RB via 2" vent        (900)
*                                   291   RB via 18" vent       (900)

*   202   drywell 723-758           220    drywell 758-779      (204)

*   203   rx/shield annulus         204    drywell 723-758      (202)
*                                   205    drywell 758-779      (204)
*                                   240    drywell 779-809      (205)
*
*   204   drywell 758-779           230    drywell 779-809      (205)
*
*   205   drywell 779-809           260    head leakage         (600)
*
*   300   downcomers                300    wetwell pool         (401)
*
*   400   wetwell inpedestal        401    wetwell pool         (401)
*                                   402    wetwell pool         (401)
*                                   403    wetwell airspace     (401)
*
*   401   wetwell                   430    VB(1)-to-downcomer   (300)
*                                   440    VB(4)-to-downcomer   (300)
*                                   490    ENV via 2" vent      (900)
*                                   491    ENV via 18" vent     (900)
*                                   495    LEAK to ENV          (900)
*
*   600   reactor pit               600    Pit-to-env           (900)
*
*   900   environment
*
*******************************************************************************
*******************************************************************************
*
*********************************************************************
*********************************************************************
*     ncg input
*********************************************************************
*********************************************************************
*
ncg004    h2  4  * hydrogen
ncg005    n2  5  * nitrogen
ncg006    co  6  * carbon monoxide
ncg007    co2 7  * carbon dioxide
ncg008    ch4 8  * methane
ncg009    o2  9  * oxygen
*
*
*@@@@@@@@@@@@@@@@@@@@@@@@@@@@@@@@@@@@@@@@@@@@@@@@@@@@@@@@@@@@@@@@@@@@@@@@@@@@
*@@@@@@@@@@@@@@@@@@@@@@@@@@@@@@@@@@@@@@@@@@@@@@@@@@@@@@@@@@@@@@@@@@@@@@@@@@@@
*@@
```

```
*@@    DEFINE EXTERNAL DATA FILES
*@@
*@@@@@@@@@@@@@@@@@@@@@@@@@@@@@@@@@@@@@@@@@@@@@@@@@@@@@@@@@@@@@@@@@@@@@@@@@@@@@@@@@@@
*@@@@@@@@@@@@@@@@@@@@@@@@@@@@@@@@@@@@@@@@@@@@@@@@@@@@@@@@@@@@@@@@@@@@@@@@@@@@@@@@@@@
*
* ----- BWRSAR SRV FLOWS -----  time  cum-water  cum-steam  cum-h2  temperature
*          edfname      channels     direct
edf10000     'sar-srv-flows'     4          read
*          filename
edf10001   sarsrv
*            format
edf10002    10f8.1
*
* ----- BWRSAR VESSEL LEAKAGE FLOWS -  time cum-water cum-steam cum-h2 temp
*
*          edfname      channels     direct
edf20000     'sar-brk-flows'     4          read
*          filename
edf20001   sarbrk
*            format
edf20002    10f8.1
*
* ----- BWRSAR DEBRIS POURS -----  time & 16 variables
*               edfname      channels     direct
edf90000     'debris pour'     16          read
*          filename
edf90001   sarpour
*            format
edf90002    5e15.8
edf90003      0.0    * pour offset
*
* ----- BWRSAR CAVITY DECAY HEAT ----- time, decay-heat(watts)
*                 edfname      channels     direct
edf70000     'cav decay heat'     1          read
*          filename
edf70001   sardecay
*            format
edf70002    4e15.8
edf70003      0.0   * decay heat offset
*@@@@@@@@@@@@@@@@@@@@@@@@@@@@@@@@@@@@@@@@@@@@@@@@@@@@@@@@@@@@@@@@@@@@@@@@@@@@@@@@@@@
*@@@@@@@@@@@@@@@@@@@@@@@@@@@@@@@@@@@@@@@@@@@@@@@@@@@@@@@@@@@@@@@@@@@@@@@@@@@@@@@@@@@

*
*---------------------- SRV source tables for testing model --------------
*
*      Steam and hydrogen sources taken from Steve's Susquehanna
*      BWRSAR calculation.
*
*      Source steam as vapor into a dummy control volume, and
*      then into the PSP pool via a flow path terminating below the
*      pool surface.
*
*      Source hydrogen into a dummy control volume, and thence into
*      the PSP pool via a flow path terminating below the pool
```

```
*     surface.
*
*
*
*   h2o liquid source table: time (s) vs  integrated flow (kg)
*
cv100c0   mass.1   800   1 * source into pool
cv100c1       te   895   9
cf80000   h2o-pool-src   equals   1   1.  0.
cf80010   1.   0.   edf.100.1
*
*
*   h2o vapor source table: time (s) vs  integrated flow (kg)
*
cv100c2   mass.3   810   1 * source into atmosphere
cv100c3       te   890   9
cf81000   h2o-vapor-src   equals   1   1.  0.
cf81010   1.   0.   edf.100.2
*
**
**   hydrogen source table: time (s) vs  integrated flow (kg)
**
cv100c6   mass.4   830   1
cv100c7       te   890   9
cf83000   h2-mass-src   equals   1   1.   0.
cf83010   1.   0.   edf.100.3
**
*****************************************************************
*****************************************************************
**
**   temperature table: time (s) vs  temp (k)
**
cf89000   temp-src   equals   1   1.   0.
cf89001  564.3  *  initialize at tsat (1100 psia) = 556.28 f = 564.3 k
cf89010   1.   0.   edf.100.4
*******************************************************************
*****************************************************************
**
**   temperature table: time (s) vs  temp (k)
**
**   This table is limited to sub-criticl temperature bounds for use
**   with mass.1 (liquid water) mass sources
**
cf89500   temp-src   equals   1   1.   0.
cf89501   564.3  *  initialize at tsat(1100 psia) = 556.28 f = 564.3 k
cf89502  3  273.15  647.2
cf89510   1.   0.   edf.100.4
*******************************************************************
*****************************************************************

*
*-------------- Vessel Break source tables for testing model ---------------
*
*
```

```
*   h2o liquid source table: time (s) vs  integrated flow (kg)
*
cv200c0   mass.1   200   1 * source into pool
cv200c1       te   295   9
cf20000   h2o-pool-src   equals   1   1.  0.
cf20010   1.   0.   edf.200.1
*
*
*   h2o vapor source table: time (s) vs  integrated flow (kg)
*
cv200c2   mass.3   210   1 * source into atmosphere
cv200c3       te   290   9
cf21000   h2o-vapor-src   equals   1   1.  0.
cf21010   1.   0.   edf.200.2
*
**
**   hydrogen source table: time (s) vs  integrated flow (kg)
**
cv200c6   mass.4   230   1
cv200c7       te   290   9
cf23000   h2-mass-src   equals   1   1.   0.
cf23010   1.   0.   edf.200.3
**
*****************************************************************
*****************************************************************
**
**   temperature table: time (s) vs  temp (k)
**
cf29000   temp-src   equals   1   1.   0.
cf29010   1.   0.   edf.200.4
******************************************************************
*****************************************************************
**
**   temperature table: time (s) vs  temp (k)
**
**   This table is limited to sub-criticl temperature bounds for use
**   with mass.1 (liquid water) mass sources
**
cf29500   temp-src   equals   1   1.   0.
cf29502  3  273.15  647.2 * limits on liq water temp
cf29510   1.   0.   edf.200.4
******************************************************************
*****************************************************************
*@@@@@@@@@@@@@@@@@@@@@@@@@@@@@@@@@@@@@@@@@@@@@@@@@@@@@@@@@@@@@@@@@@@
*@@@@@@@@@@@@@@@@@@@@@@@@@@@@@@@@@@@@@@@@@@@@@@@@@@@@@@@@@@@@@@@@@@@
*
*
******************************************************************
*************************  source volume      ************************
******************************************************************
***                                                            ***
***  This volume is required to provide a pathway for the BWRSAR   ***
***  h2 and h2o gas flows to enter the pressure suppression pool   ***
***  below the surface of the pool--like actual srv discharge      ***
```

```
***                                                                    ***
**********************************************************************
*
*
cv10000     source-volume    2   2   3
cv10001     0    0
cv100a0     3
cv100a1     pvol    117831.      rhum    .93   *  17.09 psia
cv100a2     tatm    365.85         tpol    324.11
cv100a3     zpol    204.52
cv100a4     mlfr.4  0.0          mlfr.5   0.96      mlfr.6   0.0
cv100a5     mlfr.7  0.0          mlfr.8   0.0       mlfr.9   0.04
cv100b1     190.        0.0
cv100b2     210.        500.  *  extend cv above the 16.4592 ele -- srg
*
* ------------------------ flow paths  ------------------------------
*
fl10000   steam-line-srv    100  401  198.6  198.6
fl10001   3.0000  41.3122  1.0 1.95 1.95
fl10002   3 0 0 1 * horizontal flow path, active, def, sparc
fl100s1   3.0000  41.3122   1.95    5.e-6
*
*
**********************************************************************
************************** drywell in-pedestal ************************
**********************************************************************
*
*
cv20000     'in-ped-drywell'    2   2   2
cv20001     0    0
cv200a0     3
cv200a1     pvol    117831.      rhum    .12   *  17.09 psia
cv200a2     tatm    365.85
*cv200a3     mass.1   1269.0   * seal leakage of 35#/min for 2175 sec
cv200a4     mlfr.4  0.0          mlfr.5   0.96      mlfr.6   0.0
cv200a5     mlfr.7  0.0          mlfr.8   0.0       mlfr.9   0.04
*   La Salle cavity is 9' 6.5" deep = 2.91 m
*   Start volume @ 703'11" - 9'6.5" = 694'4.5" = 211.65 m
cv200b1       214.55           0.0   * excludes La Salle cavity volume
cv200b5       224.97         225.6   * excludes La Salle cavity volume
*cv200b1       211.65           0.0   * includes La Salle cavity volume
*cv200b5       222.44         312.0   * includes La Salle cavity volume
*
*
* direct openings between reactor cavity and drywell
*
fl20100      'loped-drywell'   200   201   215.63   215.63
fl20101      2.79     1.35    1.0     2.40    2.40   * door & 2 circular ports
fl20102      3   0   0   0   * horizontal flow
fl20103      1.   1.   1.   1.
fl201s0      2.79   1.35    1.24     5.0e-5
*
fl20200      'midped-drywell'   200   201   218.24   218.24
fl20201      1.45     1.35    1.0     2.04    2.04      * crd removal hatch
```

```
fl20202      3   0   0   0   * horizontal flow
fl20203      1.   1.   1.   1.
fl202s0      1.45   1.35    1.05     5.0e-5
*
fl20300      'hiped-drywell'   200   202   221.13   221.13
fl20301      3.04    1.62    1.0     0.864   0.864       * crd line portals
fl20302      3   0   0   0    *  horizontal flow
fl20303      1.   1.   1.   1.
fl203s0      3.04   1.62    0.5     5.0e-5
*
*
*     NOTE: La Salle cavity walls below drywell floor elevation are
*           not modeled as heatslabs
*
*
*  hs20001xnn =  heat  slab for  drywell inpedestal floor
*                 elevation=700'6" to 704'= 213.51 m to 214.58 m
*                 thickness = .081" steel + 3'6"concrete +  1/4" steel
*                 id=20'3"
*                 tot thick=3.52758 ft = 1.07521 m
*
*  force use of input temperature profile, iss= -1
hs20001000  20  1  -1  0   * rectangular
hs20001001  'dw-inped-floor'
hs20001002  213.5  0.0  * elevation = 700'6"
hs20001003  1.0 * multiplicity
hs20001100  -1  1  0.0
hs20001102  0.00100  2  *  0.039"  steel
hs20001103  0.00206  3  *  0.081"  steel/concrete
hs20001104  0.00254  4  *   0.1"  concrete
hs20001105  0.00508  5  *  0.2"  concrete
hs20001106  0.01016  6  *  0.4"  concrete
hs20001107  0.02032  7  *  0.8"  concrete
hs20001108  0.04064  8  *  1.6"  concrete
hs20001109  0.08128  9  *  3.2"  concrete
hs20001110  0.16256  10  *  6.4"  concrete
hs20001111  0.32512  11  * 12.8"  concrete
hs20001112  0.536575  12  *21.125"  concrete
hs20001113  0.748030  13  *29.450"  concrete
hs20001114  0.910590  14  *35.850"  concrete
hs20001115  0.991870  15  *39.050"  concrete
hs20001116  1.032510  16  *40.650"  concrete
hs20001117  1.052830  17  *41.450"  concrete
hs20001118  1.068857  18  *42.00 "  concrete/steel
hs20001119  1.070610  19  *42.15"   steel
hs20001120  1.075207   20  *42.25"  steel
hs20001200  -1
hs20001201  'carbon steel'  2
hs20001202  'concrete'     17
hs20001203  'carbon steel' 19
hs20001300  0
hs20001400  1  400  'ext'  1.0  1.0
hs20001401  0.3   'equiv band'  5.   * steel surface
hs20001500  29.921  3.0861  .1
```

```
hs20001600  1  200  'ext'  1.0  1.0
hs20001601  0.3   'equiv band'  5.   * steel surface
hs20001700  29.921  3.0861  .1
hs20001800  -1
hs20001801  303.7   1
hs20001802  303.7   2
hs20001803  303.6   3
hs20001804  303.4   4
hs20001805  303.1   5
hs20001806  303.0   6
hs20001807  302.9   7
hs20001808  303.4   8
hs20001809  304.0   9
hs20001810  305.0  10
hs20001811  309.0  11
hs20001812  314.0  12
hs20001813  318.0  13
hs20001814  321.0  14
hs20001815  323.0  15
hs20001816  325.0  16
hs20001817  326.0  17
hs20001818  327.0  18
hs20001819  327.4  19
hs20001820  327.4  20
hsdg000010  -20001  17  'h2o-vap'
hsdg000020  -20001  17  'h2o-vap'
hsdg000030  -20001  17  'co2'
hsdg000011    59.68  2.258e6  360.8  378.0
hsdg000021    44.27  6.065e6  378.0  793.0
hsdg000031   473.06  4.157e6  823.0 1073.0
*
*
*
*  hs20002xnn  = drywell pedestal wall
*                elevation= 703'11" to 723'5 3/4"
*                id=20'3"
*                thickness = 4'5" = 1.3462 m
*
* force use of input temperature profile, iss=-1
hs20002000  19  2  -1  0    *  cylindrical
hs20002001  'dw-pedestal-wall'
hs20002002  214.5538  1.0  *elevation=703'11"
hs20002003  1.0 * multiplicity
hs20002100  -1  1  3.0861  *id=20'3"
hs20002102  3.08864  2  *0.1" concrete
hs20002103  3.09118  3  *0.2" concrete
hs20002104  3.09626  4  *0.4" concrete
hs20002105  3.10642  5  *0.8" concrete
hs20002106  3.12674  6  *1.6" concrete
hs20002107  3.16738  7  *3.2" concrete
hs20002108  3.24866  8  *6.4" concrete
hs20002109  3.41122  9  *12.8" concrete
hs20002110  3.75920  10  *26.5" concrete
hs20002111  4.10718  11  *40.2" concrete
```

```
hs20002112  4.26974  12  *46.6" concrete
hs20002113  4.35102  13  *49.8" concrete
hs20002114  4.39166  14  *51.4" concrete
hs20002115  4.41198  15  *52.2" concrete
hs20002116  4.42214  16  *52.6" concrete
hs20002117  4.42722  17  *52.8" concrete
hs20002118  4.42976  18  *52.9" concrete
hs20002119  4.43230  19  *53.0" concrete
hs20002200  -1
hs20002201  'concrete'  18
hs20002300  0
hs20002400  1  200  'int'  1.0  1.0
hs20002401  0.6   'equiv band'   5.   * concrete surface
hs20002500  1.0  6.1722  5.96265
hs20002600  1  201  'ext'  1.0  1.0
hs20002601  0.6   'equiv band'   5.   * concrete surface
hs20002700  1.0  7.52    5.96265
hs20002800  -1
hs20002801  328.6   1
hs20002802  328.3   2
hs20002803  328.0   3
hs20002804  327.0   4
hs20002805  326.5   5
hs20002806  325.5   6
hs20002807  325.2   7
hs20002808  325.2   8
hs20002809  325.2   9
hs20002810  325.2  10
hs20002811  325.2  11
hs20002812  325.2  12
hs20002813  325.2  13
hs20002814  325.2  14
hs20002815  325.3  15
hs20002816  325.7  16
hs20002817  326.8  17
hs20002818  328.0  18
hs20002819  328.6  19
hsdg000040  +20002  18  'h2o-vap'
hsdg000050  +20002  18  'h2o-vap'
hsdg000060  +20002  18  'co2'
hsdg000041   59.68  2.258e6  360.8  378.0
hsdg000051   44.27  6.065e6  378.0  793.0
hsdg000061  473.06  4.157e6  823.0 1073.0
*
*
*
*
*  hs20003xnn =  reactor pedestal wall   drywell portion
*                from elevation  723' 5 3/4"  to  729'9 5/8"
*                wall  thickness =   5'4"
*                id=   18'5"
*
*  force use of input temperature profile, iss= -1
hs20003000  20  2  -1  0    * cylindrical
```

```
hs20003001  'dw-pedestal-wall'
hs20003002  220.51645  1.0 *elevation =723'5 3/4"
hs20003003  1.0 * multiplicity
hs20003100  -1  1  2.8067  *radius=9' 2 1/2"
hs20003102  2.80924  2  *  0.1"  concrete
hs20003103  2.81178  3  *  0.2"  concrete
hs20003104  2.81686  4  *  0.4"  concrete
hs20003105  2.82702  5  *  0.8"  concrete
hs20003106  2.84734  6  *  1.6"  concrete
hs20003107  2.88798  7  *  3.2"  concrete
hs20003108  2.96926  8  *  6.4"  concrete
hs20003109  3.13182  9  * 12.8"  concrete
hs20003110  3.45694 10  * 25.6"  concrete
hs20003111  3.61950 11  * 32.0"  concrete
hs20003112  4.10718 12  * 51.2"  concrete
hs20003113  4.26974 13  * 57.6"  concrete
hs20003114  4.35102 14  * 60.8"  concrete
hs20003115  4.39166 15  * 62.4"  concrete
hs20003116  4.41198 16  * 63.2"  concrete
hs20003117  4.42214 17  * 63.6"  concrete
hs20003118  4.42722 18  * 63.8"  concrete
hs20003119  4.42976 19  * 63.9"  concrete
hs20003120  4.43230 20  * 64.0"  concrete
hs20003200  -1
hs20003201  'concrete' 19
hs20003300  0
hs20003400  1  200  'int'  1.0  1.0
hs20003401  0.6   'equiv band'   5.   * concrete surface
hs20003500  1.0  5.89  1.9
hs20003600  1  202  'ext'  1.0  1.0
hs20003601  0.6   'equiv band'   5.   * concrete surface
hs20003700  1.0  7.52  1.9
hs20003800  -1
hs20003801  328.6   1
hs20003802  328.0   2
hs20003803  327.5   3
hs20003804  327.0   4
hs20003805  326.5   5
hs20003806  326.0   6
hs20003807  325.2   7
hs20003808  325.2   8
hs20003809  325.2   9
hs20003810  325.2  10
hs20003811  325.2  11
hs20003812  325.2  12
hs20003813  325.2  13
hs20003814  325.2  14
hs20003815  325.2  15
hs20003816  325.2  16
hs20003817  325.5  17
hs20003818  326.0  18
hs20003819  327.0  19
hs20003820  328.6  20
hsdg000070  -20003  19  'h2o-vap'
```

```
hsdg000080  -20003  19  'h2o-vap'
hsdg000090  -20003  19  'co2'
hsdg000071   59.68  2.258e6  360.8  378.0
hsdg000081   44.27  6.065e6  378.0  793.0
hsdg000091  473.06  4.157e6  823.0 1073.0
*
*
*   RPV bottom head (hemisphere)
*   hs20004xxx
*   thick=7.25 inches = .18415 m
*  force use of input temperature profile, iss= -1
hs20004000  8  4  -1  0
hs20004001  'low-rpv-head'
hs20004002  221.0  *  lowermost elevation
hs20004003   1.0 *  multiplicity
hs20004100  -1  1  3.1877  * ir = 125.5 inches = 3.1877 m
*               x(i)  i
hs20004102    3.2387  2
hs20004103    3.2895  3
hs20004104    3.3149  4
hs20004105    3.3339  5
hs20004106    3.3529  6
hs20004107    3.3656  7
hs20004108    3.3719  8
hs20004200  -1
hs20004201  'carbon steel'  7
hs20004300  0  *  no heat generation
hs20004400  8890  *  use cf890 (srv gas temp) to define lhs boundary condition
hs20004600  1  200  'ext'  1.0  1.0  *  all atm heat xfer
hs20004601  .3  'equiv band'  3.0
hs20004700  71.44  3.37  4.77
hs20004800  -1  *  enter nodal temps
hs20004801  533.0  8  *  500 f
*
*
*********************************************************************
******************   drywell ex-pedestal 705'-723' ********************
*********************************************************************
*
*
cv20100      drywell-bot    2    2    2
cv20101      0    0
cv201a0      3
cv201a1     pvol    117831.      rhum    .12  *  17.09 psia
cv201a2     tatm    365.85
cv201a3     vpol    0.
cv201a4     mlfr.4  0.0          mlfr.5   0.96      mlfr.6   0.0
cv201a5     mlfr.7  0.0          mlfr.8   0.0       mlfr.9   0.04
cv201b1       214.5        0.0   * 703.7'
cv201b4       220.52      1860.  * 722.99'
*
*
*
fl21000      '201-to-202'    201   202   219.   221.
```

```
f121001      164.    2.    1.0    0.001    0.001
f121002      0   0   0   0   * vertical flow
f121003      1.   1.   1.   1.
f1210s0      164.   2.   13.4    5.0e-5
*
f125000      'downcomer inlet'    201   300   215.04   215.04
f125001      23.88   13.87   1.0    0.001    0.001
*NOTE: DOWNCOMER ID = 24"-(2*(3/8)")=23.25"
*NOTE: FLOW AREA = 23.88 = 85*PI*(23.25*.0348/12)**2/4
f125002      0   0   0   0   * vertical flow
f125003      1.   1.   1.   1.
f1250s0      23.88   13.87   0.59    5.0e-5
*
*NOTE: FOLLOWING NI INERTING LINE INPUT IS LA SALLE-SPECIFC !!
*
*      DOES NOT APPLY TO SUSQUEHANNA !  (re C.K. 6/16/89)
*
* nitrogen inerting system has a 1-1/2 inch line which is normally open
* and remains open during station blackout (see 2vq15a,16a,18a,19a) which
* directly connects the drywell and wetwell between levels m20 and m66.
*f102900      'n2-bypass'         201   401     14.9    -9.2
*f102901      0.00114     30.0     1.0     0.0381     0.0381
*f102902      0   0   0   0
*f102903      8.0    8.0    8.0   8.0
*f1029s0      0.00114     30.0     0.0381      5.0e-5
*
*NOTE: containment venting flow path input from LA SALLE
*
f129000   dw-2-inch    201     900     217.   217.
f129001   0.002027      1.0     0.0
f129002   3
f129003   15.0   15.0
f1290s1   0.002027      1.0    0.0508
f1290v1   -1    171    171
*
          cf17100   dw-2-valve   equals   1    1.0   0.0
          cf17101   0.0
          cf17111   0.0   0.0   time
*
f129100   dw-18-inch   201    900     217.   217.
f129101   0.1642       20.0     0.0
f129102   3
f129103   10.0    10.0
f1291s1   0.1642      20.0    0.4572
f1291v1   -1    172    172
*
          cf17200   dw-18-valve   equals   1    1.0   0.0
          cf17201   0.0
          cf17211   0.0    0.0   time
*
*
*
*  hs20101xnn = lowest drywell cell floor
*               thickness= 0.081" steel + 3'6"concrete  +  1/4" steel
```

```
*                od=86'3"
*                id=29'1"
*                delta r =8.7122m
*                elevation begins  at 700' 6"
*
*  force use of input temperature profile, iss= -1
hs20101000  20  1  -1  0   * rectangular
hs20101001  'low-dw-floor'
hs20101002  213.5124  0.0  *elevation=700'6"
hs20101003  1.0
hs20101100  20001  1  0.0
hs20101200  20001
hs20101300  0
hs20101400  1  401  'ext'  1.0  1.0
hs20101401  0.3   'equiv band'  5.   * steel surface
hs20101500  481.08  8.7122  0.1
hs20101600  1  201  'ext'  1.0  1.0
hs20101601  0.3   'equiv band'  5.   * steel surface
hs20101700  481.08  8.7122  0.1
hs20101800  20001 *  same initial temp as 20001
hsdg000100  -20101  17  'h2o-vap'
hsdg000110  -20101  17  'h2o-vap'
hsdg000120  -20101  17  'co2'
hsdg000101   59.68  2.258e6  360.8  378.0
hsdg000111   44.27  6.065e6  378.0  793.0
hsdg000121  473.06  4.157e6  823.0 1073.0
*
*hs20105xnn =  heat slab for lowest drywell cell wall
*
*  force use of input temperature profile, iss= -1
hs20102000  13  1  -1  0   * rectangular
hs20102001  'low-dw-cell-wall'
hs20102002 214.5792  0.2734 *elevation=704'
hs20102003  1.0 * multiplicity
hs20102100  -1  1  0.0
hs20102102  0.00254  2  *0.1" steel
hs20102103  0.00508  3  *0.20" steel
hs20102104  0.00635  4  *0.25" steel/concrete
hs20102105  0.01270  5  *0.50" concrete
hs20102106  0.02540  6  *1.0"  concrete
hs20102107  0.05080  7  *2.0"  concrete
hs20102108  0.10160  8  *4.0"  concrete
hs20102109  0.20320  9  *8.0"  concrete
hs20102110  0.40640  10 *16.0"  concrete
hs20102111  0.81280  11 *32.0"  concrete
hs20102112  1.62560  12 *64.0"  concrete
hs20102113  1.83515  13 *72.25"  concrete
hs20102200  -1
hs20102201  'carbon steel'  3
hs20102202  'concrete'  12
hs20102300  0
hs20102400  1  201  'ext'  1.0  1.0
hs20102401  0.3   'equiv band'  5.   * steel surface
hs20102500  477.05  6.17242  6.17242
```

```
hs20102600  0 * insulated
hs20102800  -1
hs20102801  328.6   1
hs20102802  328.6   2
hs20102803  328.6   3
hs20102804  328.6   4
hs20102805  327.0   5
hs20102806  326.0   6
hs20102807  325.0   7
hs20102808  324.0   8
hs20102809  322.0   9
hs20102810  319.0  10
hs20102811  314.0  11
hs20102812  304.0  12
hs20102813  299.7  13
*
*
*   hs20103xnn = lowest dw cell misc. steel
*
*  force use of input temperature profile, iss= -1
hs20103000  9  1  -1  0
hs20103001  'low-dw-misc-st'
hs20103002  214.580   1.0  *
hs20103003  1.0 * multiplicity
hs20103100  -1  1  0.0  *slab  1" thick
hs20103102  0.00254  2  *0.1" steel
hs20103103  0.00508  3  *0.2" steel
hs20103104  0.01016  4  *0.4" steel
hs20103105  0.01270  5  *0.5" steel
hs20103106  0.01524  6  *0.6" steel
hs20103107  0.02032  7  *0.8" steel
hs20103108  0.02286  8  *0.9"  steel
hs20103109  0.02540  9  *1.0" steel
hs20103200  -1
hs20103201  'carbon steel'  8
hs20103300  0
hs20103400  1  201  'ext'  1.0  1.0
hs20103401  0.3   'equiv band'  5.   * steel surface
hs20103500  961.2  5.9373  5.9373
hs20103600  1  201  'ext'  1.0  1.0
hs20103601  0.3   'equiv band'  5.   * steel surface
hs20103700  961.2  5.9373  5.9373
hs20103800  -1
hs20103801  328.6   1
hs20103802  328.6   2
hs20103803  328.6   3
hs20103804  328.6   4
hs20103805  328.6   5
hs20103806  328.6   6
hs20103807  328.6   7
hs20103808  328.6   8
hs20103809  328.6   9
*
*
```

```
*********************************************************************
******************  drywell ex-pedestal 723'-758'  *********************
*********************************************************************
*
*
cv20200      drywell-2   2    2    2
cv20201      0    0
cv202a0      3
cv202a1     pvol    117831.      rhum    .12  *  17.09 psia
cv202a2     tatm    365.85
cv202a3     vpol    0.
cv202a4     mlfr.4  0.0          mlfr.5   0.96      mlfr.6   0.0
cv202a5     mlfr.7  0.0          mlfr.8   0.0       mlfr.9   0.04
cv202b1       220.37        0.0   * 723'
cv202b4       231.0       2596.   * 758'
*
*
*
fl22000      '202-to-204'    202   204   230.   232.
fl22001      93.   2.     1.0    0.001    0.001
fl22002      0   0   0   0   * vertical flow
fl22003      1.   1.   1.   1.
fl220s0      93.   2.  0.59687    5.0e-5
*
*
*
*  hs20202xnn = heat slab for 2nd drywell  cell  exterior wall
*
*  force use of input temperature profile, iss= -1
hs20202000  13  1  -1  0
hs20202001  '2nd-dw-cell-wall'
hs20202002  220.5164  0.2734  *elevation=723'5  3/4"
hs20202003  1.0 * multiplicity
hs20202100  20102  1  0.0
hs20202200  20102
hs20202300  0
hs20202400  1  202  'ext'  1.0  1.0
hs20202401  0.3   'equiv band'  5.   * steel surface
hs20202500  684.67  10.94  10.94
hs20202600  0
hs20202800  20102  * initial temp is same as 20102
*
*
*  hs20201xnn =  lower shield wall
*                    1/2"steel + 1'9"concrete + 1.5"steel
*                    elevation =729' 9 5/8" to 758'
*                    height  = 8.59473 m
*                    thickness = 1.9167 ft = .5842 m
*                    ir=12.7917 ft = 3.8989 m
*                    or=14.7084 ft = 4.4831 m
*
*  force use of input temperature profile, iss= -1
hs20201000  19  2  -1  0
hs20201001  'low-shield-wall'
```

```
hs20201002  222.4440  1.0  *elevation=729'9 5/8"
hs20201003 1.0 * multiplicity
hs20201100  -1  1  3.8989  *id=25' 7"
hs20201102  3.90144  2  * 0.1" steel
hs20201103  3.90398  3  *0.2"  steel
hs20201104  3.90906  4  *0.4"  steel
hs20201105  3.91160  5  *0.5"  steel/concrete
hs20201106  3.92430  6  *  concrete
hs20201107  3.9497   7  *  concrete
hs20201108  4.0005   8  *  concrete
hs20201109  4.10210  9  *  concrete
hs20201110  4.16560 10  *  concrete
hs20201111  4.22910 11  *  concrete
hs20201112  4.33070 12  *  concrete
hs20201113  4.38150 13  *  concrete
hs20201114  4.4450  14  *  concrete/steel
hs20201115  4.4500  15  *  steel
hs20201116  4.4600  16  *  steel
hs20201117  4.4700  17  *  steel
hs20201118  4.4750  18  *  steel
hs20201119  4.4831  19  *  steel
hs20201200  -1
hs20201201  'carbon steel'  4
hs20201202  'concrete'  13
hs20201203  'carbon steel'  18
hs20201300  0
hs20201400  1  203  'int'  1.0  1.0 * cv203 is lhs
hs20201401  0.3   'equiv band'  5.   * steel surface
hs20201500  1.0  7.7978  8.5
hs20201600  1  202  'ext'  1.0  1.0 * cv202 is rhs
hs20201601  0.3   'equiv band'  5.   * steel surface
hs20201700  1.0      8.38      8.5
hs20201800  -1
hs20201801  327.4   1
hs20201802  327.0   2
hs20201803  326.9   3
hs20201804  326.7   4
hs20201805  326.5   5
hs20201806  326.0   6
hs20201807  325.2   7
hs20201808  325.2   8
hs20201809  325.2   9
hs20201810  325.2  10
hs20201811  325.2  11
hs20201812  325.2  12
hs20201813  325.2  13
hs20201814  325.2  14
hs20201815  325.2  15
hs20201816  326.0  16
hs20201817  326.5  17
hs20201818  327.0  18
hs20201819  327.4  19
hsdg000130  +20201  13  'h2o-vap'
hsdg000140  +20201  13  'h2o-vap'
```

```
hsdg000150  +20201  13  'co2'
hsdg000131   59.68  2.258e6  360.8  378.0
hsdg000141   44.27  6.065e6  378.0  793.0
hsdg000151  473.06  4.157e6  823.0 1073.0
*
*
*    hs20203xnn = 2nd drywell cell misc. steel
*
*  force use of input temperature profile, iss=-1
hs20203000  9  1 -1  0
hs20203001  '2nd-dw-misc-st'
hs20203002  220.51645  1.0  *elevation=723' 5 3/4"
hs20203003  1.0 * multiplicity
hs20203100  20103  1  0.0  *slab=1"thick
hs20203200  20103
hs20203300  0
hs20203400  1  202  'ext'  1.0  1.0
hs20203401  0.3   'equiv band'  5.   * steel surface
hs20203500  1123.8  10.48  10.48
hs20203600  1  202  'ext'  1.0  1.0
hs20203601  0.3   'equiv band'  5.   * steel surface
hs20203700  1123.8  10.48  10.48
hs20203800  20103 * initial temp is same as 20103
*
*
*
**********************************************************************
******************  reactor/shield wall annulus    *********************
**********************************************************************
*
*
cv20300      shield-annulus    2    2    2
cv20301      0    0
cv203a0      3
cv203a1     pvol    117831.      rhum    .12  *  17.09 psia
cv203a2     tatm    365.85
cv203a3     vpol    0.
cv203a4     mlfr.4  0.0          mlfr.5   0.96      mlfr.6   0.0
cv203a5     mlfr.7  0.0          mlfr.8   0.0       mlfr.9   0.04
cv203b1       222.4         0.0  * 729'9"
cv203b4       237.363       18.4  * elev. & vol. includes DW head*
*
*
*
fl20400   annulus-to-202    203     202     227.37   227.37
fl20401   15.78    .584    1.    .89    .89
fl20402   3   * horizontal flow
fl20403   1.0    1.0   1.0   1.0
fl204s1   15.78    .584    .895    5.0e-5
*
fl20500   annulus-to-204    203     204     234.19   234.19
fl20501   11.01    .584    1.    3.37    3.37
fl20502   3   * horizontal flow
fl20503   1.0    1.0   1.0   1.0
```

```
fl205s1   11.01    .584    1.    5.0e-5
*
fl24000   'annulus-to-head'    203   205   237.   238.
fl24001   1.24     .50      1.0    0.001    0.001 * assume 2" annular
*                                                   gap @ 12'9.5" rad
fl24002   0   0   0   0   * vertical flow
fl24003   1.   1.   1.   1.
fl240s0   1.24    .50   1.8    5.0e-5
*
*
*  hs20302xnn = upper shield wall
*               elevation =758' to 778'9"
*               height = 6.3246 m
*               id=25'7"
*               od=29'1"
*               thickness = 1.75'
*
*  force use of input temperature profile, iss=-1
hs20302000  19  2  -1  0
hs20302001  'upper-shld-wall'
hs20302002  231.0384  1.0  *elevation=758'
hs20302003  1.0 * multiplicity
hs20302100  20201  1  3.8989 *id=25'7"
hs20302200  20201
hs20302300  0
hs20302400  1  203  'int'  1.0  1.0
hs20302401  0.3   'equiv band'  .15   * steel surface
hs20302500  1.0  7.7978  6.3246
hs20302600  1  204  'ext'  1.0  1.0
hs20302601  0.3   'equiv band'  5.   * steel surface
hs20302700  1.0  8.38  6.3246
hs20302800 20201  *  initial temp same as 20201
hsdg000160  +20302  13  'h2o-vap'
hsdg000170  +20302  13  'h2o-vap'
hsdg000180  +20302  13  'co2'
hsdg000161   59.68  2.258e6  360.8  378.0
hsdg000171   44.27  6.065e6  378.0  793.0
hsdg000181  473.06  4.157e6  823.0 1073.0
*
*
*
*     heat slab for reactor vessel (wall insulation neglected)
*     average wall thickness = 6.85"
*     hs20305xnn = rx vessel wall
*     vessel id =  20.9'
*
*  force use of input temperature profile, iss=-1
hs20305000  8  2  -1  0
hs20305001  'rx-vessel-wall'
hs20305002   222.444  1.0  *elevation=729' 9 5/8"
hs20305003  1.0 * multiplicity
hs20305100  -1  1  3.18516  *id=20.9 ft
hs20305102  3.26136  2  *3" thick
hs20305103  3.31216  3  *5" thick
```

```
hs20305104  3.33756  4  *6" thick
hs20305105  3.35026  5  *6.5" thick
hs20305106  3.35661  6  *6.75" thick
hs20305107  3.35788  7  *6.80" thick
hs20305108  3.35915  8  *6.85" thick
hs20305200  -1
hs20305201  'carbon steel'  7
hs20305300  0 * no volumetric power
hs20305400  8890 * use cf890 (srv gas temp) to define lhs boundary temp
hs20305600  1  203  'ext'  1.0  1.0
hs20305601  0.3   'equiv band'  .15   * steel surface
hs20305700  1.0  6.37032  14.9
hs20305800  -1
hs20305801  533.0  8  *initial temp=500 f
*
*
**********************************************************************
******************  drywell ex-pedestal 758'-779'  *********************
**********************************************************************
*
*
cv20400      drywell-3    2    2    2
cv20401      0    0
cv204a0      3
cv204a1     pvol    117831.      rhum    .12  *  17.09 psia
cv204a2     tatm    365.85
cv204a3     vpol    0.
cv204a4     mlfr.4  0.0          mlfr.5   0.96      mlfr.6   0.0
cv204a5     mlfr.7  0.0          mlfr.8   0.0       mlfr.9   0.04
cv204b1       231.0       0.0   * 758'
cv204b4       237.44       722.  * 779'
*
*
fl23000 '204-to-205'   204   205   237.   238.
fl23001  55.   2.   1.   .001   .001
fl23002   0   0   0   0   * vertical flow
fl23003  1.   1.   1.   1.
fl230s0  55.   2.   5.9   5.0e-5
*
*
*    hs20403xnn  = 3rd drywell cell misc. steel
*
* force use of input temperature profile, iss= -1
hs20403000  9  1  -1  0
hs20403001  '3rd-dw-misc-st'
hs20403002 231.0384  1.0  *  elevation = 758'
hs20403003  1.0 * multiplicity
hs20403100  20103  1  0.0 *slab=1'thick
hs20403200  20103
hs20403300  0
hs20403400  1  204  'ext'  1.0  1.0
hs20403401  0.3   'equiv band'  5.   * steel surface
hs20403500  388.75  6.3246  6.3246
hs20403600  1  204  'ext'  1.0  1.0
```

```
hs20403601  0.3   'equiv band'  5.   * steel surface
hs20403700  388.75  6.3246  6.3246
hs20403800  20103  *  initialize temp same as 20103
*
* hs20401xnn =  heat slab for 3rd drywell cell exterior wall
*                  elevation=758' to 791' 9"
*
*
*  force use of input temperature profile, iss= -1
hs20401000  13  1  -1  0
hs20401001  '3rd-dw-cell-wall'
hs20401002  231.0384  1.0  *elevation=758'
hs20401003  1.0 * multiplicity
hs20401100  20102  1  0.0
hs20401200  20102
hs20401300  0
hs20401400  1  204  'ext'  1.0  1.0
hs20401401  0.3   'equiv band'  5.   * steel surface
hs20401500  312.64   6.4    6.4
hs20401600  0
hs20401800  20102  *  initialize temp same as 20102
*
*
*********************************************************************
******************  drywell ex-pedestal 779'-809' (top)   *********************
*********************************************************************
*
*
cv20500      drywell-top    2    2    2
cv20501      0    0
cv205a0      3
cv205a1     pvol    117831.      rhum    .12  *  17.09 psia
cv205a2     tatm    365.85
cv205a3     vpol    0.
cv205a4     mlfr.4  0.0          mlfr.5   0.96      mlfr.6   0.0
cv205a5     mlfr.7  0.0          mlfr.8   0.0       mlfr.9   0.04
cv205b1       237.363        0.0     * 779'
cv205b4       246.5878       1052.   * 806.7'
**
** drywell head leak flow path -- DEACTIVATED FOR C0 RUN
**
** Start leaking if drywell head temp has ever > CF245 and if gauge pressure >
** than the value set in CF246
*
* --- Maximum leakage area based on CBI Peach Bottom study for case
* --- with no gasket springback
*
* --- use Susquehanna head dimensions for hydraulic diameter = 4A/P
* ---  P = Pi * 37'-7.5" = 36.0281 m  Dhyd = 4 (.04)/ 36.0281 = .00444
* ---  Assume flow path length = flange thickness = 4" = .10160
*
*fl26000      'dw-hd-failure'        205   600    241.2   241.2
*fl26001      0.04   .1016   1.       * maximum open area = .04
*fl26002      3
```

```
*fl26003      1.0  1.0
*fl260s0      0.04   .1016   0.00444    1.0e-4    16.0
*fl260v0      -1    470   470
*
            cf47000      dwhead-fail-frac     l-a-ifte  3   1.0   0.0
            cf47001      0.0
            cf47011      1.0   0.0   cfvalu.450
            cf47012      1.0   0.0   cfvalu.400
            cf47013      0.0   0.0   time
*
            cf45000      'dwhead-fail'  l-and    2     1.0    0.0
            cf45001      .false.
            cf45011      1.0     0.0     cfvalu.245  * temperature criterion
            cf45012      1.0     0.0     cfvalu.246  * psid criterion
*
            cf24500      'temp-criterion'    l-gt   2     1.0   0.0
            cf24501      .false.
            cf24505      latch
            cf24511      1.0      0.0   hs-temp.2050408 * midpoint flange temp
            cf24512      0.0    644.3   time  *  head fail temp = 700 F
*
            cf24600      'dp-criterion'   l-gt    2   1.0   0.0
            cf24601      .false.
            cf24611      1.0       0.0   cfvalu.197   * dw head dp
            cf24612      0.0  565370.   time  * head fail dp = 82 psid
*
            cf19700      'diff-pressure'   add    2     1.0    0.0
            cf19711      1.0     0.0     cvh-p.205  *  DP = P(205) - Env
            cf19712     -1.0     0.0     cvh-p.600
*
            cf40000    'frac-open-cf'  tab-fun   1   1.0   0.0
            cf40003     252
            cf40011     1.0    0.0   cfvalu.197

* base on data from CBI Peach Bottom Study for case of no gasket springback
*
            tf25200   'area-vs-dp'    4    1.0    0.0
            tf25211       -1.e9      0.0    *
            tf25212    565370.07     0.0    *  82 psid   0.0 sq meters
            tf25213    1378951.4     1.0    * 200 psid   0.04 sq meters
            tf25214        1.e9      1.0    *hold area constant above 200 psid
*
*
*
*
*   hs20501xnn = rx vessel head
*   thickness varies form 3.5" to 4 15/16" avg =4.25"
*
*  force use of input temperature profile, iss=-1
hs20501000  10  5  -1  0
hs20501001  'rx-vessel-head'
hs20501002  241.3254  *elevation = 791'9"
hs20501003  1.0 * multiplicity
hs20501100  -1  1  3.1877  *radius=125.5"
```

```
hs20501102  3.2258  2  *1.5" steel
hs20501103  3.2512  3  *2.0" steel
hs20501104  3.2639  4  *3.0" steel
hs20501105  3.27025  5  *3.25" steel
hs20501106  3.27660  6  *3.50" steel
hs20501107  3.28295  7  *3.75" steel
hs20501108  3.28930  8  *4.0" steel
hs20501109  3.29311  9  *4.15" steel
hs20501110  3.29565  10 *4.25" steel
hs20501200  -1
hs20501201  'carbon steel'  9
hs20501300  0
hs20501400  8890  *  use cf890 (srv gas temp) to define lhs boundary condition
hs20501600  1 205  'ext'  1.0  1.0
hs20501601  0.3   'equiv band'  3.   * steel surface
hs20501700  1.0  3.1877  1.0
hs20501800  -1
hs20501801  533.0  10  *initial temp=500f*
*
*
*  hs20502xnn =upper head region external  wall
*             elevation = 778'9" to 791'9"
*
*  force use of input temperature profile, iss=-1
hs20502000  13  1  -1  0
hs20502001  'upper-head-wall'
hs20502002  237.363  0.2734  *elevation = 778'9"
hs20502003  1.0
hs20502100  20102  1  0.0
hs20502200  20102
hs20502300  0
hs20502400  1  205  'ext'  1.0  1.0
hs20502401  0.3   'equiv band'  2.   * steel surface
hs20502500  158.03  4.1194  4.1194
hs20502600  0
hs20502800  20102 * initialize temp same as 20102
*
*
*hs20503  is retangular approximation of drywell head
*
*  steady state temperature profile calculated, iss= 1
hs20503000  9  1  1  0
hs20503001  'dw-head-retang'
hs20503002  246.58  0. * horizontal slab, bottom at 246.58 m
hs20503003  1.0 * multiplicity
hs20503100  -1  1  0.0
hs20503102  0.00254  2  *0.1" steel
hs20503103  0.00508  3  *0.2" steel
hs20503104  0.01016  4  *0.4" steel
hs20503105  0.01905  5  *0.75" steel
hs20503106  0.02794  6  *1.1" steel
hs20503107  0.03302  7  *1.3" steel
hs20503108  0.03556  8  *1.4" steel
hs20503109  0.03810  9  *1.5" steel
```

```
hs20503200  -1
hs20503201  'carbon steel'  8
hs20503300  0
hs20503400  1  205  'int'  1.0  1.0
hs20503401  0.3   'equiv band'  5.   * steel surface
hs20503500  317.65   5.2243   1.0   * use Steve's calculated area
hs20503600  1  600  'ext'  0.1   0.1
hs20503601  0.3   'equiv band'  5.   * steel surface
hs20503700  317.65   5.2243  1.0
hs20503800  -1
hs20503801  294.29  9  * not used
*
*
*  hs20504xnn     = drywell head flange
*                   elevation 791'9" to  797' 1-3/8"
*                   thickness = 4" = 0.1016 m
*                   i.d. = 37' 7-1/2"  =  11.4681 m
*                   radius = 5.73405 m
*
*  steady state temperature profile calculated, iss= 1
hs20504000   15   2   1   0   * cylindrical slab
hs20504001   'dw-head-flange'
hs20504002   241.3254   1.0   * bottom @ 791' 9", vertical structure
hs20504003   1.0 * multiplicity
hs20504100   -1   1   5.73405
hs20504102   5.73659   2   * 0.1" steel
hs20504103   5.73913   3   * 0.2" steel
hs20504104   5.74421   4   * 0.4"
hs20504105   5.75437   5   * 0.8"
hs20504106   5.76453   6   * 1.2"
hs20504107   5.77469   7   * 1.6"
hs20504108   5.78485   8   * 2.0"
hs20504109   5.79501   9   * 2.4"
hs20504110   5.80517  10   * 2.8"
hs20504111   5.81533  11   * 3.2"
hs20504112   5.82549  12   * 3.6"
hs20504113   5.83057  13   * 3.8"
hs20504114   5.83311  14   * 3.9"
hs20504115   5.83565  15   * 4.0"
hs20504200   -1
hs20504201   'carbon steel'  14
hs20504300   0
hs20504400   1   205   'ext'   1.0   1.0
hs20504401  0.3   'equiv band'  2.   * steel surface
hs20504500   1.0   1.635   1.635
hs20504600   1   600   'ext'   0.1   0.1
hs20504601  0.3   'equiv band'  2.   * steel surface
hs20504700   1.0   1.635   1.635
hs20504800   -1
hs20504801   311.   15   * not used
*
*
*hs20505xnn  = drywell head misc steel
*
```

```
*  force use of input temperature profile, iss= -1
hs20505000  9  1  -1  0
hs20505001  'dw-head-misc-st'
hs20505002  237.363  1.0 * elevation=778'9"
hs20505003  1.0 * multiplicity
hs20505100  20103  1  0.0  *slab=1"thick
hs20505200  20103
hs20505300  0
hs20505400  1  205  'ext'  1.0  1.0
hs20505401  0.3   'equiv band'  2.   * steel surface
hs20505500  158.25  3.9624  3.9624
hs20505600  1  205  'ext'  1.0  1.0
hs20505601  0.3   'equiv band'  2.   * steel surface
hs20505700  158.25  3.9624  3.9624
hs20505800  20103  * initial temp same as 20103
*
*
*
*********************************************************************
*************************      downcomers     ************************
*********************************************************************
*
*
cv30000     downcomers    2   2   3
cv30001     0    0
cv300a0     3
cv300a1     pvol    117831.      rhum    .93   *  17.09 psia
cv300a2     tatm    340.11         tpol   324.11
cv300a3     zpol    204.52
cv300a4     mlfr.4  0.0          mlfr.5   0.96      mlfr.6   0.0
cv300a5     mlfr.7  0.0          mlfr.8   0.0       mlfr.9   0.04
cv300b1      201.16          0.0
cv300b2      215.04        330.6  * volume = all 87 downcomers
*
*-------------------------  flow paths  -------------------------
*
fl30100      'downcomer exit'     300   401   201.16   201.16
fl30101      22.4    2.6  1.0   0.001    0.001 * use small opening heights
*  82 uncapped downcomer pipes
*   5   capped downcomer pipes with 3 inch drains to ww pool
*NOTE: 22.4 = 82*Pi*(0.59**2)/4+(5*Pi*(3*.3048/12)**2/4)
fl30102      0   0   0   1   * vertical flow, sparc physics
fl30103      1.0    1.0   1.0   1.0
fl301s0      22.4     6.94   0.59   5.0e-5
*
*
*
*
*   hs30002xnn  down comer wall air portion
*
*  force use of input temperature profile, iss= -1
hs30002000  5  2  -1  0
hs30002001  'downcomers-air'
hs30002002  204.5208  1.0  *elevation=671 ft
```

```
hs30002003  87.0 * multiplicity
hs30002100  -1  1  0.295275
hs30002102  0.299720  2     *0.175"   steel
hs30002103  0.302260  3     *0.275" steel
hs30002104  0.302895  4     *0.30" steel
hs30002105  0.304800  5     *0.375" steel
hs30002200  -1
hs30002201  'carbon steel'  4
hs30002300   0
hs30002400   1  300  'int'  1.0  1.0
hs30002401  0.3   'equiv band'  .5    * steel surface
hs30002500   1.0    0.59055   8.9792
hs30002600   1  401  'ext'  1.0  1.0
hs30002601  0.3   'equiv band'  5.   * steel surface
hs30002700    1.0   0.60960   8.9792
hs30002800  -1
hs30002801  303.9   1
hs30002802  303.9   2
hs30002803  303.9   3
hs30002804  303.9   4
hs30002805  303.9   5
*
*   hs30001xnn  downcomers submerged
*
*  force use of input temperature profile, iss=-1
hs30001000  5  2  -1  0
hs30001001  'downcomers-water'
hs30001002  201.168  1.0* elevation=660'
hs30001003  87.0 * multiplicity
hs30001100  30002   1  0.295275
hs30001200  30002
hs30001300  0
hs30001400  -1  300  'int'  0.0  0.0
hs30001500  1.0  0.59055  3.3528
hs30001600   -1  401  'ext'  0.0  0.0
hs30001700  1.0  0.69060   3.3528
hs30001800  -1
*  set temp close to wetwell pool temp
hs30001801  324.1   1
hs30001802  324.1   2
hs30001803  324.1   3
hs30001804  324.1   4
hs30001805  324.1   5
*
*
*
*
*
*
*
*********************************************************************
************************** wetwell in-pedestal ************************
*********************************************************************
*
```

```
*
cv40000     'wetwell cavity'    2    2    3
cv40001     0    0
cv400a0     3
cv400a1     pvol    109006.      rhum    .93    *  15.81 psia
cv400a2     tatm    307.83         tpol   324.11
cv400a3     zpol    204.52
cv400a4     mass.2   0.0
cv400a5     mlfr.4  0.0          mlfr.5   0.96      mlfr.6   0.0
cv400a6     mlfr.7  0.0          mlfr.8   0.0       mlfr.9   0.04
cv400b1      197.5          0.0   *  648'
cv400b2      213.5124       447.7  *  703'11" - 3.5' = 700.42 = 213.5124 m
*                                    *  pedestal ID = 19'7"
*
fl40100   ped-to-WW-bottom  400   401   198.91   198.91
fl40101   1.167     1.55   1.0    .609   .609
fl40102   3 * horizontal flow path
fl40103   1.5     1.5 * kfor=krev
fl401s1   1.167     1.55   .61     5.e-6
*
fl40200   ped-to-WW-middle  400   401   202.41   202.41
fl40201   1.167     1.55   1.0    .609    .609
fl40202   3 * horizontal flow path
fl40203   1.5     1.5 * kfor=krev
fl402s1   1.167     1.55   .61     5.e-6
*
fl40300   ped-to-WW-top  400   401   208.65   208.65
fl40301   1.53     1.55    1.0    .914   .914
fl40302   3 * horizontal flow path
fl40303   1.5     1.5
fl403s1   1.53     1.55   .71     5.e-6
*
*
*
*     hs40002xnn  wetwell inpedestal  wall-pool
*      .25 inch steel inside
*    60.00 inches concrete
*      .50 inch steel outside
*
*  force use of input temperature profile, iss= -1
hs40002000  19  2  -1  0
hs40002001  'ww-ped-wall-wat'
hs40002002  197.5104   1.0 *water begins at 648'
hs40002003  1.0 * multiplicity
hs40002100  -1  1  2.9845  *id=19'7"
hs40002102  2.98704  2  *0.1    steel
hs40002103  2.99085  3  *0.25"  steel/concrete
hs40002104  2.99720  4  *0.5"  concrete
hs40002105  3.00990  5  *1.0" concrete
hs40002106  3.03530  6  *2.0" concrete
hs40002107  3.08610  7  *4.0" concrete
hs40002108  3.18770  8  *8.0" concrete
hs40002109  3.39090  9  *16.0" concrete
hs40002110  3.75920 10  *30.5" concrete
```

```
hs40002111  4.12750  11  *45.0" concrete
hs40002112  4.33070  12  *53.0" concrete
hs40002113  4.43230  13  *57.0" concrete
hs40002114  4.48310  14  *59.0" concrete
hs40002115  4.50850  15  *60.0" concrete
hs40002116  4.52120  16  *60.5" concrete/steel
hs40002117  4.52755  17  *60.75" steel
hs40002118  4.53136  18   *60.90" steel
hs40002119  4.53390  19  *61.0" steel
hs40002200  -1
hs40002201  'carbon steel'  2
hs40002202  'concrete'  15
hs40002203  'carbon steel'  18
hs40002300  0
hs40002400  -1  400  'int'  0.0  0.0 * ht to pool only
hs40002500  1.0  5.969    7.0104
hs40002600  -1  401  'ext'  0.0  0.0 * ht to pool only
hs40002700  1.0  9.0678  7.0104
hs40002800  -1
hs40002801  324.11  19 *  initialize close to wetwell pool temp
*
*   hs40003xnn  wet well in pedestal -  air
*                  length of air portion=29.5'
*
*
*  force use of input temperature profile, iss= -1
hs40003000  19  2  -1  0
hs40003001  'ww-ped-wall-air'
hs40003002  204.5208  1.0* air  begins at   671'
hs40003003  1.0 * multiplicity
hs40003100  40002  1  2.9845 *id=19'7"
hs40003200   40002
hs40003300   0
hs40003400   1  400  'int'  1.0  1.0
hs40003401  0.3   'equiv band'  5.   * steel surface
hs40003500  1.0   5.969    8.9792
hs40003600   1  401  'ext'  1.0  1.0
hs40003601  0.3   'equiv band'  5.   * steel surface
hs40003700  1.0  9.0678  8.9792
hs40003800  -1
hs40003801  303.7   1
hs40003802  303.4   2
hs40003803  303.0   3
hs40003804  302.8   4
hs40003805  302.6   5
hs40003806  302.4   6
hs40003807  302.4   7
hs40003808  302.4   8
hs40003809  302.4   9
hs40003810  302.4  10
hs40003811  302.4  11
hs40003812  302.4  12
hs40003813  302.4  13
hs40003814  302.4  14
```

```
hs40003815  302.6  15
hs40003816  302.8  16
hs40003817  303.0  17
hs40003818  303.4  18
hs40003819  303.7  19
hsdg000190  +40003  15  'h2o-vap'
hsdg000200  +40003  15  'h2o-vap'
hsdg000210  +40003  15  'co2'
hsdg000191   59.68  2.258e6  360.8  378.0
hsdg000201   44.27  6.065e6  378.0  793.0
hsdg000211  473.06  4.157e6  823.0 1073.0
*
*hs40001xnn   wet  well inpedestal floor is 8'thick with 1/4" liner
*
*  force use of input temperature profile, iss= -1
hs40001000  12  1  -1  0
hs40001001  'ww inped floor'
hs40001002  195.0616   0.0  * bottom elevation=640' (=648'-8')
hs40001003  1.0 * multiplicity
hs40001100  -1  1  0.0    * x=0.0 begins at elevation  640' and points upwards
hs40001102  0.812800  2  * 32" concrete
hs40001103  1.625600  3  * 32" concrete
hs40001104  2.032000  4  * 16" concrete
hs40001105  2.235200  5  *  8" concrete
hs40001106  2.336800  6  *  4" concrete
hs40001107  2.387600  7  *  2" concrete
hs40001108  2.413000  8  *  1" concrete
hs40001109  2.425700  9  *0.5" concrete
hs40001110  2.432050 10  *.25" concrete
hs40001111  2.435860 11  *.15" steel
hs40001112  2.438400 12  *0.1" steel  slab thickness =8'
hs40001200  -1
hs40001201  'concrete'  9
hs40001202   'carbon steel' 11
hs40001300  0
hs40001400    0 * lhs at bottom
hs40001600  1  400  'ext'  0.0  0.0
hs40001700  27.98  5.97   0.1 * floor dia. = 19'7" (5.97 m)
hs40001800  -1 * nodal temps
hs40001801  285.0    9      *  ground temperature  =  55 f
hs40001802  324.11  12      *  wetwell pool temperature
*
*
*
*
*
*************************************************************************
************************** wetwell ex-pedestal ************************
*************************************************************************
*
*
cv40100     wetwell    2    2    3
cv40101     0    0
cv40103     490.25   * control volume area used for velocity calc.
```

```
cv401a0     3
cv401a1     pvol    109006.      rhum    .95    *  15.81 psia
cv401a2     tatm    307.83         tpol   324.11
cv401a3     zpol    204.52
cv401a4     mlfr.4  0.0          mlfr.5   0.96      mlfr.6   0.0
cv401a5     mlfr.7  0.0          mlfr.8   0.0       mlfr.9   0.04
cv401b1      197.5        0.0
cv401b3      213.5124       7485.
*
*------------------------ vacuum breakers -------------------------
*
* --- this breaker represents the first 25 % of the first vb
*
* --- This is done to aid in determining the fraction of the flow path
* --- which opens each time the vacuum breakers actuate.
*
*  Use PPL data for vacuum breakers:
*               7467.0 pa-diff(1.083 psid) to crack the breakers
*              16182.0 pd-diff(2.347 psid) to fully open breakers
*        max opening area at 65 degrees is .175 m**2(1.885 ft**2)
*
fl43000   vac-brk-1a  401   300   211.76   211.76
fl43001   0.04375    0.9144   0.0    .5 .5 * initially closed
fl43002   3 * horizontal flow path
fl43003   8.47     1.0e6 * PPL kforward, large kreverse
fl430s1   0.04375    0.9144   1.     5.e-6
fl430v0   -1  102  102
*
*         control functions for vacuum breakers
          cf10100   '401-300-dp'  add 2  1.0  0.0
          cf10110   1.0  0.0  cvh-p.401 * not corrected for pool elev.
          cf10111  -1.0  0.0  cvh-p.300
*
          cf10200   'vb-1a-tab'  tab-fun  1  1.0  0.0
          cf10203   11  * tabular function number
          cf10210   1.0  0.0  cfvalu.101
*
          tf01100   'vb-1a-fract-open'  4  1.0  0.0
*                  delta-p   fraction-open
          tf01110    -1.0e6   0.0
          tf01111    7467.    0.0    * start opening @ 1.083 psid
          tf01112    7902.75  1.0    * full open @ 1.146 psid
          tf01113    +1.0e6   1.0
*
* --- this breaker represents the second 25 % of the first vb
*
fl43100   vac-brk-1b  401   300   211.76   211.76
fl43101   0.04375    0.9144   0.0    .5 .5 * initially closed
fl43102   3 * horizontal flow path
fl43103   8.47     1.0e6
fl431s1   0.04375    0.9144   1.     5.e-6
fl431v0   -1  103  103
*
          cf10300   'vb-1b-tab'  tab-fun  1  1.0  0.0
```

```
          cf10303   12  * tabular function number
          cf10310   1.0  0.0  cfvalu.101
*
          tf01200   'vb-1b-fract-open'  4  1.0  0.0
*                   delta-p   fraction-open
          tf01210     -1.0e6   0.0
          tf01211    7902.76   0.0    * start opening @ 1.146 psid
          tf01212    8338.5    1.0    * full open @ 1.209 psid
          tf01213     +1.0e6   1.0
*
*
* --- this breaker represents the third 25 % of the first vb
*
fl43200   vac-brk-1c  401   300   211.76   211.76
fl43201   0.04375    0.9144   0.0    .5 .5 * initially closed
fl43202   3 * horizontal flow path
fl43203   8.47     1.0e6
fl432s1   0.04375    0.9144   1.     5.e-6
fl432v0   -1  104  104
*
          cf10400   'vb-1c-tab'  tab-fun  1  1.0  0.0
          cf10403   13  * tabular function number
          cf10410   1.0  0.0  cfvalu.101
*
          tf01300   'vb-1c-fract-open'  4  1.0  0.0
*                   delta-p   fraction-open
          tf01310     -1.0e6   0.0
          tf01311    8338.51   0.0    * start opening @ 1.209 psid
          tf01312    8774.25   1.0    * full open @ 1.273 psid
          tf01313     +1.0e6   1.0
*
* --- this breaker represents the last 25 % of the first vb
*
fl43400   vac-brk-1d  401   300   211.76   211.76
fl43401   0.04375    0.9144   0.0    .5 .5 * initially closed
fl43402   3 * horizontal flow path
fl43403   8.47     1.0e6
fl434s1   0.04375    0.9144   1.     5.e-6
fl434v0   -1  105  105
*
          cf10500   'vb-1d-tab'  tab-fun  1  1.0  0.0
          cf10503   14  * tabular function number
          cf10510   1.0  0.0  cfvalu.101
*
          tf01400   'vb-1d-fract-open'  4  1.0  0.0
*                   delta-p   fraction-open
          tf01410     -1.0e6   0.0
          tf01411    8774.26   0.0    * start opening @ 1.273 psid
          tf01412    9210.0    1.0    * full open @ 1.336 psid
          tf01413     +1.0e6   1.0
*
* ------ this vacuum breaker represents the 2nd of 5 breakers
*
* --- this vacuum breaker will only be allowed to open after the first
```

```
* --- vacuum breaker is fully open
*
f144000   vac-brk-2of5  401   300   211.76   211.76
f144001   0.175    0.9144   0.0    .5 .5 * initially closed
f144002   3 * horizontal flow path
f144003   8.47     1.0e6
f1440s1   0.175    0.9144   1.     5.e-6
f1440v0   -1  109  109
*
          cf10900   'vb-2-tab'  tab-fun  1  1.0  0.0
          cf10903   19 * tabular function number
          cf10910   1.0  0.0  cfvalu.101
*
          tf01900   'vb-2-frac-op'  4  1.0  0.0
*                   delta-p   fraction-open
          tf01910    -1.0e6    0.0
          tf01911    9210.1    0.0    * start opening @ 1.336 psid
          tf01912   10953.0    1.0    * full open @ 1.589 psid
          tf01913    +1.0e6    1.0
*
*
*---This vacuum breaker represents the final 3 breakers combined
f145000  'vac-brk-345' 401  300  211.76  211.76
f145001  0.525  0.9144  0.0  0.5  0.5  * initially closed
f145002  3  * horizontal flow path
f145003  8.47  1.0e6
f1450s1  0.525  0.9144  1.0  5.0e-6
f1450v0  -1  451  451
*
          cf45100  'vb-345-tab'  tab-fun  1  1.0  0.0
          cf45103  451  *  tab function number
          cf45110  1.0  0.0  cfvalu.101
*
          tf45100  'vb-345-frac-op'  4  1.0  0.0
*                  delta-p  frac-open
          tf45110   -1.0e6     0.0
          tf45111  10953.1     0.0  *  start open @ 1.589 psid
          tf45112  16182.0     1.0  *  full open @ 2.347 psid
          tf45113   +1.0e6     1.0
*
*
f149000   ww-2-inch    401     900     210.    210.
f149001   0.002027     1.0    0.0
f149002   3
f149003   15.0    15.0
f1490s1   0.002027    1.0    0.0508
f1490v1   -1    173     173
*
          cf17300   ww-2-valve    equals    1    1.0   0.0
          cf17301   0.0
          cf17311   0.0    0.0    time
*
f149100   ww-18-inch   401     900     210.    210.
f149101   0.1642    20.0    0.0
```

```
f149102    3
f149103    10.0     10.0
f1491s1    0.1642      20.0     0.4572
f1491v1    -1     182     182
*
          cf18200    ww-18-valve    equals    1    1.0    0.0
          cf18201    0.0
          cf18211    0.0    0.0      time
***
* wetwell leak flow path - DEACTIVATED FOR C0 RUN
*
* Start leaking if wetwell gauge pressure > value set in CF 150
*
* leakage is from wetwell about half way between the water and ceiling
*f149500      'ww-failure'         401    900     210.    210.
*f149501      0.00929023    1.219    0.0                      * 0.1 ft2
*f149502      3
*f149503      1.0  1.0
*f1495s0      0.00929023    1.219    0.109     1.0e-4     16.0
*f1495v0      -1     151    151
*
            cf15100      ww-fail-frac     1-a-ifte  3    1.0    0.0
            cf15101      0.0
            cf15111      1.0    0.0    cfvalu.150
            cf15112      0.0    1.0    time
            cf15113      0.0    0.0    time
*
            cf15000      'ww-fail'    1-gt     2      1.0     0.0
            cf15001      .false.
            cf15005      latch
            cf15011      1.0      0.0      cfvalu.149
            cf15012      0.0      930792.      time   * fail wetwell at 135 psig
*
            cf14900      'diff-pressure'    add     2      1.0     0.0
            cf14911      1.0      0.0      cvh-p.401   *  DP = WW - Env
            cf14912     -1.0      0.0      cvh-p.900
*
*-------------- deactivate SNL La SAlle WW failure CFs ------------------*
*
*            cf29300      'liner-fail'    1-gt    2      1.0    0.0
*            cf29301      .false.
*            cf29305      latch
*            cf29311      1.0       0.0    hs-temp.4010303
*            cf29312      0.0    1273.0    time * ww liner fail temp (K)
*
*            cf29600      ww-fail-thresh    1-gt     2    1.0    0.0
*            cf29601      .false.
*            cf29605      latch
*            cf29611      1.0    0.0    cfvalu.151
*            cf29612      1.0    0.0    cfvalu.297
*
* calculate ww leak failure pressure
*            cf29700     'fail-pres'   tab-fun    1    1.0    0.0
*            cf29701      1.3445e6
```

```
*            cf29702     3      4.8263e5    1.3445e6
*            cf29703     299
*            cf29711     1.0    0.0    cfvalu.298
*
* containment failure pressure .vs. average ww wall temperature
* base on data from expert opinions
*            tf29900   'p.vs.t fail'    4    1.0    0.0
*            tf29911      0.0     1.3445e6    *
*            tf29912    533.33    1.3445e6    *  500 f   195 psig
*            tf29913    700.00    1.0342e6    *  800 f   150 psig
*            tf29914    922.22    4.8263e5    * 1200 f    70 psig
*
* average wetwell wall concrete temperature
*
*            cf29800     'tave-ww-wall'    add     9   0.824544   0.0
*            cf29812      0.00326        0.0     hs-temp.4010304
*            cf29813      0.00653        0.0     hs-temp.4010305
*            cf29814      0.01308        0.0     hs-temp.4010306
*            cf29815      0.02852        0.0     hs-temp.4010307
*            cf29816      0.05049        0.0     hs-temp.4010308
*            cf29817      0.10673        0.0     hs-temp.4010309
*            cf29818      0.21820        0.0     hs-temp.4010310
*            cf29819      0.45538        0.0     hs-temp.4010311
*            cf29820      0.11780        0.0     hs-temp.4010312
*
*
*
*heat slab input for  cv  401
*
*   hs40101xnn   wet  well   floor
*
*  force use of input temperature profile, iss= -1
hs40101000  12  1  -1  0
hs40101001  'wet-well-floor'
hs40101002  195.0616   0.0  *  bottom elevation=640' (=648'-8')
hs40101003  1.0 * multiplicity
hs40101100  40001  1  0.0 * slab geometry
hs40101200  40001
hs40101300  0
hs40101400   0
hs40101600   1  401 'ext' 0.0 0.0
hs40101700   500.47  8.8773  .1
hs40101800  40001  *  initialize temp same as 40001
*
*hs40104xxnn   air   portion of  dry well  floor support  columns
*
*  force use of input temperature profile, iss= -1
hs40104000  6  2  -1  0
hs40104001  'support  cols-air'
hs40104002  204.5208  1.0  *air  portion begins  at  671'  elevation
hs40104003  12.0 * multiplicity
hs40104100  -1  1  0.50165    *id=39.5"
hs40104102  0.50419   2  *   steel
hs40104103  0.50927   3  *   steel
```

```
;40104104  0.51689   4  *   steel
hs40104105  0.52451   5  *   steel
hs40104106  0.53340   6  *   steel
hs40104200    -1
hs40104201  'carbon steel'  5
hs40104300  0
hs40104400   0  -401 * insulated lhs
hs40104600   1  401  'ext'  1.0  1.0 * ht to atm
hs40104601  0.3   'equiv band'  5.   * steel surface
hs40104700     1.0  1.0668  8.9792
hs40104800 -1
hs40104801  303.9   1
hs40104802  303.9   2
hs40104803  303.8   3
hs40104804  303.8   4
hs40104805  303.8   5
hs40104806  303.7   6
*
*   hs40105xnn  water portions of support  columns
*
*  force use of input temperature profile, iss= -1
hs40105000  6  2  -1  0
hs40105001  'support cols-water'
hs40105002  197.5104  1.0 *  water  begins at 648'
hs40105003   12.0 * multiplicity
hs40105100   40104  1  0.50165  * id=39.5
hs40105200  40104
hs40105300    0
hs40105400   0  -401
hs40105600   -1  401  'ext'  0.0  0.0
hs40105700    1.0  1.0668  7.0104
hs40105800  -1
hs40105801  324.11  6   * initialize at wetwell pool temp
*
*hs40103xnn   wet-well-wall-air
*
*  force use of input temperature profile, iss= -1
hs40103000  12  2  -1  0
hs40103001  'ww-wall-air'
hs40103002  204.5208  1.0  *  elevation at 671'
hs40103003  1.0 * multiplicity
hs40103100  -1  1 13.4112  *  id=88'
hs40103102  13.41374  2  *0.1"  steel
hs40103103  13.41755  3  *0.25"  steel/concrete
hs40103104  13.42390  4  *0.5"  concrete
hs40103105  13.43660  5  * 1.0" concrete
hs40103106  13.46200  6  *2"   concrete
hs40103107  13.51720  7  *4 " concrete
hs40103108  13.61440  8  *8"   concrete
hs40103109  13.81760  9  *16"   concrete
hs40103110  14.22400  10  *32"    concrete
hs40103111  15.03680  11  *64" concrete
hs40103112  15.24000  12  *72'=6' concrete
hs40103200     -1
```

```
hs40103201  'carbon steel'  2
hs40103202  'concrete'  11
hs40103300  0
hs40103400   1  401 'ext'  1.0 1.0
hs40103401  0.3   'equiv band'  5.   * steel surface
hs40103500  1.0  26.8224  8.9792
hs40103600  0    -401
hs40103800    -1
hs40103801  303.7   1
hs40103802  303.0   2
hs40103803  302.7   3
hs40103804  302.5   4
hs40103805  302.5   5
hs40103806  302.4   6
hs40103807  302.3   7
hs40103808  302.2   8
hs40103809  301.8   9
hs40103810  301.2  10
hs40103811  300.0  11
hs40103812  299.7  12
*
*   hs40102xnn   wetwell pool--wall
*
*  force use of input temperature profile, iss= -1
hs40102000  12  2  -1   0
hs40102001  'ww-wall-water'
hs40102002  197.5104  1.0  * elevation=648'
hs40102003  1.0 * multiplicity
hs40102100  40103  1  13.4112  *id=88'
hs40102200  40103
hs40102300  0
hs40102400     -1  401  'ext'  0.0    0.0
hs40102500  1.0  26.8224  7.0104
hs40102600    0   -401
hs40102800  -1
* surface nodes near the wetwell pool temperature
hs40102801  320.0   1
hs40102802  319.5   2
hs40102803  319.0   3
hs40102804  315.0   4
hs40102805  310.0   5
hs40102806  305.0   6
hs40102807  304.0   7
hs40102808  303.0   8
hs40102809  302.0   9
hs40102810  301.2  10
hs40102811  300.0  11
hs40102812  299.7  12
*
*
*
*
*********************************************************************
****************** reactor well above drywell head *********************
```

```
*********************************************************************
*
*
*!!!!!!!!!!! temporary data !!!!!!!!! verify volume/altitude table with PPL
*
cv60000    rf/rx-well  2  2  4
cv600a0      3
cv600a1     pvol  1.01300e5
cv600a2     vpol  0.        rhum    0.5    tatm  316. * initial temp=110F
cv600a3     mlfr.5  0.79    mlfr.9  0.21
cv600b1       241.1       0.0   *  assume bottom of well is at 791' for now
cv600b2       247.5     316.0   * assume top of well is at 812' for now
*
*         Assumed vol = pit vol - dw head vol
*         Assumed vol = Pi*(48'10")**2*(812'-791')/4
*
*                 - (1/2) * (4/3) * Pi (37.75/2)**3   (approximately)
*               = 39332 - 28168 ft**3 = 11164 ft**3 = 316 m**3
*
*
fl60000      'rxwell-to-rf'    600   900   247.   249.4
*  assume 1/8" annular gap around outer perimeter of shield plug
*  A = Pi/4*(48'10-1/8"**2 - 48'10"**2) = 0.79972 ft**2 = 0.0742 m**2
fl60001      0.0742    5.    1.0    0.001    0.001  * check length
fl60002      0   0   0   0   * vertical flow
fl60003      1.   1.   1.   1.
fl600s0      0.0742   5.   13.4    5.0e-5  * check length, hyd. dia, & loss fact.
*
*
*hs60101xnn   reactor well cylindrical wall
*
*  steady state calculation for initial temp profile, iss= 1
hs60101000  12  2  1  0   * cylindrical
hs60101001  'well-wall-air'
hs60101002  241.1  1.0  *  elevation at 791'
hs60101003  1.0 * multiplicity
hs60101100  -1  1 7.4422
hs60101102  7.44855  2   *  steel/concrete
hs60101103  7.47395  3   * concrete
hs60101104  7.52475  4   * concrete
hs60101105  7.62635  5   * concrete
hs60101106  7.82955  6   * concrete
hs60101107  8.03275  7   * concrete
hs60101108  8.23595  8   * concrete
hs60101109  8.54075  9   * concrete
hs60101110  8.84555  10  * concrete
hs60101111  9.0      11  * concrete
hs60101112  9.2711   12  * concrete
hs60101200     -1
hs60101201  'carbon steel'   1
hs60101202  'concrete'  11
hs60101300  0 * no heat source
hs60101400 1 600 'int'.1 .1 * hx to pool if it covers more than 10% of structure
hs60101401  0.3   'equiv band'  5.   * steel surface
```

```
hs60101500  1.  14.888  6.4
hs60101600  0    -600 * insulated rhs
hs60101800    -1 * nodal temps
hs60101801  294.25  12  * not used
*
*
*  hs60201xnn =  reactor well shield plugs
*
*  steady state calculation for initial temp profile, iss= 1
hs60201000  15  1  1  0   * retangular
hs60201001  'shield-plugs'
hs60201002  247.5  0.0  * elevation = 812'
hs60201003  1.0
hs60201100  -1  1  0.0
hs60201104  0.00254  2  *   0.1"  concrete
hs60201105  0.00508  3  *  0.2"  concrete
hs60201106  0.01016  4  *  0.4"  concrete
hs60201107  0.02032  5  *  0.8"  concrete
hs60201108  0.04064  6  *  1.6"  concrete
hs60201109  0.08128  7  *  3.2"  concrete
hs60201110  0.16256  8  *  6.4"  concrete
hs60201111  0.32512  9  * 12.8"  concrete
hs60201112  0.536575  10  *21.125"  concrete
hs60201113  0.748030  11  *29.450"  concrete
hs60201114  0.910590  12  *35.850"  concrete
hs60201115  0.991870  13  *39.050"  concrete
hs60201116  1.032510  14  *40.650"  concrete
hs60201117  1.052830  15  *41.450"  concrete
hs60201200  -1
hs60201202  'concrete'     14
hs60201300  0
hs60201400  1  600  'ext'  1.0  1.0
hs60201401  0.6   'equiv band'  5.   * concrete surface
hs60201500  174.  4.   .1
hs60201600  1  900  'ext'  1.0  1.0
hs60201601  0.6   'equiv band'  5.   * concrete surface
hs60201700  174.  4.   .1
hs60201800  -1
hs60201801  294.26  15 * not used
*
*********************************************************************
*************************     environment     ************************
*********************************************************************
*
*
*  outer environment
cv90000    environment  1  2  6
cv900a0      3
cv900a1     pvol  1.01300e5
cv900a2     vpol  0.        rhum    0.5    tatm  305.
cv900a3     mlfr.5  0.79    mlfr.9  0.21
cv900b1       190.       0.0
cv900b2       300.       1.0e8
*
```

```
*
*--  the following heat slab is here to facilitate the
*--  RN package aerosol settling calculations
*
* steady state calculation for initial temp profile, iss= 1
hs90001000  4  1  1  0
hs90001001  'env-conc-floor'
hs90001002  213.5124  0.0  *elevation=700'6"
hs90001003  1.0 * multiplicity
hs90001100  -1   1  0.
hs90001101  0.00635  2  *0.25" concrete
hs90001102  0.00889  3  *0.35" concrete
hs90001103  0.01143  4  *0.45"  concrete
hs90001200  -1
hs90001202  'concrete'  3
hs90001300  0
hs90001400  0
hs90001600  1  900  'ext'  1.0  1.0
hs90001700  481.08  10.0  1.0
hs90001800  -1
hs90001801  305.     4  * not used
*
*
*
*
*
*********************************************************************
*
*
**********************************************************************
**********************************************************************
* material properties data
**********************************************************************
**********************************************************************
* tabular function input for thermal conductivity, heat capacity, and
* density of heat structure materials
*
**********************************************************************
* carbon steel
**********************************************************************
mpmat10000 'carbon steel'
mpmat10001 thc 100
mpmat10002 cps 101
mpmat10003 rho 102
*
tf10000   'thc carbon steel'  10        1.0       0.0
tf10010                       273.15    55.0      373.15    52.0
tf10011                       473.15    48.0      573.15    45.0
tf10012                       673.15    42.0      873.15    35.0
tf10013                      1073.15    31.0     1273.15    29.0
tf10014                      1473.15    31.0     9973.15    31.0
*
tf10100   'cp carbon steel '  2         1.0       0.0
tf10110                       273.15    0.465e3   5000.0    0.465e3
```

```
*
tf10200   'rho carbon steel'  2          1.0        0.0
tf10210                       273.15     7833.0     5000.0     7833.0
*********************************************************************
* drywell head air space gap properties
*********************************************************************
mpmat20000   'air gap 1'
mpmat20001   thc  200
mpmat20002   cps  201
mpmat20003   rho  202
*
tf20000      'thc air gap 1'   2     1.0    0.0
tf20011          273.15     17.0        10000.0      17.0
*
tf20100      'cps air gap 1'   2     1.0    0.0
tf20111          273.15    1005.0       10000.0     1005.0
*
tf20200      'rho air gap 1'   2     1.0    0.0
tf20211          273.15    1.18         10000.0      1.18
*********************************************************************
* thermal properties for limestone / common sand concrete
*********************************************************************
mpmat30000   'concrete'
mpmat30001   thc  300
mpmat30002   cps  301
mpmat30003   rho  302
*
tf30000      'thc concrete'    2     1.0     0.0
tf30011          273.15     1.3       10000.0      1.3
*
tf30100      'cps concrete'    2     1.0     0.0
tf30111          273.15   1200.0      10000.0     1200.0
*
tf30200      'rho concrete'    2     1.0     0.0
tf30211          273.15    2340.0     10000.0      2340.0
*************************************************************
*
*
*
*********************************************************************
*********************************************************************
*     decay heat input
*********************************************************************
*********************************************************************
*
* --- the dchdefcls0 card must be specified for cases in which
* --- the RN package is calculating aerosol behavior, even if
* --- no fission products are being tracked
*
dchreactor  bwr
dchshut     -1   0.
dchdecpow   origen
*
dchdefcls0    'all'
```

```
dchclsnorm yes
sc00001 3210  0.92  1   * derate power to 3293 mw, .92 = 3293/3578
*
*********************************************************************
*********************************************************************
*     transfer process input
*********************************************************************
*********************************************************************
*
*   'in' transfer process for core package
*           nmsin   nthrm
tpin10100   6       9
tpin10101     read    900
*
*    'out' transfer process for cavity package
*           nmsot   npotoi  iotmtx
tpot10200   5       101     uin.103
*
*     cor-cav translation matrix
*     *** note *** control poison mass is not conserved
*           nrow    ncol
tpm1030000  5       6
*           nrow/ncol  value
tpm1030001  1/1        1.0     * uo2 mass
tpm1030002  2/2        1.0     * zro2 mass
tpm1030003  3/3        1.0     * steel mass   * ?????????
tpm1030004  4/4        1.0     * zr mass
tpm1030005  5/5        1.0     * steel oxide mass
*     transfer processes for radionuclide transfer
tpin60100   15      1
tpot60200   15      601    def.1
*
*
*
*********************************************************************
*********************************************************************
**     dw cavity input
*********************************************************************
*********************************************************************
*
*
* -- La Salle Cavity:  Depth = 9' 6-1/2" = 2.91 m
*                      I.D.  = 20' 3" = 6.17 m
*                      O.D.  = 29' 11" = 9.12 m
*                      Approximate cavity volume = 3051 ft**3 = 86.41 m**3
*                      Sidewall thickness = 4' 10" = 1.47 m
*                      Floor thickness = 3' 9" = 1.14 m
*
* -- WNP-2 Cavity:     Depth = 6' 10" = 2.08 m
*                      I.D.  = 20' 3" = 6.17 m
*                      O.D.  = 30' 4" = 9.25 m
*                      Approximate cavity volume = 2196 ft**3 = 62.19 m**3
*                      Sidewall thickness = 5' 0.5" = 1.54 m
*                      Floor thickness = 5' = 1.52 m
```

```
*
*
cav0100    200    dw-cavity     *  drywell inpedestal cavity
cav01dh    117   118  119       * cf #'s for decay heat, oxide & metal splits
cav01tp    102                  *  transfer process number
*
cf11700   dw-cav-decay-ht   equals   1   1.  0.
cf11710    1.      0.   edf.700.1
*
cf11800   oxide-dh-fract   tab-fun   1   1.  0.
cf11803   118
cf11810    1.      0.   time
tf11800   oxide-dh-fract  2   1.   0.
tf11810      0.          .98    *  put 98% of decay heat in oxide layer
tf11811    1.0e7         .98
*
cf11900   metal-dh-fract   tab-fun   1   1.  0.
cf11903   119
cf11910    1.      0.   time
tf11900   metal-dh-fract    2   1.   0.
tf11910      0.          .02    *  put  2% of decay heat in metal layer
tf11918    1.0e7         .02
*
cav01g0   corcon  2            *  flat bottom cylinder geometry
*
*         nrays   r0   z0
cav01g1    50     0.   0.
*         zt   rad   hit   radc   rw   hbb  nbot  ncorn
cav01g2   0.  3.086  2.91   0.1  4.56  1.14   25     3 * use La Salle cavity
*
cav01ra   -1    * stop calculation when debris melts through floor
cav01rr   -1    * stop calculation when debris melts through side wall
*
*   15452.3 kg of stainless steel are added initially to the cavity
*   to account for the sump tank, gratings, liners, pipes and
*   supports melted by the corium.
*
cav0110      temp       305.0
cav0111      fe       11434.7
cav0112      cr        2781.4
cav0113      ni        1236.2
*
* test test test --- add a bit of uo2 to the debris
* this is necessary to prevent vanesa from bombing the first time it
* is called.  It is first called at the onset of concrete ablation.
*
cav0120      temp       305.0
cav0121      uo2         11.0
*
*   limestone / common sand concrete (mix446) with 0.056 kg/kg rebar
*
cav01c0   mix446
cav01c1   sio2      0.36982       tio2      0.00013
cav01c2   mno       0.00005       mgo       0.09214
```

```
cav01c3   cao       0.22255      na2o      0.00059
cav01c4   k2o       0.00148      fe2o3     0.00210
cav01c5   al2o3     0.00902      cr2o3     0.00002
cav01c6   co2       0.20173      h2oevap   0.02549
cav01c7   h2ochem   0.01888      fe        0.05600
cav01ca   densct    2340.0    * concrete density
cav01cb   tsolct    1420.0    * concrete solidus temperature
cav01cc   tliqct    1670.0    * concrete liquidus temperature
cav01cd   tablct    1503.0    * concrete ablation temperature
cav01ce   tinct      310.0    * concrete initial temperature
cav01cf   emisct      0.82    * emissivity
sc01000  2303  2920.0  4  * solidus temp. of high-melting group
sc01001  2303  2920.0  5  * liquidus temp. of high-melting group
*
*
*
*********************************************************************
*********************************************************************
**     radionuclide input
*********************************************************************
*********************************************************************
**
rn1000 0
rn1001 5 1 15 14 13 0 0
rn1100 1.0e-6 50.e-6 1000.
*
rnacoef  1  * calculate aerosol coefficients
*   ----    settling areas
*          fr   to     elev     area
rnset001  100  401    198.6      1.1     * fl100
rnset002  205  204    237.44    55.0     * fl230
rnset003  204  202    231.0     93.0     * fl220
rnset004  203  202    227.3      4.1     * fl204 (horizontal projection)
rnset005  202  201    220.52   164.0     * fl210
rnset006  300  401    201.16    20.6     * fl301 (conservatively high)
*
*
* ---- setup ww pool scrubbing for downcomer flow paths
*
rn2pls00    301
*
*//*********************************************************
*//*******  special output control functions ******************
*//*********************************************************
*
* use one-shot control functions for cf163,cf178,cf179,cf180,cf181
* cf771,cf774,and cf342 so that the editcf, restartcf, and the plotcf
* melcor features will produce one and only output as each of the
* above control functions switches from false to true, ie as each
* event occurs.
*
*
*******************************************************************
* write edit when user specified (melcor input) pressures are reached
```

```
* pressure 1
cf16000    pressure-1   equals    1    1.0   0.0
cf16001    1.0e8
cf16011    0.0    105489.78   time * pressure-1 = 15.3 psig (vent trigger)
*
cf16100    del-p-ww     add    2    1.0    0.0
cf16101    0.0
cf16111    1.0     0.0   cvh-p.401  *  dp = WW - Env
cf16112   -1.0     0.0   cvh-p.900
*
cf16200    set-pflag-1    l-gt     2     1.0   0.0
cf16201    .false.
cf16211    1.0     0.0     cfvalu.161
cf16212    1.0     0.0     cfvalu.160
*
cf16300    vent-mes-1      l-equals     1     1.0   0.0
cf16301    .false.
cf16305    one-shot
cf16306    2        'wetwell exceeded 15.3 psig'
cf16311    1.0    0.0      cfvalu.162
*
* pressure 2
cf16400    pressure-2   equals    1    1.0   0.0
cf16401    1.0e8
cf16411    0.0    310264.1   time   * pressure-2 = 45 psig = Low MK II Des. Pres
*
cf17400    set-pflag-2    l-gt     2     1.0   0.0
cf17401    .false.
cf17411    1.0     0.0     cfvalu.161
cf17412    1.0     0.0     cfvalu.164
*
cf17800    vent-mes-2      l-equals     1     1.0   0.0
cf17801    .false.
cf17805    one-shot
cf17806    2        'wetwell exceeded 45 psig'
cf17811    1.0    0.0      cfvalu.174
*
* pressure 3
cf16500    pressure-3   equals    1    1.0   0.0
cf16501    1.0e8
cf16511    0.0      758423.   time    * pressure-3 = 110 psig
*
cf17500    set-pflag-3    l-gt     2     1.0   0.0
cf17501    .false.
cf17511    1.0     0.0     cfvalu.161
cf17512    1.0     0.0     cfvalu.165
*
cf17900    vent-mes-3      l-equals     1     1.0   0.0
cf17901    .false.
cf17905    one-shot
cf17906    2        'wetwell exceeded 110 psig'
cf17911    1.0    0.0      cfvalu.175
*
* pressure 4
```

```
cf16600    pressure-4    equals    1    1.0    0.0
cf16601    1.0e8
cf16611    0.0    827371.     time    * pressure-4 = 120 psig
*
cf17600    set-pflag-4    l-gt     2     1.0   0.0
cf17601    .false.
cf17611    1.0     0.0     cfvalu.161
cf17612    1.0     0.0     cfvalu.166
*
cf18000    vent-mes-4      l-equals     1     1.0   0.0
cf18001    .false.
cf18005    one-shot
cf18006    2        'wetwell exceeded 120 psig'
cf18011    1.0    0.0      cfvalu.176
*
* pressure 5
cf16700    pressure-5   equals    1    1.0   0.0
cf16701    1.0e8
cf16711    0.0    965266.     time    * pressure-5 = 140 psig
*
cf17700    set-pflag-5    l-gt     2     1.0   0.0
cf17701    .false.
cf17711    1.0     0.0     cfvalu.161
cf17712    1.0     0.0     cfvalu.167
*
cf18100    vent-mes-5      l-equals     1     1.0   0.0
cf18101    .false.
cf18105    one-shot
cf18106    2        'wetwell exceeded 140 psig'
cf18111    1.0    0.0      cfvalu.177
*
*
*
*
* -- flag debris presence in cavity
*
cf77100     'debris-in-cav'   l-equals     1     1.0      0.0
cf77101     .false.
cf77105     one-shot
cf77106     2        'mass of STEEL pour in cavity 1 > 0.0 kg'
cf77111     1.0       0.0     cfvalu.081
*
*  cavity flag active when > 0.0 kg STEEL has poured from bwrsar
*
cf08100     cav-steel    l-gt   2    1.0   0.0
cf08101     .false.
cf08111     1.0   0.0   edf.900.3  *  steel mass on floor
cf08112     0.0   0.0   time
*
*
* --- trap time of first drywell head leakage
*
*
cf77400  dwl-edit  l-equals  1  1.  0.
```

```
cf77401  .false.
cf77405  one-shot
cf77406  2  'drywell head leakage begins (dwl)'
cf77411  1.  0.  cfvalu.450
*
*
* --- trap time of first wetwell leakage
*
*
cf34200  twl-edit  1-equals  1  1.  0.
cf34201  .false.
cf34205  one-shot
cf34206  2  'the wetwell leaked (twl)'
cf34211  1.  0.  cfvalu.150
*
*
*******  write edits using input editcf in melcor input
cf99100  edits  1-or  8  1.  0.
cf99101  .false.
cf99125  1.  0.  cfvalu.771 *melt in drywell cavity
cf99126  1.  0.  cfvalu.163 *wetwell exceeded pressure 1
cf99127  1.  0.  cfvalu.178 *wetwell exceeded pressure 2
cf99128  1.  0.  cfvalu.179 *wetwell exceeded pressure 3
cf99129  1.  0.  cfvalu.180 *wetwell exceeded pressure 4
cf99130  1.  0.  cfvalu.181 *wetwell exceeded pressure 5
cf99131  1.  0.  cfvalu.774 *drywell head leaked  (dwl)
cf99135  1.  0.  cfvalu.342 *wetwell leaked       (twl)
*********************************************************
******* write restarts using restartcf in melcor input
cf99200  restarts  1-or  8   1.  0.
cf99201  .false.
cf99214  1.  0.   cfvalu.771 *melt in drywell cavity
cf99215  1.  0.   cfvalu.163 *wetwell exceeded pressure 1
cf99216  1.  0.   cfvalu.178 *wetwell exceeded pressure 2
cf99217  1.  0.   cfvalu.179 *wetwell exceeded pressure 3
cf99218  1.  0.   cfvalu.180 *wetwell exceeded pressure 4
cf99219  1.  0.   cfvalu.181 *wetwell exceeded pressure 5
cf99231  1.  0.   cfvalu.774 *drywell head leaked  (dwl)
cf99232  1.  0.   cfvalu.342 *wetwell leaked (twl)
*************************************************************
*******  write plot dump using plotcf in melcor input
cf99300  plots  1-or  8  1.  0.
cf99301  .false.
cf99331  1.  0.  cfvalu.771 *melt in drywell cavity
cf99332  1.  0.  cfvalu.163 *wetwell exceeded pressure 1
cf99333  1.  0.  cfvalu.178 *wetwell exceeded pressure 2
cf99334  1.  0.  cfvalu.179 *wetwell exceeded pressure 3
cf99335  1.  0.  cfvalu.180 *wetwell exceeded pressure 4
cf99336  1.  0.  cfvalu.181 *wetwell exceeded pressure 5
cf99337  1.  0.  cfvalu.774 *drywell head leaked  (dwl)
cf99338  1.  0.  cfvalu.342 *wetwell leaked       (twl)
*
. * that is all
```

NUREG/CR-5565
ORNL/TM-11644
Distribution
Category RX, 1S, XA

Internal Distribution

1.	W. G. Craddick	13.	D. B. Simpson
2.	S. A. Hodge	14.	R. P. Taleyarkhan
3.	C. R. Hyman	15.	M. L. Tobias
4-8.	S. R. Greene	16.	ORNL Patent Section
9.	T. S. Kress	17.	Central Research Library
10.	L. J. Ott	18.	Document Reference Section
11.	B. W. Patton	19-20.	Laboratory Records Department
12.	C. E. Pugh	21.	Laboratory Records (RC)

External Distribution

22. J. N. Ridgely, Division of Safety Issue Resolution, U.S. Nuclear Regulatory Commission, Severe Accident Issues Branch, MS NL/S - 007, 5650 Nicholson Lane, Rockville, Maryland 20852
23. A. E. Levin, U.S. Nuclear Regulatory Commission, OW FN 8E23, Research Systems Branch, Division of Systems Technology, Washington, DC 20555
24. R. L. Palla, Jr., U.S. Nuclear Regulatory Commission, OW FN MS 10E4, Room 10E11, Washington, DC 20555
25. J. A. Mitchell, U.S. Nuclear Regulatory Commission, MS NLS - 314, Washington, DC 20555
26. W. Minners, U.S. Nuclear Regulatory Commission, MS NLS -007, Washington, DC 20555
27. Y. S. Chen, U.S. Nuclear Regulatory Commission, MS NLN - 344, Washington, DC 20555
28. F. Eltawila, U.S. Nuclear Regulatory Commission, MS NLN - 344, Washington, DC 20555
29. J. T. Han, U.S. Nuclear Regulatory Commission, MS NLN - 353, Washington, DC 20555
30. C. E. Ader, U.S. Nuclear Regulatory Commission, MS NLS - 169, Washington, DC 20555
31. B. Sheron, U.S. Nuclear Regulatory Commission, MS NLS - 007, Washington, DC 20555

32-34. R. M. Summers, R. K. Cole, E. A. Boucheron, Sandia National Laboratories, Division 6418, Kirkland Air Force Base, Albuquerque, NM 87185

35. M. L. Corradini, Dept. of Nuclear Engineering, University of Wisconsin, 153 Engineering Research Bldg., 1500 Johnson Drive, Madison, Wisconsin 53706-1687

36-37. D. L. Kelly, R. J. Dallman, Idaho National Engineering Laboratory, MS 2508, Idaho Falls, ID 83415

38. G. W. Smith, Energy Operations, P.O. Box 31995, Jackson, Mississippi 39286-1995
39. Richard Sherry, Risk & Reliability Division, NUC Corporation, 910 Clopper Road, P.O. Box 6032, Gaithersburg, Maryland 20877-0962
40. W. M. Davis, ENERCON Services, Inc., 1700 West Albany, Suite A, P.O. Box 2050, Broken Arrow, Oklahoma 74013
41. C. A. Kukielka, Pennsylvania Power & Light Company, Two North Ninth Street, Allentown, PA 18104
42. Greg Krueger, Philadelphia Electric Company, 2301 Market Street, Philadelphia, PA 19101
43. George A. Greene, Brookhaven National Laboratory, Department of Nuclear Engineering, Building 820M, Upton, NY 11973
44. B. E. Boyack, Los Alamos National Laboratory, Mail Stop K551, Los Alamos, NM 87545
45. Gulf States Utilities Company, River Bend Nuclear Group, River Bend Station, P.O. Box 220, St. Francisville, LA 70775, ATTN: J. S. Miller
46. A. C. Payne, Sandia National Laboratories, Division 6412, Kirkland Air Force Base, Albuquerque, NM 87185
47. S. E. Dingman, Sandia National Laboratories, Division 6412, Kirkland Air Force Base, Albuquerque, NM 87185
48. T. D. Brown, Sandia National Laboratories, Division 6413, Kirkland Air Force Base, Albuquerque, NM 87185
49. Mr. James A. Reafsnyder, Deputy Assistant Manger, Energy Research & Development, DOE, Oak Ridge Operations Office, Oak Ridge, TN 37831-6269

50-52. DOE, Office of Scientific and Technical Information, P.O. Box 62, Oak Ridge, TN 37831

NRC FORM 335 (2-89) NRCM 1102, 3201, 3202

U.S. NUCLEAR REGULATORY COMMISSION

BIBLIOGRAPHIC DATA SHEET

(See instructions on the reverse)

1. REPORT NUMBER (Assigned by NRC, Add Vol., Supp., Rev., and Addendum Numbers, if any.)

NUREG/CR-5565
ORNL/TM-11548

2. TITLE AND SUBTITLE

The Response of BWR Mark II Containments to Station Blackout Severe Accident Sequences

3. DATE REPORT PUBLISHED

MONTH	YEAR
May	1991

4. FIN OR GRANT NUMBER

B0853

5. AUTHOR(S)

S. R. Greene, S. A. Hodge, C. R. Hyman, M. L. Tobias

6. TYPE OF REPORT

Technical

7. PERIOD COVERED (Inclusive Dates)

8. PERFORMING ORGANIZATION – NAME AND ADDRESS (If NRC, provide Division, Office or Region, U.S. Nuclear Regulatory Commission, and mailing address; if contractor, provide name and mailing address.)

Oak Ridge National Laboratory
Oak Ridge, TN 37831-8057

9. SPONSORING ORGANIZATION – NAME AND ADDRESS (If NRC, type "Same as above"; if contractor, provide NRC Division, Office or Region, U.S. Nuclear Regulatory Commission, and mailing address.)

Division of Safety Issue Resolution
Office of Nuclear Regulatory Research
U.S. Nuclear Regulatory Commission
Washington, DC 20555

10. SUPPLEMENTARY NOTES

11. ABSTRACT (200 words or less)

This report describes the results of a series of calculations conducted to investigate the response of BWR Mark II containments to short-term and long-term station blackout severe accident sequences. The BWR-LTAS, BWRSAR, and MELCOR codes were employed to conduct quantitative accident sequence progression and containment response analyses for several station blackout scenarios. The accident mitigation effectiveness of automatic depressurization system actuation, drywell flooding via containment spray operation, and debris quenching in Mark II suppression pools is assessed.

12. KEY WORDS/DESCRIPTORS (List words or phrases that will assist researchers in locating the report.)

boiling water reactor
individual plant examination
Mark II containment
severe accident
station blackout

13. AVAILABILITY STATEMENT

unlimited

14. SECURITY CLASSIFICATION

(This Page) unclassified

(This Report) unclassified

15. NUMBER OF PAGES

16. PRICE

NRC FORM 335 (2-89)